Physik-Department

Max-Planck-Institut für Kernphysik

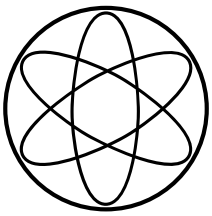

Particle Physics and Dark Energy: Beyond Classical Dynamics

Doctoral Thesis in Physics

submitted by

Mathias Garny

2008

Technische Universität München

TECHNISCHE UNIVERSITÄT MÜNCHEN

Max-Planck-Institut für Kernphysik

Particle Physics and Dark Energy: Beyond Classical Dynamics

Mathias Garny

Vollständiger Abdruck der von der Fakultät für Physik der Technischen Universität München zur Erlangung des akademischen Grades eines

Doktors der Naturwissenschaften (Dr. rer. nat.)

genehmigten Dissertation.

Vorsitzender: Univ.-Prof. Dr. Lothar Oberauer

Prüfer der Dissertation:

1. Prof. Dr. Manfred Lindner, Ruprecht-Karls-Universität Heidelberg
2. Univ.-Prof. Dr. Alejandro Ibarra

Die Dissertation wurde am 24.09.2008 bei der Technischen Universität München eingereicht und durch die Fakultät für Physik am 24.10.2008 angenommen.

Particle Physics and Dark Energy: Beyond Classical Dynamics

Abstract

In this work, quantum corrections to classical equations of motion are investigated for dynamical models of dark energy featuring a time-evolving quintessence scalar field. Employing effective quantum field theory, the robustness of tracker quintessence potentials against quantum corrections as well as their impact on cosmological observables are discussed. Furthermore, it is demonstrated that a rolling quintessence field can also play an important role for baryogenesis in the early universe. The macroscopic time-evolution of scalar quantum fields can be described from first principles within nonequilibrium quantum field theory based on Kadanoff-Baym equations derived from the 2PI effective action. A framework for the nonperturbative renormalization of Kadanoff-Baym equations is provided. Renormalized Kadanoff-Baym equations are proposed and their finiteness is shown for a special case.

Zusammenfassung

In dieser Arbeit werden Quantenkorrekturen klassischer Bewegungsgleichungen in dynamischen Modellen der Dunklen Energie untersucht, welche ein zeitabhängiges Quintessenz-Skalarfeld beinhalten. Im Rahmen effektiver Quantenfeldtheorie wird die Stabilität von Quintessenz-Potentialen bezüglich Quantenkorrekturen sowie deren Einfluß auf kosmologische Parameter diskutiert. Darüber hinaus wird gezeigt, daß ein zeitabhängiges Quintessenzfeld auch für die Baryogenese im frühen Universum eine wichtige Rolle spielen kann. Die makroskopische Zeitentwicklung von skalaren Quantenfeldern kann basierend auf Grundprinzipien der Nichtgleichgewichtsquantenfeldtheorie mittels Kadanoff-Baym Gleichungen beschrieben werden. Es wird ein Formalismus für die nichtperturbative Renormierung von Kadanoff-Baym Gleichungen entwickelt, renormierte Kadanoff-Baym Gleichungen vorgeschlagen, und deren Endlichkeit für einen Spezialfall nachgewiesen.

Contents

1 Introduction **1**

2 Dynamical Dark Energy **5**
2.1 Quintessence Cosmology 6
2.2 Tracking Solutions 9
2.3 Interacting Quintessence 12

3 Quantum Effective Action **15**
3.1 1PI Effective Action 16
3.2 2PI Effective Action 19
3.3 nPI Effective Action 21

4 Quantum Corrections in Quintessence Models **23**
4.1 Self-Interactions 24
4.2 Matter Couplings 44
4.3 Gravitational Coupling 51
4.4 Summary 60

5 Leptonic Dark Energy and Baryogenesis **61**
5.1 Quintessence and Baryogenesis 61
5.2 Creation of a $B-L$-Asymmetry 62
5.3 Stability 66

6 Quantum Nonequilibrium Dynamics and 2PI Renormalization **67**
6.1 Kadanoff-Baym Equations from the 2PI Effective Action 68
6.2 Nonperturbative 2PI Renormalization at finite Temperature 73

7 Renormalization Techniques for Schwinger-Keldysh Correlation Functions **79**
7.1 Non-Gaussian Initial States 79
7.2 Nonperturbative Thermal Initial Correlations 86
7.3 Renormalized Kadanoff-Baym Equation for the Thermal Initial State 103

8 Renormalization of Kadanoff-Baym Equations **105**
8.1 Kadanoff-Baym Equations and 2PI Counterterms 105
8.2 Renormalizable Kadanoff-Baym Equations from the 4PI Effective Action 106
8.3 Impact of 2PI Renormalization on Solutions of Kadanoff-Baym Equations 112
8.4 Summary 129

9 Conclusions **131**

A Conventions **135**

B Effective Action Techniques **137**
B.1 Low-Energy Effective Action . . . 137
B.2 Effective Action in Curved Background . . . 138
B.3 Renormalization Group Equations . . . 141

C Resummation Techniques and Perturbation Theory **145**
C.1 Relation between 2PI and 1PI . . . 145
C.2 Resummed Perturbation Theory . . . 146

D Quantum Fields in and out of Equilibrium **151**
D.1 Thermal Quantum Field Theory . . . 151
D.2 Nonequilibrium Quantum Field Theory . . . 157

E Nonperturbative Renormalization Techniques **163**
E.1 Renormalization of the 2PI Effective Action . . . 163
E.2 Renormalization of 2PI Kernels . . . 165
E.3 Two Loop Approximation . . . 167
E.4 Three Loop Approximation . . . 168

F Integrals on the Closed Real-Time Path **171**

Acknowledgements **173**

Bibliography **175**

Chapter 1

Introduction

According to the standard model of cosmology, the evolution of our universe experienced a rapidly inflating and highly correlated phase at its beginning. This phase ended in an explosive entropy production (reheating), during which all kinds of sufficiently light particles were produced and thermalized, most of them highly relativistic. Reheating was followed by a controlled expansion during which the temperature decreased and more and more massive species became non-relativistic (radiation domination). Subsequently, pressure-less baryonic and cold dark matter became the dominant contribution to the total energy density, and underwent gravitational clustering (matter domination). However, in recent cosmic history, the expansion of the universe started to accelerate. This may be attributed to the so-called dark energy, which became more and more important and makes up over two third of the energy density of the universe today.

All that is known about dark energy is based on its gravitational interaction. While the total energy density can be measured by observations of the anisotropy of the cosmic microwave background (CMB), the forms of energy which cluster gravitationally can be inferred from large-scale structure surveys together with appropriate models of structure formation. However, the clustered energy is much less than the total energy density, such that an additional, homogeneously distributed component is required. On top of that, such a dark energy component can precisely account for the accelerated expansion observed by measurements of the luminosity of distant supernovae [133]. This concordance of different observations makes the need for dark energy convincing and the question about its nature one of the most outstanding questions in astro-particle physics.

The inclusion of a cosmological constant in Einstein's equations of General Relativity provides a parameterization of dark energy which is compatible with cosmological observations [89]. The cosmological constant can be viewed as a covariantly conserved contribution to the energy-momentum tensor which is invariant under general coordinate transformations. For any quantum field theory for which coordinate invariance is unbroken, this is precisely the property of the vacuum expectation value of the energy-momentum tensor. Therefore, the cosmological constant may be interpreted as the vacuum energy within quantum field theory [188]. However, since quantum field theory together with classical gravity determines the vacuum energy only up to a constant, it is impossible to predict the value of the cosmological constant. Furthermore, the naïve summation of zero-point energies of all momentum modes of a free quantum field leads to a divergent result. Once a cutoff between the TeV and the Planck scale is imposed, this amounts to a value which is between 60 and 120 orders of magnitude too large. This fact is known as the cosmological constant problem [178]. If the value inferred from cosmological observations is taken at face value, an enormous hierarchy between the vacuum energy density and the energy density of radiation and matter must have existed in the early universe (smallness problem). Subsequently, radiation and matter get diluted due to the cosmic ex-

pansion, and the cosmological constant becomes of comparable order of magnitude precisely in the present cosmological epoch (coincidence problem).

These unsatisfactory features of the cosmological constant have motivated an extensive search for alternative explanations of dark energy. Apart from attempts to explain cosmic acceleration by modifications of the equations of General Relativity [74, 151], models of dynamical dark energy [65, 162] explore the possibility that the dark energy density might evolve with time and become diluted during cosmic expansion, similar to the radiation and matter components. In this way its smallness today could be attributed to a dynamical mechanism and the huge age of the universe.

Similar dynamical mechanisms are well-known in cosmology. For example, cosmic inflation provides a dynamical mechanism leading to a spatially flat universe in which the total energy density is naturally very close to the critical energy density [108] as observed by CMB measurements [89]. Another example is provided by baryogenesis. Here, the observed baryon density (as well as the absence of antibaryons) is attributed to a dynamically produced asymmetry. If the three Sakharov conditions [163] are fulfilled in the early universe, namely violation of baryon number conservation, violation of charge-conjugation and its combination with parity, and departure from thermal equilibrium, a baryon asymmetry can develop. For specific realizations, the final observable value of the asymmetry is even insensitive to a primordial asymmetry [48, 71]. Both examples show that a dynamical mechanism can help to explain a measurable quantity which would otherwise have required an enormous amount of fine-tuning of the "initial" state after the Big Bang.

Dynamical models for dark energy typically require the introduction of new degrees of freedom. For example, cosmic acceleration could be powered by a slowly rolling scalar field [157, 182], called quintessence field, similar to the inflaton field in the early universe. A special class of quintessence models featuring so-called tracking solutions [169] exhibits a dynamical self-adjusting mechanism of the dark energy density. This means that the evolution of the dark energy density today is insensitive to the amount of primordial dark energy in the early universe. Therefore, the energy densities of matter and dark energy can be comparable not only in the present epoch, but also in the early universe. For specific models, both energy densities are even of comparable magnitude during the entire history of the universe [85, 157]. These features represent advantages of tracker quintessence models compared to the cosmological constant.

However, quintessence models cannot address the fundamental cosmological constant problem of quantum field theory. Additionally, introducing scalar fields brings up even more theoretical questions on the quantum level. Above all, this includes the hierarchy problem. It states that a scalar field is unprotected against large quantum corrections to its mass, originating in quadratically divergent loop corrections (where "large" refers to an ultraviolet embedding scale). Nevertheless, particle physicists and cosmologists commonly resort to scalar fields. The most prominent examples are the Higgs field in the Standard Model and the inflaton field in cosmology. However, up to now no direct experimental evidence for the existence of an elementary scalar field exists.

In the context of quintessence models, it is therefore an urgent question what role quantum corrections play for the dynamics of the quintessence scalar field. In particular, the quintessence field is characterized by two striking properties, which deserve special attention. These are *(i)* the quintessence tracker potential and *(ii)* the macroscopic time-evolution of the field value over cosmic time-scales.

Quintessence tracker potentials have a form which is not well-known within particle physics, involving exponentials and inverse powers of the field. Therefore, it is important to investigate the robustness of such exceptional potentials with respect to quantum corrections.

Typically, tracker quintessence fields feature non-renormalizable self-interactions suppressed by inverse powers of the Planck scale. This indicates that tracker potentials may result from integrating

out some unknown degrees of freedom at the Planck scale. Below this scale, effective quantum field theory can be employed. The ignorance about the superior theory is encapsulated into a few effective parameters (like the potential energy at a certain field value, e.g. today) and the ultraviolet embedding scale.
In order to assess the self-consistency of quintessence tracker models, it is crucial to investigate their robustness with respect to quantum corrections originating from self-interactions. In particular, it is necessary to investigate whether the asymptotic flatness of the potential is stable under radiative corrections.
Phenomenological signatures which could reveal the existence of a rolling quintessence field include time-varying fundamental 'constants' as well as apparent violations of the equivalence principle [157]. Both effects result from couplings between quintessence and Standard Model particles. However, once quantum corrections are taken into account, such couplings destroy the desired properties of the quintessence field if they are too large. Therefore it is important to investigate their quantum backreaction and to obtain quantitative upper bounds.
Additionally, it is necessary to check whether radiatively induced non-minimal gravitational couplings are in conflict with experimental tests of General Relativity. For example, non-minimal couplings of the quintessence field can lead to a time-variation of the effective Newton constant over cosmological time-scales [181].

The second characteristic property of the quintessence field mentioned above is its macroscopic time-evolution over cosmological time-scales. Therefore, the question arises how to calculate radiative corrections for a time-evolving scalar field. If the kinetic energy of the field is much smaller than the potential energy and if its environment can be approximated by a vacuum or a thermal background, it is possible to use a derivative expansion of the effective action in vacuum or at finite temperature, respectively. At leading order, this amounts to replacing the classical potential by the effective potential in the equations of motion.
Quantum corrections within quintessence models as described in this work employ the derivative expansion of the effective action. The latter is applicable since the quintessence field is slowly rolling today. However, this might not have been the case in the early universe. Therefore, it is necessary to develop methods that can describe the quantum dynamics of scalar fields beyond the limitations of the derivative expansion. This falls into the realm of nonequilibrium quantum field theory.
Note that similar questions arise for other nonequilibrium phenomena within astro-particle and high-energy physics, like inflation and reheating, as well as baryogenesis or heavy ion collisions. Traditionally, these processes are modeled by semi-classical approximations. These include Boltzmann equations, hydrodynamic transport equations or effective equations of motion for a coherent scalar field expectation value, for example based on mean-field approximations [18, 63, 130].
Since it is of great importance to assess the reliablity of these approximations, a comparison with a completely quantum field theoretical treatment is desirable. In recent years it has been demonstrated that scalar (and fermionic) quantum fields far from equilibrium can be described based on first principles by Kadanoff-Baym equations [1, 2, 25, 32, 142]. These are evolution equations for the full one- and two-point correlation functions obtained from the stationarity conditions of the 2PI effective action [66]. The advantages of this treatment are twofold: First, its conceptual simplicity is very attractive. The only assumption entering the derivation of Kadanoff-Baym equations is the truncation of the so-called 2PI functional, which amounts to a controlled approximation in the coupling constant or the inverse number of field degrees of freedom for specific quantum field theories [25]. Otherwise, no further assumptions are required. In particular, no assumptions that would only hold close to thermal equilibrium or in the classical limit are required. Furthermore, for any time-reversal invariant quantum field theory, the Kadanoff-Baym equations are also time-reversal invariant, in contrast

to Boltzmann equations. Second, Kadanoff-Baym equations inherently incorporate typical quantum (e.g. off-shell) effects as well as "classical" (e.g. on-shell) effects in a unified manner. Therefore they are very versatile and can be employed both to assess the validity of conventional semi-classical approximations (e.g. for baryogenesis and leptogenesis), and in situations where a single effective description does not exist (e.g. for (p)reheating by inflaton decay and subsequent thermalization). In addition, Kadanoff-Baym equations can describe the quantum dynamics of a time-evolving scalar field beyond the 'slow-roll' approximation (e.g. for inflation and quintessence).
It has been shown that numerical solutions of Kadanoff-Baym equations not only provide a description of the quantum thermalization process of relativistic quantum fields for closed systems [30, 32, 33], but also feature a separation of time-scales between kinetic and chemical equilibration (prethermalization) [31]. Furthermore, they have been compared to semi-classical transport equations for bosonic and fermionic systems [1, 123, 142, 143]. Moreover, Kadanoff-Baym equations can describe the decay of a coherent, oscillating scalar field expectation value under conditions where parametric resonance occurs [33], and have also been investigated in curved space-time [115, 170].
These successes of nonequilibrium quantum field theory make it worthwhile and, in view of realistic applications, necessary to answer remaining conceptual questions, like renormalization. There are several reasons why a proper renormalization of Kadanoff-Baym equations is essential. First, it is required for a quantitative comparison with semi-classical Boltzmann equations, which are finite by construction. Second, renormalization has an important quantitative impact on the solutions of Kadanoff-Baym equations, and therefore affects thermalization time-scales. Third, it is crucial for identifying physical initial states, meaning all nonequilibrium initial states that can occur as real states of the physical ensemble. The fact that this class excludes for example an initial state featuring bare particle excitations shows that this is of significance. Finally, a proper renormalization leads to a stabilization of the computational algorithm used for the numerical solution of Kadanoff-Baym equations such that its range of applicability is extended and its robustness is improved.

In chapter 2, quintessence models with tracking solutions are briefly reviewed, and in chapter 3, an overview over perturbative as well as nonperturbative calculation techniques of the quantum effective action is given. In chapter 4, the robustness of tracker quintessence models with respect to quantum corrections is studied. Quantum corrections induced by the self-interactions of the quintessence field, by couplings to Standard Model particles, and by the gravitational interaction are investigated, and consequences for cosmology as well as for observational signatures of a rolling quintessence field are discussed. Next, in chapter 5, it is demonstrated that the quintessence field can also play an important role in the early universe. This is done by presenting a model where baryogenesis and late-time cosmic acceleration are both driven by a time-evolving complex quintessence field.
The derivation of Kadanoff-Baym equations starting from the 2PI effective action is briefly reviewed in chapter 6, as well as the nonperturbative renormalization procedure of the 2PI effective action in thermal equilibrium, which has recently been formulated [28, 29, 37, 173–175].
The remaining part of this thesis is dedicated to the renormalization of Kadanoff-Baym equations. This requires two steps. First, in chapter 7, the nonperturbative renormalization procedure for the 2PI effective action in vacuum and in thermal equilibrium is adapted to the closed Schwinger-Keldysh real-time contour, which is the starting point for nonequilibrium quantum field theory. Second, in chapter 8, extended Kadanoff-Baym equations that can be used to describe systems featuring non-Gaussian initial correlations, are derived from the 4PI effective action. An ansatz for renormalized Kadanoff-Baym equations within $\lambda\Phi^4$-theory is proposed and verified analytically for a special case. Furthermore, properties expected from solutions of renormalized Kadanoff-Baym equations are checked and the importance of renormalization for nonequilibrium quantum dynamics is demonstrated.

Chapter 2

Dynamical Dark Energy

In the following, the main theoretical motivations for dynamical dark energy models are reviewed, and it is briefly discussed in how far dynamical dark energy, and specifically quintessence models with tracking solutions, can address the problems connected to the cosmological constant. Furthermore, possible observational signatures of a quintessence field are reviewed. For a detailed discussion of the observational evidence for accelerated expansion and dark energy, it is referred to Refs. [89, 100, 133, 160].
In order to be able to distinguish clearly between the different cosmological questions it is useful to make a detailed definition:

QFT smallness problem: Why is there no huge cosmological constant contributing a vacuum energy density of order M_{pl}^4, $M_{\rm GUT}^4$, $M_{\rm SUSY}^4$ or $M_{\rm el.\,weak}^4$?

Cosmological smallness problem: How can one explain a small *nonzero* cosmological constant or dark energy density?

Coincidence of scales: The present dark energy and matter densities are[1]

$$\rho_{de} \approx 1.3 \cdot 10^{-123}\, M_{pl}^4 \qquad \text{and} \qquad \rho_{\rm M} \approx 0.5 \cdot 10^{-123}\, {\rm M}_{pl}^4 .$$

Coincidence of epochs: In our present cosmological epoch the expansion of the universe changes from decelerated to accelerated [160].

The last two items are observational statements. The question is whether there is a natural explanation for these coincidences or whether they are just an "accident".
It appears likely that these questions cannot be answered by a single approach. On the one hand, a mechanism (or a symmetry) is needed that explains why the huge field theoretical contributions including contributions from potential shifts do not exist at all or at least why they do not act as a source of gravity. On the other hand, the observed acceleration of the universe has to be explained.
The cosmological standard model with a cosmological constant and a cold dark matter component (ΛCDM) is in accordance with all present observations inside the errorbars [89]. However, it does not answer *any* of the four cosmological questions above. The value of the cosmological constant has to be fine-tuned to fulfill the two "coincidences": At the Planck epoch there is a hierarchy of order 10^{-123} between the energy density of the cosmological constant and the relativistic matter content in this model.

[1] The values are based on the "concordance model" $\Omega_{\rm DE} = 0.7$, $\Omega_M = 0.3$ and use $H_0 = 70\,{\rm km/s\,Mpc}$.

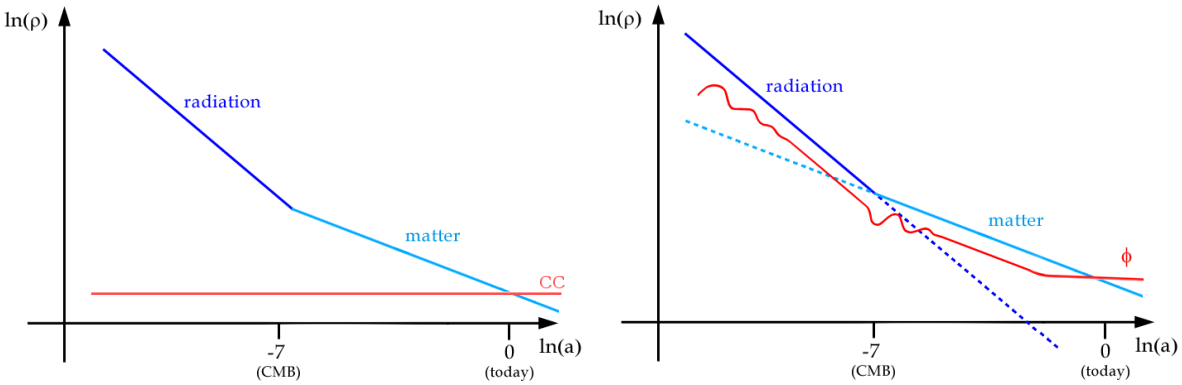

Figure 2.1: *Schematic illustration of the evolution of the radiation, matter and dark energy densities for the cosmological constant (left) and a tracking quintessence model (right).*

Starting point for *dynamical* dark energy models is the "cosmological smallness problem". The aim is to explain the smallness of dark energy by the huge age of the universe. Therefore a "time-dependent cosmological constant" can be introduced that decays (similar to matter or radiation density) during cosmic evolution thus providing a natural explanation for its smallness today (see figure 2.1). At the Planck scale the dark energy content of the universe does not have to be fine-tuned to an extraordinarily small number.

General covariance of the equations of motion dictates that the dark energy cannot only depend on time but is given by a space-time dependent *field*[2] which has to be added to the Lagrangian of the theory as a new dynamical degree of freedom. This opens up a whole field of possibilities manifesting themselves in a huge variety of scalar-field-based models, like Chaplygin Gas (a cosmic fluid derived from a Born-Infeld Lagrangian with equation of state $p \sim -1/\rho$), phantom energy (derived from a scalar-field Lagrangian with kinetic term with a "wrong sign" and with pressure $p < -\rho$) or k-essence (with nonlinear kinetic term) and of course, most straightforward and probably most elaborated, quintessence with a standard kinetic term and a self-interaction described by the quintessence potential, to name only a few (see [65, 162] for reviews, [16]).

The details of the decaying field are important when addressing the "coincidence of scales". Generally, it will therefore depend on the specific model in how far a natural explanation for this remarkable coincidence is found. Quintessence provides a special class of so-called tracking solutions that accounts for this coincidence, which will be discussed in the following.

The "coincidence of epochs" is not *generically* addressed by dynamic dark energy models. In some models the two coincidences are linked (like for a cosmological constant), while in other models they have to be discussed separately.

2.1 Quintessence Cosmology

The framework of cosmology is the general theory of relativity, and cosmological models with dynamical dark energy can be formulated within this setting. However, one should keep in mind that cosmology is based on some fundamental assumptions, like isotropy and large-scale homogeneity of all components of our universe. Their validity is assumed in the following. Scalar-fields in cosmology are actually not unusual. Already shortly after the big bang the universe may have undergone

[2] Just replacing the cosmological constant by a function $\Lambda(t)$ is not possible because the Einstein equations can only be solved for covariant conserved energy-momentum tensors $T_{\mu\nu;\rho} = 0$. However, $(\Lambda g_{\mu\nu})_{;\rho} = 0$ only if $\Lambda \equiv$ const.

an accelerated phase, the cosmic inflation, which is often described by a slowly rolling scalar-field, called inflaton [108, 139, 140]. In this section, the quintessence scalar-field will be introduced into the general theory of relativity, in close analogy to the inflaton scalar-field[3]. Starting point is the gravitational action with a standard kinetic term and a potential for the quintessence scalar-field ϕ given by [157, 182]

$$S = \int d^4x\sqrt{-g(x)}\left(-\frac{R}{16\pi G} + \frac{1}{2}g^{\mu\nu}\partial_\mu\phi\partial_\nu\phi - V(\phi) + \mathcal{L}_B\right), \tag{2.1}$$

where G is Newton's constant and $\mathcal{L}_B$ is the Lagrangian describing all other forms of energy like dark matter, baryonic matter, radiation and neutrinos, which will be called "background". Furthermore, $g(x)$ is the determinant of the metric $g_{\mu\nu}(x)$ and R is the curvature scalar as defined in appendix A. The coupling of the quintessence field to gravity is called minimal in this case since there are no explicit coupling terms like $\phi^2 R$. It is only mediated through the integration measure and the contraction of the space-time derivatives in the kinetic term dictated by general coordinate invariance. Possible constant contributions in the action (i.e. the cosmological constant) are assumed to be absorbed into the potential $V(\phi)$. Variation of the action with respect to the metric yields the Einstein equations

$$R_{\mu\nu} - \frac{R}{2}g_{\mu\nu} = 8\pi G(T^B_{\mu\nu} + T^Q_{\mu\nu}), \tag{2.2}$$

with the Ricci-tensor $R_{\mu\nu}$, the energy-momentum tensor for the background $T^B_{\mu\nu} = \frac{2}{\sqrt{-g}}\frac{\delta(\sqrt{-g}\mathcal{L}_B)}{\delta g^{\mu\nu}}$ and

$$T^Q_{\mu\nu} = \partial_\mu\phi\partial_\nu\phi - g_{\mu\nu}\left(\frac{1}{2}(\partial\phi)^2 - V\right) \equiv (\rho_\phi + p_\phi)u_\mu u_\nu - g_{\mu\nu}p_\phi\,. \tag{2.3}$$

The energy-momentum tensor can be expressed in analogy to a perfect fluid with unit 4-velocity vector $u_\mu = \partial_\mu\phi/\sqrt{(\partial\phi)^2}$ and energy density and pressure given by

$$\rho_\phi = \frac{1}{2}(\partial\phi)^2 + V(\phi) \qquad \text{and} \qquad \mathrm{p}_\phi = \frac{1}{2}(\partial\phi)^2 - \mathrm{V}(\phi)\,. \tag{2.4}$$

Variation of the action with respect to ϕ leads to the equation of motion for the quintessence field[4]

$$\Box\phi + \frac{dV(\phi)}{d\phi} = 0\,, \tag{2.5}$$

with the covariant D'Alembertian for a scalar-field

$$\Box = D_\mu D^\mu = \frac{1}{\sqrt{-g}}\partial_\mu\sqrt{-g}\partial^\mu\,.$$

Under the assumptions of isotropy, homogeneity and a spatially flat universe the Robertson-Walker-Metric for comoving coordinates $x^\mu = (t, \boldsymbol{x})$ with a dimensionless scalefactor $a(t)$ can be used,

$$ds^2 = g_{\mu\nu}dx^\mu dx^\nu = dt^2 - a(t)^2 d\boldsymbol{x}^2\,.$$

After specializing the energy-momentum tensors to contain only space-independent densities $\rho_B(t)$ and $\rho_\phi(t)$ and pressures[5] $p_B(t)$ and $p_\phi(t)$ the Einstein equations reduce to the Friedmann equations

$$\begin{aligned} 3M_{pl}^2H^2 &= \rho_\phi + \rho_B\,, \\ 3M_{pl}^2\frac{\ddot{a}}{a} &= -\frac{1}{2}(\rho_\phi + 3p_\phi + \rho_B + 3p_B)\,, \end{aligned} \tag{2.6}$$

[3] It is also possible to construct models where the quintessence and the inflaton fields are identical [154].

[4] If the background Lagrangian $\mathcal{L}_B$ contains ϕ (e.g. quintessence-dependent couplings) the right hand side of the equation of motion has to be replaced by $\delta\mathcal{L}_B/\delta\phi$. For the basic discussion of quintessence it will be assumed that this term has a negligible influence on the dynamics of the ϕ field.

[5] The energy momentum tensors for the background and the ϕ field are assumed to be of the form of an ideal fluid $T^i_{\mu\nu} = (\rho_i + p_i)u_\mu u_\nu - g_{\mu\nu}p_i$ with $u_\mu = (1, \mathbf{0})$.

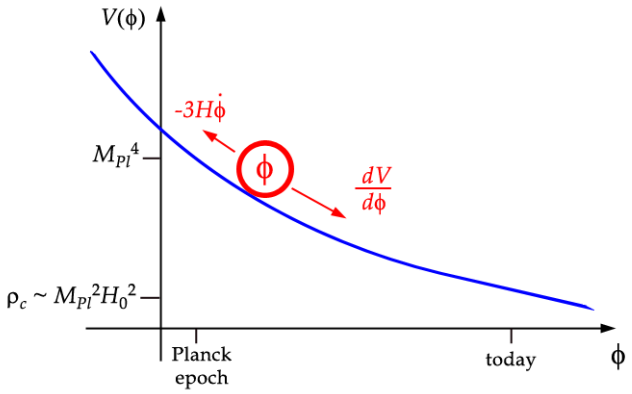

Figure 2.2: *Schematic illustration of the equation of motion of the quintessence field.*

with the Hubble parameter $H = \dot{a}/a$ and the Planck-Mass $M_{pl} = 1/\sqrt{8\pi G}$. The critical density is defined as $\rho_c \equiv 3M_{pl}^2 H^2$. The first Friedmann equation is often written in terms of $\Omega_i \equiv \rho_i/\rho_c$

$$1 = \Omega_\phi + \Omega_B \,.$$

In the case of a spatially homogeneous scalar field $\phi(t)$ the covariant D'Alembertian is

$$\Box = a^{-3}\partial_t\, a^3\, \partial_t = \partial_t^2 + 3H\partial_t \,,$$

yielding an equation of motion from (2.5) for the homogeneous quintessence field:

$$\ddot{\phi} + 3H\dot{\phi} + \frac{dV(\phi)}{d\phi} = 0 \,. \tag{2.7}$$

Illustratively, the derivative of the potential acts like a force which accelerates the scalar field value towards smaller potential energies thereby being "damped" by the $3H\dot{\phi}$-term. However, the damping depends on the contents of the universe including quintessence itself which means there is a back-reaction (see figure 2.2). The latter is responsible for the existence of non-trivial "tracking" solutions.

The equation of motion is equivalent to the "first law of thermodynamics"

$$d(a^3\rho_\phi)/dt = -p_\phi\, da^3/dt \,, \tag{2.8}$$

which can also be obtained from the requirement of covariant conservation of the energy-momentum tensor $T^{Q;\nu}_{\mu\nu} = 0$. Actually, this law is also valid for each independent[6] species i in the background

$$d(a^3\rho_i)/dt = -p_i\, da^3/dt \,. \tag{2.9}$$

Furthermore it can be shown that the corresponding equation for the total energy density $\rho_{\text{total}} \equiv \rho_\phi + \sum_i \rho_i$ and the (analogically defined) total pressure p_{total} can be derived from the Friedmann equations. Thus, assuming N species in the background, there are $4+N$ independent equations (second order differential equations are counted twice) from (2.9, 2.7, 2.6) with $4+2N$ independent variables

[6] An *independent* species should have negligible interaction with other species.

$a, \dot{a}, \phi, \dot{\phi}, \rho_i, p_i$. This means the system can only be solved by specifying N additional equations, conventionally taken to be the equations of state for the N background species,

$$p_i = p_i(\rho_i) \equiv \omega_i \rho_i \,. \tag{2.10}$$

A constant "equation of state parameter" ω_i, together with the first law of thermodynamics (2.9), yields the scaling behavior of the most important background components[7]

$\omega_M = 0$	$\rho_M \propto a^{-3}$	nonrelativistic matter,
$\omega_R = 1/3$	$\rho_M \propto a^{-4}$	relativistic matter,
$\omega_\Lambda = -1$	$\rho_\Lambda \propto a^0$	cosmological constant.

It is useful to define the equation of state parameter ω_ϕ analogously to the background for the quintessence field,

$$\omega_\phi = \frac{p_\phi}{\rho_\phi} = \frac{\dot{\phi}^2/2 - V}{\dot{\phi}^2/2 + V} \,. \tag{2.11}$$

However, the crucial difference is that this parameter will in general *not* be a constant. Therefore the scaling behavior of quintessence cannot be integrated as easily as for matter and radiation. Like in inflationary scenarios, it is used that ω_ϕ can be close to -1 if the scalar-field is slowly rolling (i.e. $\dot{\phi}^2/2 \ll V$) down its potential. It can be seen from the second Friedmann equation (2.6) that it is a necessary condition for an accelerated expansion of the universe that $\omega_\phi < -1/3$. If the quintessence field is static ($\dot{\phi} = 0$), it acts like a cosmological constant V with $\omega_\phi = -1$. On the other hand, a freely rolling field ($\dot{\phi}^2/2 \gg V$) has $\omega_\phi = +1$ and scales like a^{-6}. In any intermediate case one has

$$-1 \leq \omega_\phi \leq +1$$

if the potential is positive. Models with $\omega_\phi < -1$ can be obtained by flipping the sign of the kinetic term in the Lagrangian (tachyonic or phantom dark energy) or by introducing new terms in the action, leading to cosmologies with a Big Rip in the future. Such models allow superluminal velocities and are unstable on the quantum level since the energy density is not bounded from below [162]. These models are not considered here. Instead, the focus lies on those models which are able to address the "cosmological smallness problem" most efficiently.

2.2 Quintessence with Tracking Solutions

Within quintessence cosmology, specific models are obtained from specific choices of the potential. A priori, the potential may be an arbitrary function of the field value. From the point of view of particle physics, a polynomial which contains quadratic and quartic terms, similar to the standard Higgs potential, would be the most straightforward choice, since it is renormalizable and well-understood. Furthermore, such a potential furnishes the simplest model of cosmic inflation in the early universe, which is compatible with all observational constraints [89]. However, for dynamical dark energy, a renormalizable potential suffers from several shortcomings. First, it would be necessary to fine-tune the mass and the coupling constant to extraordinarily small values[8] in order to prevent the field from

[7] The cosmological constant is only given for completeness. It does not appear in the *background* since it is absorbed into the potential V.

[8] For a quadratic potential, the typical relaxation time-scale is given by the mass. Requiring that this time-scale is of the order of the age of the universe means that the mass has to be of the order of the Hubble constant $H_0 \sim 10^{-33}\,\mathrm{eV}$. When a quartic term is present, it is additionally required that the quartic coupling constant is extremely tiny, $\lambda \ll H_0^2/M_{pl}^2$. A similar constraint is well-known for chaotic inflation, $\lambda \ll H_{inf}^2/M_{pl}^2 \lesssim 10^{-10}$.

reaching the stable potential minimum already long before the present epoch, and thereby disqualify as *dynamical* dark energy. Second, even if the fine-tuning of the mass and the coupling constant is permitted, it would additionally be necessary to fine-tune the initial conditions of the field in the early universe in order to achieve precisely the observed dark energy density today.
On the other hand, it is possible to specify desired properties of dynamical dark energy and then try to construct potentials which yield solutions featuring these properties. This philosophy has been followed in Ref. [157], and generalized in Ref. [169] leading to the notion of tracker quintessence models, which are characterized by the following properties: First, the dynamics of the quintessence field today should be insensitive to the initial value in the early universe. Second, it should be possible to explain the smallness of the quintessence energy density today due to its dilution caused by the cosmic expansion, similar to the dark matter density. Thereby, it is desired that the ratio of dark energy and dark matter densities stays ideally of order unity during the complete cosmic history, such that their similarity is not a special "coincidence" at all. Third, a necessary property is the cross-over from matter domination to dark energy domination. The last property is the only one shared by the cosmological constant, which, however, is absolutely sensitive to the "initial" value, since it is a constant, and requires a huge hierarchy between the dark matter and dark energy densities in the early universe.
As has been shown in Ref. [169], the upper properties are realized for quintessence potentials which fulfill the so-called tracker condition. It states that the dimensionless function

$$\Gamma(\phi) \equiv \frac{V(\phi)V''(\phi)}{V'(\phi)^2}$$

has to be larger or equal to unity, and (approximately) constant for all field values for which $V(\phi)$ is between the critical energy density today and after inflation. The latter requirement can be shown to guarantee the existence of attractors in phase space, which wipe out the dependence on initial conditions for all solutions which approach the attractor solution [169]. Thus, the first desired property is fulfilled. For the attractor solution, the quintessence field dilutes with cosmic expansion with an approximately constant equation of state [169]

$$\omega_\phi^* = \omega_B - \frac{\Gamma - 1}{\Gamma - \frac{1}{2}}(1 + \omega_B)\,, \tag{2.12}$$

where $\omega_B = 1/3$ during radiation domination and $\omega_B = 0$ during matter domination. The equation of state parameter determines the evolution of the quintessence energy density in the expanding universe. For a quintessence potential where $\Gamma \sim 1$, the quintessence equation of state ω_ϕ^* is close to ω_B, such that the quintessence energy density evolves with time approximately proportional to the dominant background density. Thus, for a quintessence potential where $\Gamma \sim 1$, the dark energy density "tracks" first the radiation density and then the matter density, and thereby meets the second desired property. For $\Gamma = 1$, the ratio of the dark energy and dark matter densities would even be exactly constant during matter domination, and exhibit perfect tracking behaviour. For $\Gamma > 1$, however, one has that $\omega_\phi^* < \omega_B$. This means that the ratio of the quintessence energy density and the background energy density increases with time. Therefore, a cross-over from matter domination to dark-energy domination has to occur at some point, which was the third desired property.
The prototype tracker potentials are those for which $\Gamma(\phi)$ is precisely constant. They are given by

$$V(\phi) \;=\; \begin{cases} M_{pl}^4 \exp\left(-\lambda \frac{\phi}{M_{pl}}\right) & \text{for} \quad \Gamma = 1\,, \\ c \cdot \phi^{-\alpha} & \text{for} \quad \Gamma > 1 \qquad \text{with} \quad \Gamma = 1 + \frac{1}{\alpha}\,. \end{cases}$$

Both the exponential and the inverse power law potentials decrease monotonously with ϕ, and approach their minimal value (zero) asymptotically for infinitely large field values. For the tracker solution, the field slowly rolls down the potential, with $\phi^*(t)|_{t\to\infty} \to \infty$. Their properties have been studied extensively in the literature [9, 10, 34, 157, 169, 182], and will therefore only be briefly sketched here. Furthermore, many alternative potentials, for which Γ is only approximately constant, are typically built up from combinations of the prototype potentials, like the inverse exponential potential [169] or the so-called SUGRA potential [42, 43], and share many of their basic properties.

Exponential potential: For the exponential potential, the quintessence energy density is precisely proportional to the radiation density during radiation domination (with $\Omega_\phi = 4/\lambda^2$), and to the matter density during matter domination (with $\Omega_\phi = 3/\lambda^2$). Therefore, the exponential potential motivates the search for early dark energy, which clearly discriminates it from the cosmological constant. Constraints on early dark energy arise from its impact on BBN, structure formation and the CMB [85, 86]. A typical upper bound for the dark energy fraction at redshifts $z \gtrsim 2$ is $\Omega_\phi < 0.05$, which implies that $\lambda > 7.75$. For a single exponential potential, Ω_ϕ would *always* remain constant and no cross-over towards accelerated expansion would occur, which disqualifies it as a viable dark energy model. However, the tracking attractor just exists if $\lambda > \sqrt{3(1+\omega_B)}$, i.e. if the potential is steep enough. Otherwise, the exponential potential features an attractor for which the quintessence energy density dominates over the radiation and matter densities, with equation of state $\omega_\phi^* = -1 + \lambda^2/3$, such that accelerated expansion occurs when λ is small enough. Therefore, viable models can be constructed for which the cross-over is triggered by an effective change in the slope of the exponential potential. This can be accomplished by a potential which is given by the sum of two exponentials with different slope [21], or by a "leaping kinetic term" [111]. For the cross-over to occur now, it is necessary to adjust the relative size of the exponentials, which may be considered as an unavoidable tuning of the potential. In Ref. [111] it is argued, however, that the tuning is much less severe as required for the cosmological constant (over two instead of 120 orders of magnitude).

Inverse power law potential: The inverse power law potential alone already leads to a viable dynamical dark energy model, for which the dark energy density dilutes during cosmic expansion according to the tracking solution, but the fraction Ω_ϕ grows. At some point the quintessence density becomes comparable to the dark matter density and then leads to the onset of a dark energy dominated epoch of accelerated expansion. This cross-over occurs when the field value is of the order of the Planck scale. Therefore, it happens in the *present* epoch if $V(M_{pl}) \sim M_{pl}^2 H_0^2$. Thus, the pre-factor $c \equiv \Lambda^{4+\alpha}$ of the inverse power law potential has to have the order of magnitude

$$\Lambda = \mathcal{O}\left(\left(\frac{H_0}{M_{pl}}\right)^{\frac{2}{4+\alpha}} M_{pl}\right) = \mathcal{O}\left(10^{-\frac{122}{4+\alpha}} M_{pl}\right).$$

For example, $\Lambda \sim 10\,\mathrm{keV}$ for $\alpha = 1$. The smaller the inverse power law index α, the more shallow is the potential. Since the field rolls more slowly in shallow potentials, its equation of state today is the more negative the smaller the inverse power law index. A conservative upper bound $\omega_\phi < -0.7$ on the dark energy equation inferred from SN1a and CMB measurements leads to an upper bound $\alpha \lesssim 2$ for the inverse power law index [84].

Self-adjusting mass

For tracking solutions, not only the potential energy of the quintessence field decreases with time, but also the effective time-dependent mass $m_\phi^2(t) \equiv V''(\phi(t))$ of the quintessence field, which is given

by the second derivative of the potential, approaches zero for $t \to \infty$. For the tracking solution, it is explicitly given by [169]

$$m_\phi^2(t) = V''(\phi^*(t)) = \frac{9}{2}\Gamma\left(1 - \omega_\phi^{*2}\right) H(t)^2 . \tag{2.13}$$

Thus, for tracker quintessence potentials, the classical dynamics drive the mass of the quintessence field towards a value which is of the order of the Hubble parameter. It is emphasized that, on the classical level, this is a self-adjusting mechanism for the mass, since, even if one starts with a different value, the mass converges towards the value given above since the tracking solution is an attractor solution. A mass of the order of the Hubble scale, which corresponds to the inverse size of the horizon, is also desirable for stability reasons, since it inhibits the growth of inhomogeneities in the quintessence field [157].

Possible origins of tracker potentials

Exponential and inverse power law potentials are very unusual from the point of view of high energy physics. Nevertheless, some attempts have been made to obtain such potentials from a superior theory. In Ref. [34] it was proposed that the quintessence field can be interpreted as a fermion condensate in a strongly interacting supersymmetric gauge theory, whose dynamics may, under certain assumptions, be describable by an inverse power law potential. An extension of the upper scenario to supergravity discussed in Ref. [42] leads to the so-called SUGRA-potential. Exponential potentials may occur in the low-energy limit of extradimensional theories [165] or could result from the anomalous breaking of dilatation symmetry [182]. In any case, the quintessence field is an effective degree of freedom, described by an effective theory which is valid below an ultraviolet embedding scale. The aim of the present work is to investigate the robustness of tracker potentials under quantum corrections in a model-independent way, which includes a wide range of possibilities for the unknown underlying UV completion.

2.3 Interacting Quintessence

Interactions between the rolling quintessence field and Standard Model fields lead to striking phenomenological consequences [157, 172, 184], which can be tested experimentally in many ways. In general, interactions of the quintessence field are expected if it is embedded in an effective field theory framework [51]. For a neutral scalar field, there are plenty of possibilities for couplings between quintessence and Standard Model fields [11, 15, 36, 44, 46, 56, 64, 83, 87, 95, 137, 145, 183, 184, 186]. For tracker quintessence potentials, it is plausible that also the couplings may have a non-trivial dependence on the quintessence field. The effects described below are generic for quintessence models, and are treated as model-independent as possible.
In principle, one can discriminate between direct effects of the quintessence coupling on the properties of the Standard Model particles, and indirect backreaction effects of the Standard Model fields on the quintessence dynamics [96]. The quantum vacuum contribution of the latter is discussed in section 4.2. Here, the most prominent direct effects are briefly mentioned.

Apparent violations of the equivalence principle: Yukawa-type couplings between the quintessence field and fermion fields ψ_i may be parameterized as [157]

$$\mathcal{L}_{\text{Yuk}} = -\sum_i F_i(\phi)\, \bar{\psi}_i \psi_i . \tag{2.14}$$

Each function $F_i(\phi)$ gives a ϕ-dependent contribution to the mass (m_i) of each fermion species. Since the field value $\phi(t)$ changes during cosmic evolution, the fermion masses are also time-varying on cosmological time-scales. Actually, this is a very typical feature of quintessence models. Of course, the time-variation of the fermion mass is supposed to be tiny in comparison to the total mass.
The fermions ψ_i do not need to be fundamental fermions but should be understood as effective fields, e.g. describing neutrons or protons, with effective Yukawa couplings $F_i(\phi)$. In this case, the ϕ-dependence of the nucleon masses could also be mediated by a ϕ-dependence of the QCD scale, that could for example result from a ϕ-dependent unified gauge coupling in some GUT theory [184].
The Yukawa couplings (2.14) mediate a long-range interaction by coherent scalar-boson exchange between the fermions [157]. This interaction can be described by a Yukawa potential between two fermions of type i and j of spatial distance r

$$U_{\text{Yukawa}}(r) = -y_i y_j \frac{e^{-m_\phi r}}{r}, \tag{2.15}$$

with couplings $y_i \equiv dF_i/d\phi$ and the dynamical quintessence mass $m_\phi^2 = V''(\phi)$. As m_ϕ is typically of the order H, inside the horizon ($m_\phi r \ll 1$) this interaction is a long-range interaction like gravity. Therefore, it can be seen as a correction to the Newtonian potential,

$$U(r) = -G m_i m_j \frac{1}{r}\left(1 + 8\pi M_{pl}^2 \frac{y_i}{m_i}\frac{y_j}{m_j}\right), \tag{2.16}$$

where the first term in the brackets represents the Newtonian contribution and the second term the quintessence contribution for an interaction of species i with j. One consequence of the species dependence is a violation of the equivalence principle. This turns out to put the most stringent bound on the couplings y_i. The acceleration of different materials towards the sun has been shown to be the same up to one part in 10^{10} [157] from which a bound for the Yukawa couplings of neutrons and protons can be derived[9] [157]:

$$y_n, y_p \lesssim 10^{-24}. \tag{2.17}$$

This means a coupling of quintessence to baryonic matter has to be highly suppressed. In other words, the strength of the interaction for baryonic matter is of the order $y_n^2/m_n^2 \sim y_p^2/m_p^2 \sim (10^{24}\text{GeV})^{-2}$ and thus 10 orders of magnitude weaker than the gravitational coupling $G \sim (10^{19}\text{GeV})^{-2}$.

Time-variation of masses and couplings: Not only the fermion masses, but basically *all* "constants" in the Standard model (and beyond) could depend on the quintessence field[10]. A time-variation of fundamental gauge couplings can be induced by the term

$$\mathcal{L}_{\text{Gauge}} = \frac{1}{2} Z(\phi)\text{Tr}(\text{F}_{\mu\nu}\text{F}^{\mu\nu}),$$

where $F_{\mu\nu}$ is the field strength tensor of some gauge symmetry [184]. The time-dependent normalization can also be expressed by replacing the gauge coupling g according to $g^2 \to g^2/Z(\phi)$ which leads to a time-dependent effective coupling. For the photon field, this leads to a time-varying fine-structure "constant" α_{em}. Actually, a detection of such a variation could be considered as a possible signal for quintessence [82]. Furthermore, a variation in the strong coupling (and thereby the QCD scale) could

[9] Numerically, this bound corresponds to $M_{pl}^2 y^2/m^2 < 10^{-10}$ where m is the nucleon mass.

[10] The presence of the non-constant field ϕ will also alter the classical conservation laws since it is possible that e.g. energy and momentum is exchanged with the quintessence field. However, the *total* energy and momentum are still conserved.

lead to varying masses of baryons. If the Standard Model is embedded in a GUT theory, it is even possible to relate the variation of the various gauge couplings, yielding interrelations between the variation of nucleon masses and the fine-structure constant [184]. Thus quintessence could predict a relation between the violation of the equivalence principle and the change of $\alpha_{\rm em}$.
The effect of changing fundamental constants can show up in many different ways, giving the possibility to extract experimental bounds (see [184]). Besides geonuclear bounds (Oklo, $|\Delta\alpha_{\rm em}(z\approx 0.13)|/\alpha_{\rm em} < 10^{-7}$) and astronuclear bounds (decay rates in meteorites, $|\Delta\alpha_{\rm em}(z\approx 0.45)|/\alpha_{\rm em} < 3\cdot 10^{-7}$), there are measurements from the observation of absorption lines in Quasars (typically $\Delta\alpha_{\rm em}(z\approx 2)/\alpha_{\rm em}\sim -7\cdot 10^{-6}$ with errors of the same order [168, 176]). Furthermore, Big Bang Nucleosynthesis (BBN) constrains $|\Delta\Lambda_{\rm QCD}(z\approx 10^{10})|/\Lambda_{\rm QCD} < 10^{-2}$ and $|\Delta\alpha_{\rm em}(z\approx 10^{10})|/\alpha_{\rm em} < 10^{-2}(10^{-4})$ where the latter bound applies if a GUT-motivated relation between $\alpha_{\rm em}$ and $\Lambda_{\rm QCD}$ is used [50, 75, 118, 172]. Possible time variations of the electron to proton mass ratio are investigated in Refs. [119, 158]. The experimental bounds imply that the functions $Z(\phi)$ and $F_i(\phi)$ may only vary *slightly* while ϕ changes of the order M_{pl} or more during a Hubble time.

Time-variation of the effective Newton constant: Non-minimal gravitational couplings of the quintessence field lead to modifications of Einstein gravity [52, 55, 73, 94, 155, 171]. A non-minimal coupling which is linear in the curvature scalar can be understood as an additional contribution to the Newton constant in the Einstein-Hilbert action,

$$\int d^4x\sqrt{-g}\left(-\frac{R}{16\pi G}-f(\phi)R+\ldots\right)\equiv\int d^4x\sqrt{-g}\left(-\frac{R}{16\pi G_{\mathit{eff}}}+\ldots\right),$$

where

$$\frac{1}{16\pi G_{\mathit{eff}}}=\frac{1}{16\pi G}+f(\phi)\,.$$

Hereby G_{eff} is an effective Newton constant which appears in the gravitational force law for systems which are small compared to the time- and space-scales on which $\phi(x)$ varies, analogically to Brans-Dicke scalar-tensor theories [41]. For a scalar field with time-dependent field value, a non-minimal coupling which is linear in R thus leads to a time-variation of the effective Newton constant over cosmological time-scales. Of course, a variation in the strength of gravity is highly restricted by experiments [155, 181]. Laboratory and solar system experiments testing a time variation of G restrict today's value to $\left|\dot{G}_{\rm eff}/G_{\rm eff}\right|_{\rm today}\ \leq\ 10^{-11}{\rm yr}^{-1}$ and an independent constraint from effects induced on photon trajectories gives $\left|f'^2/(f-1/16\pi G)\right|_{\rm today}\leq 1/500$. The requirement that the expansion time-scale H^{-1} during BBN may not deviate by more than 10% from the standard value means that the value of the gravitational constant during BBN may not have differed by more than 20% from today's value [181]. This can be rewritten in the form

$$\left|\frac{(G_{\rm eff})_{\rm BBN}-(G_{\rm eff})_{\rm today}}{(G_{\rm eff})_{\rm today}}\right|\leq 0.2\,.$$

Chapter 3

Quantum Effective Action

The effective action contains the complete information about a quantum theory. In this chapter, approximation techniques for the effective action of a scalar quantum field in Minkowski space-time are reviewed, which is described by the classical action

$$S[\phi] = \int d^4x \left(\frac{1}{2}(\partial\phi)^2 - V_{cl}(\phi) \right) . \tag{3.1}$$

The extension to curved space-time and the calculation of the contribution to the effective action from couplings between the scalar field and heavier degrees of freedom is discussed in appendix B.
The quantum field operator $\Phi(x)$ and its conjugate $\partial_{x^0}\Phi(x)$ obey equal-time commutation relations (units where $\hbar = 1$ are used hereafter),

$$\begin{aligned} [\Phi(x^0,\boldsymbol{x}),\Phi(x^0,\boldsymbol{y})]_- &= 0\,, \\ [\Phi(x^0,\boldsymbol{x}),\partial_{x^0}\Phi(x^0,\boldsymbol{y})]_- &= i\hbar\,\delta^{(3)}(\boldsymbol{x}-\boldsymbol{y})\,, \\ [\partial_{x^0}\Phi(x^0,\boldsymbol{x}),\partial_{x^0}\Phi(x^0,\boldsymbol{y})]_- &= 0\,. \end{aligned} \tag{3.2}$$

A statistical ensemble of physical states in the Hilbert space belonging to the real scalar quantum field theory can be described by a density matrix ρ. In any orthonormal basis $\{|n\rangle\}$ of the Hilbert space, the density matrix

$$\rho = \sum_n p_n |n\rangle\langle n| \tag{3.3}$$

describes a statistical ensemble in which the state $|n\rangle$ can be found with probability p_n. The expectation value of an observable described by the operator $\mathcal{O}$ is given by

$$\langle\mathcal{O}\rangle = \mathrm{Tr}\,(\rho\,\mathcal{O})\,. \tag{3.4}$$

Total conservation of probability implies that $\mathrm{Tr}\,\rho = 1$. Since $0 \le p_n \le 1$, it follows that $\mathrm{Tr}\,\rho^2 \le 1$. If $\mathrm{Tr}\,\rho^2 = 1$, the ensemble can be described by a pure state[1] $|\psi\rangle$ with density matrix $\rho = |\psi\rangle\langle\psi|$. An example for the latter case is an ensemble in the vacuum state $|0\rangle$,

$$\rho = |0\rangle\langle 0|\,. \tag{3.5}$$

The vacuum state is defined as the eigenstate of the Hamiltonian

$$H(x^0) = \int d^3x \left(\frac{1}{2}(\dot\Phi(x))^2 + \frac{1}{2}(\nabla\Phi(x))^2 + V_{cl}(\Phi(x)) \right) \tag{3.6}$$

[1] This can easily be seen by choosing a basis of the Hilbert space which contains the state $|\psi\rangle$.

with lowest energy. For any external classical source $J(x)$ coupled to the quantum field $\Phi(x)$ the state $|0\rangle_J$ is defined as the eigenstate of the Hamiltonian

$$H_J(x^0) = \int d^3x \left(\frac{1}{2}(\dot{\Phi}(x))^2 + \frac{1}{2}(\nabla\Phi(x))^2 + V_{cl}(\Phi(x)) - J(x)\Phi(x) \right) \tag{3.7}$$

with lowest energy. The density matrix of a canonical ensemble in thermal equilibrium[2] at temperature T is known explicitly,

$$\rho = \frac{1}{Z} \exp(-\beta H) , \tag{3.8}$$

where[3] $\beta = 1/(kT)$ and $Z^{-1} = \mathrm{Tr} \exp(-\beta H)$. The vacuum ensemble is obtained from the thermal ensemble in the limit $T \to 0$. Any density matrix which can not be written in the form of eq. (3.5) or eq. (3.8) characterizes a nonequilibrium ensemble. The computation of the effective action for ensembles which are characterized by a Gaussian density matrix at some initial time $t_{init} = 0$ is treated in appendix D, and the generalization to arbitrary density matrices with initial non-Gaussian correlations can be found in section 7.1.

3.1 1PI Effective Action

In this section, the effective action for ensembles described by the density matrix

$$\rho = |0\rangle_{J\,J}\langle 0| , \tag{3.9}$$

including the vacuum state for vanishing external source $J(x) = 0$, is treated. The expectation value of the field operator $\Phi(x)$ in the presence of the external classical source $J(x)$,

$$\phi(x) \equiv \mathrm{Tr}(\rho\,\Phi(x)) = \frac{\delta W[J]}{\delta J(x)} , \tag{3.10}$$

can be obtained from the derivative of the generating functional $W[J]$ for connected correlation functions, which is given by the path integral [180]

$$\exp\left(iW[J]\right) = \int \mathcal{D}\varphi \exp\left(iS[\varphi] + i\int d^4x J(x)\varphi(x) \right) . \tag{3.11}$$

The effective action $\Gamma[\phi]$ is the Legendre transform of $W[J]$,

$$\Gamma[\phi] = W[J] - \int d^4x J(x)\phi(x) , \tag{3.12}$$

where the dependence on J is expressed by a dependence on ϕ using relation (3.10). By construction, the equation of motion determining the field expectation value $\phi(x)$ including all quantum corrections for vanishing external source is obtained from the stationary point of the effective action,

$$\frac{\delta\Gamma[\phi]}{\delta\phi(x)} = 0 . \tag{3.13}$$

[2] When considering a quantum field theory with conserved global charges, there is an additional contribution from the corresponding chemical potentials in the equilibrium density matrix. For the real scalar quantum field, there are no symmetries which could lead to conserved charges, and thus the chemical potential vanishes in thermal equilibrium.

[3] In the following, units where $k = 1$ are used.

The effective action can be calculated using its expansion in terms of "one-particle-irreducible" (1PI) Feynman diagrams [122],

$$\begin{aligned}\Gamma[\phi] &= S[\phi]+\frac{i}{2}\mathrm{Tr}\ln\mathcal{G}_0^{-1}+\Gamma_1[\phi]\,, \qquad (3.14)\\ i\Gamma_1[\phi] &= \quad + \quad + \ \ldots \\ &= \frac{1}{8}\int d^4x[-iV_{cl}^{(4)}(\phi(x))]\mathcal{G}_0(x,x)^2+\frac{1}{12}\int d^4x\int d^4y[-iV_{cl}'''(\phi(x))]\mathcal{G}_0(x,y)^3[-iV_{cl}'''(\phi(y))]\\ &\quad +\ldots .\end{aligned}$$

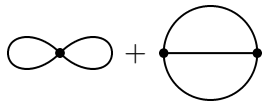

The functional $i\Gamma_1[\phi]$ is equal to the sum of all 1PI Feynman diagrams [122] without external lines. A Feynman diagram is "one-particle-reducible" (1PR) if it can be separated into two disconnected parts by cutting one of its internal lines. Conversely, a Feynman diagram is 1PI if it is not 1PR. The lines of the 1PI Feynman diagrams represent the classical, field-dependent propagator

$$\mathcal{G}_0^{-1}(x,y)=\frac{-i\delta^2 S[\phi]}{\delta\phi(x)\delta\phi(y)}=i(\Box_x+V_{cl}''(\phi(x)))\delta^4(x-y)\,, \qquad (3.15)$$

and the field-dependent interaction vertices are given by the third and higher derivatives of the classical action,

$$\begin{aligned}\frac{i\delta^3 S[\phi]}{\delta\phi(x_1)\ldots\delta\phi(x_3)} &= -iV_{cl}'''(\phi(x_1))\delta^4(x_1-x_2)\delta^4(x_2-x_3)\,,\\ \frac{i\delta^4 S[\phi]}{\delta\phi(x_1)\ldots\delta\phi(x_4)} &= -iV_{cl}^{(4)}(\phi(x_1))\delta^4(x_1-x_2)\delta^4(x_2-x_3)\delta^4(x_3-x_4)\,,\end{aligned} \qquad (3.16)$$

and so on.
Each 1PI Feynman diagram contributing to the loop expansion of the effective action formulated in terms of the field-dependent classical propagator $\mathcal{G}_0(x,y)$ and the field-dependent classical vertices (3.16) resums an infinite set of Feynman diagrams which are being composed of the free field-independent propagator

$$G_0^{-1}(x,y)=i(\Box_x+V_{cl}''(0))\delta^4(x-y)\,,$$

and the field-independent vertices which are given by the derivatives $i\delta^k S[\phi]/\delta\phi^k|_{\phi=0}$ ($k\geq 3$) of the classical action evaluated at $\phi=0$, and an arbitrary number of external lines given by the field value $\phi(x)$. This infinite resummation can be recovered from each 1PI Feynman diagram by replacing the classical propagator $\mathcal{G}_0(x,y)$ by its Schwinger-Dyson expansion around the free propagator $G_0(x,y)$,

$$\begin{aligned}\mathcal{G}_0(x,y) &= G_0(x,y)+\int d^4v\, G_0(x,v)[-iV_{cl}''(\phi(v))-iV_{cl}''(0)]\mathcal{G}_0(v,y)\\ &= G_0(x,y)+\int d^4v\, G_0(x,v)[-iV_{cl}''(\phi(v))-iV_{cl}''(0)]G_0(v,y)\ +\\ &\quad +\int d^4v\int d^4u\, G_0(x,v)[-iV_{cl}''(\phi(v))-iV_{cl}''(0)]G_0(v,u)[-iV_{cl}''(\phi(u))-iV_{cl}''(0)]G_0(u,y)\\ &\quad +\ \ldots\,,\end{aligned}$$

and performing a Taylor expansion with respect to the field value ϕ around $\phi=0$,

$$V_{cl}''(\phi(x))=V_{cl}''(0)+V_{cl}'''(0)\phi(x)+\frac{1}{2}V_{cl}^{(4)}(0)\phi(x)^2+\ldots\,, \qquad (3.17)$$

as well as inserting a similar Taylor expansion of the higher derivatives of the classical potential into the classical field-dependent vertices (3.16). In general, the effective action can equivalently be expanded in terms of Feynman diagrams involving the classical propagator and in terms of Feynman diagrams involving the free propagator. The former possibility has the advantage that only a finite number of Feynman diagrams contributes to the effective action at each loop order, since no infinite resummation of external lines is required as in the latter case [122]. Furthermore, the 1PI resummed loop expansion in terms of the classical propagator has a larger range of applicability. In the case of spontaneous symmetry breaking, for example, the free propagator is formally ill-defined since $V''_{cl}(0) < 0$. This is due to an unsuitable choice of the expansion point (here $\phi = 0$) in the field. In contrast to that, the 1PI resummed loop expansion does not require a Taylor expansion in the field and is therefore manifestly independent of the expansion point. It is well-defined for all field values ϕ where $V''_{cl}(\phi) > 0$, and is therefore applicable to theories with spontaneous symmetry breaking [122]. Alternatively to the expansion in 1PI Feynman diagrams, the effective action can be expanded in powers of space-time derivatives of the field $\phi(x)$,

$$\Gamma[\phi] = \int d^4x \left(-V_{\mathit{eff}}(\phi) + \frac{Z(\phi)}{2}(\partial\phi)^2 + \dots \right) . \tag{3.18}$$

The lowest order of the derivative expansion is called effective potential. The next Lorentz-invariant order contains two derivatives. Both expansions may be combined to obtain an expansion of the effective potential in terms of 1PI Feynman diagrams,

$$\begin{aligned} V_{\mathit{eff}}(\phi) &= V_{cl}(\phi) + \frac{1}{2}\int \frac{d^4k}{(2\pi)^4} \ln\left(\frac{k^2 + V''_{cl}(\phi)}{k^2}\right) + V_1(\phi) , \\ -V_1(\phi) &= \quad + \quad + \dots \\ &= \frac{1}{8}\left[-V^{(4)}_{cl}(\phi)\right]\left[\int \frac{d^4k}{(2\pi)^4}\frac{1}{k^2 + V''_{cl}(\phi)}\right]^2 \\ &\quad + \frac{1}{12}\left[-V'''_{cl}(\phi)\right]^2 \int \frac{d^4k}{(2\pi)^4}\int \frac{d^4q}{(2\pi)^4} \frac{1}{(k^2 + V''_{cl})(q^2 + V''_{cl})((q+k)^2 + V''_{cl})} \\ &\quad + \dots , \end{aligned}$$

formulated in Euclidean momentum space using the Euclidean classical propagator

$$\mathcal{G}_0^{-1}(k) = k^2 + V''_{cl}(\phi) .$$

The momentum integral over $\ln((k^2 + V''_{cl}(\phi))/k^2)$ in the first line is obtained from the one-loop contribution $i/2\mathrm{Tr}\ln\mathcal{G}_0^{-1}$ to the effective action, see eq. (3.14), up to a field-independent constant. The Feynman diagrams are obtained from the Feynman rules given above transferred to Euclidean momentum space, i.e. with lines representing the field-dependent classical propagator $\mathcal{G}_0(k)$ and field-dependent classical vertices given by $-V^{(k)}_{cl}(\phi)$ ($k \geq 3$).

The integrals over the loop momenta contain ultraviolet (UV) divergences. Therefore, it is either necessary to remove these divergences by a suitable renormalization of the parameters appearing in the classical action, which is, for a given fixed UV regulator, possible for the renormalizable classical potential

$$V_{cl}(\phi) = V_0 + \mu^3\phi + \frac{1}{2}m^2\phi^2 + \frac{1}{3!}g\phi^3 + \frac{1}{4!}\lambda\phi^4 , \tag{3.19}$$

or to embed the quantum theory at a physical UV scale and treat it as an effective field theory. In the latter case, the loop momenta are confined to be below the UV scale since the theory is only valid up to this scale, such that there are no UV divergences. Instead, the result explicitly depends on the energy scale of the UV embedding.

3.2 2PI Effective Action

The 2PI effective action is a straightforward generalization of the expansion of the effective action in terms of 1PI Feynman diagrams. It can be derived from the generating functional $W[J,K]$ including local and bilocal external classical sources $J(x)$ and $K(x,y)$,

$$\exp\Big(iW[J,K]\Big) = \int \mathcal{D}\varphi \exp\left(iS[\varphi] + iJ\varphi + \frac{i}{2}\varphi K\varphi\right), \tag{3.20}$$

with the short-hand notation

$$J\varphi = \int d^4x J(x)\varphi(x), \quad \varphi K\varphi = \int d^4x \int d^4y\, \varphi(x)K(x,y)\varphi(y). \tag{3.21}$$

The field expectation value and the connected two-point correlation function ("full propagator") in the presence of the sources $J(x)$ and $K(x,y)$ can be obtained from the derivatives of the generating functional $W[J,K]$,

$$\begin{aligned} \phi(x) &\equiv \mathrm{Tr}(\rho\,\Phi(x)) = \frac{\delta W[J,K]}{\delta J(x)}, \\ G(x,y) &\equiv \mathrm{Tr}\left(\rho\,(\Phi(x)-\phi(x)(\Phi(y)-\phi(y)\right) = \frac{2\delta W[J,K]}{\delta K(y,x)} - \phi(x)\phi(y). \end{aligned} \tag{3.22}$$

The 2PI effective action is defined as the double Legendre transform of the generating functional,

$$\Gamma[\phi,G] = W[J,K] - \int d^4x J(x)\phi(x) - \frac{1}{2}\int d^4x \int d^4y K(y,x)(G(x,y)+\phi(x)\phi(y)). \tag{3.23}$$

The equations of motion of the field expectation value $\phi(x)$ and the full propagator $G(x,y)$ are

$$\frac{\delta\Gamma[\phi,G]}{\delta\phi(x)} = -J(x) - \int d^4y K(x,y)\phi(y), \quad \frac{\delta\Gamma[\phi,G]}{\delta G(x,y)} = -\frac{1}{2}K(x,y). \tag{3.24}$$

For vanishing external sources the equations of motion including all quantum corrections are, by construction, given by the stationarity conditions of the 2PI effective action,

$$\frac{\delta\Gamma[\phi,G]}{\delta\phi(x)} = 0, \quad \frac{\delta\Gamma[\phi,G]}{\delta G(x,y)} = 0. \tag{3.25}$$

The 2PI effective action can be calculated using its expansion in terms of "two-particle-irreducible" (2PI) Feynman diagrams [66],

$$\Gamma[\phi,G] = S[\phi] + \frac{i}{2}\mathrm{Tr}\ln G^{-1} + \frac{i}{2}\mathrm{Tr}\left(\mathcal{G}_0^{-1}G\right) + \Gamma_2[\phi,G], \tag{3.26}$$

$i\Gamma_2[\phi,G]$ =

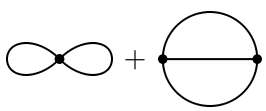

(3.27)

$$= \frac{1}{8}\int d^4x [-iV_{cl}^{(4)}(\phi(x))]G(x,x)^2 + \frac{1}{12}\int d^4x \int d^4x [-iV_{cl}'''(\phi(x))]G(x,y)^3[-iV_{cl}'''(\phi(y))] + \dots .$$

The functional $i\Gamma_2[\phi, G]$ is equal to the sum of all 2PI Feynman diagrams [66] without external lines. A Feynman diagram is "two-particle-reducible" (2PR) if it can be separated into two disconnected parts by cutting two of its internal lines. A Feynman diagram is 2PI if it is not 2PR. The field-dependent interaction vertices of the 2PI Feynman diagrams are given by the third and higher derivatives of the classical action as before, see eq. (3.16). However, in contrast to the 1PI effective action, the lines of the 2PI Feynman diagrams contributing to the 2PI effective action represent the *full* propagator $G(x,y)$.
Using the upper parameterization of the 2PI effective action, the equation of motion for the full propagator $G(x,y)$ is

$$\frac{\delta\Gamma[\phi,G]}{\delta G(y,x)} = 0 \quad \Leftrightarrow \quad G^{-1}(x,y) = \mathcal{G}_0^{-1}(x,y) - \frac{2i\delta\Gamma_2[\phi,G]}{\delta G(y,x)}\,. \tag{3.28}$$

This equation of motion can be written in the form of a self-consistent Schwinger-Dyson equation,

$$G^{-1}(x,y) = \mathcal{G}_0^{-1}(x,y) - \Pi(x,y)\,, \tag{3.29}$$

where the self-energy $\Pi(x,y)$ is obtained from opening one line of each 2PI Feynman diagram contributing to the 2PI functional $\Gamma_2[\phi,G]$,

$$\Pi(x,y) \equiv \frac{2i\delta\Gamma_2[\phi,G]}{\delta G(y,x)}\,. \tag{3.30}$$

In contrast to the perturbative Schwinger-Dyson equation, the self-energy contains Feynman diagrams with lines given by the *full* propagator $G(x,y)$ which appears also on the left hand side of the self-consistent Schwinger-Dyson equation. Therefore, the self-consistent Schwinger-Dyson is an implicit, i.e. nonperturbative, and in general non-linear equation for the propagator $G(x,y)$. In spite of these complications, the self-consistency of the 2PI formalism has some advantages which are indispensable when studying the time-evolution of quantum fields. For example, approximations based on a loop truncation of the 2PI effective action lead to evolution equations for the two-point function which are free of the secularity-problem (see appendix D) in contrast to approximations based on a loop truncation of the 1PI effective action, which break down at late times even for arbitrarily small values of the coupling constant. Thus, approximations based on a loop truncation of the 2PI effective action have a larger range of applicability than those based on a loop truncation of the 1PI effective action. This is similar to the difference between free perturbation theory and 1PI resummed perturbation theory discussed in the previous section.
For the exact theory, the 2PI effective action evaluated with the field-dependent solution $\bar{G}[\phi]$ of the self-consistent Schwinger-Dyson equation agrees with the 1PI effective action [66],

$$\Gamma[\phi,\bar{G}[\phi]] = \Gamma[\phi]. \tag{3.31}$$

Truncations of the 2PI effective action, for example up to a certain loop order, correspond to an infinite resummation of 1PI Feynman diagrams of all loop orders but with certain restrictions on their topology [37,66]. Assume the 2PI functional is truncated such that it contains just some finite or infinite subset of all 2PI diagrams, denoted by $i\Gamma_2^{trunc}[\phi,G]$. Then the propagator in this approximation is determined by solving the equation of motion

$$G^{-1}(x,y) = \mathcal{G}_0^{-1}(x,y) - \Pi^{trunc}(x,y;G)\,, \tag{3.32}$$

where the self-energy $\Pi^{trunc}(x,y;G)$ is derived from $i\Gamma_2^{trunc}[\phi,G]$, but still contains the propagator $G(x,y)$, i.e. the equation of motion is still a self-consistent equation [120]. The solution of this equation for a given ϕ, denoted by $\bar{G}[\phi]$, is therefore called the "full" propagator [120] (even though it is

not the *exact* propagator due to the truncation of $i\Gamma_2[\phi,G]$). An approximation to the exact effective action is obtained by inserting $\bar{G}[\phi]$ into the truncated 2PI effective action, $\Gamma^{appr}[\phi]=\Gamma^{trunc}[\phi,\bar{G}[\phi]]$. In principle, the same approximation can also be obtained via the perturbative expansion of the effective action in terms of 1PI Feynman diagrams containing the classical propagator. However, even if just one single Feynman diagram was kept in the 2PI functional $i\Gamma_2^{trunc}[\phi,G]$, it yields an approximation $\Gamma^{appr}[\phi]$ to the effective action which corresponds to a selective infinite series of perturbative 1PI Feynman diagrams [120] (see also appendix C.1). In the following the superscripts are omitted and truncations of the 2PI functional are also denoted by $i\Gamma_2[\phi,G]$.

3.3 nPI Effective Action

The nPI effective action is derived from the generating functional $W[J_1,\ldots,J_n]$ including external classical sources $J_k(x_1,\ldots,x_k)$ for $1\leq k\leq n$,

$$\exp\Big(iW[J_1,\ldots,J_n]\Big)=\int\mathcal{D}\varphi\,\exp\left(iS[\varphi]+i\sum_{k=1}^{n}\frac{1}{k!}J_{12\cdots k}\,\varphi_1\varphi_2\cdots\varphi_k\right), \tag{3.33}$$

with the short-hand notation

$$J_{12\cdots k}\,\varphi_1\varphi_2\cdots\varphi_k=\int d^4x_1\cdots\int d^4x_n\,J(x_1,\ldots,x_k)\,\varphi(x_1)\cdots\varphi(x_k)\,. \tag{3.34}$$

The nPI effective action is obtained by the multiple Legendre transform

$$\Gamma[\phi,G,V_3,\ldots,V_n]=W[J_1,\ldots,J_n]-\sum_{k=1}^{n}J_{12\cdots k}\frac{\delta W}{\delta J_{12\cdots k}}\,. \tag{3.35}$$

The equations of motion of the field expectation value $\phi(x)$, the full propagator $G(x,y)$ and the full connected vertex functions $V_k(x_1,\ldots,x_k)$ including all quantum corrections for vanishing external sources are, by construction, given by the stationarity conditions of the nPI effective action,

$$\frac{\delta\Gamma}{\delta\phi(x)}=0,\quad \frac{\delta\Gamma}{\delta G(x,y)}=0,\quad \frac{\delta\Gamma}{\delta V_{12\cdots k}}=0\,. \tag{3.36}$$

For the exact theory, all nPI effective actions with propagator and vertices evaluated at the stationary point agree with the 1PI effective action in the absence of sources,

$$\Gamma[\phi]=\Gamma[\phi,\bar{G}]=\Gamma[\phi,\bar{G},\bar{V}_3]=\ldots=\Gamma[\phi,G,\bar{V}_3,\ldots,\bar{V}_n]\,.$$

Loop approximations still obey an equivalence hierarchy for vanishing sources [26],

$$\begin{array}{ccccccccc}
\Gamma[\phi]_{1-loop} & = & \Gamma[\phi,\bar{G}]_{1-loop} & = & \Gamma[\phi,\bar{G},\bar{V}_3]_{1-loop} & = & \Gamma[\phi,G,\bar{V}_3,\bar{V}_4]_{1-loop} & = & \ldots\,,\\
 & & \Gamma[\phi,G]_{2-loop} & = & \Gamma[\phi,G,\bar{V}_3]_{2-loop} & = & \Gamma[\phi,G,\bar{V}_3,\bar{V}_4]_{2-loop} & = & \ldots\,,\\
 & & & & \Gamma[\phi,G,V_3]_{3-loop} & = & \Gamma[\phi,G,V_3,\bar{V}_4]_{3-loop} & = & \ldots\,.
\end{array}$$

4PI Effective Action

As an example, the 4PI effective action $\Gamma[G,V_4]=\Gamma[0,G,0,V_4]$ for a theory with Z_2-symmetry $\phi\to-\phi$ is considered. In this case, the connected two- and four-point functions are given by

$$G(x_1,x_2)=G_{12}=\frac{2\delta W[K,L]}{\delta K_{12}},\quad V_4(x_1,x_2,x_3,x_4)=\frac{4!\delta W[K,L]}{\delta L_{1234}}-G_{12}G_{34}-G_{13}G_{24}-G_{14}G_{23}\,,$$

in terms of the generating functional $W[K,L] = W[0,K,0,L]$. For $\lambda\Phi^4/4!$-theory, the three-loop approximation of the 4PI effective action reads [27]

$$\Gamma[G,V_4] = \frac{i}{2}\mathrm{Tr}\ln G^{-1} + \frac{i}{2}\mathrm{Tr}\left(\mathcal{G}_0^{-1}G\right) + \Gamma_2[G,V_4], \tag{3.37}$$

$i\Gamma_2[G,V_4]$ =

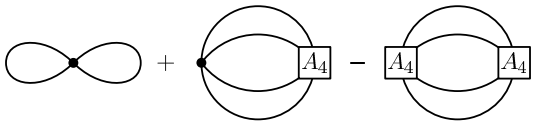

$$\begin{aligned} &= \frac{1}{8}\int d^4x\,[-i\lambda]G(x,x)^2 \\ &\quad + \frac{1}{24}\int d^4x_{1234}\int d^4y\,[iA_4(x_1,x_2,x_3,x_4)]G(x_1,y)G(x_2,y)G(x_3,y)G(x_4,y)[-i\lambda] \\ &\quad - \frac{1}{48}\int d^4x_{1234}\int d^4y_{1234}\,[iA_4(x_1,x_2,x_3,x_4)]G(x_1,y_1)G(x_2,y_2)\times \\ &\qquad\qquad \times G(x_3,y_3)G(x_4,y_4)[iA_4(y_1,y_2,y_3,y_4)]\,, \end{aligned} \tag{3.38}$$

where a compact notation $d^4x_{1234} = d^4x_1\cdots d^4x_4$ is used, and the kernel A_4 is defined via

$$V_4(x_1,x_2,x_3,x_4) = \int d^4y_{1234}\,G(x_1,y_1)G(x_2,y_2)G(x_3,y_3)G(x_4,y_4)[iA_4(y_1,y_2,y_3,y_4)]\,.$$

The equation of motion for V_4 in the absence of sources is obtained from the stationarity condition,

$$\frac{\delta\Gamma[G,V_4]}{\delta V_4} = 0 \quad \Leftrightarrow \quad iA_4(x_1,x_2,x_3,x_4) = -i\lambda\,\delta^4(x_1-x_2)\delta^4(x_1-x_3)\delta^4(x_1-x_4)\,.$$

Thus, the full 4-point function $\bar{V}_4(x_1,x_2,x_3,x_4)$ is, in this approximation, given by the classical vertex with four full propagators attached to it. Inserting the 4-point kernel into the 4PI effective action yields the corresponding approximation of the 2PI effective action,

$$i\Gamma_2[G] = i\Gamma_2[G,\bar{V}_4] = \frac{1}{8}\int d^4x\,[-i\lambda]G(x,x)^2 + \frac{1}{48}\int d^4x\int d^4y\,[-i\lambda]G(x,y)^4[-i\lambda]\,.$$

This is precisely the three-loop approximation of the 2PI effective action $\Gamma[G] = \Gamma[\phi=0,G]$, i.e.

$$\Gamma[G]_{3-loop} = \Gamma[G,\bar{V}_4]_{3-loop}\,,$$

for vanishing sources. According to the equivalence hierarchy, one would expect that only the nPI effective actions for $n \geq 3$ coincide at three-loop level. However, due to the Z_2-symmetry all correlation functions involving an odd number of fields vanish, such that 2PI and 3PI also coincide, and therefore also 2PI and 4PI.

Chapter 4

Quantum Corrections in Quintessence Models

Quintessence models admitting tracking solutions [169] feature attractors in phase-space which wipe out the dependence on the initial conditions of the field in the early universe, as discussed in chapter 2. Furthermore, tracking solutions exhibit a dynamical self-adjusting mechanism yielding an extremely small time-evolving classical mass $m_\phi(t) \sim H(t)$ of the quintessence field of the order of the Hubble parameter. The smallness of $m_\phi(t)$ inhibits the growth of inhomogeneities of the scalar field [157] and makes quintessence a viable dark energy candidate. In this context, it is an important question whether the self-adjusting mechanism for the classical mass and its smallness are robust under quantum corrections [22, 43, 83, 102, 132, 152, 159, 171]. The long-standing "cosmological constant problem" can be reformulated as the problem to determine the overall normalization of the effective quintessence potential. Apart from that, quantum corrections can influence the dynamics by distorting the *shape* or the *flatness* (i.e. the derivatives) of the scalar potential $V_{cl}(\phi) \to V_{eff}(\phi)$. Additionally, quantum corrections can induce non-minimal gravitational couplings between the field ϕ and the curvature scalar R, or a non-standard kinetic term.

Note that the fundamental "cosmological constant problem" of quantum field theory is not addressed in this work. Since quantum field theory together with classical gravity determines the effective potential only up to a constant, it will always be assumed here that the freedom to shift the potential by an arbitrary constant, $V_{eff}(\phi) \to V_{eff}(\phi) + \text{const}$, is used in such a way that it yields the observed value for dark energy in the present cosmological epoch. However, as mentioned above, even with this assumption there remain quantum corrections to the dynamics of the quintessence field which can be addressed by quantum field theory. In this chapter, these impacts of quantum fluctuations on the dynamics of a light quintessence field from three different sources are investigated. These sources are self-couplings, couplings to Standard Model particles and couplings to gravity.

In section 4.1, quantum corrections to the shape of the scalar potential originating from the quintessence self-couplings are investigated in the framework of effective field theory. In this framework, it is assumed that the quintessence field arises from a high-energy theory, which is governed by a UV-scale of the order of the GUT or Planck scales. This is possible, since the self-couplings of the dark energy field, although typically non-renormalizable, are Planck-suppressed in tracking quintessence models [9, 10, 34, 157, 169, 182]. Suitable approximations of the effective action are discussed, and previous studies [43, 83] are extended by identifying and resumming the relevant contributions, which explicitly depend on the UV-scale. For two exemplary classes of models the resulting effective potential is used to study their robustness.

In section 4.2, quantum corrections induced by couplings between the quintessence field and Stan-

dard Model particles are investigated. The low-energy effective action is studied, which contains the quintessence-field-dependent contributions of the Standard Model fields to the vacuum energy [20, 81]. Even under relatively conservative assumptions, these contributions dominate the effective potential unless the couplings are tiny [20,81]. Upper bounds on the couplings of a tracker quintessence field are quantified and translated into upper bounds for time-variations of Standard Model particle masses on cosmological time-scales caused by these couplings, as well as into upper bounds on the coupling strength to a long-range fifth force mediated by the quintessence field. These are linked to potentially observable effects like a variation of the electron to proton mass ratio [119, 158] over cosmological time-scales or tiny apparent violations of the equivalence principle [172, 184].
In section 4.3 it is investigated which kinds of non-minimal gravitational couplings are induced by quantum fluctuations of the dark energy scalar field. Gravitational couplings of the quintessence field are a crucial property of dark energy. The minimal gravitational coupling contained in the covariant derivative in the kinetic term of the quintessence action and the covariant integration measure are required due to general coordinate invariance. Non-minimal gravitational couplings between the rolling scalar field and the curvature scalar lead to a time-variation of the effective Newton constant over cosmological time-scales. This is constrained observationally by solar system tests of gravity and by Big Bang Nucleosynthesis [39, 52, 53, 55, 73, 94, 101, 155]. The non-minimal couplings which are generated radiatively for a tracker quintessence field in one-loop approximation are derived and compared to the observational bounds. Corrections to the kinetic term are also discussed in section 4.3.

4.1 Quantum Corrections from Self-Interactions

If the light scalar field responsible for dark energy has itself fluctuations described by quantum field theory, quantum corrections induced by its self-interactions do contribute to the quantum effective action. In this section, this contribution is investigated. Typical potentials used in the context of quintessence contain non-renormalizable self-couplings, involving e.g. exponentials of the field, $V_{cl}(\phi) = V_0 \exp\left(-\lambda\phi/M_{pl}\right)$ [9, 10, 34, 157, 169, 182]. These enter the effective action via the field-dependent vertices (see eq. (3.16))

$$-iV_{cl}^{(k)}(\phi) = -iV_{cl}(\phi)/M^k, \qquad M = M_{pl}/\lambda \sim M_{pl}\sqrt{\Omega_{de}/3}\,, \tag{4.1}$$

which are suppressed by a scale M between the GUT and the Planck scale. Such couplings could arise from an effective theory by integrating out some unknown high-energy degrees of freedom at an ultraviolet scale $\Lambda \sim \mathcal{O}(M)$. The effective field theory is only valid up to this physical embedding scale Λ, and the quantum effective action explicitly depends on the value of Λ. Ultraviolet divergent contributions to the effective action lead to marginal dependence $\propto \ln\Lambda$ (for logarithmic divergences) or relevant dependence $\propto \Lambda^n$ (e.g. $n = 2$ for quadratic divergences) on the embedding scale Λ. In the simplest case, Λ can be imagined as a cutoff for the momentum cycling in the loops of the Feynman diagrams.
It turns out that it is useful to keep track of the dependence on the suppression scale M of the vertices and the embedding scale Λ separately, although they are closely related in a way depending on the unknown underlying high-energy theory. Since the suppression scale M is of the order of the GUT or the Planck scale, the same is possibly true for Λ. Because unknown quantum gravity effects dominate above the Planck scale, an upper bound $\Lambda \lesssim M_{pl}$ is assumed. In order to establish a meaningful approximation, it is desirable to resum all relevant contributions proportional to powers of

$$\Lambda^2/M^2 \sim \mathcal{O}(1)\,,$$

whereas the tiny mass $m_\phi^2 \sim V''(\phi)$ of the quintessence field, which is typically of the order of the Hubble scale, admits a perturbative expansion in powers of

$$V''(\phi)/M^2 \sim V(\phi)/M^4 \lll 1\,.$$

In section 4.1.1 power counting rules for tracker potentials within effective field theory are derived and used to identify the dependence of Feynman diagrams on $V(\phi)$, M and Λ within this scheme. In section 4.1.2 an approximation to the effective action which resums the field-dependent relevant contributions at leading order in $V(\phi)/M^4$ is discussed. In section 4.1.3 the same approximation is applied to a quantum field theory in 1+1 space-time dimensions where the effective potential is known independently due to the symmetry properties of the theory, and it is demonstrated that the resummation introduced in section 4.1.2 yields concordant results. In section 4.1.4 the robustness of the prototype tracker potentials, namely the exponential and the inverse power-law potential, is studied.

4.1.1 Effective Field Theory for Tracker Potentials

An effective theory describes the dynamics of a system by reducing it to effective degrees of freedom with effective interactions, which are not fundamental, but only exist up to a certain energy scale Λ. Above this ultraviolet scale Λ of the effective theory, it has to be replaced by another (effective or fundamental) theory.
An example for an effective field theory is the Fermi model of β-decay [97], based on an effective point-like 4-fermion interaction between the electron, the neutrino, the neutron (down quark) and the proton (up quark). The interaction strength is given by the Fermi constant $G_F = 1.166 \cdot 10^{-5}\mathrm{GeV}^{-2}$. The non-renormalizable effective interaction has to be replaced by the electroweak W-boson exchange at the UV scale of the order $\Lambda \sim 1/\sqrt{G_F}$.
An example for a loop calculation within an effective field theory is provided by the Nambu–Jona-Lasinio model [149], which features a 4-fermion self-interaction which is invariant under the chiral transformation $\psi \to e^{i\alpha\gamma_5}\psi$,

$$\mathcal{L} = \overline{\psi} i\gamma^\mu \partial_\mu \psi + \frac{G}{4}\left[(\overline{\psi}\psi)^2 - (\overline{\psi}\gamma_5\psi)^2\right]\,.$$

Similar to the Fermi model, it is an effective field theory with UV scale $\Lambda \sim 1/\sqrt{G}$. If the interaction strength is stronger than a critical value, the chiral symmetry is broken dynamically, such that the vacuum expectation value $\langle\overline{\psi}\psi\rangle \equiv -2M/G$ is non-zero. The scale M of the dynamical chiral symmetry breaking is determined by a self-consistent Schwinger-Dyson equation (gap equation) which involves a one-loop "tadpole" Feynman integral. If the UV scale of the theory is implemented by a Lorentz invariant cutoff for the Euclidean loop momentum, the gap equation reads [149]

$$M = \underset{\cdot}{\bigcirc} = 2GM \int\limits_{k^2<\Lambda^2} \frac{d^4k}{(2\pi)^4}\frac{1}{k^2+M^2} = 2GM\,\frac{\Lambda^2}{16\pi^2} f_1(M^2/\Lambda^2)\,, \tag{4.2}$$

with $f_1(M^2/\Lambda^2) = 1 + \frac{M^2}{\Lambda^2}\ln\left(\frac{M^2}{\Lambda^2+M^2}\right)$, $f_1(0) = 1$. It has a non-zero solution M if $G > G_{crit} = 8\pi^2/\Lambda^2$.

Loop integrals in effective field theory

In order to resum the relevant contributions to the quantum effective action for the scalar field described by the action (3.1) with a tracker potential $V_{cl}(\phi)$, it is important to identify the dependence

on the embedding scale Λ. In analogy to the Nambu–Jona-Lasinio model, the embedding scale is assumed to cut off the ultraviolet divergences in the loop integrals. However, the form of this cut-off depends on the unknown degrees of freedom at the embedding scale. In general, this lack of knowledge can be captured by a form factor $F_\Lambda(k)$, which parameterizes the cutoff-function. For our purpose, it is not required to know this form factor in detail, but it is sufficient to know its asymptotic behaviour,

$$F_\Lambda(k) = \begin{cases} 1 & \text{for} \quad |k_\mu| \ll \Lambda, \\ 0 & \text{for} \quad |k_\mu| \gg \Lambda. \end{cases} \tag{4.3}$$

The form factor modifies the high-momentum contribution of the loop integrals, accomplished by modifying the integration measure[1]

$$d^4k \to d^4k F_\Lambda(k) \equiv d^4_\Lambda k\,.$$

A hard momentum cutoff in Euclidean momentum space corresponds to a form factor $F_\Lambda(k) = \theta(k^2 - \Lambda^2)$. As an illustrative example, the two-loop contributions to the effective action (see eq. (3.14)) are considered. The same parameterization of the quadratically divergent Feynman integral ("tadpole") is used as in eq. (4.2),

$$\int \frac{d^4_\Lambda k}{(2\pi)^4} \frac{1}{k^2+m^2} = \frac{\Lambda^2}{16\pi^2} f_1(m^2/\Lambda^2)\,, \tag{4.4}$$

where the shape of the dimensionless function $f_1(x)$ depends on the form factor, but, as above, is of order one for $m^2 \ll \Lambda^2$, i.e. $f_1(x) \sim \mathcal{O}(1)$ for $0 \le x \ll 1$. Similarly, the following quadratically divergent two-loop Feynman integral ("setting sun") is parameterized as

$$\int \frac{d^4_\Lambda k}{(2\pi)^4} \int \frac{d^4_\Lambda q}{(2\pi)^4} \frac{1}{(k^2+m^2)(q^2+m^2)((q+k)^2+m^2)} = \frac{\Lambda^2}{(16\pi^2)^2} f_2(m^2/\Lambda^2)\,,$$

where the dimensionless function $f_2(x)$ has been defined such that $f_2(x) \sim \mathcal{O}(1)$ for $0 \le x \ll 1$. With these definitions, the two-loop contributions to the effective action in the limit $m^2_\phi = V''_{cl}(\phi) \lll \Lambda^2$ can be evaluated,

$$\begin{aligned} &= \frac{1}{8} V^{(4)}_{cl}(\phi) \left[\int \frac{d^4_\Lambda k}{(2\pi)^4} \frac{1}{k^2 + V''_{cl}(\phi)} \right]^2 \\ &= \frac{1}{8} V^{(4)}_{cl}(\phi) \left[\frac{\Lambda^2}{16\pi^2} f_1(V''_{cl}/\Lambda^2) \right]^2 \approx \frac{1}{8} V^{(4)}_{cl}(\phi) \left[\frac{\Lambda^2}{16\pi^2} f_1(0) \right]^2 \\ &= V_{cl}(\phi) \cdot \left\{ \frac{\lambda^4}{8M^4_{pl}} \left[\frac{\Lambda^2}{16\pi^2} f_1(0) \right]^2 \right\} \quad \text{for } V_{cl}(\phi) = V_0 \exp(-\lambda\phi/M_{pl})\,, \end{aligned} \tag{4.5}$$

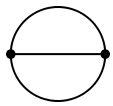

$$\begin{aligned} &= \frac{1}{12} \left[V'''_{cl}(\phi) \right]^2 \iint \frac{d^4_\Lambda k d^4_\Lambda q}{(2\pi)^8} \frac{1}{(k^2+V''_{cl})(q^2+V''_{cl})((q+k)^2+V''_{cl})} \\ &= \frac{1}{12} \left[V'''_{cl}(\phi) \right]^2 \frac{\Lambda^2}{(16\pi^2)^2} f_2(V''_{cl}/\Lambda^2) \approx \frac{1}{12} \left[V'''_{cl}(\phi) \right]^2 \frac{\Lambda^2}{(16\pi^2)^2} f_2(0) \\ &= V_{cl}(\phi) \cdot \underbrace{\frac{V_{cl}(\phi)}{M^4_{pl}}}_{10^{-120}} \cdot \left\{ \frac{\lambda^6}{12M^2_{pl}} \frac{\Lambda^2}{(16\pi^2)^2} f_2(0) \right\} \quad \text{for } V_{cl}(\phi) = V_0 \exp(-\lambda\phi/M_{pl})\,. \end{aligned} \tag{4.6}$$

[1] The most general form factor $F_\Lambda(k_1,\ldots,k_n)$ for overlapping loop integrals can depend on all loop momenta $k_1,\ldots,k_n$. Here, it is assumed for simplicity that $F_\Lambda(k_1,\ldots,k_n) = F_\Lambda(k_1)F_\Lambda(k_2)\cdots F_\Lambda(k_n)$. This choice is sufficient to identify the relevant contributions. The results below do not depend on this assumption.

As an example, the two diagrams are also evaluated for an exponential potential. First it can be observed that both are proportional to the classical potential $V_{cl}(\phi)$ in this case. Second, it is emphasized that the second diagram is suppressed with respect to the first one by a relative factor

$$V_{cl}(\phi)/M_{pl}^4 \approx \rho_\phi/M_{pl}^4 \approx 10^{-120}\,.$$

The value 10^{-120} applies for the present epoch. Even if the quintessence energy density was much larger in cosmic history, the ratio $\rho_\phi(t)/M_{pl}^4 \lll 1$ is a very small number[2]. It turns out that the suppression of the non-local diagram with two vertices with respect to the local diagram with one vertex is a result which can be generalized for tracker potentials.

Power counting rules for tracker potentials

In order to identify proper approximations for quintessence tracker potentials, it is necessary to estimate the orders of magnitude of the contributions to the effective action. Since these involve derivatives of the (classical) quintessence potential, it is desirable to set up a power counting rule giving an estimate of their order of magnitude.
For tracker quintessence potentials, it turns out that the scale height M yields such an estimate,

$$V_{cl}^{(k)}(\phi) \sim V_{cl}(\phi)/M^k\,. \tag{4.7}$$

It is an exact relation for exponential potentials, see eq. (4.1), where $V_{cl}(\phi)$ is of the order of the critical energy density $\sim M_{pl}^2H^2$ and M is between the GUT and the Planck scales. For inverse power law potentials, the scale height depends on the field value, $M \sim \phi$. However, during the present epoch, the field value is also of the order of the Planck scale.
By dimensional analysis, a 2PI Feynman diagram with $\mathcal{V}$ vertices and L loops can, within effective field theory, be estimated with the upper power counting rule. For example, an extension of the upper analysis leads to

$$\begin{aligned}
\text{Diagrams with } \mathcal{V}=1 \quad &\sim \quad V_{cl}(\phi)\cdot\left\{\Lambda^2/M^2\right\}^L\,,\\
\text{Diagrams with } \mathcal{V}=2 \quad &\sim \quad V_{cl}(\phi)\cdot\frac{V_{cl}(\phi)}{M^4}\cdot\left\{\Lambda^2/M^2\right\}^{L-1}\,.
\end{aligned}$$

In general, only the maximally divergent L-loop diagrams yield relevant contributions, which are not suppressed by powers of $V(\phi)/M_{pl}^4 \lll 1$ compared to the classical potential. These diagrams are precisely those which only involve "tadpole" integrals, i.e. those with one vertex. Apart from the "double bubble" diagram discussed above, all higher-dimensional operators suppressed by powers of M yield a "multi bubble" diagram with one vertex.
Motivated by the above estimate, it will be shown in the next section that, for tracker potentials, the leading quantum correction to the classical potential can be obtained in terms of 2PI Feynman diagrams with $\mathcal{V}=1$ but with arbitrarily high number of loops. The resummation of all diagrams with $\mathcal{V}=1$ is accomplished by a generalized Hartree-Fock approximation of the 2PI effective action.

4.1.2 Hartree-Fock Approximation

Within the framework of the 2PI effective action the Hartree-Fock approximation consists of a truncation of the 2PI functional $i\Gamma_2[\phi,G]$ containing all local 2PI Feynman diagrams [66]. In the context

[2] An upper bound $\rho_\phi < \rho_{max}$ for the energy density of the quintessence field is assumed, where ρ_{max} is the maximal energy density at the end of the inflation, $\rho_{max} \sim M_{pl}^2H_{inf}^2 \sim 10^{-8}M_{pl}^4(H_{inf}/10^{14}\text{GeV})^2$.

of $\lambda\Phi^4$-theory, there is only a single local 2PI Feynman diagram, the "double bubble" diagram which is the first contribution in eq. (3.28). In general, a 2PI Feynman diagram $\mathcal{F}$ contained in $i\Gamma_2[\phi,G]$ is "local" if its contribution to the 2PI self-energy $\Pi(x,y)$, see eq. (3.30), can be written in the form $2\delta\mathcal{F}/\delta G(x,y) = -i\Pi_{loc}(x)\delta^4(x-y)$, i.e. it is only supported at coincident space-time points. For a general scalar potential $V_{cl}(\phi)$ of interest here, there are infinitely many local 2PI Feynman diagrams, which are precisely given by all diagrams with one vertex ("multi-bubble" diagrams). The 2PI effective action in Hartree-Fock approximation is thus given by

$$i\Gamma_2[\phi,G] \;=\; \sum_{L=2}^{\infty}\frac{1}{2^L L!}\int d^4x\,(-iV_{cl}^{(2L)}(\phi(x)))G(x,x)^L\,, \tag{4.8}$$

where the $L=2$ contribution is the "double-bubble". The factor $1/2^L L!$ takes into account the correct symmetry factor for the "multi-bubble" contributions, which contain a $2L$-vertex.
The self-consistent Schwinger-Dyson equation for the full propagator $G(x,y)$ in Hartree-Fock approximation follows from the stationarity condition of the 2PI action, see eqs. (3.29,3.30),

$$\begin{aligned} G^{-1}(x,y) &= \mathcal{G}_0^{-1}(x,y) - \frac{2i\delta\Gamma_2[\phi,G]}{\delta G(y,x)} \\ &= i(\Box_x + V_{cl}''(\phi(x))\delta^4(x-y) \;-\; \sum_{L=2}^{\infty}\frac{L}{2^L L!}(-iV_{cl}^{(2L)}(\phi(x)))G(x,x)^{L-1}\delta^4(x-y)\,. \end{aligned} \tag{4.9}$$

Due to the locality of the self-energy, it is possible to make the Hartree-Fock ansatz

$$G^{-1}(x,y) = i(\Box_x + M_{\mathit{eff}}^2(x))\delta^4(x-y)\,, \tag{4.10}$$

for which the full propagator in Hartree-Fock approximation is parameterized by a local effective mass $M_{\mathit{eff}}(x)$. The upper self-consistent Schwinger-Dyson equation is indeed solved by a propagator of this form[3], which reduces to a self-consistent "gap equation" for the effective mass $M_{\mathit{eff}}^2(x)$,

$$M_{\mathit{eff}}^2(x) = V_{cl}''(\phi(x)) + \sum_{L=2}^{\infty}\frac{L}{2^L L!}V_{cl}^{(2L)}(\phi(x))G(x,x)^{L-1}\,.$$

This equation can equivalently be written in a compact form with an exponential derivative operator,

$$M_{\mathit{eff}}^2(x) = \exp\left[\frac{1}{2}G(x,x)\frac{d^2}{d\phi^2}\right]V_{cl}''(\phi(x))\,. \tag{4.11}$$

The gap-equation is still a self-consistent equation for $M_{\mathit{eff}}^2(x)$, since the effective mass enters also in the propagator $G(x,x)$ on the right-hand side. The effective potential is obtained from the effective mass in the limit of a space-time independent field value (see below). In this limit the effective mass is also space-time independent, and the self-consistency of the gap equation can explicitly be seen by switching to Euclidean momentum space,

$$M_{\mathit{eff}}^2 = \exp\left[\frac{1}{2}\left(\int\frac{d_\Lambda^4 k}{(2\pi)^4}\frac{1}{k^2+M_{\mathit{eff}}^2}\right)\frac{d^2}{d\phi^2}\right]V_{cl}''(\phi)\,.$$

[3]Note that this is due to the structure of the Hartree-Fock approximation. For truncations containing non-local diagrams, one indeed has to solve the equation in the complete $x-y$ plane if the self-consistency should not be sacrificed. This is important for nonequilibrium quantum fields discussed in chapter 6 and also for the renormalizability of general approximations based on the 2PI formalism, see appendix E.

In order to obtain the effective potential $V_{eff}(\phi)$ at some range of field values ϕ, the gap equation has to be solved for these values of ϕ. Since the solution depends on ϕ, it is denoted by $M_{eff}(\phi)$, and determined by the requirement

$$M^2_{eff}(\phi) = \exp\left[\frac{1}{2}\left(\int \frac{d^4_\Lambda k}{(2\pi)^4}\frac{1}{k^2+m^2}\right)\frac{d^2}{d\phi^2}\right] V''_{cl}(\phi)\Big|_{m^2=M^2_{eff}(\phi)} . \tag{4.12}$$

More generally, for a space-time dependent field $\phi(x)$, the solution of the gap equation (4.11) is a function of the space-time point x and a functional of the field $\phi(\cdot)$ which is denoted by $M_{eff}(x;\phi)$. It is determined by the requirement

$$M^2_{eff}(x;\phi) \;=\; \exp\left[\frac{1}{2}G(x,x)\frac{d^2}{d\phi^2}\right] V''_{cl}(\phi(x))\Big|_{G(x,x)=G\left(x,x;M^2_{eff}(\cdot;\phi)\right)} , \tag{4.13}$$

where, for any function $M^2(x)$, $G\left(x,y;M^2(\cdot)\right)$ is the solution of the equation

$$\left(\Box_x + M^2(x)\right) G\left(x,y;M^2(\cdot)\right) = -i\delta^4(x-y) .$$

The Hartree-Fock approximation to the effective action $\Gamma_{hf}[\phi]$ follows from inserting the field-dependent full propagator $\bar{G}[\phi](x,y) \equiv G\left(x,y;M^2_{eff}(\cdot;\phi)\right)$ determined by the solution $M^2_{eff}(x;\phi)$ of the gap equation into the 2PI effective action (see section 3.2, [66]). Up to a field-independent constant, the effective action is obtained from eqs. (4.8, 3.26, 4.10),

$$\begin{aligned}\Gamma_{hf}[\phi] \;&=\; \Gamma[\phi,\bar{G}[\phi]] \\ &=\; \int d^4x\left(\frac{1}{2}(\partial\phi)^2 - V_{hf}(\phi)\right) + \frac{i}{2}\mathrm{Tr}\left[\ln\left(\Box_x + M^2_{eff}(x;\phi)\right) - iM^2_{eff}(x;\phi)\bar{G}[\phi]\right] ,\end{aligned}$$

where

$$V_{hf}(\phi(x)) \equiv \exp\left[\frac{1}{2}\bar{G}(x,x;\phi)\frac{d^2}{d\phi^2}\right] V_{cl}(\phi(x)) . \tag{4.14}$$

The effective potential in Hartree-Fock approximation is the lowest order contribution to the derivative expansion of $\Gamma_{hf}[\phi]$,

$$V^{hf}_{eff}(\phi) = V_{hf}(\phi) + \frac{1}{2}\int \frac{d^4_\Lambda k}{(2\pi)^4}\left[\ln\left(\frac{k^2+M^2_{eff}(\phi)}{k^2}\right) - \frac{M^2_{eff}(\phi)}{k^2+M^2_{eff}(\phi)}\right] , \tag{4.15}$$

where $V_{hf}(\phi)$ can be written as

$$V_{hf}(\phi) \;=\; \exp\left[\frac{1}{2}\left(\int \frac{d^4_\Lambda k}{(2\pi)^4}\frac{1}{k^2+m^2}\right)\frac{d^2}{d\phi^2}\right] V_{cl}(\phi)\Big|_{m^2=M^2_{eff}(\phi)} \;=\; \overline{V}(\phi,m^2)\big|_{m^2=M^2_{eff}(\phi)} .$$

In order to simplify the notation, an auxiliary potential has been introduced,

$$\overline{V}(\phi,m^2) \equiv \exp\left[\frac{1}{2}\left(\int \frac{d^4_\Lambda k}{(2\pi)^4}\frac{1}{k^2+m^2}\right)\frac{d^2}{d\phi^2}\right] V_{cl}(\phi) , \tag{4.16}$$

which is obtained from applying the exponential derivative operator containing a propagator with an auxiliary mass m^2 to the classical potential $V_{cl}(\phi)$. The gap equation for $M^2_{eff}(\phi)$ can also be expressed via the auxiliary potential,

$$M^2_{eff}(\phi) \;=\; \frac{\partial^2\overline{V}(\phi,m^2)}{\partial\phi^2}\Big|_{m^2=M^2_{eff}(\phi)} . \tag{4.17}$$

Resummed perturbation theory

In order to check the validity of the Hartree-Fock approximation, it is necessary to have a formalism available which allows to estimate the corrections. Since the Hartree-Fock approximation is based on the intrinsically nonperturbative self-consistent gap equation derived from the 2PI effective action, the calculation of corrections to this approximation is not straightforward as in perturbation theory. Instead, the exact propagator has to be expanded around the self-consistently determined Hartree-Fock propagator, similar to the expansion of the full propagator around the classical propagator (see appendix C.1), in order to obtain an expansion of the exact effective action around the Hartree-Fock result. In appendix C.2, it is shown that this yields an expansion of the exact effective action in terms of tadpole-free 1PI Feynman diagrams with dressed propagators and dressed vertices. Applying the result from eq. (C.9) to the lowest order of the derivative expansion of the effective action yields a corresponding expansion of the exact effective potential $V_{eff}^{exact}(\phi)$ in terms of 1PI Feynman diagrams without tadpoles,

$$
\begin{aligned}
V_{eff}^{exact}(\phi) &= V_{eff}^{hf}(\phi) + V_{eff}^{notad}(\phi) \qquad (4.18)\\
-V_{eff}^{notad}(\phi) &= \quad + \quad + \quad + \quad + \quad + \ldots \\
&= \frac{1}{12}\left[-\overline{V}^{(3)}(\phi)\right]^2 \int \frac{d_\Lambda^4 k}{(2\pi)^4} \int \frac{d_\Lambda^4 q}{(2\pi)^4} \frac{1}{(k^2+\overline{V}^{(2)})(q^2+\overline{V}^{(2)})((q+k)^2+\overline{V}^{(2)})} \\
&\quad + \ldots ,
\end{aligned}
$$

where $V_{eff}^{hf}(\phi)$ is the effective potential in Hartree-Fock approximation as given in eq. (4.15), and $-V_{eff}^{notad}(\phi)$ is the sum of all 1PI Feynman diagrams *without tadpoles* with lines representing the field-dependent dressed propagator in Euclidean momentum space

$$G_{hf}^{-1}(k) = k^2 + M_{eff}^2(\phi) = k^2 + \overline{V}^{(2)}(\phi)\,,$$

determined self-consistently by the solution of the gap equation (4.12), and field-dependent dressed vertices given by the derivatives of the auxiliary potential (4.16) evaluated with auxiliary mass $m^2 = M_{eff}^2(\phi)$,

$$-i\overline{V}^{(k)}(\phi) \equiv \left.\frac{-i\partial^k \overline{V}(\phi, m^2)}{\partial \phi^k}\right|_{m^2 = M_{eff}^2(\phi)}, \qquad (4.19)$$

for $k \geq 3$. The gap equation (4.12) can be rewritten as $M_{eff}^2(\phi) = \overline{V}^{(2)}(\phi)$ (see also eq. 4.17), which was already used above. A Feynman diagram contains a "tadpole" if it contains at least one line which begins and ends at the same vertex. The effective potential expanded in terms of the dressed propagator and vertices defined above contains only Feynman diagrams which have no "tadpoles".

Hartree-Fock approximation for tracker potentials

The gap equation and the effective potential in Hartree-Fock approximation are now evaluated within effective field theory for a tracker potential characterized by the power-counting rules discussed in section 4.1.1. The dependence of the effective mass on the UV embedding scale Λ is obtained by inserting eq. (4.4) into the gap equation (4.12),

$$M_{eff}^2(\phi) = \exp\left[\frac{1}{2}\left(\frac{\Lambda^2}{16\pi^2} f_1(m^2/\Lambda^2)\right)\frac{d^2}{d\phi^2}\right] V_{cl}''(\phi)\Big|_{m^2 = M_{eff}^2(\phi)} .$$

In the limit $M_{eff}^2(\phi) \ll \Lambda^2$, the gap equation has an approximate solution

$$M_{eff}^2(\phi) \simeq \exp\left[\frac{\Lambda^2}{32\pi^2} f_1(0) \frac{d^2}{d\phi^2}\right] V_{cl}''(\phi) \cdot \left\{1 + \mathcal{O}\left(\frac{M_{eff}^2}{\Lambda^2}\right)\right\}.$$

This solution can be trusted for all values of ϕ where the approximate solution fulfills the assumption $M_{eff}^2(\phi) \ll \Lambda^2$. Within the range of field values where this is the case, the approximate solution of the gap equation can be used in order to obtain a corresponding approximation of the effective potential using eq. (4.15). The momentum integral in the second term in eq. (4.15) is only logarithmically divergent, since the quadratic divergences of the two contributions to the integrand cancel (this can be verified using $\ln(1+x) \approx x$). Therefore, it has a marginal dependence on the UV scale Λ, and may be parameterized in the form

$$\int \frac{d_\Lambda^4 k}{(2\pi)^4} \left[\ln\left(\frac{k^2+m^2}{k^2}\right) - \frac{m^2}{k^2+m^2}\right] = \frac{m^4}{16\pi^2} f_0(m^2/\Lambda^2), \tag{4.20}$$

where $f_0(x) \sim \mathcal{O}(1)$ (for $0 \leq x \ll 1$) contains a logarithmic dependence on Λ. Thus, all relevant contributions are captured by the first term in eq. (4.15). Using that $M_{eff}^2(\phi) \ll \Lambda$, one finally obtains the effective potential in leading order in M_{eff}^2/Λ^2 and $V_{eff}/\tilde{M}^4$ from eq (4.15),

$$V_{eff}(\phi) \simeq \exp\left[\frac{\Lambda^2}{32\pi^2} f_1(0) \frac{d^2}{d\phi^2}\right] V_{cl}(\phi) \cdot \left\{1 + \mathcal{O}\left(\frac{M_{eff}^2}{\Lambda^2}\right) + \mathcal{O}\left(\frac{V_{eff}}{\tilde{M}^4}\right)\right\}, \tag{4.21}$$

where, for simplicity, the effective potential is denoted by $V_{eff}(\phi) \equiv V_{eff}^{hf}(\phi)$ unless otherwise stated. Here, the suppression scale $\tilde{M}$ is defined as the scale height of the effective potential $V_{eff}(\phi)$,

$$V_{eff}^{(k)}(\phi) \sim V_{eff}(\phi)/\tilde{M}^k, \tag{4.22}$$

analogously to the scale height M of the classical potential $V_{cl}(\phi)$. In section 4.1.4, it will be shown that the effective potentials obtained for classical tracker potentials indeed fulfill a relation of this type. The corrections of the order M_{eff}^2/Λ^2 are inherited from the corrections to the approximate solution of the gap equation, and the corrections of order $V_{eff}/\tilde{M}^4$ originate from the marginal contributions to the effective potential which have been neglected. The latter can be seen in the following way. The marginal contributions can be written in the form

$$\delta V_{eff}^{marginal}(\phi) = \frac{1}{2} \frac{M_{eff}^4(\phi)}{16\pi^2} f(M_{eff}^2(\phi)/\Lambda^2),$$

where $f(x) \equiv f_0(x) + \delta f(x) \sim \mathcal{O}(1)$ (for $0 \leq x \ll 1$) contains a logarithmic Λ-dependence. Here, $f_0(x)$ is the marginal contribution to the effective potential in Hartree-Fock approximation (see eqs. (4.15, 4.20)), and $\delta f(x)$ stands for marginal corrections to the Hartree-Fock approximation (see also below). The power counting rule (4.22) for the effective tracker potential directly yields that $V_{eff}'' \sim V_{eff}/\tilde{M}^2$, i.e. the order of magnitude of the effective mass can be estimated as $M_{eff}^2 \sim V_{eff}/\tilde{M}^2$ at leading order in M_{eff}^2/Λ^2. Thus, the marginal corrections $\delta V_{eff}^{marginal} \sim M_{eff}^4 \cdot \ln\Lambda \sim [V_{eff} \cdot (V_{eff}/\tilde{M}^4) \cdot \ln\Lambda]$ are suppressed by a factor of the order $V_{eff}/\tilde{M}^4$ compared to the leading contribution to the effective potential.

Using the resummed perturbation theory, the order of magnitude of corrections to the Hartree-Fock effective potential can also be estimated. The first correction comes from the non-local tadpole-free

1PI Feynman diagrams with two vertices connected by $l+1$ lines ($l \geq 2$). Within effective field theory, their contribution is of the order (see eq. (4.6))

$$\delta V_{eff}^{nonloc}(\phi) = \sum_{l=2}^{\infty} \frac{1}{2(l+1)!} \left[\overline{V}^{(l+1)}(\phi)\right]^2 \frac{\Lambda^{2(l-1)}}{(16\pi^2)^l} f_l(M_{eff}^2(\phi)/\Lambda^2)\,,$$

where again $f_l(x) \sim \mathcal{O}(1)$ (for $0 \leq x \ll 1$). Using the upper power counting rule (4.22), the dressed vertices (4.19) for the effective potential (4.21) can be estimated as $\overline{V}^{(l+1)} \sim V_{eff}/\tilde{M}^{l+1}$, such that $[\overline{V}^{(l+1)}]^2\Lambda^{2(l-1)} \sim V_{eff} \cdot V_{eff}/\tilde{M}^4 \cdot (\Lambda/\tilde{M})^{2(l-1)}$. Thus, $\delta V_{eff}^{nonloc} \sim V_{eff} \cdot V_{eff}/\tilde{M}^4 \cdot F(\Lambda/\tilde{M})$, is also suppressed by the tiny factor of order $V_{eff}/\tilde{M}^4 \lll 1$, where $F(\Lambda/\tilde{M})$ contains a resummation of the subleading relevant contributions $\sim (\Lambda/\tilde{M})^{2(l-1)} f_l(0)/[2(l+1)!(16\pi^2)^l] \lesssim \mathcal{O}(1)$ (for $\Lambda \lesssim \tilde{M}$).
In summary, the approximation to the effective potential from eq. (4.21) can be used in the range of field values ϕ where the conditions

$$M_{eff}^2(\phi) \ll \Lambda^2 \lesssim \tilde{M}^2 \qquad \text{and} \qquad V_{eff}(\phi) \ll \tilde{M}^4$$

are fulfilled. For a quintessence tracker potential, both conditions are in fact identical if the UV embedding scale and the suppression scale of the non-renormalizable interactions are of the same order (as expected for an effective field theory) $\Lambda \sim \tilde{M}$, since $M_{eff}^2 \sim V_{eff}/\tilde{M}^2$ at leading order in M_{eff}^2/Λ^2. Furthermore, for exponential tracker potentials, the suppression scale $\tilde{M} \sim M \lesssim M_{pl}$ turns out to be close to the Planck scale (see section 4.1.4), such that the corrections to the leading effective potential in eq. (4.21) within the effective field theory framework are indeed of the order[4] $V_{eff}/M_{pl}^4 \sim 10^{-120}$ during the present cosmological epoch. Clearly, the corrections are negligible even if some of the upper assumptions are relaxed, for example if a UV embedding scale $\Lambda \ll M_{pl}$ is allowed, as will be discussed in detail in section 4.1.4.
For simplicity, it may be assumed that the function $f_1(x)$ appearing in the parameterization of the "tadpole" Feynman integral in eq. (4.4) is normalized to $f_1(0) = \pm 1$. This can be achieved without loss of generality by rescaling the precise value of Λ by a factor of order one. For generality, the possibility that $f_1(0)$ can be positive or negative has been included, for the following reason. Since the Feynman integral (4.4) has a relevant dependence on Λ, the value of the integral is dominated by contributions close to the UV embedding scale, at which the unknown underlying theory becomes important. Thus, although the integral (4.4) is of the order of magnitude $\sim \Lambda^2$, the precise numerical value will strongly depend on the form factor $F_\Lambda(k)$. Therefore, due to the unknown shape of the form factor, it cannot be decided a priori whether $f_1(x)$ is positive or negative, even though the integrand without the form factor is positive definite. There are also similar examples like the Casimir effect, where the sign of the renormalized 0-0-component of the energy-momentum tensor can be positive or negative, depending e.g. on boundary conditions and geometry, even though the unrenormalized contribution is positive definite [35].
Finally, an approximation of the effective potential is obtained, which resums all relevant contributions for quintessence tracker potentials (which are characterized by the power-counting rule (4.7)), and which explicitly depends on the UV embedding scale Λ,

$$V_{eff}(\phi) \simeq \exp\left[\pm \frac{\Lambda^2}{32\pi^2} \frac{d^2}{d\phi^2}\right] V_{cl}(\phi)\,. \tag{4.23}$$

The corrections have been estimated to be of the order $M_{eff}^2(\phi)/\Lambda^2$ and $V_{eff}(\phi)/\tilde{M}^4$. This result can be compared to the one-loop analysis of Refs. [43, 83]. The one-loop result can be recovered by

[4] As mentioned in the beginning, it is assumed here that the freedom to shift the effective potential by a constant is used to match the present quintessence energy density with the observed value today.

inserting the Taylor-expansion $\exp[c\cdot\partial^2]=\sum_{L=0}^{\infty}c^L\partial^{2L}/L!$ of the exponential derivative operator up to first order,

$$V_{1-loop}(\phi)\simeq\left[1\pm\frac{\Lambda^2}{32\pi^2}\frac{d^2}{d\phi^2}\right]V_{cl}(\phi)\,.$$

For tracker potentials obeying the power counting rule (4.7), the higher-order contributions which are resummed by the Taylor-series of the exponential derivative operator are proportional to

$$\Lambda^{2L}/M^{2L},\qquad L=2,3,4,\ldots\,.$$

These relevant corrections are unsuppressed for an effective theory where the UV embedding scale Λ is of the order of the suppression scale M of non-renormalizable interactions, and therefore it is important to take them into account. As discussed above, this is accomplished by the effective potential (4.23) in Hartree-Fock approximation which is valid as long as the effective quintessence mass and potential energy are much smaller than $\Lambda\sim M\lesssim M_{pl}$.
It should be mentioned that the upper results are valid under the assumption that the embedding scale Λ itself does not depend (strongly) on the value of the scalar field ϕ. This is a reasonable assumption if the UV completion is generically connected to quantum gravity effects, in which case $\Lambda\sim M_{pl}$ can be expected [58, 65], which is also compatible with $M\sim M_{pl}$. On the other hand, in principle, the UV embedding scale Λ might depend on the field value ϕ in a way which is specific for the UV completion. If, for example, the quintessence field influences the size $R(\phi)$ of a compactified extra-dimension, and if the embedding scale $\Lambda\propto R^{-1}(\phi)$ corresponds to the compactification scale of this extra-dimension, it might depend on ϕ. The parametric dependence of Λ on ϕ thus has to be studied case-by-case for any possible UV completion and will depend on the details of the embedding. In order to be able to investigate the robustness of tracker potentials in a model-independent way, the analysis is restricted to those classes of UV completions where the field-dependence of the embedding scale is negligible compared to the field-dependence of the classical tracker potential in the Hartree-Fock approximated effective potential (4.23). An analogous restriction has also been made in the one-loop analysis of Refs. [43, 83].

4.1.3 Manifestly finite Effective Potential in 1+1 Dimensions

Before studying the robustness of quintessence potentials using the generalized Hartree-Fock approximation, it will be applied to quantum field theory in 1+1 space-time dimensions in order to check whether the approximation introduced above yields correct results in a case where the exact effective potential is known independently due to the symmetry properties of the theory. Furthermore, it turns out that the generalized Hartree-Fock approximation can be used efficiently to compute the renormalized effective potential for a scalar quantum field in 1+1 dimensions with non-derivative self-interactions.
The Hartree-Fock approximation discussed in section 4.1.2 can be extended in a straightforward way to d-dimensional quantum field theory described by the classical action

$$S[\phi]=\int d^dx\left(\frac{1}{2}(\partial\phi)^2-V_{cl}(\phi)\right)\,. \tag{4.24}$$

Since the action is dimensionless ($\hbar=1$ in natural units), the field has mass-dimension $[\phi]=(d-2)/2$. The expansion of the effective action in terms of 1PI or 2PI diagrams described in sections 3.1 and 3.2, respectively, can be transferred to d dimensions by replacing all 4-dimensional integrals in position and momentum space by d-dimensional integrals, $d^4x\to d^dx$, $d^4k/(2\pi)^4\to d^dk/(2\pi)^d$, as well as $\delta^4(x-y)\to\delta^d(x-y)$.

For $d = 1+1$, i.e. for two-dimensional Minkowski space, the field value ϕ is dimensionless, and therefore all non-derivative k-point self-interactions with classical vertices given by the derivatives $-iV_{cl}^{(k)}(\phi)$ of the potential ($k \geq 3$) are renormalizable. It will now be shown that it is even possible to perform the renormalization explicitly for the self-consistent Hartree-Fock approximation and for a general potential $V_{cl}(\phi)$ in $d = 1+1$.
The effective action in d dimensions in Hartree-Fock approximation is given by eq. (4.14) with $d^4x \to d^dx$, and with a full propagator $G(x,y)$ parameterized, as in eq. (4.10), by an effective mass M_{eff}^2 which is determined self-consistently by the field-dependent gap equation (4.13). For simplicity, the lowest order of the derivative expansion of the effective action, i.e. the effective potential, is treated here. The effective potential in d dimensions in Hartree-Fock approximation is, up to a field-independent constant, given by (see eq. 4.15)

$$V_{eff}^{hf}(\phi) = V_{hf}(\phi) + \frac{1}{2}\int \frac{d^dk}{(2\pi)^4}\left[\ln\left(\frac{k^2+M_{eff}^2(\phi)}{k^2}\right) - \frac{M_{eff}^2(\phi)}{k^2+M_{eff}^2(\phi)}\right]. \tag{4.25}$$

As above (see eqs. (4.12, 4.14, 4.17)), $M_{eff}^2(\phi)$ and $V_{hf}(\phi)$ can be rewritten as

$$M_{eff}^2(\phi) = \left.\frac{\partial^2\overline{V}(\phi,m^2)}{\partial\phi^2}\right|_{m^2=M_{eff}^2(\phi)}, \quad V_{hf}(\phi) = \left.\overline{V}(\phi,m^2)\right|_{m^2=M_{eff}^2(\phi)}, \tag{4.26}$$

using the d-dimensional auxiliary potential

$$\overline{V}(\phi,m^2) \equiv \exp\left[\frac{1}{2}\left(\int\frac{d^dk}{(2\pi)^4}\frac{1}{k^2+m^2}\right)\frac{d^2}{d\phi^2}\right]V_{cl}(\phi). \tag{4.27}$$

Renormalization in $1+1$ dimensions

For $d = 1+1$, the momentum integral in the second term in eq. (4.25) is convergent and can be explicitly calculated, such that the effective potential in Hartree-Fock approximation is (the effective potential has mass-dimension two in $d = 1+1$)

$$V_{eff}^{hf}(\phi) = V_{hf}(\phi) + \frac{1}{8\pi}M_{eff}^2(\phi) = \left(\overline{V}(\phi,m^2) + \frac{1}{8\pi}\frac{\partial^2\overline{V}(\phi,m^2)}{\partial\phi^2}\right)_{m^2=M_{eff}^2(\phi)}. \tag{4.28}$$

In the second expression on the right-hand side, the effective potential is rewritten in terms of the auxiliary potential $\overline{V}(\phi,m^2)$. Obviously, the effective mass and the effective potential are finite if $\overline{V}(\phi,m^2)$ is finite. In order to completely renormalize all divergences in Hartree-Fock approximation it is thus sufficient (in $d = 1+1$) to introduce counterterms which remove the divergences of the "tadpole" Feynman integral appearing in eq. (4.27). Note that this integral is only logarithmically divergent in $d = 1+1$, such that dimensional regularization [61] may be used without loss of generality. With $\varepsilon \equiv 1 - d/2$ for d near 2, the dimensionally regulated "tadpole" integral is given by

$$\int\frac{d^dk}{(2\pi)^d}\frac{1}{k^2+m^2} = \frac{\Gamma(\varepsilon)}{(4\pi)^{d/2}}m^{d-2} = \frac{\tilde{\mu}^{-2\varepsilon}}{4\pi}\left(\frac{1}{\varepsilon} + \ln\frac{4\pi e^{-\gamma}\tilde{\mu}^2}{m^2} + \mathcal{O}(\varepsilon)\right), \tag{4.29}$$

where the renormalization scale $\tilde{\mu}$ has been introduced in the last equality, and $\gamma \approx 0.5772$ is Euler's constant. To keep the field value a dimensionless quantity as in $d = 2$, the replacement $\phi \to \tilde{\mu}^{-\varepsilon}\phi$ is made. In order to remove the term which diverges when $\varepsilon \to 0$, all coupling constants appearing

in the (bare) classical potential $V_{cl}^B(\phi)$ are split into a renormalized part and a counterterm[5], and all renormalized terms are collected in $V_{cl}^R(\phi)$ and all counterterms in $\delta V_{cl}(\phi)$, to get

$$V_{cl}^B(\phi) = V_{cl}^R(\phi) + \delta V_{cl}(\phi)\,.$$

Here, the bare classical potential $V_{cl}^B(\phi)$ can be identified with the potential appearing in the (bare) classical action (4.24), such that the dimensionally regulated auxiliary potential is

$$\overline{V}(\phi, m^2) = \exp\left[\frac{1}{8\pi}\left(\frac{1}{\varepsilon} + \ln\frac{4\pi e^{-\gamma}\tilde{\mu}^2}{m^2} + \mathcal{O}(\varepsilon)\right)\frac{d^2}{d\phi^2}\right] V_{cl}^B(\phi)\,.$$

The auxiliary potential can be renormalized according to the minimal subtraction scheme if the counterterms are chosen according to

$$\delta V_{cl}(\phi) \equiv \left(\exp\left[-\frac{1}{8\pi}\frac{1}{\varepsilon}\frac{d^2}{d\phi^2}\right] - 1\right) V_{cl}^R(\phi)\,. \tag{4.30}$$

Note that the counterterms do not depend on m^2, which is crucial for the self-consistency of the gap equation (4.26). With this, the auxiliary potential can be written in terms of the renormalized classical potential (for $\varepsilon \to 0$),

$$\overline{V}(\phi, m^2) = \exp\left[\frac{1}{8\pi}\ln\frac{\mu^2}{m^2}\frac{d^2}{d\phi^2}\right] V_{cl}^R(\phi)\,, \tag{4.31}$$

where $\mu^2 \equiv 4\pi e^{-\gamma}\tilde{\mu}^2$. The auxiliary potential is thus manifestly finite for an arbitrary finite renormalized classical potential $V_{cl}^R(\phi)$, and arbitrary auxiliary mass m^2, and depends on the renormalization scale μ. Consequently, it can be seen from eqs. (4.26) and (4.28) that the effective mass $M_{eff}^2(\phi)$ and the effective potential $V_{eff}(\phi)$ in Hartree-Fock approximation are also manifestly finite in $d = 1+1$. In particular, the self-consistent gap equation which determines the field-dependent effective mass can be rewritten in terms of the renormalized classical potential,

$$M_{eff}^2(\phi) = \exp\left[\frac{1}{8\pi}\ln\frac{\mu^2}{m^2}\frac{d^2}{d\phi^2}\right] V_{cl}^R{}''(\phi)\Big|_{m^2 = M_{eff}^2(\phi)}\,, \tag{4.32}$$

and is also manifestly finite in $d = 1+1$.

Renormalized resummed perturbation theory

Before calculating the renormalized effective potential for a specific example, it should be noted that the counterterms contained in $\delta V_{cl}(\phi)$ as defined in eq. (4.30) are actually already the *exact* counterterms, i.e. the exact effective potential is rendered finite by this choice of $\delta V_{cl}(\phi)$. This can be seen using the resummed perturbation theory discussed above (see also appendix C.2), where an expansion of the exact effective action in terms of 1PI Feynman diagrams without tadpoles, but with dressed propagators and vertices, has been derived.

The corresponding expansion (4.18) of the exact effective potential can easily be transferred to an arbitrary dimension d. In $d = 1+1$ dimensions, it was shown above that the auxiliary potential $\overline{V}(\phi, m^2)$ is rendered finite by the counterterms (4.30) for arbitrary auxiliary masses m^2. Therefore, the dressed propagator $G_{hf}(k)$ and the dressed vertices (4.19) $-i\overline{V}^{(k)}(\phi)$ are themselves finite in $d = 1+1$, and can be calculated explicitly from the manifestly finite expression (4.31) for $\overline{V}(\phi, m^2)$.

[5] A field rescaling Z is not introduced here since this in not necessary in $d = 1+1$.

Furthermore, there is only one type of Feynman integral which is divergent in $d = 1+1$, given by the logarithmically divergent "tadpole" integral[6] (4.29). Since the expansion (4.18) of the effective potential is characterized by the property that it just contains Feynman diagrams without tadpoles, and precisely these diagrams do not contain any divergent loop integrals, the effective potential in $d = 1+1$ is completely renormalized by the counterterms (4.30).
This result can be interpreted in the following way: All divergences have been resummed into the dressed propagator and the dressed vertices (4.19) introduced above, which are renormalized by the counterterms (4.30). The Feynman diagrams without tadpoles contributing to $V_{eff}^{notad}(\phi)$ according to the expansion (4.18) are convergent in $d = 1+1$, and thus no further counterterms are required. For example, the two loop contribution to $V_{eff}^{notad}(\phi)$ is convergent, and equal to

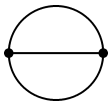

$$= \frac{1}{(8\pi)^2} \frac{\psi'(\frac{1}{6}) + \psi'(\frac{1}{3}) - \psi'(\frac{2}{3}) - \psi'(\frac{5}{6})}{54} \frac{\left(\overline{V}^{(3)}(\phi)\right)^2}{\overline{V}^{(2)}(\phi)}, \tag{4.33}$$

where $\psi'(x) = d\psi(x)/dx$ is the first derivative of the digamma function $\psi(x) = \Gamma'(x)/\Gamma(x)$. Note that due to the self-consistently determined dressed propagator and dressed vertices this diagram corresponds to an infinite resummation of perturbative diagrams (see section 3.2 and appendix C).
Since all contributions to $V_{eff}^{notad}(\phi)$ are convergent, it is possible to calculate an arbitrary Feynman diagram up to its numerical prefactor by dimensional analysis. Let $\mathcal{F}$ be a diagram contributing to $V_{eff}^{notad}(\phi)$ with $\mathcal{V}_k$ vertices with k legs ($k \geq 3$). Then it has $\mathcal{V} = \sum_k \mathcal{V}_k$ vertices, $P = \sum_k k\mathcal{V}_k/2$ internal lines and $L = P - \mathcal{V} + 1$ loops [179]. Since all vertices have mass-dimension two in $d = 1+1$, their product contributes a factor with dimension $2\mathcal{V}$. Since $\mathcal{F}$ has also mass-dimension two and the only further scale which appears in the convergent loop integrals is the effective mass $M_{eff}^2 = \overline{V}^{(2)}$ contained in the dressed propagator $G_{hf}(k)$, the diagram can be written as

$$\mathcal{F} = \frac{1}{(8\pi)^L} g(\mathcal{F}) \frac{\prod_{k\geq 3} \left(\overline{V}^{(k)}(\phi)\right)^{\mathcal{V}_k}}{\left(\overline{V}^{(2)}(\phi)\right)^{\mathcal{V}-1}}, \tag{4.34}$$

with a constant numerical prefactor denoted by $g(\mathcal{F})$. For example, for the two loop diagram (4.33) it is $g(\mathcal{F}) = (\psi'(\frac{1}{6}) + \psi'(\frac{1}{3}) - \psi'(\frac{2}{3}) - \psi'(\frac{5}{6}))/54 \approx 0.781$.
Altogether, it was shown that the exact and completely renormalized effective potential (4.18) for a scalar quantum field in 1+1 dimensions with non-derivative self-interactions can be written as

$$\begin{aligned} V_{eff}^{exact}(\phi) &= V_{eff}^{hf}(\phi) + V_{eff}^{notad}(\phi) \\ &= \left(\overline{V}(\phi) + \frac{1}{8\pi}\overline{V}^{(2)}(\phi)\right) + \sum_{\mathcal{F}} \frac{g(\mathcal{F})}{(8\pi)^L} \frac{\prod_{k\geq 3} \left(\overline{V}^{(k)}(\phi)\right)^{\mathcal{V}_k}}{\left(\overline{V}^{(2)}(\phi)\right)^{\mathcal{V}-1}}, \end{aligned} \tag{4.35}$$

where $V_{eff}^{hf}(\phi)$ is the effective potential in Hartree-Fock approximation (4.28), which was rewritten using $\overline{V}(\phi) \equiv \overline{V}^{(0)}(\phi) = V_{hf}(\phi)$ and $\overline{V}^{(2)}(\phi) = M_{eff}^2(\phi)$. The sum runs over all 1PI Feynman diagrams

[6] A Feynman diagram for a scalar quantum field is convergent if the superficial degree of divergence of the diagram and all its subdiagrams is negative [38, 61, 113, 177, 191]. For a diagram with $\mathcal{V}$ momentum-independent vertices, P internal scalar lines and an arbitrary number of external lines, the superficial degree of divergence is $D = dL - 2P$ [179], where $L = P - \mathcal{V} + 1$ is the number of loops. In $d = 1+1$, $D = 2L - 2P = -2(\mathcal{V} - 1)$, i.e. only (sub-)diagrams with one vertex can contain divergences. The internal lines of loop diagrams with one vertex have to begin and end at this vertex, i.e. they are "tadpoles" attached to this vertex.

$\mathcal{F}$ without tadpoles for which the dimensionless numerical constants $g(\mathcal{F})$ are defined via eq. (4.34), and with dressed vertices (4.19)

$$\overline{V}^{(k)}(\phi) \equiv \left.\frac{\partial^k \overline{V}(\phi, m^2)}{\partial \phi^k}\right|_{m^2 = M^2_{\mathit{eff}}(\phi)},$$

derived from the "tadpole-resummed" auxiliary potential $\overline{V}(\phi, m^2)$ (4.31) evaluated with the effective mass $m^2 = M^2_{\mathit{eff}}(\phi)$ determined by the renormalized gap equation (4.32).

Exponential potential — Liouville theory

In this section the Hartree-Fock approximation is applied to a quantum field with an exponential potential,

$$V_{cl}(\phi) = V_0 \exp(-\lambda\phi), \tag{4.36}$$

with a dimensionless parameter λ, known as Liouville Theory [76, 148]. In 1+1 dimensions, this is a renormalizable potential. In the following, it will be show that the effective potential can be renormalized and computed explicitly with the techniques introduced above, and yields a result which agrees with an independent method based on the conformal symmetry of Liouville Theory [67, 76, 156] (which exists, for the exponential potential, in 1+1 dimensions only).
The Hartree-Fock approximation is ideally suited for the exponential potential. It is possible to find an exact solution of the gap equation (4.32), since the derivative $d^2/d\phi^2$ appearing in the exponential derivative operator can be just replaced by λ^2,

$$M^2_{\mathit{eff}} = \exp\left[\frac{\lambda^2}{8\pi}\ln\frac{\mu^2}{M^2_{\mathit{eff}}}\right] V^{R\prime\prime}_{cl}(\phi) = \lambda^2 V_0 \exp\left[\frac{\lambda^2}{8\pi}\ln\left(\frac{\mu^2}{M^2_{\mathit{eff}}}\right) - \lambda\phi\right]. \tag{4.37}$$

Inserting eq. (4.36) for $V^R_{cl}(\phi)$, the gap equation can be easily solved algebraically for each value of ϕ by dividing the equation by the renormalization scale μ^2 and taking the logarithm on both sides,

$$\begin{aligned} \ln\left(\frac{M^2_{\mathit{eff}}}{\mu^2}\right) &= \ln\left(\frac{\lambda^2 V_0}{\mu^2}\right) + \frac{\lambda^2}{8\pi}\ln\left(\frac{\mu^2}{M^2_{\mathit{eff}}}\right) - \lambda\phi \\ \Rightarrow \quad \ln\left(\frac{M^2_{\mathit{eff}}(\phi)}{\mu^2}\right) &= \frac{1}{1+\lambda^2/(8\pi)}\left[\ln\left(\frac{\lambda^2 V_0}{\mu^2}\right) - \lambda\phi\right]. \end{aligned}$$

The solution of the gap equation thus reads

$$\ln\left(\frac{M^2_{\mathit{eff}}(\phi)}{\mu^2}\right) = \ln\left(\frac{M_r^2}{\mu^2}\right) - \frac{\phi}{\lambda^{-1} + \lambda/(8\pi)},$$

where $\ln(M_r^2/\mu^2) \equiv [\ln(\lambda^2 V_0/\mu^2)]/(1+\lambda^2/(8\pi))$. Furthermore, using eqs. (4.26, 4.31) yields

$$V_{hf}(\phi) = \exp\left[\frac{\lambda^2}{8\pi}\ln\left(\frac{\mu^2}{M^2_{\mathit{eff}}(\phi)}\right)\right] V^R_{cl}(\phi) = V_r \exp\left[-\frac{\phi}{\lambda^{-1} + \lambda/(8\pi)}\right],$$

where $\ln(V_r/V_0) \equiv -[\ln(M_r^2/\mu^2)]\,\lambda^2/(8\pi)$. Together with the solution of the gap equation, the effective potential in Hartree-Fock approximation is obtained from eq. (4.28),

$$V^{hf}_{\mathit{eff}}(\phi) = V_{hf}(\phi) + \frac{1}{8\pi}M^2_{\mathit{eff}}(\phi) = \left(V_r + \frac{1}{8\pi}M_r^2\right)\exp\left[-\tilde{\lambda}\phi\right].$$

The effective potential in Hartree-Fock approximation is also an exponential of the field ϕ, with a renormalized pre-factor $V_r + M_r^2/(8\pi)$ and with slope given by

$$\tilde{\lambda}^{-1} = \lambda^{-1} + \lambda/(8\pi)\,.$$

The upper relation can also be obtained completely independently from the transformation properties of the energy-momentum tensor, which is highly constrained by the conformal symmetry of Liouville Theory in 1+1 dimensions [67, 76].
Using the expansion of the exact effective potential in terms of 1PI tadpole-free Feynman diagrams with dressed propagator and dressed vertices, it is additionally possible to show that the effective potential in Hartree-Fock approximation captures basically already all quantum corrections to the potential. The dressed vertices and propagator for the exponential potential (4.36) are given by

$$\overline{V}^{(k)}(\phi) = \left.\frac{\partial^k \overline{V}(\phi, m^2)}{\partial \phi^k}\right|_{m^2 = M_{eff}^2(\phi)} = (-\lambda)^k V_{hf}(\phi) = (-\lambda)^k V_r \exp\left[-\tilde{\lambda}\phi\right].$$

Using this, it can be seen from eq. (4.34) that the contribution from a tadpole-free diagram $\mathcal{F}$ with $\mathcal{V}_k$ vertices with k legs ($k \geq 3$), i.e. with $\mathcal{V} = \sum_k \mathcal{V}_k$ vertices, $P = \sum_k k\mathcal{V}_k/2$ internal lines and $L = P - \mathcal{V} + 1$ loops has the form

$$\mathcal{F} \;=\; \frac{1}{(8\pi)^L}\, g(\mathcal{F})\, \frac{\prod\limits_{k\geq 3} \left((-\lambda)^k V_{hf}(\phi)\right)^{\mathcal{V}_k}}{\left(\lambda^2 V_{hf}(\phi)\right)^{\mathcal{V}-1}} \;=\; \frac{1}{(8\pi)^L}\, g(\mathcal{F})\, \frac{(-\lambda)^{2P}}{\lambda^{2(\mathcal{V}-1)}} V_{hf}(\phi) \;=\; g(\mathcal{F}) \left(\frac{\lambda^2}{8\pi}\right)^L V_{hf}(\phi)\,.$$

Thus *all* contributions to the effective potential are proportional to $V_{hf}(\phi)$. Consequently, using eq. (4.35) the exact effective potential is obtained

$$V_{eff}^{exact}(\phi) = V_R \exp\left[-\tilde{\lambda}\phi\right], \tag{4.38}$$

where all contributions have been resummed into the constant prefactor

$$V_R = V_r \left(1 + \frac{\lambda^2}{8\pi} + \sum_{\mathcal{F}} g(\mathcal{F}) \left(\frac{\lambda^2}{8\pi}\right)^L\right) = V_r \left(1 + \frac{\lambda^2}{8\pi} + 0.781 \left(\frac{\lambda^2}{8\pi}\right)^2 + \ldots\right).$$

The sum runs over all 1PI Feynman diagrams $\mathcal{F}$ without tadpoles, $L \geq 2$ is the number of loops of $\mathcal{F}$, and $g(\mathcal{F})$ is the dimensionless numerical prefactor defined in eq. (4.34). This diagrammatic calculation of the effective potential also agrees with the result given in Ref. [76] without derivation.

4.1.4 Robustness of Quintessence Potentials

For tracker potentials which obey the power-counting rule (4.7), non-renormalizable interactions are suppressed by a high-energy scale $M \lesssim M_{pl}$. Within effective field theory embedded at a UV scale $\Lambda \sim M$, the effective potential (4.23) obtained from the Hartree-Fock approximation is the leading contribution to the effective potential for classical tracker potentials. Therefore, eq. (4.23) yields a useful prescription to estimate the stability of tracker quintessence potentials $V_{cl}(\phi)$ under quantum corrections induced by its self-interactions. This prescription consists of applying the exponential derivative operator

$$\exp\left[\pm\frac{\Lambda^2}{32\pi^2}\frac{d^2}{d\phi^2}\right] \tag{4.39}$$

to the classical potential $V_{cl}(\phi)$. In the following, the effect of this operator on the prototype tracker quintessence potentials is investigated. Furthermore, the dependence on the embedding scale Λ is discussed, as well as the validity conditions of the Hartree-Fock approximation. The impact on cosmological tracking solutions is studied for some examples.

Exponential potential

One prototype class of tracker potentials are (combinations of [21, 150]) exponential potentials [10, 157, 182]. Remarkably, an exponential of the field ϕ is form-invariant under the action of the operator (4.39). Consider e.g. the following finite or infinite sum of exponentials,

$$V_{cl}(\phi) = \sum_j V_j \exp\left(-\lambda_j \frac{\phi}{M_{pl}}\right). \tag{4.40}$$

The only effect of applying the operator (4.39) is a simple rescaling of the prefactors V_j according to

$$V_j \;\rightarrow\; V_j \exp\left[\pm \frac{\lambda_j^2 \Lambda^2}{32\pi^2 M_{pl}^2}\right]. \tag{4.41}$$

This extends the result of Ref. [83] for the one-loop case, which would correspond to the first term in a Taylor expansion of (4.39). Note that if $\Lambda \sim M_{pl}$ the correction can be of an important size, and can influence the relative strength of the exponentials in (4.40). The necessary conditions of validity, $V''_{eff}(\phi) \ll \Lambda^2$, and $V_{eff}(\phi) \ll \tilde{M}^4 \sim M_{pl}^4$, for the Hartree-Fock approximation are both fulfilled when

$$V_{eff}(\phi) \ll \Lambda^2 M_{pl}^2 \lesssim M_{pl}^4,$$

which implies that it is applicable if $\Lambda \gg H_{max}$, where H_{max} is the maximum value of the Hubble parameter where the field ϕ plays a role. For example, H_{max} could be the inflationary scale H_{inf}. For chaotic inflation with quadratic potential, it is typically of the order $H_{inf} \sim (\delta T_{CMB}/T_{CMB}) \cdot M_{pl} \sim 10^{-5} M_{pl} \sim 10^{13}$GeV [140, 141]. Furthermore, note that the effective potential indeed fulfills the power-counting rule (4.22) for tracker potentials with scale-height of the order $\tilde{M} \sim M \lesssim M_{pl}$ for $\lambda_j \gtrsim \mathcal{O}(1)$.
Altogether, it is found that exponential potentials are stable under radiative corrections from self-interactions in the domain of validity of the Hartree-Fock approximation within effective field theory. In particular, ultraviolet embedding scales up to the Planck scale $\Lambda \lesssim M_{pl}$ are possible. The subleading corrections, which would lead to a distortion of the exponential shape, are suppressed by a factor of the order of $V_{eff}(\phi)/M_{pl}^4$. This is an extremely tiny number of the order H^2/M_{pl}^2 in the context of quintessence models.

Inverse power law potential

The second prototype class of tracker potentials are (combinations) of inverse powers of the quintessence field ϕ [43, 83, 157, 169],

$$V_{cl}(\phi) = \sum_\alpha c_\alpha \phi^{-\alpha}. \tag{4.42}$$

The action of the operator (4.39) yields

$$\begin{aligned} V_{eff}(\phi) &= \sum_\alpha \frac{c_\alpha \phi^{-\alpha}}{\Gamma(\alpha)} \sum_{L=0}^{\infty} \frac{\Gamma(\alpha+2L)}{L!} \left(\frac{\pm\Lambda^2}{32\pi^2\phi^2}\right)^L \\ &= \sum_\alpha \frac{c_\alpha \phi^{-\alpha}}{\Gamma(\alpha)} \int_0^\infty dt\, t^{\alpha-1} \exp\left(-t \pm \frac{\Lambda^2}{32\pi^2\phi^2} t^2\right), \end{aligned} \tag{4.43}$$

where the Γ-function inside the sum over L has been replaced by an integration over the positive real axis in the second line, by using its definition. This integral gives a finite result if the negative sign in the exponent is used, which will therefore be assumed from now on. First two limiting cases

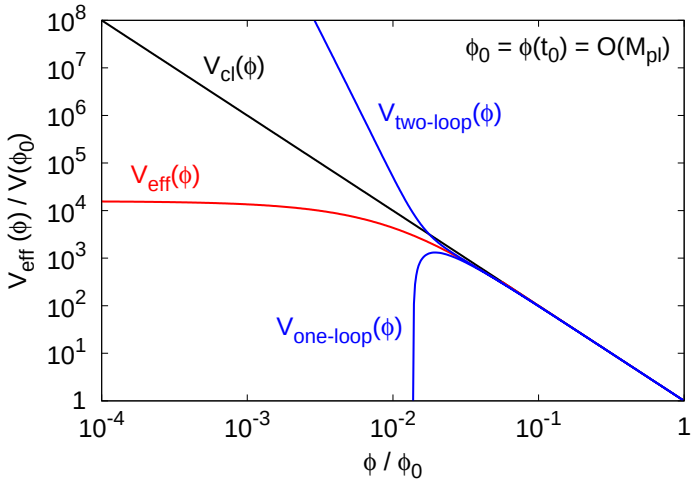

Figure 4.1: *Comparison of the Hartree-Fock approximation of the effective potential $V_{eff}(\phi)$ (red) with the leading one- and two-loop contributions as given by the Taylor expansion of the derivative operator (4.39) up to first and second order, respectively, (blue) as well as the classical potential $V_{cl}(\phi) \propto \phi^{-\alpha}$ (black) for $\alpha = 2$. The loop expansion breaks down at small field values $\phi \ll \Lambda$. The non-perturbative "multi-bubble" resummation accomplished by the Hartree-Fock approximation allows to extend the range of validity to the complete admissible range of field values $\phi > 0$.*

will be discussed, where the integral can be solved analytically. For large field values $\phi \gg \Lambda$, which corresponds to small potential energy and -curvature, the second term in the exponent appearing in the second line of eq. (4.43) can be neglected, which implies that asymptotically

$$V_{eff}(\phi) \to V_{cl}(\phi) \equiv \sum_\alpha c_\alpha \phi^{-\alpha}, \quad \phi \to \infty. \tag{4.44}$$

This means the low energy regime where the potential and its derivatives go to zero is not changed by quantum corrections. For the opposite limit where $\phi \ll \Lambda$, the integral in the last line of (4.43) can be calculated by neglecting the first term in the argument of the exponential,

$$V_{eff}(\phi) \;\to\; \sum_\alpha \frac{c_\alpha \phi^{-\alpha}}{\Gamma(\alpha)} \frac{1}{2}\Gamma(\frac{\alpha}{2}) \left(\frac{\Lambda^2}{32\pi^2\phi^2}\right)^{-\frac{\alpha}{2}} = \sum_\alpha \frac{\Gamma(\frac{\alpha}{2})}{2\Gamma(\alpha)} c_\alpha \left(\frac{\Lambda}{4\pi\sqrt{2}}\right)^{-\alpha} = \text{const}. \tag{4.45}$$

Thus the effective potential approaches a constant finite value for $\phi \lesssim \Lambda/(4\pi\sqrt{2})$ of the order $V_{cl}(\Lambda)$ in the small-field limit $\phi \ll \Lambda$ (see figures 4.1 and 4.2). Furthermore, it is easy to see that also the second derivative of the effective potential approaches a constant value

$$V''_{eff}(\phi) \to \sum_\alpha \frac{\Gamma(\frac{\alpha+2}{2})}{2\Gamma(\alpha)} c_\alpha \left(\frac{\Lambda}{4\pi\sqrt{2}}\right)^{-(\alpha+2)}. \tag{4.46}$$

Similarly, all higher derivatives approach constant values for $\phi \ll \Lambda$. Therefore, the effective potential $V_{eff}(\phi)$ fulfills the power-counting rule (4.22) with scale height given by

$$\tilde{M} \sim \begin{cases} \Lambda & \text{for} \quad \phi \ll \Lambda \\ \phi & \text{for} \quad \phi \gg \Lambda \end{cases}. \tag{4.47}$$

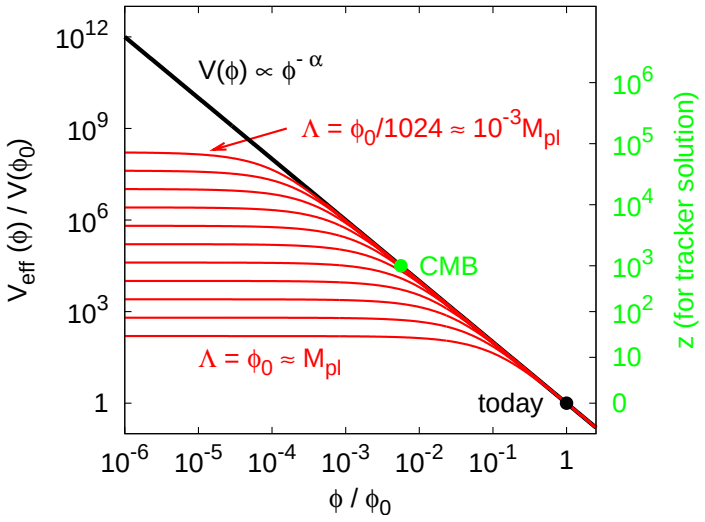

Figure 4.2: *Dependence of the effective potential $V_{eff}(\phi)$ on the UV embedding scale Λ for an inverse power law potential $V_{cl}(\phi) \propto \phi^{-\alpha}$ with $\alpha = 2$. The potential is normalized to the value of the potential $V_{cl}(\phi_0)$ at redshift $z = 0$. From top to bottom, Λ is enlarged by a factor 2 for each red line. The black line is the classical potential $V_{cl}(\phi)$, which is a straight line due to the double logarithmic scale. For $\phi \ll \Lambda$, the effective potential $V_{eff}(\phi)$ approaches a constant value, whereas $V_{cl}(\phi)$ grows unboundedly. The redshift-scale on the right-hand side applies for the classical tracking solution only and illustrates when the deviations of the effective potential $V_{eff}(\phi)$ from the classical potential $V_{cl}(\phi)$ become relevant in cosmic history going backward from $\phi/\phi_0 = 1$ (today).*

The scale-height $\tilde{M}$ of the effective potential approaches a constant value for small field values ϕ, in contrast to the scale height $M \sim \phi$ of the classical potential $V_{cl}(\phi)$. Thus, the singularity of the classical potential $V_{cl}(\phi)$, see eq. (4.42), for $\phi \to 0$ is not present for the effective potential $V_{eff}(\phi)$, where a constant value of the order $V_{cl}(\Lambda)$ is approached instead.
The Hartree-Fock approximation requires that $V''_{eff}(\phi) \ll \Lambda^2 \lesssim \tilde{M}^2$ and $V_{eff}(\phi) \ll \tilde{M}^4$. From eq. (4.47), it can be seen that the requirement $\Lambda^2 \lesssim \tilde{M}^2$ is fulfilled in the whole range of possible field values $\phi > 0$. In order to check the other conditions of validity, the case where the potential consists of only one inverse power-law term $V_{cl}(\phi) = c_\alpha \phi^{-\alpha}$ will be treated first for simplicity. In the range $\phi \ll \Lambda$, the limits of the effective potential (4.44) and the effective mass (4.45) can be used,

$$\begin{aligned} V''_{eff}(\phi) \sim c_\alpha \Lambda^{-(\alpha+2)} \ll \Lambda^2 \quad &\Leftrightarrow \quad \Lambda \gg c_\alpha^{1/(\alpha+4)}, \\ V_{eff}(\phi) \sim c_\alpha \Lambda^{-\alpha} \ll \tilde{M}^4 \sim \Lambda^4 \quad &\Leftrightarrow \quad \Lambda \gg c_\alpha^{1/(\alpha+4)}. \end{aligned}$$

Thus, both conditions of validity yield the same lower bound on the embedding scale Λ. The conditions of validity in the range $\phi \gg \Lambda$ can be evaluated using that $V_{eff}(\phi) \simeq V_{cl}(\phi)$ in this range,

$$\begin{aligned} V''_{eff}(\phi) \sim c_\alpha \phi^{-(\alpha+2)} \ll \Lambda^2 \quad &\Leftrightarrow \quad \Lambda \gg c_\alpha^{1/(\alpha+4)} (\Lambda/\phi)^{\frac{\alpha+2}{\alpha+4}}, \\ V_{eff}(\phi) \sim c_\alpha \phi^{-\alpha} \ll \tilde{M}^4 \sim \phi^4 \quad &\Leftrightarrow \quad \Lambda \gg c_\alpha^{1/(\alpha+4)} (\Lambda/\phi). \end{aligned}$$

Since $\Lambda/\phi \ll 1$ by assumption, the bounds obtained in the large-field range are weaker than the bounds obtained in the small-field range. All conditions of validity are thus fulfilled if the embedding

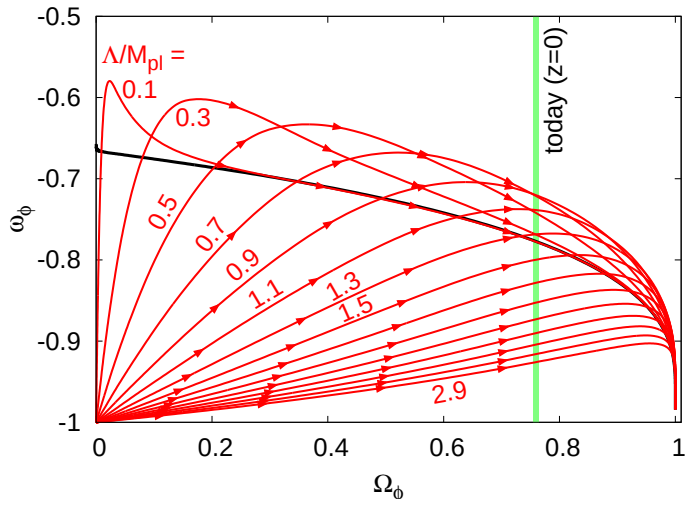

Figure 4.3: *Evolution in the $(\Omega_\phi, \omega_\phi)$-plane for the effective potential $V_{eff}(\phi)$ of an inverse power-law potential $V_{cl}(\phi) \propto \phi^{-\alpha}$ with $\alpha = 1$ for various values of Λ keeping $H_0 = 73\,\mathrm{km/sMpc}$ and $\Omega_{de} \equiv \Omega_\phi(z=0) = 0.76$ fixed. The UV embedding scale Λ is enlarged by $0.2\,M_{pl}$ for each red line starting from $\Lambda = 0.1\,M_{pl}$. The black line is the tracking solution in the classical potential $V_{cl}(\phi)$, from which the solutions deviate considerably for embedding scales Λ close to the Planck scale. The four arrows on each trajectory mark the points with redshifts $z = 2, 1, 0.5, 0.1$ from left to right.*

scale fulfills the lower bound $\Lambda \gg c_\alpha^{1/(\alpha+4)}$. For the classical potential (4.42) which contains a sum of inverse power-laws, the generalized bound is

$$\Lambda \gg \max_\alpha c_\alpha^{1/(\alpha+4)}.$$

For a single inverse power-law, the order of magnitude of the constant c_α required to reproduce the correct abundance of dark energy is [169]

$$c_\alpha^{1/(\alpha+4)} \sim \left(H_0^2 M_{pl}^{\alpha+2}\right)^{1/(\alpha+4)} \sim \left((100\,\mathrm{MeV})^6 M_{pl}^{\alpha-2}\right)^{1/(\alpha+4)}.$$

Thus, the lower bound on the embedding scale is a relatively mild restriction $\Lambda \gg 100\,\mathrm{MeV}$ for observationally allowed [169] values of the inverse power-law index $\alpha \lesssim 2$. For extremely steep potentials, $\alpha \to \infty$, the lower bound asymptotically approaches the Planck scale. It is emphasized that loop approximations to the effective potential break down in the limit $\phi \to 0$, whereas the Hartree-Fock approximation is applicable (see figure 4.1). The dependence of the effective potential on the UV embedding scale Λ is shown in figure 4.2 for the case $V_{cl}(\phi) \propto \phi^{-2}$.

Finally, the question in how far typical tracking quintessence models are changed by considering the effective potential from eq. (4.43) is investigated. Since the field value today is typically of the order of the Planck scale [169], the large-field limit eq. (4.44), where the effective potential approaches the classical potential and the corrections are negligible, is only applicable when $\Lambda \lll M_{pl}$. For values up to $\Lambda \lesssim M_{pl}/10$ the field ϕ can have a tracking solution. The redshift z_{quant} in cosmic history where the effective potential starts to deviate from the classical tracking potential, see figure 4.2, gives a rough estimate at which redshift the tracking sets in. For a potential dominated by a single inverse

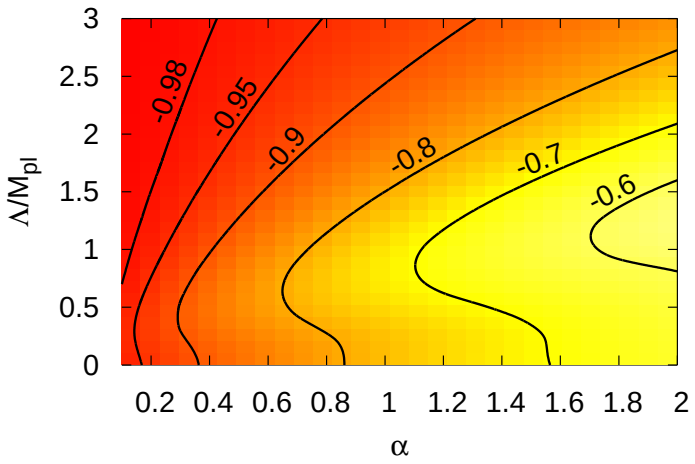

Figure 4.4: *Contour plot of the equation of state ω_{de} today ($z = 0$) using the effective potential $V_{eff}(\phi)$ obtained from the classical potential $V_{cl}(\phi) \propto \phi^{-\alpha}$ depending on the embedding scale Λ and the inverse power-law index α. The limit $\Lambda = 0$ corresponds to the classical limit $V_{eff} \equiv V_{cl}$. Again, H_0 and $\Omega_{de} = 0.76$ are chosen as in figure 4.3.*

power-law $V_{cl}(\phi) \propto \phi^{-\alpha}$,

$$z_{\text{quant}} \sim \left(\frac{M_{pl}/10}{\Lambda/(4\pi\sqrt{2\alpha(\alpha+1)})} \right)^{\frac{\alpha+2}{3(1+\omega_B)}},$$

is obtained by requiring a deviation of the effective potential of less than 1% and using the tracking solution during matter and radiation domination with equation of state $\omega_\phi = \frac{\alpha}{\alpha+2}(1+\omega_B) - 1$ [169], with $\omega_B = 0, 1/3$ respectively. For example, assuming $\Lambda \sim M_{pl}/100$ (where $M_{pl} \equiv 1/\sqrt{G}$), the tracking sets in at redshift $z_{\text{quant}} \sim 300$ for $\alpha = 2$ and $z_{\text{quant}} \sim 130$ for $\alpha = 1$. Similar bounds also hold for other types of potentials, e.g. like the SUGRA-potential [43], which are dominated by an inverse power-law behaviour at redshifts $z \gg 0.5$. For values $\Lambda \gtrsim M_{pl}/10$, there are large deviations from the tracking solution even at low redshifts and today, as is shown in figure 4.3 for an exemplary case with $V_{cl}(\phi) \propto \phi^{-\alpha}$. If the UV embedding scale Λ is of the order of the Planck scale, there is a direct transition from the slow roll regime with $\phi \lesssim \Lambda$, equation of state $\omega_\phi \sim -1$ and dark energy fraction $\Omega_\phi \lll 1$ in the flattened effective potential $V_{eff}(\phi)$ to the dark energy dominated accelerating solution for $\phi \gtrsim M_{pl}$ with $\Omega_\phi \to 1$ and $\omega_\phi \to -1$. Thus the solution never performs tracking with $\omega_\phi = -\frac{2}{\alpha+2}$ as for the classical potential $V_{cl}(\phi)$. In the case $\alpha = 1$, the equation of state today $\omega_{de} \equiv \omega_\phi(z = 0)$ is enhanced for $0.1 \lesssim \Lambda/M_{pl} \lesssim 1.3$ compared to the tracking value, and gets smaller for even larger[7] Λ, see figures 4.3 and 4.4. Moreover, the sign of $d\omega_\phi/dz$ can change depending on the value of the embedding scale Λ.

[7] Note that even when $\Lambda \gtrsim M_{pl}$ the pre-factor of the tadpole integral (4.4) is still sub-Planckian due to the loop factor $1/16\pi^2$.

4.2 Quantum Corrections from Matter Couplings

If the quintessence dynamics is governed by a low-energy effective theory which is determined by integrating out some unknown high energy degrees of freedom, involving e.g. quantum gravity, string theory or supergravity [58, 65], the low-energy theory should generically contain couplings and self-couplings of the quintessence field suppressed by some large scale, e.g. the Planck scale. In this section, radiative corrections induced by couplings between the quintessence field and "low-energy" particle species will be investigated. In this context, "low-energy" stands for degrees of freedom which exist well below the UV embedding scale of the quintessence field, including the well-known Standard Model particles.

On the one hand, such couplings can influence the properties of the Standard Model particles. The rolling quintessence field can, for example, drive a time-variation of particle masses and couplings over cosmological time-scales. Quintessence models leading to time-varying Standard Model masses and couplings, as well as mass-varying neutrinos (MaVaNs), have been frequently investigated, see e.g. [11, 15, 36, 44, 46, 56, 64, 83, 87, 95, 137, 145, 183, 184, 186]. In some cases such couplings can be directly constrained observationally, like for a coupling to Standard Model gauge fields [51]. For the photon, quintessence couplings can lead to tiny time-variations of the fine-structure constant α_{em} [54, 176], and a coupling to the gluons could manifest itself by a tiny time-variation of the proton mass [119, 158] over cosmic history. Such time-variations can be tested observationally, for example by comparing the frequency of spectral lines which depends on first and second powers of α_{em} respectively, from spectra emitted by quasars at various redshifts [54, 176]. Other constraints arise from the impact of time-varying couplings and masses on Big Bang Nucleosynthesis [50, 75, 172] predictions. Additionally, the coupling to a light quintessence field mediates a gravity-like long range force, leading to tiny apparent violations of the equivalence principle [172, 184], which is constrained by high-precision test of General Relativity [155, 181]. A significant interaction with dark matter is less constrained [13] and is considered in many contexts, e.g. [14, 96, 117, 189, 190], often accompanied by a varying dark matter mass (varying mass particles, VAMP) [62, 99, 114, 161].

On the other hand, the interactions of matter with the quintessence field can also influence the dynamics of the quintessence field itself via the backreaction effect, i.e. due to the contributions to the equation of motion of the scalar field originating from its matter interaction [96]. Illustratively, classical backreaction occurs due to a background matter density which the quintessence field feels due to the matter interaction. As a consequence, only the sum of the energy-momentum tensor of the quintessence field and of the interacting particles are conserved. Such a backreaction effect might trigger the cross-over from matter domination to quintessence domination. For example, a coupling to neutrinos, which leads to growing neutrino masses, slows down the rolling quintessence field due to the presence of the cosmic neutrino background. If the increase of the neutrino masses becomes strong enough, the rolling quintessence field gets stopped and yields a cosmic expansion similar to the cosmological constant which can be linked to the neutrino mass scale in specific models [11].

Due to the presence of vacuum quantum fluctuations, the interactions of the quintessence field lead to a backreaction effect even in the limit of vanishing background matter density. For cosmological matter densities, it turns out that this "quantum vacuum" backreaction generically overwhelms the classical backreaction for particle species much heavier than the dark energy scale around $\sim$ meV, as will be investigated in the following using the low-energy effective action.

Note that the low-energy effective action as defined in appendix B.1 captures quantum fluctuations of (renormalizable) Standard Model degrees of freedom, i.e. the quintessence field is treated as a classical background field here. Thus, the opposite limit as in the previous section is taken, where the impact of quantum fluctuations of the quintessence field itself has been investigated but matter couplings have been assumed to be absent. As discussed in appendix B.1, the *full* quantum effective

action for a coupled quintessence field can be obtained in two steps by first calculating the low-energy effective action by a path integral over the matter fields, and then calculating the effective action by a path integral over the quintessence field. This means, if the low-energy effective action discussed here is considered as the input for the "classical" action in the previous section, one could recover, in principle, the full effective action for a coupled quintessence field[8].
At lowest order in a derivative expansion of the low-energy effective action, the quantum vacuum backreaction is determined by the response of the quantum vacuum energy to variations of the quintessence field value. This response, in turn, is given by the quintessence-field-dependence of the low-energy effective potential, obtained from integrating out all matter fields heavier than the quintessence field.

4.2.1 Quantum Backreaction

Generically, the light classical mass $m_\phi^2(\phi) = V_{cl}''(\phi)$ of the quintessence field is unprotected against huge corrections induced by quantum fluctuations of heavier degrees of freedom coupled to the quintessence field ("hierarchy problem"). Furthermore, this is not only the case for the classical mass, but also for all higher derivatives $V_{cl}^{(k)}(\phi)$ and the slope $V_{cl}'(\phi)$ of the classical potential, as well as the total potential energy $V_{cl}(\phi)$. The latter is the "old cosmological constant problem", which is not addressed here. As before, the freedom to shift the effective potential by an arbitrary field-independent amount will be used instead, such that the total effective potential energy *today* has the value required for dark energy. Furthermore, if a huge amount of fine-tuning is accepted, also the quintessence mass and slope can be chosen to have the required values *today* by a suitable renormalization of the quantum fluctuations of (renormalizable) heavier degrees of freedom coupled to the quintessence field, like the Standard Model particles. However, even in this case there may still be huge corrections to the classical potential and its derivatives evaluated at a quintessence field value which is slightly displaced from todays value. Since the scalar field is rolling, such corrections would affect the behaviour of the quintessence field in the past, and could destroy some of the desired features (like tracking behaviour) of dynamical dark energy if they are too large.
The effective quintessence potential slope and mass are given by the first and second field derivatives of the low-energy effective quintessence potential, respectively. Their values *today* may be fixed by imposing renormalization conditions on the low-energy effective quintessence potential. Even if these are chosen such that the corrections to the quintessence potential are minimized *today*, the quantum vacuum still leads to a remaining "minimal response" on the dynamics of the quintessence field. In the following, the minimal response of one-loop quantum fluctuations of Standard Model particles on the quintessence field will be calculated. It will be shown that the low-energy effective potential can be renormalized by imposing three independent renormalization conditions (linked to the quartic, quadratic and logarithmic divergences) in this case. The minimal response is obtained by choosing the three renormalization conditions such that the quantum contributions to the low-energy effective potential $V_{eff}(\phi)$ and its first and second derivative vanish *today*,

$$\begin{aligned} V_{eff}(\phi = \phi_0) &= V_{cl}(\phi = \phi_0)\,, \\ V_{eff}'(\phi = \phi_0) &= V_{cl}'(\phi = \phi_0)\,, \\ V_{eff}''(\phi = \phi_0) &= V_{cl}''(\phi = \phi_0)\,, \end{aligned} \tag{4.48}$$

[8] This would require, however, to know details about the UV completion of the quintessence field combined with the Standard Model, which imposes constraints on the combination of the field-dependence of the self-interactions and the field-dependence of the couplings. At the level of approximation represented by the low-energy effective action, radiative corrections induced by quintessence couplings can be investigated in a model-independent way, i.e. no information about the details of the unknown UV completion is required.

where $\phi_0 \equiv \phi(t_0)$ is the quintessence field value today ($t = t_0$). Here $V_{cl}(\phi)$ represents the (renormalized) classical quintessence potential, in terms of which the low-energy effective potential can be expanded as

$$V_{eff}(\phi) = V_{cl}(\phi) + V_{1L}(\phi) + \dots ,$$

where $V(\phi)_{1L}$ denotes the (renormalized) one-loop contribution. Since the quintessence field generically changes only slowly on cosmological time-scales, one expects that the leading effect of quantum fluctuations is suppressed by a factor of the order

$$V_{cl}'''(\phi = \phi_0)_{1L}(\dot{\phi}(t_0)\,\Delta t)^3 , \tag{4.49}$$

with Δt of the order of a Hubble time, compared to the classical potential $V_{cl}(\phi)$.
The coupling between quintessence and any massive particle species j is modeled by assuming a general dependence of the mass on the quintessence field. This general form includes many interesting and potentially observable possibilities, like a time-varying (electron- or proton-) mass $m_j(\phi(t))$, a Yukawa coupling $dm_j/d\phi$ to fermions (e.g. protons and neutrons) mediating a new long-range gravity-like force, or a coupling between dark energy and dark matter (dm) of the form (see e.g. [13])

$$\dot{\rho}_{dm} + 3H\rho_{dm} = \rho_{dm}\frac{d\ln m_{dm}(\phi)}{d\phi}\dot{\phi} . \tag{4.50}$$

In terms of particle physics, a dependence of the mass on the dark energy field ϕ could be produced in many ways, which are just briefly mentioned here. One possibility would be a direct ϕ-dependence of the Higgs Yukawa couplings or of the Higgs VEV. For Majorana neutrinos, the Majorana mass of the right-handed neutrinos could depend on ϕ leading to varying neutrino masses via the seesaw mechanism [107, 186]. The mass of the proton and neutron could also vary through a variation of the QCD scale, for example induced by a ϕ-dependence of the GUT scale [185]. Additionally, a variation of the weak and electromagnetic gauge couplings could directly lead to a variation of the radiative corrections to the masses [81]. Possible parameterizations of the ϕ-dependence are $m(\phi) = m_0(1+\beta f(\phi/M_{pl}))$ with a dimensionless coupling parameter β and a function $f(x)$ of order unity or $m(\phi) = m_0\exp(\beta\phi/M_{pl})$ [83].

One-loop low-energy effective potential

The one-loop contribution to the low-energy effective potential for the quintessence field can be calculated from the functional determinants of the propagators with mass $m(\phi)$ (see section B.1),

$$V_{1L}(\phi) = \frac{1}{2}\int\frac{d^4k}{(2\pi)^4}\left(\sum_B g_B\ln(k^2+m_B(\phi)^2) - \sum_F g_F\ln(k^2+m_F(\phi)^2)\right) , \tag{4.51}$$

where B and F run over all bosons and fermions with internal degrees of freedom g_B and g_F respectively. The momentum has been Wick-rotated to Euclidean space. To implement the renormalization conditions (4.48), the following integrals are considered,

$$\begin{aligned} I_0(m^2) &\equiv \int\frac{d^4k}{(2\pi)^4}\ln(k^2+m^2) , \\ I_l(m^2) &\equiv \int\frac{d^4k}{(2\pi)^4}\frac{1}{(k^2+m^2)^l} = \frac{(-1)^{l-1}}{(l-1)!}\frac{d^l}{(dm^2)^l}I_0(m^2) , \end{aligned} \tag{4.52}$$

which are finite for $l \geq 3$. Following the procedure described in Ref. [179], the divergences in I_0, I_1 and I_2 are isolated by integrating I_3 with respect to m^2, yielding

$$I_0(m^2) \;=\; 2\int^{m^2} dm_3^2 \int^{m_3^2} dm_2^2 \int^{m_2^2} dm_1^2\, I_3(m_1^2) \quad + D_0 + D_1 m^2 + D_2 m^4\,, \tag{4.53}$$

with infinite integration constants D_0, D_1 and D_2. Thus one is led to introduce three counterterms proportional to m^0, m^2 and m^4 to cancel the divergences, which can be easily reabsorbed by a shift of the scalar potential $V_{cl}(\phi)$. This leaves a finite part I_0^{finite} of the same form as (4.53) but with the three infinite constants replaced by three finite parameters that have to be fixed by the three renormalization conditions (4.48). The appropriate choice can be expressed by choosing the lower limits in the integration over the mass m^2 to be equal to its todays value m_0^2,

$$\begin{aligned} I_0^{\text{finite}}(m^2;m_0^2) &= 2\int_{m_0^2}^{m^2} dm_3^2 \int_{m_0^2}^{m_3^2} dm_2^2 \int_{m_0^2}^{m_2^2} dm_1^2\, I_3(m_1^2) \\ &= \frac{1}{32\pi^2}\left(m^4\left(\ln\frac{m^2}{m_0^2} - \frac{3}{2}\right) + 2m^2 m_0^2 - \frac{1}{2}m_0^4\right), \end{aligned} \tag{4.54}$$

where $I_3(m^2) = 1/(32\pi^2 m^2)$ has been used.
Thus, the renormalized one-loop contribution to the low-energy effective potential which fulfills the renormalization conditions (4.48) is uniquely determined to be

$$V_{1L}(\phi) = \frac{1}{2}\left(\sum_B g_B I_0^{\text{finite}}(m_B(\phi)^2; m_B(\phi_0)^2) - \sum_F g_F I_0^{\text{finite}}(m_F(\phi)^2; m_F(\phi_0)^2)\right). \tag{4.55}$$

The higher loop corrections involve interaction vertices of the (Standard Model) matter particles. The one-loop result is exact in the limit of vanishing interaction strength. Thus, the best approximation to the full low-energy effective potential is obtained by applying the one-loop approximation to the effective low-energy degrees of freedom of the Standard Model, i.e. to nucleons instead of quarks.
The low-energy effective potential renormalized in this way can be regarded as the result of a fine-tuning of the contributions from the quantum fluctuations of heavy degrees of freedom to the quintessence potential energy, slope and mass at its todays values, i.e. evaluated for $\phi = \phi_0$. However, when the quintessence field had different values in the cosmic history, the cancellation does not occur any more and one expects the huge corrections of order m^4 to show up again, unless the coupling is extremely weak. Indeed, this argument yields extremely strong bounds for the variation of the masses with the rolling field ϕ [20, 81]. To obtain a quantitative limit it is required that the one-loop contribution to the potential should be subdominant during the relevant phases of cosmic history up to now, which is taken to be of the order of a Hubble time, in order to ensure that the quintessence dynamics, e.g. tracking behaviour, are not affected. For the corresponding ϕ-values this means that

$$V_{1L}(\phi) \ll V_{cl}(\phi)\,, \tag{4.56}$$

is required. If the one-loop effective potential (4.55) is Taylor-expanded around todays value ϕ_0, the first non-vanishing contribution is by construction of third order,

$$\begin{aligned} V_{1L}(\phi) &\approx \frac{1}{3!}V_{1L}'''(\phi_0)(\phi-\phi_0)^3 \approx \frac{1}{3!}\frac{1}{32\pi^2}\sum_j \frac{(-1)^{2s_j} g_j}{m_j(\phi_0)^2}\left(\frac{dm_j^2}{d\phi}(\phi-\phi_0)\right)^3 \\ &\approx \frac{1}{96\pi^2}\sum_j (-1)^{2s_j} g_j m_j(\phi_0)^4 \left(\frac{d\ln m_j^2}{d\ln V_{cl}''}\ln\frac{V_{cl}''(\phi)}{V_{cl}''(\phi_0)}\right)^3. \end{aligned} \tag{4.57}$$

Here the index j runs over bosons B and Fermions F (with spin s_j), and eq. (4.54) has been used. In the last line, the dependence on the quintessence field ϕ has been rewritten as a dependence on its mass $m_\phi^2 \equiv V_{cl}''(\phi)$. Today, the mass is of the order of the Hubble constant $H_0 \sim 10^{-33}$eV. For tracking quintessence models [169], the quintessence mass also scales proportional to the Hubble parameter H during cosmic evolution. Therefore, it is assumed that

$$\ln V_{cl}''(\phi)/V_{cl}''(\phi_0) \sim \ln H^2/H_0^2 \lesssim 3\ln(1+z)\,. \tag{4.58}$$

In order to investigate under which conditions the inequality (4.56) is fulfilled up to a redshift z_{max}, the most conservative assumption is to replace the logarithm in the last line in (4.57) by its maximal value of order $3\ln(1+z_{max})$ and the right hand side of (4.56) by the minimal value $V_{cl}(\phi_0)$. Furthermore, the inequality (4.56) is certainly fulfilled if each individual contribution to the one-loop potential (4.55) respects it. Altogether, under these assumptions the requirement (4.56) that the quintessence dynamics are unaltered up to a redshift z_{max} yields a bound for the variation of the mass m_j of a species j (with g_j internal degrees of freedom) with the quintessence mass scale $V_{cl}'' \sim H^2$

$$\left|\frac{d\ln m_j^2}{d\ln V_{cl}''}\right| \ll \frac{1}{3\ln(1+z_{max})}\left(\frac{96\pi^2 V_{cl}(\phi_0)}{g_j m_j(\phi_0)^4}\right)^{\frac{1}{3}}. \tag{4.59}$$

This bound is the main result of this section. It scales with mass like $m^{-4/3}$, i.e. the bound gets tighter for heavier particles. Inserting $z_{max} \sim z_{eq} \sim 10^3$ and expressing the potential energy

$$V_{cl}(\phi_0) = \frac{1-\omega_{de}}{2}\,\Omega_{de}\,\frac{3H_0^2}{8\pi G}$$

in terms of the dark energy fraction Ω_{de} and equation of state ω_{de} with $H_0 \sim 70\mathrm{km/s\,Mpc}$ yields

$$\left|\frac{d\ln m_j^2}{d\ln V_{cl}''}\right| \ll \left(\frac{1-\omega_{de}}{2}\frac{\Omega_{de}}{0.7}\right)^{\frac{1}{3}}\frac{1}{\sqrt[3]{g_j}}\left(\frac{1.3\mathrm{meV}}{m_j(\phi_0)}\right)^{\frac{4}{3}}. \tag{4.60}$$

Finally, it should be remarked that there remains the possibility that several masses $m_j(\phi)$ change in such a way that the *total* contribution to the low-energy effective potential stays small [81]. Generically, this would require an additional dynamical mechanism or symmetry which leads to such fine-tuned correlated changes at the required level. The total low-energy effective action would then depend on the details of such an unknown explicit mechanism, presumably closely related to the UV embedding. An example for such a mechanism could be based on supersymmetry, where the masses of fermions and their superpartners would have to change in the same way if SUSY was unbroken, so that their contributions in eq. (4.51) would always cancel. However, this is not the case below the SUSY breaking scale. The bound (4.59), which applies for mass-variations with arbitrary *relative* size for all species, is independent of the details of the unknown UV completion.

4.2.2 Bounds on Quintessence Couplings

The upper bound (4.59) can be directly related to upper bounds for the coupling strength to the long-range force mediated by the light scalar field, and for cosmic mass variation. The relative change of the mass m_j since redshift z can be related to the derivative $d\ln m_j^2/d\ln V_{cl}''$ using eq. (4.58),

$$\frac{\Delta m_j}{m_j} \approx \frac{d\ln m_j^2}{d\ln V_{cl}''}\ln\frac{V_{cl}''(\phi)}{V_{cl}''(\phi_0)} \lesssim 3\ln(1+z)\frac{d\ln m_j^2}{d\ln V_{cl}''}\,, \tag{4.61}$$

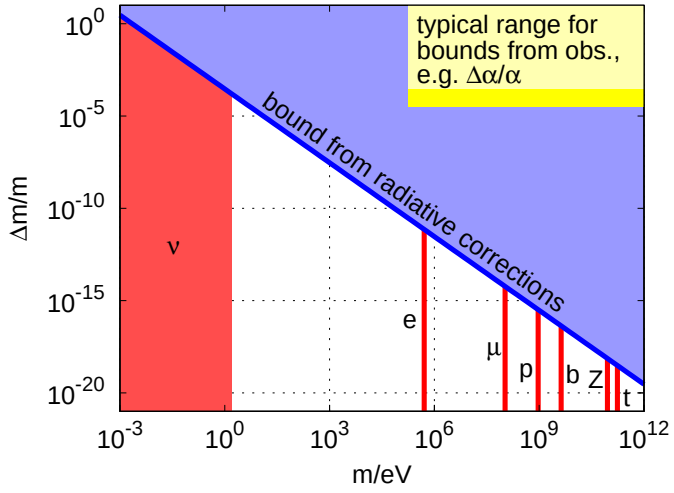

Figure 4.5: *Bounds for cosmic mass variation since redshift $z \sim 2$ from the radiative correction to the quintessence potential in dependence of the mass m. The red (vertical) lines mark the masses of some Standard Model particles. The limits inferred from observations, e.g. of $\Delta\alpha_{em}/\alpha_{em}$ strongly depend on the considered particle type and further assumptions, but typically lie around 10^{-4} to 10^{-5} [172].*

which means the bound (4.60) directly gives an upper limit for the relative mass variation of species j since redshift z. For example, for the variation of the electron mass since $z \sim 2$, the upper bound

$$\frac{\Delta m_e}{m_e} \ll 0.7 \cdot 10^{-11} \left(\frac{1-\omega_{de}}{2} \frac{\Omega_{de}}{0.7} \right)^{\frac{1}{3}}, \tag{4.62}$$

is obtained, which is at least six orders of magnitude below direct observational constraints for a change in the electron-proton mass ratio [172]. For heavier particles, the bounds are even stronger by a factor $(m_e/m)^{4/3}$, see figure 4.5, e.g. of the order $\Delta m_p/m_p \ll 10^{-15}$ for the proton. It should be emphasized that these upper bounds are valid under the assumption that the mass-variation is driven by a rolling scalar field with tracker properties, and in the absence of cancellations among the contributions from different particle species. In this case, however, the upper bound is a conservative upper bound due to the renormalization conditions which correspond to the "minimal response". This means that for any other choice of renormalization conditions, the upper bounds will be even stronger.

The only known particles which could have a sizeable mass variation due to the bound (4.60) are neutrinos. Thus, models considering mass-varying neutrinos or a connection between dark energy and neutrinos (see e.g. [11, 45, 95]) are not disfavored when considering quantum fluctuations. If the bound (4.60) is saturated, quantum backreaction effects are of the same order of magnitude as classical backreaction effects, and can have an impact on the quintessence dynamics in the recent past, where the turnover to a dark energy dominated cosmos occurs.
Fermions with quintessence-field-dependent masses are subject to a Yukawa-like interaction mediated by the quintessence field ("fifth force"), with typical range given by the inverse mass of the quintessence field $m_\phi^{-1} \sim H_0^{-1}$ and Yukawa coupling strength given by the derivative of the fermion mass [157],

$$y_j = \frac{dm_j(\phi)}{d\phi},$$

which can be described by a Yukawa potential (see section 2.3). Since this interaction leads to an apparent violation of the equivalence principle, an upper bound on the effective quintessence Yukawa couplings for nucleons can be inferred [157]. On the other hand, for a rolling quintessence field the coupling strength is constrained by the bound (4.59) via the relation

$$y_j = \frac{dm_j}{d\phi} = \frac{1}{2} m_j \frac{V_{cl}'''}{V_{cl}''} \frac{d\ln m_j^2}{d\ln V_{cl}''} \equiv \frac{m_j}{2M} \frac{d\ln m_j^2}{d\ln V_{cl}''},$$

where the scale height $M \equiv (d\ln V_{cl}''/d\phi)^{-1}$ of the quintessence mass was introduced, which is typically of the order of the Planck scale today [169]. For the proton and neutron an upper limit

$$y_{p,n} \ll 0.4 \cdot 10^{-35} \left(\frac{M_{pl}}{M}\right) \left(\frac{1\text{GeV}}{m_{p,n}}\right)^{\frac{1}{3}} \left(\frac{1-\omega_{de}}{2} \frac{\Omega_{de}}{0.7}\right)^{\frac{1}{3}}, \tag{4.63}$$

is obtained which is far below the limit from the tests of the equivalence principle [157], see eq. (2.17). These limits can be compared to the corresponding gravitational coupling given by m_j/M_{pl}, e.g. of the order 10^{-19} for the nucleons. Thus the bound in eq. (4.60) also directly gives a bound for the *relative* suppression

$$\beta_j \equiv \frac{y_j}{m_j/M_{pl}} = \frac{d\ln m_j}{d(\phi/M_{pl})}$$

of the coupling strength to the fifth force mediated by the quintessence field compared to the gravitational coupling, giving (for $M \sim M_{pl}$, $\omega_{de}+1 \lesssim 1$, $\Omega_{de} \sim 0.7$)

$$\beta_j \lesssim \frac{\Delta m_j}{m_j} \ll 4 \left(\frac{\text{meV}}{m_j}\right)^{4/3} \sim 10^{-11} \left(\frac{m_e}{m_j}\right)^{4/3}. \tag{4.64}$$

Note that the bound from eq. (4.63) also holds for other species (with mass-scaling $\sim m^{-1/3}$), whose quintessence couplings are in general *not* constrained by the tests of the equivalence principle [157]. This is also true for dark matter, if it consists of a new heavy species like e.g. a weakly interacting massive particle (WIMP), which severely constrains any coupling via a ϕ-dependent mass,

$$y_{dm} = dm_{dm}/d\phi \ll 10^{-36}\,(\text{TeV}/m_{dm})^{1/3},$$

corresponding to a limit of the order

$$\Delta m_{dm}/m_{dm} \ll 10^{-19}\,(\text{TeV}/m_{dm})^{4/3},$$

for a mass variation between $z \sim 2$ and now from eq. (4.64).

4.3 Quantum Corrections from Gravitational Coupling

Since any dynamical dark energy scenario is necessarily situated in a curved space-time setting, for example described by a Robertson-Walker metric, it is important to study the quantum corrections on such a background. In ϕ^4-theory, one-loop radiative corrections induce a non-minimal coupling (NMC)

$$\xi R\phi^2/2$$

between the curvature scalar R and the scalar field ϕ, with a dimensionless coupling ξ [35]. Even if the renormalization condition

$$\xi(\mu_0) = 0$$

is chosen at some renormalization point characterized by a scale $\mu = \mu_0$, the corresponding renormalization-group improved effective action which is applicable at very different scales $\mu \neq \mu_0$ contains a non-zero non-minimal coupling as described by the renormalization group running of $\xi(\mu)$ [92, 116].
For a scalar field with non-zero field expectation value ϕ, the non-minimal coupling $\xi R\phi^2/2$ leads to a rescaling of the Newton constant $G = M_{pl}^{-2}$ (see section 2.3),

$$\frac{1}{16\pi G_{eff}(\phi)} = \frac{1}{16\pi G} + \frac{1}{2}\xi\phi^2\,,$$

where the effective Newton constant $G_{eff}(\phi)$ appears in the gravitational force law for systems which are small compared to the time- and space-scales on which $\phi = \phi(x)$ varies. A rolling quintessence field with a non-minimal coupling which is linear in R thus leads to a time-variation of the (effective) Newton "constant" on cosmic time-scales,

$$\frac{\Delta G_{eff}}{G_{eff}} \equiv \frac{G_{eff}(\phi(t)) - G_{eff}(\phi(t_0))}{G_{eff}(\phi(t_0))} = -\frac{\xi}{2}\left(\phi^2(t) - \phi^2(t_0)\right) 16\pi G_{eff}(\phi(t))\,,$$

which is constrained by precision tests of General Relativity and Big Bang Nucleosynthesis [55, 155, 181].
For tracking quintessence models, the scalar field value today is of the order of the Planck scale, $\phi(t_0)^2 \sim M_{pl}^2 = 1/G$. Thus, a non-minimal coupling of the form $R\phi^2$ potentially yields a large contribution to the effective Newton constant, unless the coupling ξ is small enough. For inverse-power-law potentials, constraints on the time-variation of the Newton constant lead to an upper limit $|\xi| \lesssim 3 \cdot 10^{-2}$ [55, 155].
Radiative corrections which lead to a non-minimal coupling of the form $R\phi^2$ as for the ϕ^4-theory could thus lead to a conflict with experimental constraints on a time-varying Newton constant. However, dynamical dark energy scenarios making use of a scalar field involve non-renormalizable interactions suppressed by some high-energy scale up to the Planck scale, described by a tracker potential $V_{cl}(\phi)$, with properties which are very different compared to a ϕ^4-potential. Therefore it is important to include the non-renormalizable interactions in the investigation of radiatively induced non-minimal couplings between the dark energy scalar field and gravity.
In the following, this analysis will be performed based on the semi-classical[9] one-loop effective action on a curved background discussed in appendix B.2, which is obtained using Heat Kernel Expansion [35] and zeta-function regularization [91, 110].

[9] The metric $g_{\mu\nu}(x)$ is treated as a classical background field in this approach.

4.3.1 Radiatively induced Non-minimal Coupling for ϕ^4-Theory

The action of a scalar field in curved space-time with standard kinetic term,

$$S[\phi, g_{\mu\nu}] = \int d^4x \sqrt{-g} \left(\frac{1}{2} g^{\mu\nu} \partial_\mu \phi \partial_\nu \phi - V_{cl}(\phi) \right), \tag{4.65}$$

contains minimal couplings to the metric via the integration measure and the contraction of the space-time derivatives in the kinetic term required by general coordinate invariance. In quantum field theory, radiative corrections to the classical action furthermore lead to additional non-minimal couplings to gravity.

Before investigating non-minimal couplings for a quintessence theory, the calculation of radiative corrections in curved space-time will be reviewed for a theory described by the ϕ^4-potential

$$V_{cl}(\phi) = \Lambda + m^2\phi^2/2 + \lambda\phi^4/4!,$$

in order to compare the generalized formalism discussed in appendix B, which is also suitable for the quintessence case, with known results. The minimal scalar action in curved space-time which is stable under one-loop quantum corrections is [35, 92, 116]

$$\begin{aligned} S[\phi, g_{\mu\nu}] &= \int d^4x \sqrt{-g}\, \mathcal{L}(\phi(x), g_{\mu\nu}(x)) \\ &= \int d^4x \sqrt{-g} \left(\frac{1}{2} g^{\mu\nu} \partial_\mu \phi \partial_\nu \phi - V(\phi, R) + \varepsilon_1 C + \varepsilon_2 G + \Box B(\phi, R) \right), \end{aligned} \tag{4.66}$$

where

$$\begin{aligned} V(\phi, R) &= V_{cl}(\phi) + \frac{1}{2}\xi R\phi^2 + \frac{R}{16\pi G} + \varepsilon_0 R^2, \\ B(\phi, R) &= \varepsilon_3\phi^2 + \varepsilon_4 R, \\ C &= R_{\mu\nu\rho\sigma}R^{\mu\nu\rho\sigma} - 2R_{\mu\nu}R^{\mu\nu} + R^2/3, \\ G &= R_{\mu\nu\rho\sigma}R^{\mu\nu\rho\sigma} - 4R_{\mu\nu}R^{\mu\nu} + R^2, \end{aligned} \tag{4.67}$$

with dimensionless constants ε_i and including the Einstein-Hilbert term linear in R[10]. The necessity to include all the upper terms can be seen from the renormalization group improved effective action, which arises in the following way. Assume that some given approximation to the effective action contains parameters which can describe the dynamics around a typical energy scale μ_0. At another energy scale $\mu \neq \mu_0$, radiative corrections may change the effective values of these parameters, as described by the renormalization group. Then the renormalization group improved effective action is an improved approximation to the effective action where the running of the parameters is incorporated such that it is applicable also at scales $\mu \neq \mu_0$ (see appendix B).

The renormalization-group improvement of the one-loop effective action ("leading logarithm approximation") is accomplished by starting with the classical action at the reference scale μ_0, and taking the running into account as described by the renormalization group equations obtained from the one-loop approximation. As shown in appendix B, the renormalization-group improved effective action in leading logarithm approximation for a scalar in curved space and for the renormalization scheme discussed in section B.2 is

$$\begin{aligned} \Gamma_{LL}[\phi, g_{\mu\nu}; \mu] &= \int d^4x \sqrt{-g} \left(\frac{1}{2} g^{\mu\nu} \partial_\mu \phi \partial_\nu \phi - V_{LL}(\phi, R; \mu) \right. \\ &\quad \left. + \varepsilon_1(\mu) C + \varepsilon_2(\mu) G + \Box B_{LL}(\phi, R; \mu) \right), \end{aligned} \tag{4.68}$$

[10] The latter two terms are total derivatives and thus not relevant for the dynamics, but they are needed for the cancellation of divergences and do appear in the dynamics if their running is considered [92, 116].

where, for ϕ^4-theory, it is possible to make the ansatz

$$\begin{aligned} V_{LL}(\phi,R;\mu) &= \Lambda(\mu)+\frac{m^2(\mu)}{2}\phi^2+\frac{\lambda(\mu)}{4!}\phi^4+\frac{1}{2}\xi(\mu)R\phi^2+\frac{R}{16\pi G(\mu)}+\varepsilon_0(\mu)R^2, \\ B_{LL}(\phi,R;\mu) &= \varepsilon_3(\mu)\phi^2+\varepsilon_4(\mu)R\,. \end{aligned}$$

Inserting the ansatz into the partial differential equations (B.19) for V_{LL} and B_{LL} yields

$$\begin{aligned} \frac{\partial V_{LL}}{\partial t} &= \frac{d\Lambda}{dt}+\frac{1}{2}\frac{dm^2}{dt}\phi^2+\frac{1}{4!}\frac{d\lambda}{dt}\phi^4+\frac{1}{2}\frac{d\xi}{dt}R\phi^2-\frac{R}{16\pi G^2}\frac{dG}{dt}+\frac{d\varepsilon_0}{dt}R^2 \\ &= \frac{1}{64\pi^2}\left(\frac{\partial^2 V_{LL}}{\partial\phi^2}-\frac{R}{6}\right)^2=\frac{1}{64\pi^2}\left(m(\mu)^2+\frac{\lambda(\mu)}{2}\phi^2+\left(\xi(\mu)-\frac{1}{6}\right)R\right)^2 \\ \frac{\partial\Box B_{LL}}{\partial t} &= \frac{d\varepsilon_3}{dt}\Box\phi^2+\frac{d\varepsilon_4}{dt}\Box R \\ &= \frac{1}{192\pi^2}\left(\frac{\partial^2\Box V_{LL}}{\partial\phi^2}-\frac{\Box R}{5}\right)=\frac{1}{192\pi^2}\left(\frac{\lambda(\mu)}{2}\Box\phi^2+\left(\xi(\mu)-\frac{1}{5}\right)\Box R\right), \end{aligned}$$

where $t=\ln(\mu^2/\mu_0^2)$. By comparing the coefficients of the terms proportional to ϕ^2, ϕ^4, $R\phi^2$, R, R^2 and $\phi^0R^0=$ const in the two upper expressions for $\partial V_{LL}/\partial t$ and the coefficients of the terms proportional to $\Box\phi^2$ and $\Box R$ in the two upper expressions for $\partial\Box B_{LL}/\partial t$, the one-loop renormalization group equations for ϕ^4-theory in curved space [92, 116] within the renormalization scheme from section B.2 are obtained,

$$\begin{aligned} \frac{d\lambda}{dt} &= \frac{3\lambda^2}{32\pi^2}, & \frac{dm^2}{dt} &= \frac{\lambda m^2}{32\pi^2}, \\ \frac{dG}{dt} &= -\frac{8\pi G^2m^2(\xi-\frac{1}{6})}{32\pi^2}, & \frac{d\Lambda}{dt} &= \frac{m^4}{64\pi^2}, \\ \frac{d\xi}{dt} &= \frac{\lambda(\xi-\frac{1}{6})}{64\pi^2}, & \frac{d\varepsilon_0}{dt} &= \frac{(\xi-\frac{1}{6})^2}{64\pi^2}, \\ \frac{d\varepsilon_1}{dt} &= -\frac{1}{120\cdot 32\pi^2}, & \frac{d\varepsilon_2}{dt} &= -\frac{1}{360\cdot 32\pi^2}, \\ \frac{d\varepsilon_3}{dt} &= \frac{\lambda}{12\cdot 32\pi^2}, & \frac{d\varepsilon_4}{dt} &= \frac{\xi-\frac{1}{5}}{6\cdot 32\pi^2}, \end{aligned} \tag{4.69}$$

where the β-functions from eq. (B.17) for the parameters ε_1 and ε_2 were also included. The first line, which describes the running of the quartic coupling and the mass, is identical to the $\overline{\text{MS}}$ result in flat space. The second line describes the running of the Newton- and the cosmological constants. The running of the non-minimal coupling ξ is given in the third line, along with the running of the coefficients of higher curvature scalars whose presence in the action leads to modifications of standard General Relativity. For non-zero quartic coupling λ, the renormalization group equation for the non-minimal coupling ξ has *no* fixed point at $\xi=0$. Thus, even if the renormalization condition $\xi(\mu_0)=0$ is imposed at the reference scale $\mu=\mu_0$, a radiatively induced non-minimal coupling is generated in the renormalization-group improved effective action applicable at other scales $\mu\neq\mu_0$. For generic values $\lambda\neq 0$, $m^2\neq 0$ and $\xi\neq 1/6$, the same is true for all the running parameters, for which reason the action (4.66) is indeed the minimal scalar action in curved space which is stable under one-loop renormalization group running. Note that the fixed point $\xi=1/6$ of the non-minimal coupling corresponds to the value of ξ for which the classical action is conformal invariant in the limit $m,\Lambda,G^{-1}\to 0$ [35].

4.3.2 Radiatively induced Non-minimal Coupling for Quintessence

In order to study radiatively induced non-minimal couplings for a quintessence field, it is desirable to generalize the renormalization group equations to general scalar potentials $V_{cl}(\phi)$, for which effective field theory is applicable. Within effective field theory, ultraviolet divergences are absent since the theory is only valid up to the UV embedding scale Λ. Nevertheless, for a given approximation to the effective action within effective field theory, which can describe the dynamics around an energy scale $\mu_0 \ll \Lambda$, radiative corrections can lead to a rescaling of the effective parameters at different scales $\mu \neq \mu_0$, $\mu \ll \Lambda$. Similarly as before, this scale-dependence can be incorporated in a renormalization group improved effective action which yields generalized renormalization group equations for an effective field theory below the embedding scale.
For a quintessence field, the UV embedding scale is typically of the order of the Planck or the GUT scale, whereas the dynamical scale is of the order of the Hubble scale $\mu \sim H(t) \lll \Lambda$. If it is assumed, for example, that non-minimal gravitational couplings of the quintessence field are absent for some reference scale $\mu_0 \sim H(t_0) \lll \Lambda$, non-minimal couplings can be generated radiatively at different scales $\mu \sim H(t)$. Since the dynamical scale $H(t)$ changes (slowly) in cosmic history, radiatively generated non-minimal couplings could manifest themselves, as described above, by a time-variation of the effective Newton constant. In general, non-minimal couplings between the field ϕ and the curvature scalar R which are linear in R, i.e. of the form $f_1(\phi)R$ with some (scale-dependent) function $f_1(\phi)$, lead to an effective Newton "constant"

$$\frac{1}{16\pi G_{eff}(\phi)} = \frac{1}{16\pi G} + f_1(\phi)\,,$$

which varies over cosmic time-scales due to the rolling quintessence field $\phi(t)$. Such a time-variation is constrained observationally between Big Bang Nucleosynthesis (BBN) $H(t_{BBN}) \sim T_{BBN}^2/M_{pl} \sim 10^{-15}$eV and today $H_0 \sim 10^{-33}$eV to be less than $\sim 20\%$ [181]. Therefore, it is important that radiatively induced non-minimal couplings from renormalization group running between these scales do not violate this bound. Since both scales are far below the UV scale Λ and far below any other thresholds of known particle masses, one may focus on the logarithmic scale dependence $\sim \ln(\mu^2/\mu_0^2)$ as described by the renormalization group derived from the one-loop β-functions obtained via zeta-function regularization [110] in curved space (see appendix B).
In the following it will be shown that the minimal scalar action in curved space-time with general scalar potential $V_{cl}(\phi)$, which is stable under one-loop quantum corrections, has the same form as for ϕ^4-theory, see eq. (4.66), however with a "generalized potential" $V(\phi,R)$ and a function $B(\phi,R)$ with a more general dependence on ϕ and R. In order to capture radiatively induced non-minimal couplings involving higher powers of ϕ and R, the ansatz

$$\begin{aligned} V(\phi,R) &= \sum_{nm} c_{nm}\phi^n R^m\,, \\ B(\phi,R) &= \sum_{nm} \bar{c}_{nm}\phi^n R^m\,, \end{aligned} \tag{4.70}$$

is made, with coefficients c_{nm} and $\bar{c}_{nm}$, respectively. This ansatz is possible for all functions which can be written as a Taylor series around $\phi = 0$ and $R = 0$. Equivalently, it is possible to expand around any other values $\phi = \phi_0$ and $R = R_0$, if necessary. Since the final result does not depend on the choice of the expansion point, it is set to zero for simplicity. It should be emphasized however, that the result is applicable to all theories where $V(\phi,R)$ and $B(\phi,R)$, including especially the potential $V_{cl}(\phi)$, possess Taylor expansions around at least one arbitrary expansion point, which does not necessarily have to be at $\phi = R = 0$. The generalized potential $V(\phi,R)$ and the function $B(\phi,R)$ from eq. (4.67) for

ϕ^4-theory correspond to the choice

$$c_{00}=\Lambda,\; c_{20}=\frac{m^2}{2},\; c_{40}=\frac{\lambda}{4!},\; c_{21}=\frac{\xi}{2},\; c_{01}=\frac{1}{16\pi G},\; c_{02}=\varepsilon_0,\; \bar{c}_{20}=\varepsilon_3,\; \bar{c}_{01}=\varepsilon_4\,.$$

The one-loop effective action for the action given in eq. (4.66) with $V(\phi,R)$ and $B(\phi,R)$ parameterized as in the ansatz (4.70) has been derived in appendix B.2. Inserting the first three terms of the Heat Kernel Expansion (B.15) into eq. (B.14) yields

$$\begin{aligned}\Gamma[\phi,g_{\mu\nu}]_{1L} &= \int\frac{d^4x}{32\pi^2}\sqrt{-g}\Bigg[-\frac{(X-R/6)^2}{2}\left(\ln\frac{X-R/6}{\mu^2}-\frac{3}{2}\right)\\ &\quad-\left(\frac{1}{120}C-\frac{1}{360}G-\frac{1}{30}\Box R+\frac{1}{6}\Box X\right)\ln\frac{X-R/6}{\mu^2}+\sum_{j=3}^{\infty}\frac{\bar{g}_j(x,x)(j-3)!}{(X-R/6)^{j-2}}\Bigg]\\ &\equiv \Gamma_{1L}[\phi,g_{\mu\nu};\mu]+\Gamma_{1L,HD}[\phi,g_{\mu\nu}]\,,\end{aligned}\tag{4.71}$$

where

$$X=X(\phi,R)=\partial^2V(\phi,R)/\partial\phi^2\,,$$

and μ is the renormalization scale. In the last line of eq. (4.71), the contribution $\Gamma_{1L,HD}[\phi,g_{\mu\nu}]$ is defined, which contains the sum over the higher terms of the Heat Kernel Expansion ($j\geq 3$). These involve curvature scalars built from higher powers of the curvature tensor and higher derivative terms which are independent of the renormalization scale (see appendix B.2 and Ref. [121]). In contrast to this, the first two terms (which correspond to $j=0,2$, see eq.(B.15)), denoted by $\Gamma_{1L}[\phi,g_{\mu\nu};\mu]$, do depend on μ.

In appendix B, the renormalization group improved effective action for the one-loop effective action (4.71) was derived. It has a similar form as for ϕ^4-theory, see eq. (4.68). However, it contains a renormalization group improved "generalized potential" $V_{LL}(\phi,R;\mu)$ and a function $B_{LL}(\phi,R;\mu)$ with a more general dependence on ϕ and R compared to ϕ^4-theory. The scale-dependence of V_{LL} and B_{LL} is determined by the partial differential equations (see eq. (B.19), $t=\ln(\mu^2/\mu_0^2)$)

$$\begin{aligned}\frac{\partial}{\partial t}V_{LL}(\phi,R;\mu) &= \frac{1}{64\pi^2}\left(\frac{\partial^2V_{LL}(\phi,R;\mu)}{\partial\phi^2}-\frac{R}{6}\right)^2,\; V_{LL}(\phi,R;\mu_0)=V(\phi,R),\\ \frac{\partial}{\partial t}\Box B_{LL}(\phi,R;\mu) &= \frac{1}{192\pi^2}\left(\frac{\partial^2\Box V_{LL}(\phi,R;\mu)}{\partial\phi^2}-\frac{\Box R}{5}\right),\; \Box B_{LL}(\phi,R;\mu_0)=0\,.\end{aligned}$$

This result is indeed independent of the choice of the expansion point in eq. (4.70). The running of the parameters $\varepsilon_1(\mu)$ and $\varepsilon_2(\mu)$ in the action (4.68) is identical to that of ϕ^4-theory (see eqs. (B.17) and (4.69)).

In order to investigate the radiatively induced non-minimal couplings, the "generalized potential" $V_{LL}(\phi,R;\mu)$ is expanded in powers of R,

$$V_{LL}(\phi,R;\mu)=f_0(\phi;\mu)+f_1(\phi;\mu)R+f_2(\phi;\mu)R^2+\cdots\,.$$

As discussed above, the non-minimal coupling of the form $f_1(\phi;\mu)R$ which is linear in R results in a time-variation of the effective Newton constant. The partial differential equation determining $V_{LL}(\phi,R;\mu)$ yields a hierarchy of partial differential equations for $\{f_k(\phi;\mu)\,|\,0\leq k\leq N\}$. The lowest two are

$$\begin{aligned}\frac{\partial}{\partial t}f_0(\phi;\mu) &= \frac{1}{64\pi^2}\left(\frac{\partial^2f_0(\phi;\mu)}{\partial\phi^2}\right)^2,\quad f_0(\phi;\mu_0)=V_{cl}(\phi)\,,\\ \frac{\partial}{\partial t}f_1(\phi;\mu) &= \frac{1}{32\pi^2}\frac{\partial^2f_0(\phi;\mu)}{\partial\phi^2}\left(\frac{\partial^2f_1(\phi;\mu)}{\partial\phi^2}-\frac{1}{6}\right),\quad f_1(\phi;\mu_0)=f_1(\phi)\,.\end{aligned}\tag{4.72}$$

The renormalization group equation in the first line describes the running of the quintessence potential, and the second line yields the running of the non-minimal coupling which is linear in R ("NMC"). The renormalization group equations for ϕ^4-theory are recovered by inserting $f_0(\phi;\mu) = \Lambda(\mu) + m^2(\mu)\phi^2/2 + \lambda(\mu)\phi^4/4!$ and $f_1(\phi;\mu)R = R/(16\pi G(\mu)) + \xi(\mu)R\phi^2/2$. It is emphasized that, in general, the functional dependence of $f_0(\phi;\mu)$ and $f_1(\phi;\mu)$ on the field is only subject to the restriction that it can be written as a Taylor series around some field value $\phi = \phi_0$, which need not necessarily be $\phi_0 = 0$. The partial differential equation for $B_{LL}(\phi, R;\mu)$ can be decomposed similarly by an expansion in R.

Here, it is demanded that the potential is given by a (tracker) quintessence potential $V_{cl}(\phi)$ at the reference scale μ_0. Furthermore, a renormalization condition $f_1(\phi;\mu_0) = f_1(\phi)$ is imposed on the non-minimal coupling parameterized by the function $f_1(\phi)$. If

$$\partial f_1(\phi;\mu_0)/\partial\phi = \partial f_1(\phi)/\partial\phi \equiv 0\,, \qquad \text{(mNMC)} \tag{4.73}$$

is set, i.e. $f_1(\phi;\mu) \equiv$ const, then the quintessence field is minimally coupled at the reference scale μ_0 (e.g. $\mu_0 \sim H(t_{BBN}) \sim 10^{-15}$eV). Note that the partial differential equation describing the running of $f_1(\phi;\mu)$ does *not* have a fixed point at $f_1(\phi;\mu) \equiv$ const. Therefore, the renormalization group improved effective action contains a non-vanishing NMC at all scales $\mu \neq \mu_0$ (e.g. $\mu \sim H_0 \sim 10^{-33}$eV) even though $\partial f_1(\phi;\mu_0)/\partial\phi \equiv 0$, which is purely generated by radiative corrections. Since this non-minimal gravitational coupling is unavoidably present in the theory, it is denoted by mNMC ("minimal NMC").

Note that the scale-dependence of the functions $f_0(\phi;\mu)$ and $f_1(\phi;\mu)$ already includes the running of the "cosmological constant" $\Lambda(\mu) \equiv f_0(\phi;\mu)|_{\phi=0}$ and the "Newton constant" $1/(16\pi G(\mu)) \equiv f_1(\phi;\mu)|_{\phi=0}$, respectively. In fact, the non-minimal coupling[11] $f_1(\phi(t);\mu(\phi(t)))$ for a rolling field $\phi(t)$ evaluated with a renormalization scale of the order of the dynamical scale of the quintessence field $\mu^2(\phi(t)) \sim m_\phi^2(\phi(t))$ encodes the time-variation of the effective Newton "constant" (which is relevant for astrophysical and laboratory measurements since it appears in the gravitational force law)

$$\frac{1}{16\pi G_{eff}(\phi(t))} = \frac{1}{16\pi G} + f_1(\phi(t);\mu(\phi(t)))\,,$$

caused by both the renormalization group running and the rolling quintessence field, in a unified manner[12]. It is emphasized that the choice of the renormalization scale μ is not free here, but is fixed by the matching of the renormalization group improved effective potential with the one-loop effective potential (see appendix B and Ref. [60]),

$$\begin{aligned} \mu^2(\phi) &\equiv V_{cl}''(\phi) + \left(\xi_0 - \frac{1}{6}\right)R \\ &= \left[\frac{9}{2}\Gamma\left(1-\omega_\phi^{*2}\right) + 9\left(\xi_0 - \frac{1}{6}\right)\left(\omega_B - \frac{1}{3}\right)\right]H^2 \;\propto\; H^2\,, \end{aligned} \tag{4.74}$$

where the renormalization condition $f_1(\phi;\mu_0) = \xi_0\phi^2/2 + \text{const}$ has been inserted as an example, as well as the dynamical mass (2.13) of a tracker quintessence potential $V_{cl}(\phi)$ and the curvature scalar R of a FRW solution with $\omega_B = 0, 1/3$ during matter/radiation domination. The mNMC (4.73) corresponds to the choice $\xi_0 = 0$.

[11] For the rolling quintessence field $\phi(t)$, t denotes the time.

[12] Similarly, the time-variation of the effective energy density $\rho_\phi = \frac{1}{2}\dot\phi^2 + f_0(\phi(t);\mu(\phi(t)))$ encodes the time-variation of dark energy caused by both the rolling quintessence field and the renormalization group running of the cosmological constant due to quantum fluctuations of the quintessence field in a unified manner. However, the latter is negligible here (see below).

Finally, note that the renormalization group equation (4.72) for the non-minimal coupling $f_1(\phi;\mu)R$ has fixed-points of the form

$$f_1(\phi;\mu) = f_1^*(\phi) \equiv \frac{1}{16\pi G} + b\phi + \frac{1}{2}\xi^*\phi^2,$$

for the "conformal coupling" $\xi^* = 1/6$ and arbitrary constant values G and b.

4.3.3 Robustness of Quintessence Actions

The impact of radiative corrections which are not encoded in the effective potential, i.e. non-minimal gravitational couplings and corrections to the kinetic term, on tracker quintessence fields will now be investigated. Therefore, the results of the previous section are applied to a quintessence field with classical action containing a tracker potential $V_{cl}(\phi)$, characterized by the power-counting rules (4.7).

Linear non-minimal gravitational coupling

The renormalization group improved effective action contains the scale-dependent "generalized potential" $V_{LL}(\phi,R;\mu) = \sum_{k=0}^{\infty} f_k(\phi;\mu)R^k$, which simultaneously encodes the renormalization group running of the potential $f_0(\phi;\mu)$ and all non-minimal couplings between the field ϕ and the curvature scalar R in leading logarithm approximation. It is determined by the partial differential equation (B.19), which can be decomposed into a hierarchy of partial differential equations for the contributions $f_k(\phi;\mu)$, see eq. (4.72).
For scales where $|t| = |\ln(\mu^2/\mu_0^2)| \ll 32\pi^2$, the solution of the renormalization group equations (4.72) for $f_k(\phi;\mu)$ $(k = 0, 1)$ in linear approximation is

$$\begin{aligned} f_0(\phi;\mu) &= V_{cl}(\phi) + \frac{t}{64\pi^2}\left(V_{cl}''(\phi)\right)^2 + \mathcal{O}\left(\frac{t}{32\pi^2}\right)^2, \\ f_1(\phi;\mu) &= f_1(\phi) + \frac{t}{32\pi^2}V_{cl}''(\phi)\left(f_1''(\phi) - \frac{1}{6}\right)^2 + \mathcal{O}\left(\frac{t}{32\pi^2}\right)^2. \end{aligned} \tag{4.75}$$

For example, for the running between the Big Bang Nucleosynthesis era, $\mu_0 \sim H(t_{BBN}) \sim 10^{-15}$eV, and today, $\mu \sim H_0 \sim 10^{-33}$eV, $|t|/(32\pi^2) \approx 0.26$. According to the power counting rules (4.7), the running of the quintessence potential is completely negligible, since the scale-dependent part proportional to $V_{cl}''(\phi)^2 \sim V_{cl}(\phi)(V_{cl}(\phi)/M^4)$ is suppressed by the tiny factor $V_{cl}(\phi)/M^4 \lll 1$, which is of the order 10^{-120} today, compared to the classical potential. This is in agreement with the suppression of logarithmic corrections with respect to the UV scale found in section 4.1.
Assuming, for example, that the non-minimal coupling at the reference scale is quadratic in the field, $f_1(\phi;\mu_0) = f_1(\phi) = \xi_0\phi^2/2 + \text{const}$, the radiative correction to the non-minimal coupling is

$$f_1(\phi;\mu) = f_1(\phi;\mu_0) + \frac{t}{32\pi^2}V_{cl}''(\phi)\left(\xi_0 - \frac{1}{6}\right)^2 + \mathcal{O}\left(\frac{t}{32\pi^2}\right)^2. \tag{4.76}$$

The combined effect of the rolling quintessence field and the running non-minimal coupling thus leads to a time-variation of the effective Newton constant given by

$$\begin{aligned} \frac{\Delta G_{eff}}{G_{eff}} &= \frac{G_{eff}(\phi(t)) - G_{eff}(\phi(t_0))}{G_{eff}(\phi(t_0))} = -\Big(f_1(\phi(t);\mu) - f_1(\phi(t_0);\mu_0)\Big)\,16\pi G_{eff}(\phi(t)) \\ &= -\frac{\xi_0}{2}\Big(\phi^2(t) - \phi^2(t_0)\Big)\,16\pi G_{eff}(\phi(t)) \\ &\quad -\frac{1}{32\pi^2}\ln\left(\frac{\mu^2(\phi(t))}{\mu_0^2}\right)V_{cl}''(\phi(t))\left(\xi_0 - \frac{1}{6}\right)^2 16\pi G_{eff}(\phi(t)), \end{aligned}$$

where the renormalization scale is given by eq. (4.74). The first contribution is the classical contribution, and the second is the one induced by radiative corrections. Even if the non-minimal coupling at the reference scale μ_0 vanishes, i.e. $\xi_0 = 0$, radiative corrections induce a non-minimal coupling ("mNMC") which leads to a time-variation of the effective Newton constant.
For tracker quintessence fields, the time variation of the effective Newton constant between BBN and today is ($G_{eff} \equiv G_{obs} = 1/M_{pl}^2$, $\Delta\phi^2 \equiv \phi^2(t) - \phi^2(t_0)$)

$$\frac{\Delta G_{eff}}{G_{eff}} \approx -8\pi\xi_0 \frac{\Delta\phi^2}{M_{pl}^2} - \frac{1}{32\pi^2} \ln\left(\frac{H_0^2}{H_{BBN}^2}\right) \frac{V_{cl}''(\phi(t))}{H_0^2} \left(\xi_0 - \frac{1}{6}\right)^2 \frac{16\pi H_0^2}{M_{pl}^2}\,.$$

The first term on the right-hand side is the classical contribution. It vanishes if the quintessence field is minimally coupled at the reference (BBN) scale, i.e. in the limit $\xi_0 \to 0$. The second term on the right-hand is the quantum contribution. It denotes the non-minimal coupling which is generated radiatively between the reference scale and today.
The agreement between the abundances of light elements and predictions from BBN lead to the upper bound $\Delta G_{eff}/G_{eff} \lesssim 20\%$ [181]. Since the rolling quintessence field is of the order of the Planck scale today, $\Delta\phi^2/M_{pl}^2$ can be of order one. Therefore the BBN bound yields restrictive upper bounds on $|\xi_0| \lesssim 0.05$ [55, 155]. However, the radiatively induced contribution to the non-minimal coupling (the mNMC) is suppressed by the tiny factor H_0^2/M_{pl}^2. Therefore, if the non-minimal coupling $|\xi_0|$ is small enough at the BBN scale, tracker quintessence models are robust against radiative corrections to the non-minimal coupling between the BBN scale and today.
Note that the linear approximation in t to the solutions (4.75) of the renormalization group equations has to be extended if the scope of the running is enlarged, for example, to be between the GUT scale and today. Using the power-counting rules (4.7) for tracker potentials, it is found that the coefficients of the contributions proportional to higher powers of $t/(32\pi^2)$ are highly suppressed by powers of $V_{cl}(\phi)/M^4 \sim V_{cl}(\phi)/M_{pl}^4$. However, it is also possible to show that for specific examples, e.g $V_{cl}(\phi) \propto \exp(-\lambda\phi/M_{pl})$, the expansion in powers of t is an asymptotic expansion, in which case a non-perturbative treatment is obligatory for $|t|/(32\pi^2) \to \infty$.

Nonlinear non-minimal gravitational coupling

Apart from the non-minimal coupling which is linear in the curvature scalar R, the scale-dependent "generalized potential" $V_{LL}(\phi, R; \mu) = \sum_{k=0}^{\infty} f_k(\phi;\mu) R^k$ also encodes the running of non-minimal couplings $f_k(\phi;\mu)$ between the scalar field and higher powers of R for $k \geq 2$.
The presence of nonlinear terms in the curvature scalar leads to modifications of General Relativity, which are suppressed if their contribution to the action is suppressed with respect to the Einstein-Hilbert term [12]. This is the case if $f_k(\phi;\mu) \ll M_{pl}^2/R^{1-k}$ for all relevant values of the curvature scalar R. For cosmology, the curvature scalar is of the order of the Hubble scale, $R \sim H^2$.
The running of the non-minimal coupling $f_2(\phi;\mu)R^2$, as obtained from eq. (B.19), is given by the partial differential equation

$$\begin{aligned} \frac{\partial}{\partial t} f_2(\phi;\mu) &= \frac{1}{64\pi^2}\left[2\frac{\partial^2 f_0(\phi;\mu)}{\partial\phi^2}\frac{\partial^2 f_2(\phi;\mu)}{\partial\phi^2} + \left(\frac{\partial^2 f_1(\phi;\mu)}{\partial\phi^2} - \frac{1}{6}\right)^2\right], \\ f_2(\phi;\mu_0) &= f_2(\phi)\,. \end{aligned} \tag{4.77}$$

For ϕ^4-theory, $f_2(\phi;\mu) \equiv \varepsilon_0(\mu)$ does not explicitly depend on ϕ. The running of the coupling $\varepsilon_0(\mu)$ in ϕ^4-theory is recovered by inserting $\partial^2 f_2(\phi;\mu)/\partial\phi^2 = 0$ and $\partial^2 f_1(\phi;\mu)/\partial\phi^2 = \xi(\mu)$.

In order to estimate the radiatively induced non-minimal coupling $\propto R^2$, the initial conditions

$$f_2(\phi;\mu_0) = f_2(\phi) \equiv \varepsilon_0 \equiv \text{const} \quad \textit{and} \quad f_1(\phi;\mu_0) = f_1(\phi) \equiv \xi_0\phi^2/2 + \text{const}$$

are assumed. With this choice, the field is minimally coupled at the reference scale $\mu = \mu_0$ for $\xi_0 = 0$. The approximate solution of the renormalization group equation is

$$f_2(\phi;\mu) = \varepsilon_0 + \frac{t}{64\pi^2}\left(\xi_0 - \frac{1}{6}\right)^2 + \frac{1}{2}\left(\frac{t}{32\pi^2}\right)^2 V_{cl}^{(4)}(\phi)\left(\xi_0 - \frac{1}{6}\right)^3 + \mathcal{O}\left(\frac{t}{32\pi^2}\right)^3 .$$

Up to linear order in $t = \ln(\mu^2/\mu_0^2)$, $f_2(\phi;\mu)$ does not explicitly depend on ϕ, similar to ϕ^4-theory. A non-minimal coupling $\propto V_{cl}^{(4)}(\phi)R^2$ arises at order t^2, which is extremely suppressed by the factor $V_{cl}^{(4)}(\phi) \sim V_{cl}(\phi)/M^4$ for a tracker potential.
For a potential $V_{cl}(\phi)$ involving higher-dimensional operators, radiative corrections also induce non-minimal couplings between the field and higher powers R^k, $k \geq 3$, of the curvature scalar. For example, for a potential which contains a dimension six (or higher) operator, a radiatively induced non-minimal coupling $\propto V_{cl}^{(6)}(\phi)R^3$ arises at order t^3,

$$f_3(\phi;\mu) \;=\; \frac{1}{3!}\left(\frac{t}{32\pi^2}\right)^3 V_{cl}^{(6)}(\phi)\left(\xi_0 - \frac{1}{6}\right)^4 + \mathcal{O}\left(\frac{t}{32\pi^2}\right)^4 ,$$

where $f_3(\phi;\mu_0) = 0$ was assumed. For a tracker potential, this is extremely suppressed compared to the linear term $\propto R/(16\pi G) \sim RM_{pl}^2$ since

$$V_{cl}^{(6)}(\phi)R^3/(RM_{pl}^2) \sim (M^2/M_{pl}^2)\cdot(V_{cl}(\phi)/M^4)\cdot(R^2/M^4) ,$$

where $R \sim H^2$ and $M \sim M_{pl}$.

Kinetic term

The one-loop effective action (4.71) contains, apart from one-loop non-minimal gravitational couplings, also the one-loop higher-derivative contributions to the effective action. The first contribution to the derivative expansion (3.18) has the form of a modification of the kinetic term $Z(\phi)(\partial\phi)^2/2$. In the flat space-time limit, the one-loop contribution obtained from the Heat Kernel Expansion (4.71) is

$$\begin{aligned}
\Gamma[\phi,\eta_{\mu\nu}]_{1L} \;&=\; \int\frac{d^4x}{32\pi^2}\left[-V_{1L}(\phi) - \left(\frac{1}{6}\Box X\right)\ln\frac{X}{\mu^2}\right.\\
&\qquad \left. + \left(-\frac{1}{12}\partial_\mu X\partial^\mu X - \frac{1}{60}\Box^2 X\right)\frac{1}{X} + \sum_{j=4}^{\infty}\frac{\bar{g}_j(x,x)(j-3)!}{X^{j-2}}\right]\\
&=\; \int\frac{d^4x}{32\pi^2}\left[-V_{1L}(\phi) + \frac{1}{12X}\partial_\mu X\partial^\mu X + \mathcal{O}\left(\partial^4\right)\right]\\
&=\; \int\frac{d^4x}{32\pi^2}\left[-V_{1L}(\phi) + \frac{1}{2}Z_{1L}(\phi)(\partial\phi)^2 + \mathcal{O}\left(\partial^4\right)\right] ,
\end{aligned}$$

where the third coefficient of the Heat Kernel Expansion $g_3(x,x)$ (see Ref. [121]) was inserted in the Minkowski limit in the second line. The one-loop correction to the kinetic term is thus given by

$$Z(\phi) = 1 + Z_{1L}(\phi), \qquad Z_{1L}(\phi) = \left[V_{cl}'''(\phi)\right]^2/V_{cl}''(\phi) .$$

It is independent of the renormalization scale μ, in accordance with the vanishing anomalous dimension, see eq. (B.17). For a tracker potential, the one-loop correction to the kinetic term is suppressed by the factor $Z_{1L} \sim V_{cl}'''(\phi)^2/V_{cl}''(\phi) \sim V_{cl}(\phi)/M^4 \lll 1$ compared to the classical value $Z = 1$.

4.4 Summary

In this chapter quantum corrections to quintessence models have been investigated. These provide a form of dynamical dark energy for which an extremely light rolling scalar field is responsible for the present cosmic acceleration, similar to the inflaton in the early universe.

First an approximation scheme suitable to investigate the impact of quintessence self-couplings on the shape of the effective potential has been introduced. An additive constant has been fine-tuned to be zero, thus bypassing the unresolved "cosmological constant problem". It has been shown that the quantum corrections to the scalar potential can be self-consistently calculated in leading order in $V''(\phi)/\Lambda^2$. Hereby Λ denotes the embedding scale characteristic for an underlying theory and $V''(\phi)$ denotes the square of the quintessence mass, which is of the order of the Hubble parameter for tracking solutions. While potentials involving exponentials just get rescaled, inverse power law potentials are flattened at small field values. The effective potential approaches a finite maximum value, thus truncating the singular behaviour of the inverse power law. This distortion of the potential directly plays a role cosmologically if Λ is large, roughly $\Lambda \gtrsim M_{pl}/10$, and affects general properties like tracking behaviour.

Second couplings between the quintessence field and heavier degrees of freedom, like the Standard Model fermions or dark matter, have been discussed. The discussion has been constrained to couplings that can effectively be written in the form of quintessence-field-dependent mass terms. The quantum corrections induced by these couplings have been described by the low-energy effective action obtained from integrating out the Standard Model degrees of freedom. An upper bound for the couplings was quantified under the assumption that fine-tuning in the form of renormalization conditions for the low-energy effective potential is admitted. This fine-tuning was used to minimize the quantum corrections in the present cosmological epoch. The remaining corrections constitute the minimal quantum vacuum backreaction of the Standard Model fields on the dynamics of the quintessence field.
Next, the upper bounds on the couplings have been translated into upper bounds for potentially observable effects, like tiny time-variations of particle masses between redshift $z \sim 2$ and now, or tiny apparent violations of the equivalence principle. Note that it has been assumed that the mass variations are uncorrelated. In this case, they are constrained to be far below observational bounds for all Standard Model particles. The latter are of the order $|\Delta m/m| \lesssim 10^{-5}$ [119, 158]. However, it has been found that massive neutrinos can have large relative mass variations of order one. The bound can be avoided for correlated mass variations of different species which are finely tuned in such a way that their quintessence-field-dependent contributions to the vacuum energy cancel.

Third non-minimal gravitational couplings induced by quantum corrections have been investigated. For ϕ^4-theory, a non-minimal coupling of the form $\phi^2 R$ is induced by radiative corrections in the effective action, where R denotes the curvature scalar. For a tracker potential, however, all couplings of the form $\phi^n R^m$ with integers n and m have to be included at one loop level, and will be induced by quantum corrections unless the field is exactly conformally coupled. Potentially, non-minimal couplings of the quintessence field can lead to conflicts with tests of General Relativity. However, for tracker potentials, it has been shown that the radiatively induced non-minimal couplings as obtained from the one-loop renormalization group analysis are suppressed by powers of $H^2/M_{pl}^2 \ll 1$ and therefore do not lead to sizeable deviations from General Relativity.

Chapter 5

Leptonic Dark Energy and Baryogenesis

Scalar fields with time-dependent expectation value are not only considered in quintessence models, but are commonly invoked in cosmology, above all to describe the inflationary phase [108] of the early universe. Furthermore, rolling fields are the basis of a number of baryogenesis models [8, 78] and also play an important role in the context of a possible time-variation of fundamental constants over cosmological time-scales [172]. Due to the similarity of the underlying concepts, it is an interesting question whether some of these issues could be related. This has been studied for example for the early- and late time acceleration, called quintessential inflation [154], or for the combination of spontaneous lepto- and baryogenesis with quintessence [138, 187] and quintessential inflation [72]. Here, a toy model is discussed where baryogenesis and cosmic acceleration are driven by a leptonic quintessence field coupled indirectly to the Standard Model sector via a massive mediating scalar field. It does not require the introduction of new interactions which violate baryon (B) or lepton (L) number below the inflationary scale. Instead, a $B-L$-asymmetry is stored in the quintessence field, which compensates for the corresponding observed baryon asymmetry.

5.1 Quintessence and Baryogenesis

Complex scalar fields have been discussed as candidates for dynamical dark energy [40, 106], which offer the possibility that the field carries a $U(1)$-charge [8, 78], and thus could itself store a baryon or lepton density [23]. This approach can very well be accommodated within the so-called "baryosymmetric baryogenesis" [79, 80] scenario, where one attempts to explain the overabundance of matter over antimatter without postulating new baryon- or lepton number violating interactions, nevertheless starting with no initial asymmetry. This requires the introduction of an invisible sector, in which an asymmetry is hidden that exactly compensates the one observed in the baryon (and lepton) sector, thereby circumventing one of the Sakharov conditions [163]. Here a possible realization is discussed where the anomaly-free combination $B-L$ is conserved below the inflationary scale, and the invisible sector, which compensates for the $B-L$-asymmetry of the Standard Model (SM) baryons and leptons, is leptonic dark energy [23, 103]. For other realizations involving dark matter or neutrinos see e.g. Refs. [77, 79].

Toy Model

In this section the question is addressed of how $B-L$-asymmetries in the dark energy sector, realized by a complex quintessence field charged under $B-L$, and in the SM sector can be created by a dynamical evolution within an underlying $B-L$-symmetric theory. For this, it is necessary to con-

sider a suitable interaction between both sectors. Direct couplings between the quintessence field and SM fields are commonly investigated for example in the context of time-varying coupling constants and/or -masses [172] or violations of the equivalence principle [157], which leads to strong constraints in the case of a coupling e.g. to photons or nucleons [51, 102, 157] (see also section 4.2). Here, a toy model is discussed where it is assumed that direct interactions between the quintessence field ϕ and the SM are sufficiently suppressed, allowing however an indirect interaction mediated by a "mediating field" χ which couples to ϕ and the SM. In the late universe, the χ-interactions should freeze out. This means that the massive scalar χ is hidden today and also that the transfer of asymmetry between the quintessence and the SM sector freezes out. Thus, once an asymmetry has been created in each sector in the early universe, it will not be washed out later on. In the specific setup considered here the quintessence field is taken to carry lepton number -2, so that it carries a $B-L$-density given by

$$n_\phi = -2|\phi|^2\dot{\theta}_\phi \qquad (\text{with } \phi \equiv |\phi|e^{i\theta_\phi}), \tag{5.1}$$

and analogously for the mediating field χ which carries the same lepton number. The effective toy-model Lagrangian for ϕ and χ is

$$\begin{aligned}\mathcal{L} &= \frac{1}{2}(\partial_\mu\phi)^*(\partial^\mu\phi) - V(|\phi|) + \frac{1}{2}(\partial_\mu\chi)^*(\partial^\mu\chi) - \frac{1}{2}\mu_\chi^2|\chi|^2 \\ &\quad -\frac{1}{2}\lambda_1|\phi|^2|\chi|^2 - \frac{1}{4}\lambda_2(\phi^2\chi^{*2} + \text{h.c.}) + \mathcal{L}_{\mathcal{SM}}(\chi,\ldots),\end{aligned}$$

with dimensionless coupling constants $\lambda_1 > 0$ and $\lambda_2 < \lambda_1$ responsible for the coupling between the quintessence and the mediating field. This Lagrangian has a global $U(1)$-symmetry under a common phase rotation of ϕ and χ which corresponds to a $B-L$-symmetric theory. The coupling of the mediating field to the SM encoded in the last contribution should also respect this symmetry. This is compatible e.g. with a Yukawa-like coupling of the form $\mathcal{L}_{SM} \ni -g\chi\overline{\nu_R^c}\nu_R + \text{h.c.}$ to right-handed neutrinos, see Ref. [23]. For the quintessence potential an exponential potential of the form [21, 98, 157, 182]

$$V(|\phi|) = V_0\left(e^{-\xi_1|\phi|/M_{pl}} + ke^{-\xi_2|\phi|/M_{pl}}\right) \tag{5.2}$$

is assumed, which leads to tracking of the dominant background component and a crossover towards an accelerating attractor at the present epoch for $\xi_1 \gg \sqrt{3} \gg \xi_2$ and a suitable choice of k [21]. For the dynamics in the early universe one can safely neglect the second term. Since the vacuum expectation value (VEV) of ϕ increases and typically $|\phi| \gtrsim M_{pl}$ today, the effective mass $m_\chi^2 \approx \mu_\chi^2 + \lambda_1|\phi|^2$ of the mediating field gets huge and the field indeed decouples the quintessence and the SM sectors in the late universe. However, before the electroweak phase transition the dynamics of ϕ and χ can lead to a creation of the baryon asymmetry.

5.2 Creation of a $B-L$-Asymmetry

To study the evolution of the scalar fields ϕ and χ in the early universe, it is described by a flat FRW metric after the end of inflation with a Hubble parameter $H = H_{inf}$ and with VEVs $\phi = \phi_0$ and $\chi = \chi_0 e^{-i\alpha_0}$ inside our Hubble patch which are displaced by a relative angle α_0 in the complex plane. These initial conditions correspond to dynamical CP violation if $\sin(2\alpha_0) \neq 0$, which is necessary for the formation of an asymmetry [19,80]. Under these conditions, the fields start rotating in the complex plane and thus develop a $B-L$-density, see eq. (5.1). This asymmetry is then partially transferred to the SM by the $B-L$-conserving decay of the χ-field into SM particles, leading to a decay term for the

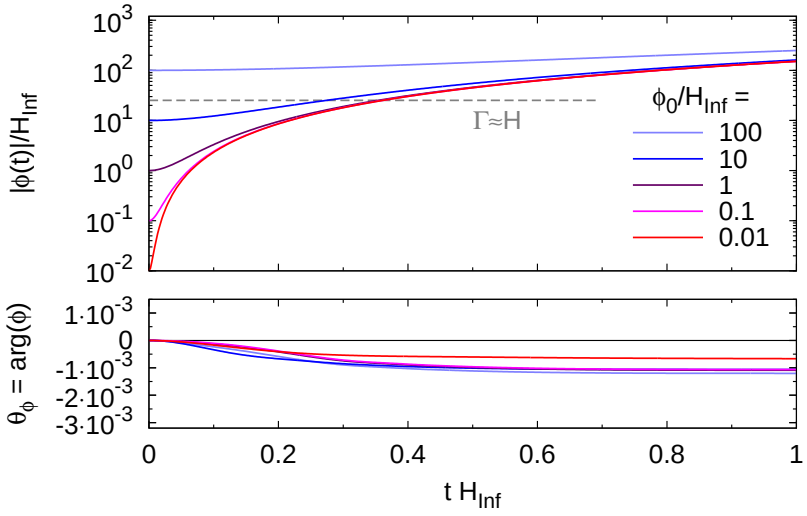

Figure 5.1: *Numerical solution for the absolute value of the quintessence VEV $|\phi|$ (upper) and its complex phase (lower) for various initial conditions ϕ_0 and the choice $\lambda_1 = 1, \lambda_2 = 0.1, V_0/\rho_0 = 10^{-5}, \xi_1 = 7, \chi_0 = H_{inf} = 10^{12}\text{GeV}, \alpha_0 = \pi/4, g = 1$ of parameters.*

χ-field in the equations of motion [23]

$$\begin{aligned} \ddot{\phi} + 3H\dot{\phi} &= -2\frac{\partial V}{\partial \phi^*} - \lambda_1|\chi|^2\phi - \lambda_2\phi^*\chi^2\,, \\ \ddot{\chi} + 3H\dot{\chi} + 3\Gamma_{\chi\to\text{SM}}\dot{\chi} &= -\mu_\chi^2\chi - \lambda_1|\phi|^2\chi - \lambda_2\chi^*\phi^2\,, \end{aligned}$$

where $\Gamma_{\chi\to\text{SM}} = \frac{g^2}{8\pi}m_\chi$ is the decay rate and g^2 stands for the squared sum of the Yukawa couplings corresponding to the relevant decay channels. Provided that the quintessence behaviour is dominated by the exponential and not by the mixing terms (which is roughly the case if $|V'(\phi_0)| \gg \chi_0^2\phi_0, \chi_0^3$), it will roll to larger field values with only small changes in the radial direction (see figure 5.1), whereas the χ-field oscillates and decays once $\Gamma_{\chi\to\text{SM}} \gtrsim H$ (see figure 5.2).
Due to the $B-L$-symmetry, the total $B-L$-density is conserved, and thus the asymmetries stored in the different components always add up to the initial value which was assumed to be zero after inflation, i.e.

$$n_\phi + n_\chi + n_{\text{SM}} \equiv 0\,. \tag{5.3}$$

After the decay of the χ-field, the comoving asymmetry freezes (see figure 5.3) since there is no more exchange between the quintessence and the SM sectors[1] [23],

$$n_{\text{SM}}a^3 \to -n_\phi a^3 \to \text{const} = \int_0^\infty \text{d}t\, a^3\Gamma_{\chi\to\text{SM}}\cdot n_\chi \equiv A_\infty\,, \tag{5.4}$$

and thus the $B-L$-asymmetry in the SM is exactly compensated by the $B-L$-asymmetry stored in the quintessence field. The final yield of the $B-L$-asymmetry

$$n_{\text{SM}}/s = D\cdot\kappa \equiv D\cdot\frac{-A_\infty}{3.2\rho_0^{3/4}} \propto A_\infty \tag{5.5}$$

[1] Here, $t \equiv 0$ and $a \equiv 1$ at the end of inflation.

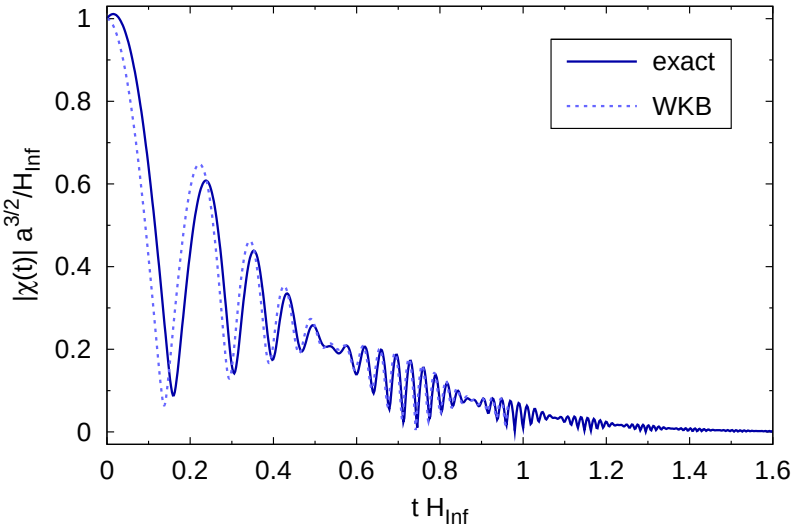

Figure 5.2: *Numerical and approximate WKB solution for the absolute value of the mediating field VEV* $|\chi|$ *for the same parameter values as in figure 5.1 despite* $\phi_0 = H_{inf}$.

(where $\rho_0 \equiv 3H_{inf}^2 M_{pl}^2$) can actually be calculated either numerically or, for a restricted parameter range, analytically via the integral in eq. (5.4) using an approximate WKB solution for $\chi(t)$ [23] (see figure 5.2 and figure 5.3),

$$\kappa \approx -\frac{\mathcal{N}}{2}\sin(2\alpha_0)\left(\frac{\chi_0}{H_{inf}}\right)^2 \cdot \begin{cases} 3.6\cdot 10^{-10}\dfrac{\phi_0}{10^{13}\mathrm{GeV}}\left(\dfrac{H_{inf}}{10^{12}\mathrm{GeV}}\right)^{\frac{1}{2}} & \text{if } \phi_0^3 \gg \chi_0^2\phi_0, |V'(\phi_0)| \\ 1.7\cdot 10^{-8}\left(\dfrac{\xi_1}{7}\dfrac{V_0}{\rho_0}\right)^{\frac{1}{3}}\left(\dfrac{H_{inf}}{10^{12}\mathrm{GeV}}\right)^{\frac{7}{6}} & \text{if } |V'(\phi_0)| \gg \phi_0^3, \chi_0^3\,, \end{cases} \tag{5.6}$$

where $\mathcal{N} \equiv \mathcal{N}(\lambda_1, \lambda_2, g)$ contains the the dependence on the coupling constants, with $\mathcal{N} \sim 1$ for $g^2/(8\pi) \sim \lambda_2/\lambda_1 \ll \lambda_1 \sim 1$ [23]. The analytic estimate agrees well with the numerical results (see figure 5.3) inside the respective domains of validity. In the notation of eq. (5.5) $\kappa \propto A_\infty$ is the contribution which depends on the dynamics of the quintessence and the mediating field, and D is a factor of proportionality which depends on the expansion history of the universe after inflation and can vary in the range $1 \gtrsim D \gtrsim 10^{-6}$ for various models of inflation and re/preheating [23]. Thus, arriving at the observed value[2] $n_{\mathrm{SM}}/s \sim 10^{-10}$ is possible if the asymmetry parameter κ is in the range

$$10^{-10} \lesssim \kappa \lesssim 10^{-4}\,, \tag{5.7}$$

which is indeed the case for a broad range of values for the initial energy density and VEV of the quintessence field (see figure 5.4).

[2]Note that the $B-L$-asymmetry and the baryon asymmetry differ by an additional sphaleron factor of order one, see Ref. [109].

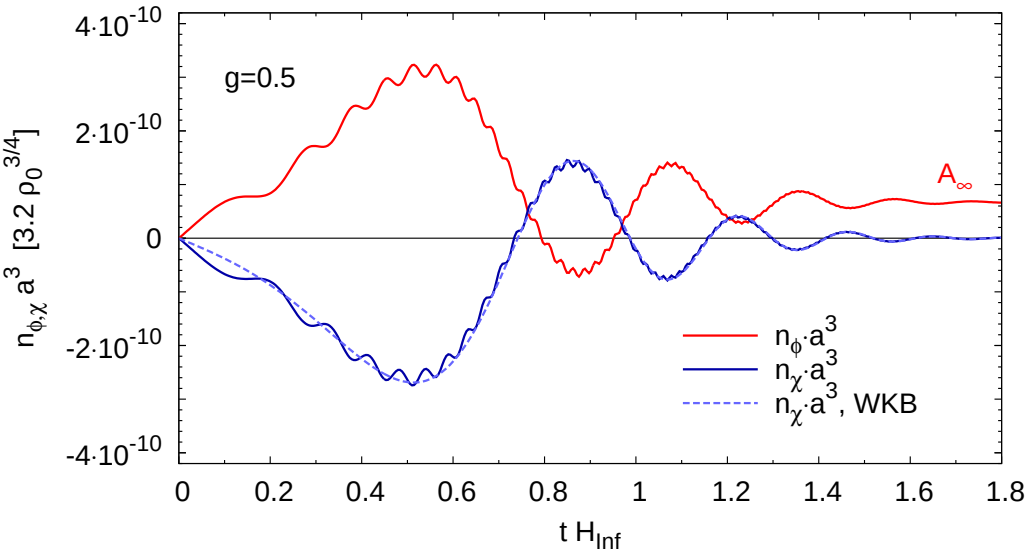

Figure 5.3: *Time-evolution of the comoving asymmetry of the quintessence (red) and the mediating (blue) fields for the same parameters as in figure 5.1 despite $g = 0.5$. After an initial phase of oscillations, the χ-field decays and the asymmetry stored in the quintessence field goes to a constant asymptotic value A_∞ which is of equal amount but opposite sign as the asymmetry created in the SM. The analytic WKB approximation for n_χ is also shown (dashed).*

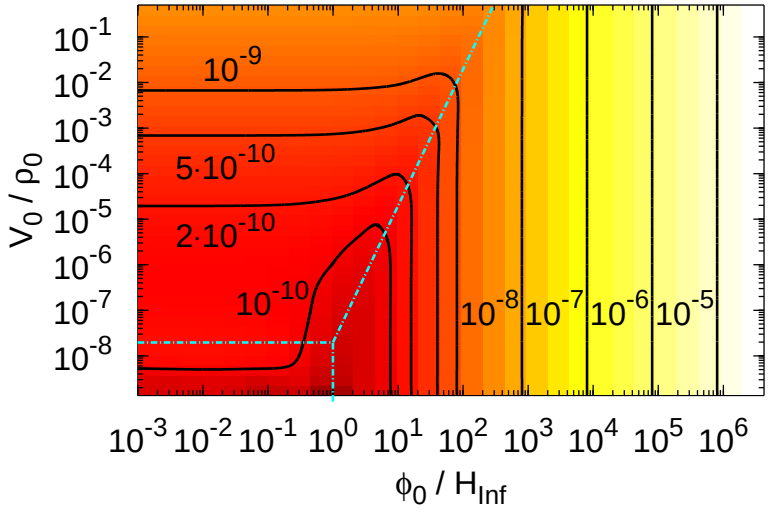

Figure 5.4: *Contour plot of the created asymmetry $\kappa \propto A_\infty$. V_0/ρ_0 corresponds to the fraction of quintessence energy density after inflation and ϕ_0 is the initial quintessence VEV. The other parameters are chosen as in figure 5.1. The dashed lines divide the regions where the analytic approximations from eq. (5.6) are valid.*

5.3 Stability

An important issue in the context of complex quintessence models is to study the stability against the formation of inhomogeneities, which could otherwise lead to the formation of so-called Q-balls [59], and destroy the dark energy properties. Once the comoving asymmetry is frozen one can estimate from eq. (5.1) the phase velocity $\dot{\theta}_\phi$ which is necessary to yield an asymmetry $n_\phi/s \sim 10^{-10}$,

$$\frac{|\dot{\theta}_\phi|}{H} = \frac{|n_\phi|}{2H|\phi|^2} \sim 10^{-10}\frac{2\pi^2}{45}g_{*S}(T)\frac{T^3}{2H|\phi|^2} \lesssim 10^{-8}\frac{(HM_{\rm Pl})^{3/2}}{2H|\phi|^2} \ll 10^{-8}\,, \tag{5.8}$$

where it was assumed that $g_{*S}(T) \sim 100$ and $|\phi| \gtrsim M_{pl}$. Thus the field is moving extremely slowly in the radial direction compared to the expansion rate of the universe, which is exactly the opposite limit as that which was studied for example in the spintessence models [40]. Quantitatively, one can show [134] that there exist no growing modes for linear perturbations in $|\phi|$ and θ_ϕ for any wavenumber k provided that

$$\dot{\theta}_\phi^2 < \frac{3H + 2\dot{\varphi}/\varphi}{3H + 6\dot{\varphi}/\varphi}V''\,, \tag{5.9}$$

(with $\varphi \equiv |\phi|$, $V'' \equiv d^2V/d\varphi^2$). Since the mass $V'' \sim H^2$ of the quintessence field tracks the Hubble scale [169] and since $\dot{\varphi}/\varphi > 0$ this inequality is safely fulfilled once the tracking attractor is joined, and thus there are no hints for instabilities in this regime. Details of the analysis, including also the early moments of evolution as well as additional particle processes, can be found in Ref. [23].
Finally, it is mentioned that, since the underlying Lagrangian is $B-L$-symmetric, it offers a possibility to combine Dirac-neutrinos with baryogenesis aside from the Dirac-leptogenesis mechanism [77]. Note that the lepton-asymmetry in the SM is of opposite sign compared to Dirac-leptogenesis. Furthermore, there is no specific lower bound on the reheating temperature like in thermal leptogenesis [70].
In conclusion, the coupled leptonic quintessence model discussed here can account for the observed baryon asymmetry of the universe without introducing new $B-L$-violating interactions below the inflationary scale by storing a lepton asymmetry in the dark energy sector.

Chapter 6

Quantum Nonequilibrium Dynamics and 2PI Renormalization

The standard big bang paradigm implies that cosmology is nonequilibrium physics. As has been seen in the previous chapters, nonequilibrium phenomena do not only occur in the early universe (like baryogenesis). A rolling quintessence field, for which the expectation value evolves with time during all cosmological epochs, also provides an example for a nonequilibrium situation.

The description of nonequilibrium phenomena within quantum field theory has traditionally been limited to semi-classical approximations. These can either describe highly correlated systems, like a system with time-varying field expectation value, or systems where correlations are quickly lost, but which are nevertheless sufficiently dilute, such that quantum nonequilibrium effects, like off-shell effects, are sufficiently suppressed, and Boltzmann equations may be used. However, in situations where neither of the two limits described above can be applied, a full quantum field theoretical description is required. An example is a system where a time-evolving field expectation value and a non-thermal distribution of particle-like excitations have to be treated simultaneously, as it occurs for the inflaton field during reheating, and could also occur for a quintessence field.

A self-consistent quantum field theoretical description of quantum fields far from equilibrium is available in the form of Kadanoff-Baym Equations derived from the 2PI effective action, and many interesting nonequilibrium questions have been addressed within this framework in the recent years. Their derivation is briefly reviewed in section 6.1.

Due to the inherently nonperturbative structure of Kadanoff-Baym equations, their renormalization is still an unresolved question, which is tackled in chapters 7 and 8 of this work. There are various reasons why a proper renormalization of Kadanoff-Baym equations is desirable, as mentioned in the introduction. In particular, it is required for quantitative comparisons with semi-classical approaches. Renormalization is indispensable in order to obtain reliable predictions from realistic applications of Kadanoff-Baym equations.

The renormalization techniques for Kadanoff-Baym equations developed in this work are based on the nonperturbative renormalization procedure of the 2PI effective action, which has been recently formulated at finite temperature, and which is reviewed in section 6.2.

For concreteness, the nonequilibrium formalism is discussed for a real scalar $\lambda\Phi^4/4!$ quantum field theory, although the underlying concepts are more general and can be adapted to more realistic quantum field theories. The fundamental action in Minkowski space is given by

$$S[\phi] = \int d^4x \left(\frac{1}{2}(\partial\phi)^2 - \frac{1}{2}m^2\phi^2 - \frac{\lambda}{4!}\phi^4 \right) . \tag{6.1}$$

6.1 Kadanoff-Baym Equations from the 2PI Effective Action

The closed real-time path

Within quantum nonequilibrium dynamics, one is interested in the time-evolution of correlation functions for a system which can be described by a density matrix ρ at a given initial time $t_{init} \equiv 0$. In general, the correlation functions are defined as expectation values of products of field operators and their conjugates with respect to the statistical ensemble. Such expectation values can be calculated using the so-called *in-in* or closed-time-path (CTP) formalism [68, 126, 166]. In contrast to the usual *in-out* formalism, the calculation of expectation values requires the evaluation of matrix elements where the left state and the right state are both specified at the initial time. For a Heisenberg operator $\mathcal{O}_H(t)$, which may be an arbitrary product of field operators and their conjugates all evaluated at a common time argument t, the expectation value is given by [68]

$$\begin{aligned} \langle \mathcal{O}_H(t) \rangle &= \mathrm{Tr}\left(\rho\, U(t_{init},t)\, \mathcal{O}_I(t)\, U(t,t_{init}) \right) \\ &= \mathrm{Tr}\left(\rho\, \tilde{T}\left[\exp\left(+i \int_{t_{init}}^{t} dt' H_I(t') \right) \right] \mathcal{O}_I(t)\, T\left[\exp\left(-i \int_{t_{init}}^{t} dt' H_I(t') \right) \right] \right) , \end{aligned} \tag{6.2}$$

where $\mathcal{O}_I(t) = \exp(itH_0)\, \mathcal{O}_H(0) \exp(-itH_0)$ denotes the interaction picture operator. The interaction picture time-evolution operator is given by [68]

$$\begin{aligned} U(t,t') &= \exp(itH_0) \exp\left(-i(t-t')H\right) \exp\left(-it'H_0\right) \\ &= \begin{cases} T\left[\exp\left(-i \int_{t'}^{t} dt'' H_I(t'') \right) \right] & \text{for } t > t' \\ \tilde{T}\left[\exp\left(+i \int_{t}^{t'} dt'' H_I(t'') \right) \right] & \text{for } t < t' , \end{cases} \end{aligned} \tag{6.3}$$

where H_0 is the quadratic part of the Hamiltonian and the interactions are contained in $H_I(t) = \exp(itH_0)\,(H - H_0) \exp(-itH_0)$. T and $\tilde{T}$ denote the chronological and the antichronological time-ordering operator, respectively. The product of operators appearing in the trace (6.2) contains a chronologically ordered part and an antichronologically ordered part. Therefore the contour $\mathcal{C}$ shown in figure 6.1 is defined, which is running along the real axis from t_{init} to $t_{max} = t$ and back to t_{init}, as well as a time-ordering operator $T_{\mathcal{C}}$ on the contour. The time arguments of the operators may also be assigned to the contour $\mathcal{C}$. The operator $T_{\mathcal{C}}$ becomes the chronological time-ordering operator on the branch running forward in time and the antichronological time-ordering operator on the branch running backward in time. All operators belonging to the antichronological branch $\mathcal{C}_-$ are placed left of the operators belonging to the chronological branch $\mathcal{C}_+$. In this way, the expectation value in eq. (6.2) can be written as

$$\langle \mathcal{O}_H(t) \rangle = \mathrm{Tr}\left(\rho\, T_{\mathcal{C}} \left[\exp\left(-i \int_{\mathcal{C}} dt H_I(t) \right) \mathcal{O}_I(t) \right] \right) , \tag{6.4}$$

where the time integral is performed along the contour $\mathcal{C} = \mathcal{C}_+ + \mathcal{C}_-$. Note that it is possible to extend the contour to a maximal time $t_{max} > t$ by inserting the unity operator $1 = U(t,t_{max})U(t_{max},t)$ left or right of the operator $\mathcal{O}_I(t)$ in eq. (6.2).

The Schwinger-Keldysh propagator

The Schwinger-Keldysh propagator is defined as the connected two-point correlation function on the closed real-time contour $\mathcal{C}$,

$$G(x,y) = \langle T_{\mathcal{C}}\, \Phi(x)\Phi(y) \rangle - \langle \Phi(x) \rangle \langle \Phi(y) \rangle . \tag{6.5}$$

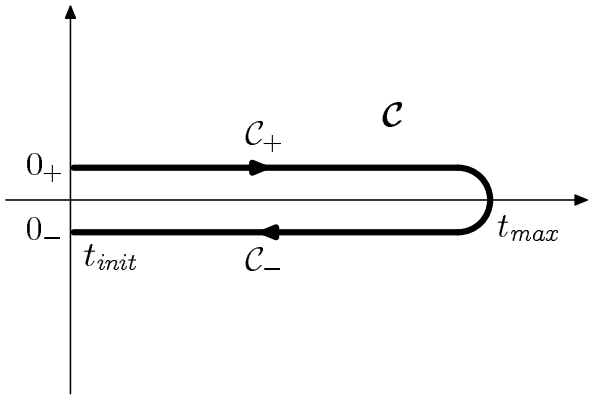

Figure 6.1: *Closed real-time contour [68, 126, 166].*

The Schwinger-Keldysh propagator can be obtained by functional differentiation from the generating functional for correlation functions formulated on the closed real-time path. The generating functional in the presence of a local external source $J(x)$ and a bilocal external source $K(x,y)$, written down using a complete basis of common eigenstates of the field operator $\Phi(x)$ at the initial time $t_{init} \equiv 0$,

$$\Phi(0,\boldsymbol{x})|\varphi,0\rangle = \varphi(\boldsymbol{x})|\varphi,0\rangle\,, \tag{6.6}$$

is given by

$$\begin{aligned} Z_\rho[J,K] &= \mathrm{Tr}\left(\rho\, T_\mathcal{C}\left[\exp\left(i\int_\mathcal{C} d^4x J(x)\Phi(x) + \frac{i}{2}\int_\mathcal{C} d^4x \int_\mathcal{C} d^4y\, \Phi(x)K(x,y)\Phi(y)\right)\right]\right) \\ &= \int\mathcal{D}\varphi_+\int\mathcal{D}\varphi_-\,\langle\varphi_+,0\,|\rho|\,\varphi_-,0\rangle \times \left\langle \varphi_-,0\left|T_\mathcal{C}\left[\exp\left(iJ\Phi + \frac{i}{2}\Phi K\Phi\right)\right]\right|\varphi_+,0\right\rangle\,, \end{aligned}$$

where the short hand notation (3.21) applies (with $\int \to \int_\mathcal{C}$). The second matrix element can be expressed by a path integral over all field configurations $\varphi(x)$ with time argument attached to the contour $\mathcal{C}$ fulfilling the boundary conditions $\varphi(0_\pm,\boldsymbol{x}) = \varphi_\pm(\boldsymbol{x})$ [49],

$$\begin{aligned} Z_\rho[J,K] &= \int\mathcal{D}\varphi_+\int\mathcal{D}\varphi_-\,\langle\varphi_+,0\,|\rho|\,\varphi_-,0\rangle \int\limits_{\varphi(0_+,\boldsymbol{x})=\varphi_+(\boldsymbol{x})}^{\varphi(0_-,\boldsymbol{x})=\varphi_-(\boldsymbol{x})}\mathcal{D}\varphi\,\exp\left(iS[\varphi] + iJ\varphi + \frac{i}{2}\varphi K\varphi\right) \\ &\equiv \int\mathcal{D}\varphi\,\langle\varphi_+,0\,|\rho|\,\varphi_-,0\rangle\,\exp\left(iS[\varphi] + iJ\varphi + \frac{i}{2}\varphi K\varphi\right)\,. \end{aligned} \tag{6.7}$$

The information about the initial state enters via the matrix element of the density matrix. The standard case which has been used for numerical studies so far is a Gaussian initial state.

2PI effective action for a Gaussian initial state

A Gaussian initial state is an initial state for which all connected n-point correlation functions vanish for $n \geq 3$. The density matrix element for a Gaussian initial state can be parameterized as

$$\langle\varphi_+,0\,|\rho|\,\varphi_-,0\rangle = \exp\left(i\alpha_0 + i\alpha_1\varphi + \frac{i}{2}\varphi\alpha_2\varphi\right)\,. \tag{6.8}$$

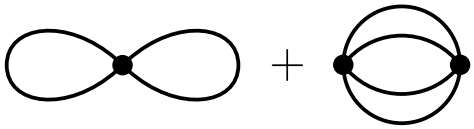

Figure 6.2: *Diagrams contributing to the three-loop truncation of the 2PI effective action in the symmetric phase (setting-sun approximation) for a Gaussian initial state.*

Therefore, in the Gaussian case, the contribution of the density matrix to the generating functional (6.7) can be absorbed into the external sources, $J+\alpha_1 \to J$ and $K+\alpha_2 \to K$ (the constant α_0 can be absorbed into the normalization of the path integral measure).
The 2PI effective action is the double Legendre transform of the generating functional (6.7) with respect to the external sources. The latter has the same structure as the generating functional (3.20) in vacuum, except that all time-integrations are performed over the closed real-time path. Consequently, the 2PI effective action for a Gaussian initial state is obtained from the parameterization given in eq. (3.26) by replacing the time-integrations $\int \to \int_{\mathcal{C}}$. For example, the three-loop truncation of the 2PI effective action $\Gamma[G] \equiv \Gamma[\phi=0,G]$ in the Z_2-symmetric phase ($\langle\Phi(x)\rangle = 0$), which is referred to as setting-sun approximation, is given by (see figure 6.2)

$$\begin{aligned} \Gamma[G] &= \frac{i}{2}\mathrm{Tr}\ln G^{-1} + \frac{i}{2}\mathrm{Tr}\left(G_0^{-1}G\right) + \Gamma_2[G]\,, \\ i\Gamma_2[G] &= \frac{-i\lambda}{8}\int_{\mathcal{C}} d^4x\, G(x,x)^2 + \frac{(-i\lambda)^2}{48}\int_{\mathcal{C}} d^4x \int_{\mathcal{C}} d^4y\, G(x,y)^4\,. \end{aligned} \tag{6.9}$$

Here, $G_0^{-1}(x,y) = i(\Box_x + m^2)\delta_{\mathcal{C}}^4(x-y)$ is the free inverse Schwinger-Keldysh propagator which contains the (bare) mass and the Dirac distribution on the time path $\mathcal{C}$.

Kadanoff-Baym equations for a Gaussian initial state

The equation of motion for the full Schwinger-Keldysh propagator is obtained from evaluating the functional derivative of the 2PI effective action with respect to the two-point function (which yields a stationarity condition for vanishing external source $K(x,y)$ by construction)

$$\frac{\delta}{\delta G(x,y)}\,\Gamma[G] = -\frac{1}{2}K(x,y)\,. \tag{6.10}$$

Here, the external sources are formally not zero for the physical situation, but $J(x) = \alpha_1(x)$ and $K(x,y) = \alpha_2(x,y)$, due to the density matrix element. However, their contribution to the equation of motion will be omitted below because it vanishes in the Kadanoff-Baym equations. Instead, the information about the initial state only enters via the initial conditions for the two-point function for a Gaussian initial state (see appendix D).
In setting-sun approximation, the equation of motion for the propagator is given by (see figure 6.3)

$$G^{-1}(x,y) = G_0^{-1}(x,y) - \Pi(x,y)\,, \tag{6.11}$$

$$\Pi(x,y) \equiv \frac{2i\delta\Gamma_2[G]}{\delta G(y,x)} = \frac{-i\lambda}{2}G(x,x)\delta_{\mathcal{C}}^4(x-y) + \frac{(-i\lambda)^2}{6}G(x,y)^3\,, \tag{6.12}$$

where $\Pi(x,y)$ is the full self-energy. The Kadanoff-Baym equations are an equivalent formulation of

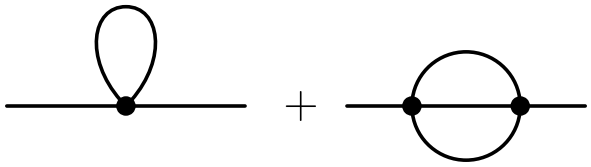

Figure 6.3: *Diagrams contributing to the self-energy* $\Pi(x,y)$ *in setting-sun approximation for a Gaussian initial state.*

the equation of motion. They are obtained by convolving eq. (6.11) with the full propagator

$$\left(\Box_x + m^2 + \frac{\lambda}{2}G(x,x)\right) G(x,y) = -i\delta^4_{\mathcal{C}}(x-y) - i\int_{\mathcal{C}} d^4z\,\Pi(x,z)G(z,y)\,, \tag{6.13}$$

and inserting the decomposition of the full two-point function into the statistical propagator $G_F(x,y)$ and the spectral function $G_\rho(x,y)$,

$$G(x,y) = G_F(x,y) - \frac{i}{2}\,\mathrm{sgn}_{\mathcal{C}}(x^0-y^0)\,G_\rho(x,y)\,. \tag{6.14}$$

The Kadanoff-Baym equations read

$$\begin{aligned}
\left(\Box_x + M^2(x)\right) G_F(x,y) &= \int_0^{y^0} d^4z\,\Pi_F(x,z)G_\rho(z,y) \\
&\quad - \int_0^{x^0} d^4z\,\Pi_\rho(x,z)G_F(z,y)\,, \\
\left(\Box_x + M^2(x)\right) G_\rho(x,y) &= \int_{x_0}^{y^0} d^4z\,\Pi_\rho(x,z)G_\rho(z,y)\,.
\end{aligned} \tag{6.15}$$

The effective mass $M^2(x) = m^2 + \frac{\lambda}{2}G(x,x)$ contains the bare mass and the local part of the self-energy (6.12). The non-local part of the self-energy can be decomposed into statistical and spectral components similarly as the propagator. In setting-sun approximation, one has

$$\Pi_{non-local}(x,y) = \Pi_F(x,y) - \frac{i}{2}\,\mathrm{sgn}_{\mathcal{C}}(x^0-y^0)\,\Pi_\rho(x,y) = \frac{(-i\lambda)^2}{6}G(x,y)^3\,. \tag{6.16}$$

A more detailed derivation can be found in appendix D.

For a Gaussian initial state, the complete information about the initial state enters via the initial values of the connected one- and two-point functions and their time derivatives (up to one derivative of each time argument, see section D.2.2). For the spectral function, these initial conditions are fixed by the equal-time commutation relations (see eq. (D.49)). For the statistical propagator, it is convenient to parameterize the initial conditions in terms of an effective kinetic energy density $\omega(t=0,\boldsymbol{k})$ and effective particle number density $n(t=0,\boldsymbol{k})$ at the initial time $t=0$ for each spatial momentum mode $\boldsymbol{k}$ (see eq. (D.51)). The definitions obtained from the free-field ansatz [25] (where $G(x^0,y^0,\boldsymbol{k}) = \int d^3x\, e^{-i\boldsymbol{k}(\boldsymbol{x}-\boldsymbol{y})}\,G(x,y)$)

$$\begin{aligned}
\omega^2(t,\boldsymbol{k}) &= \left(\frac{\partial_{x^0}\partial_{y^0}G_F(x^0,y^0,\boldsymbol{k})}{G_F(x^0,y^0,\boldsymbol{k})}\right)\Bigg|_{x^0=y^0=t}\,, \\
n(t,\boldsymbol{k}) &= \omega(t,\boldsymbol{k})G_F(t,t,\boldsymbol{k}) - \frac{1}{2}\,,
\end{aligned} \tag{6.17}$$

have proven to yield meaningful results, although there is no unique definition.

Quantum dynamics far from equilibrium

With the formalism presented above, it is possible to answer the question of how a quantum field evolves out of equilibrium for a wide class of circumstances. In particular, the quantum thermalization process can be studied from first principles for a closed system [32]. It is interesting to note that the derivation of Kadanoff-Baym equations within quantum field theory does not require any further approximations or assumptions. The Kadanoff-Baym equation (6.15) is an exact evolution equation for the full two-point correlation function (the approximation enters on the level of a truncation of the self-energy $\Pi(x,y)$, like in eq. (6.12)). In particular, no assumptions are required which would only hold for systems close to equilibrium [32]. Kadanoff-Baym equations are suitable to study quantum fields arbitrarily far from equilibrium as long as the underlying quantum field theory is valid. Furthermore, Kadanoff-Baym equations do not violate time-reversal invariance [32], in contrast e.g. to Boltzmann-equations [164]. Due to the unitary time-evolution, thermal equilibrium can never be reached completely. Nevertheless, observables like the two-point correlation function have been shown to converge towards a thermal value at late times for closed systems involving scalar quantum fields on a lattice in 1+1 [32], 1+2 [123] and 1+3 [33,142] space-time dimensions (see also [69] for the nonrelativistic case) as well as for fermionic quantum fields in 1+3 space-time dimensions [30, 143].

Furthermore, in contrast to semi-classical descriptions given e.g. by Boltzmann equations [164], Kadanoff-Baym equations include memory effects since they are non-local in time and are capable of describing scattering processes which involve exchange of virtual (quasi-)particles ("off-shell") as well as on-shell particles in a unified, quantum-field theoretical manner. Therefore, in situations where the upper effects become important, the application of standard Boltzmann equations, including e.g. the lowest order 2-to-2 scattering process, might lead to quantitatively or even qualitatively incorrect results [142, 143, 147]. Since standard Boltzmann equations are widely used in all areas of physics, it seems worth to investigate under which circumstances they are reliable and in how far various extensions of Boltzmann-equations [147] can capture the off-shell and memory effects included in the quantum-field theoretical Kadanoff-Baym treatment. For such a comparison to work quantitatively, it is desirable to have a proper renormalization procedure available which allows to compare the evolution of semi-classical Boltzmann-ensembles with physical renormalized excited states rather than bare excited states.

There are also situations where semi-classical descriptions are not available, e.g. for highly correlated systems, which may undergo an instability. A typical situation of this type is the decay of a scalar condensate. A coherent scalar condensate which periodically oscillates in its potential starts to decay, due to its couplings, into (quasi-)particle excitations. This decay may additionally be resonantly enhanced if parametric resonance conditions are fulfilled [127, 128], creating a highly non-thermal population of field quanta, which are then expected to thermalize on a much longer time-scale. However, this subsequent thermalization process cannot be described in the conventional 1PI framework. Within a quantum field theoretical treatment based on Kadanoff-Baym equations, the evolution of the system can be followed at all stages starting from the coherent condensate to the thermalized plasma [33]. If the oscillating field is the inflaton, the upper scenario is known as reheating (or preheating if parametric resonance occurs) [5, 128, 129, 167]. Using Kadanoff-Baym equations it is thus possible to explore the period between the end of inflation and the beginning of the radiation dominated regime [3, 4]. This is relevant e.g. for the production of primordial gravitational waves [88], which will be tested by future precision measurements of the polarization of the cosmic microwave background [125], and for the reheating temperature. This is the maximal temperature of the plasma in the early universe, which is relevant e.g. for leptogenesis [70] and the production of long-lived thermal relics ("gravitinos") [93].

In principle, Kadanoff-Baym equations can even be applied in regimes where a priori no well-defined

notion of (quasi-)particle excitations exists, as might occur in strongly coupled theories under extreme nonequilibrium conditions [27]. Such a situation may be encountered in high-energy Heavy Ion Collisions performed at RHIC and planned at the LHC [6, 7].
Finally, it is mentioned that it is possible to analyze kinetic and chemical equilibration using Kadanoff-Baym equations. Kinetic equilibration requires energy-momentum exchange between different momentum modes, e.g. via quantum scattering processes, while chemical equilibration occurs due to energy-momentum transfer between different species, e.g. via decay and recombination processes. Due to these different underlying microscopic processes, one expects that kinetic and chemical equilibration occur on different time-scales. Such a separation of time-scales has indeed been found for the quantum equilibration process described by Kadanoff-Baym equations [143]. Microscopic kinetic equilibration already occurs long before macroscopic observables have reached their final equilibrium values [31]. An important requirement for the applicability of effective, e.g. hydrodynamic, descriptions of nonequilibrium processes is the validity of local thermal equilibrium [112]. The "prethermalization" [31] featured by solutions of Kadanoff-Baym equations is a justification from first principles regarding the domain of applicability of hydrodynamic equations, used e.g. for the interpretation of data from high-energy Heavy Ion Collisions [131].

6.2 Nonperturbative Renormalization of the 2PI Effective Action at finite Temperature

The 2PI effective action provides the appropriate framework for the investigation of quantum nonequilibrium dynamics. However, due to its nonperturbative nature, renormalization is more complicated compared to the conventional perturbative approach.
In general, a perturbative approximation (for example a loop approximation of the 1PI effective action) is compatible with the renormalizability of the underlying quantum field theory if the following condition holds: Let $\mathcal{M}$ denote the set of perturbative Feynman diagrams belonging to the approximation of interest. Then, for any diagram in $\mathcal{M}$, it is necessary that all diagrams which are required to cancel its UV divergences and subdivergences (as determined by the BPHZ renormalization procedure [38, 113, 191]) do also belong to $\mathcal{M}$.
Since the solution of the self-consistent equation of motion for the full 2PI propagator corresponds to a selective infinite resummation of perturbative Feynman diagrams, it is non-trivial whether an approximation based on a truncation of the 2PI effective action is compatible with renormalizability. Recently, it has been shown [28, 29, 37, 173–175] that systematic (e.g. loop, $1/N$) truncations of the 2PI effective action lead to approximations which are compatible with renormalizability, and a completely nonperturbative renormalization procedure for the 2PI effective action in vacuum and at finite temperature has been formulated. The 2PI vacuum counterterms, which render all n-point functions finite, have to be determined self-consistently.
The derivation of the nonperturbative renormalization procedure at finite temperature is briefly reviewed in this section for the setting-sun approximation (6.9) of the 2PI effective action.

The thermal time path

The density matrix $\rho = Z^{-1}\exp(-\beta H)$ in thermal equilibrium at temperature $T = 1/\beta$ is explicitly known in terms of the full Hamiltonian. The exponential appearing in the thermal density matrix can be interpreted as the full time-evolution operator $\exp(-itH)$ evaluated for the imaginary time $t = -i\beta$. Accordingly, the matrix element of the thermal density matrix can be written as a path integral over field configurations $\varphi(x)$ with time argument on a time contour $\mathcal{I}$ running along the

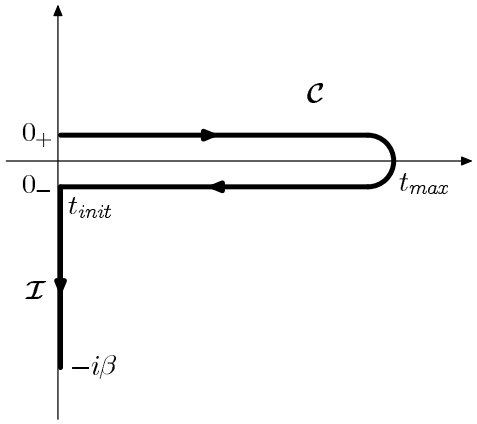

Figure 6.4: *Thermal time contour $\mathcal{C}+\mathcal{I}$ [136].*

imaginary axis from $t=0$ to $t=-i\beta$ [49] (see section D.1.1),

$$\langle \varphi_+, 0 \,|\rho|\, \varphi_-, 0\rangle \;=\; \int\limits_{\varphi(0_-,\boldsymbol{x})=\varphi_-(\boldsymbol{x})}^{\varphi(-i\beta,\boldsymbol{x})=\varphi_+(\boldsymbol{x})} \mathcal{D}\varphi \, \exp\left(i \int_{\mathcal{I}} d^4x \, \mathcal{L}(x) \right) . \tag{6.18}$$

The upper path integral representation of the thermal density matrix element yields a generating functional for the thermal state by concatenating the time contours $\mathcal{C}$ and $\mathcal{I}$ (the derivation is analogous to that of eq. (6.7)),

$$\begin{aligned} Z_\beta[J,K] &= \mathrm{Tr}\left(\rho \, T_{\mathcal{C}+\mathcal{I}} \left[\exp\left(i \int_{\mathcal{C}+\mathcal{I}} d^4x J(x)\Phi(x) + \frac{i}{2} \int_{\mathcal{C}+\mathcal{I}} d^4x \int_{\mathcal{C}+\mathcal{I}} d^4y \, \Phi(x) K(x,y) \Phi(y) \right) \right] \right) \\ &= \int \mathcal{D}\varphi \exp\left(i \int_{\mathcal{C}+\mathcal{I}} d^4x \left\{ \mathcal{L}(x) + J(x)\varphi(x) \right\} + \frac{i}{2} \int_{\mathcal{C}+\mathcal{I}} d^4x \int_{\mathcal{C}+\mathcal{I}} d^4y \, \varphi(x) K(x,y) \varphi(y) \right) . \end{aligned} \tag{6.19}$$

The path integral is performed over all field configurations $\varphi(x)$ with time argument attached to the thermal time path $\mathcal{C}+\mathcal{I}$ (see figure 6.4) which fulfill the periodicity relation $\varphi(0_+,\boldsymbol{x}) = \varphi(-i\beta,\boldsymbol{x})$. The time arguments of the external sources are also attached to the thermal time path $\mathcal{C}+\mathcal{I}$.

The thermal propagator

The thermal propagator is defined as the connected two-point correlation function on the thermal time contour $\mathcal{C}+\mathcal{I}$,

$$G_{th}(x,y) = \langle T_{\mathcal{C}+\mathcal{I}} \Phi(x)\Phi(y) \rangle - \langle \Phi(x) \rangle \langle \Phi(y) \rangle . \tag{6.20}$$

The thermal propagator can be obtained from the generating functional (6.19) for correlation functions formulated on the thermal time path by functional differentiation.
For calculations in thermal equilibrium, it is sometimes convenient to use a pure imaginary time formalism by setting $t_{max}=0$ such that only the path $\mathcal{I}$ contributes. Since thermal correlation functions considered here are space-time translation invariant, it is convenient to Fourier transform the thermal two-point function with respect to the relative imaginary times and spatial coordinates,

$$G_{th}(x,y) = \int_q e^{iq(x-y)} G_{th}(q) \qquad \text{for } x^0, y^0 \in \mathcal{I} . \tag{6.21}$$

The meaning of $\int_q$ depends on the context. For zero-temperature calculations $\int_q \equiv \int \frac{d^4q}{(2\pi)^4}$ denotes the integral over Euclidean momentum space. For finite-temperature calculations, however, $\int_q \equiv \int_q^T \equiv T\sum_n \int \frac{d^3q}{(2\pi)^3}$, where $q^0 = i\omega_n$ and the sum runs over the Matsubara frequencies $\omega_n = 2\pi n/T$ (see section D.1.2).

2PI effective action and Schwinger-Dyson equation

The 2PI effective action in thermal equilibrium is the double Legendre transform of the generating functional (6.19) with respect to the external sources. The latter has the same structure as the generating functional (3.20) in vacuum, except that all time-integrations are performed over the thermal time path. Consequently, the 2PI effective action in thermal equilibrium is obtained from the parameterization given in eq. (3.26) by replacing the time-integrations $\int \to \int_{\mathcal{C}+\mathcal{I}}$. Especially, the setting-sun approximation of the 2PI effective action is obtained from eq. (6.9) by replacing $\int_{\mathcal{C}} \to \int_{\mathcal{C}+\mathcal{I}}$.
The equation of motion for the full thermal propagator is obtained from the stationarity condition (3.28) of the 2PI effective action with respect to variations of the two-point function. In setting-sun approximation, it is given by

$$G_{th}^{-1}(x,y) = G_{0,th}^{-1}(x,y) - \Pi_{th}(x,y)\,, \tag{6.22}$$

$$\Pi_{th}(x,y) \equiv \frac{2i\delta\Gamma_2[G_{th}]}{\delta G_{th}(y,x)} = \frac{-i\lambda}{2} G_{th}(x,x)\delta^4_{\mathcal{C}+\mathcal{I}}(x-y) + \frac{(-i\lambda)^2}{6} G_{th}(x,y)^3\,, \tag{6.23}$$

where $\Pi_{th}(x,y)$ is the full thermal self-energy, and $G_{0,th}^{-1}(x,y) = i(\Box_x + m^2)\delta^4_{\mathcal{C}+\mathcal{I}}(x-y)$ is the free inverse thermal propagator. Note that $x^0, y^0 \in \mathcal{C}+\mathcal{I}$ take real as well as imaginary values.

Nonperturbative renormalization procedure — derivation

Starting from the bare classical action

$$S[\phi] = \int d^4x \left(\frac{1}{2}(\partial\phi)^2 - \frac{1}{2}m_B^2\phi^2 - \frac{\lambda_B}{4!}\phi^4 \right), \tag{6.24}$$

the field is rescaled and the bare mass m_B and the bare coupling λ_B are split into renormalized parts and counterterms,

$$\phi_R = Z^{-1/2}\phi, \quad Zm_B^2 = m_R^2 + \delta m^2, \quad Z^2\lambda_B = \lambda_R + \delta\lambda, \quad Z = 1 + \delta Z\,, \tag{6.25}$$

where Z is the rescaling factor of the field value. The equation of motion for the renormalized 2PI propagator $G_{th,R} = Z^{-1}G_{th}$ in setting-sun approximation and at finite temperature is obtained by using eq. (6.22) on the imaginary time path $\mathcal{I}$ and switching to 4-momentum space,

$$G_{th,R}^{-1}(k) = k^2 + m_R^2 - \Pi_{th,R}(k)\,, \tag{6.26}$$

$$\Pi_{th,R}(k) = -\delta Z_0 k^2 - \delta m_0^2 - \frac{\lambda_R + \delta\lambda_0}{2}\int_q G_{th,R}(q) + \frac{\lambda_R^2}{6}\int_{pq} G_{th,R}(p)G_{th,R}(q)G_{th,R}(k-q-p)\,.$$

Here, δZ_0, δm_0^2 and $\delta\lambda_0$ denote the 2PI counterterms in setting-sun approximation, which have to be chosen such that the divergences in the tadpole- and setting-sun contributions to the renormalized self-energy $\Pi_{th,R}(k)$ as well as the divergences hidden in the full propagator are removed independent of the temperature. As will be shown in the following, this is accomplished by imposing two renormalization conditions

$$G_{T_0}^{-1}(k=\tilde{k}) = \tilde{k}^2 + m_R^2\,, \qquad \frac{d}{dk^2}G_{T_0}^{-1}(k=\tilde{k}) = +1\,, \tag{6.27}$$

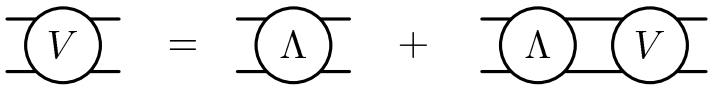

Figure 6.5: *Bethe-Salpeter equation.*

for the propagator supplemented by a third renormalization condition for an appropriate 4-point function. Here $G_{T_0}(k)$ is the solution of eq. (6.26) for an (arbitrary) reference temperature T_0, and $\tilde{k}$ is an (arbitrary) reference scale (e.g. $T_0 = 0, \tilde{k} = 0$).
The aim is to find a set of counterterms which also renormalizes the propagator $G_T(k)$ for all $T \neq T_0$, the equation for which can be written as

$$\begin{aligned} G_T^{-1}(k) &= G_{T_0}^{-1}(k) - \Delta\Pi(k)\,, \\ \Delta\Pi(k) &= -\frac{\lambda_R + \delta\lambda_0}{2}\left[\int_q^T G_T(q) - \int_q^{T_0} G_{T_0}(q)\right] \\ &\quad + \frac{\lambda_R^2}{6}\left[\int_{pq}^T G_T(p)G_T(q)G_T(k-q-p) - \int_{pq}^{T_0} G_{T_0}(p)G_{T_0}(q)G_{T_0}(k-q-p)\right]. \end{aligned} \tag{6.28}$$

Inverting the first line yields an expansion

$$G_T(k) = G_{T_0}(k) + \Delta G(k) = G_{T_0}(k) + G_{T_0}(k)\Delta\Pi(k)G_{T_0}(k) + \Delta^2 G(k)\,. \tag{6.29}$$

At large momenta $k^2 \gg T^2, T_0^2$, both propagators agree asymptotically, such that $\Delta\Pi(k) \sim c_1 \ln k + c_2(\ln k)^2 + \ldots$ (with coefficients c_i) just grows logarithmically. Thus, $\Delta G(k)$ and $\Delta^2 G(k)$ fall off like k^{-4} and k^{-6} times powers of logarithms, respectively. Furthermore, $\int_q^T \equiv \int_q^{T_0} + \int_q^{\Delta T}$ where the latter is exponentially suppressed for $q^2 \gg T^2, T_0^2$. Altogether, using Weinbergs theorem [177] one finds that

$$\Delta\Pi(k) = \frac{1}{2}\left[\int_q^{T_0} \Delta G(q) + \int_q^{\Delta T} G_T(q)\right]\Lambda_{T_0}(q,k) + \mathcal{F}(k)\,, \tag{6.30}$$

where $\mathcal{F}(k)$ contains all finite contributions (and falls off like k^{-2} times powers of logarithms), and where $\Lambda_{T_0}(q,k)$ is equal to

$$\Lambda_R(q,k) = -\lambda_R - \delta\lambda_0 + \lambda_R^2 \int_p G_{th,R}(p)G_{th,R}(k-q-p)\,, \tag{6.31}$$

evaluated at temperature T_0. Using the second part of eq. (6.29) in eq. (6.30), one can write

$$\int_q^{T_0} \Delta\Pi(q)\left[\delta(q-k) - \frac{1}{2}G_{T_0}^2(q)\Lambda_{T_0}(q,k)\right] = \frac{1}{2}\left[\int_q^{T_0} \Delta^2 G(q) + \int_q^{\Delta T} G_T(q)\right]\Lambda_{T_0}(q,k) + \mathcal{F}(k)\,.$$

Multiplying by $\delta(k-p) + G_{T_0}^2(k)V_{T_0}(k,p)/2$ (with V_{T_0} arbitrary) and integrating over k yields

$$\begin{aligned} &\int_q^{T_0} \Delta\Pi(q)\left\{\delta(q-p) - \frac{1}{2}G_{T_0}^2(q)\left[V_{T_0}(q,p) - \Lambda_{T_0}(q,p) - \frac{1}{2}\int_k^{T_0} \Lambda_{T_0}(q,k)G_{T_0}^2(k)V_{T_0}(k,p)\right]\right\} = \\ &= \frac{1}{2}\int_k^{T_0}\left\{\left[\int_q^{T_0} \Delta^2 G(q) + \int_q^{\Delta T} G_T(q)\right]\Lambda_{T_0}(q,k) + \mathcal{F}(k)\right\}\left(\delta(k-p) + \frac{1}{2}G_{T_0}^2(k)V_{T_0}(k,p)\right). \end{aligned}$$

If one demands that $V_{T_0}(q,p)$ fulfills the "Bethe-Salpeter equation" (see figure 6.5) at temperature T_0,

$$V_R(q,p) = \Lambda_R(q,p) + \frac{1}{2}\int_k \Lambda_R(q,k) G^2_{th,R}(k) V_R(k,p)\,, \tag{6.32}$$

it is possible to encapsulate all divergences of the upper equation into $V_{T_0}(q,p)$,

$$\Delta\Pi(p) = \frac{1}{2}\int_q^{T_0} \left[\Delta^2 G(q) + \mathcal{F}(q) G^2_{T_0}(q)\right] V_{T_0}(q,p) + \frac{1}{2}\int_q^{\Delta T} G_T(q) V_{T_0}(q,p)\,.$$

The momentum integrals are finite provided that the 2PI 4-point function $V_{T_0}(q,p)$ is finite and grows at most logarithmically when one of its arguments tends towards infinity while the other is fixed. It turns out [28] that this is achieved by requiring $V_{T_0}(q,p)$ to be finite at the renormalization point,

$$V_{T_0}(q=\tilde{k}, p=\tilde{k}) = -\lambda_R\,. \tag{6.33}$$

Finally, since $\Delta\Pi(p)$ is finite, eq. (6.28) implies that the renormalized 2PI propagator $G_T(k)$ is finite for all temperatures T.
In summary, the renormalization conditions eq. (6.27) for the propagator $G_{th,R}(k)$ and eq. (6.33) for the 4-point function $V_R(q,p)$ (evaluated at some arbitrary reference temperature T_0) together with the nonperturbative Schwinger-Dyson equation (6.26) and Bethe-Salpeter equation (6.32) form a closed set of equations for the determination of the 2PI counterterms.

Chapter 7

Renormalization Techniques for Schwinger-Keldysh Correlation Functions

In this chapter, a framework appropriate for the nonperturbative renormalization of Kadanoff-Baym equations is developed and applied to the three-loop truncation of the 2PI effective action.

The nonperturbative 2PI renormalization procedure is transferred to the 2PI effective action formulated on the closed Schwinger-Keldysh real-time contour. Therefore, a Kadanoff-Baym equation for the full thermal propagator formulated on the closed real-time contour is derived. This requires the incorporation of initial states characterized by non-Gaussian n-point correlation functions (for arbitrary n) into the Kadanoff-Baym equations.

In section 7.1, Kadanoff-Baym equations for non-Gaussian initial states are derived. In section 7.2, it is shown how to calculate the thermal values of the non-Gaussian n-point correlation functions for a given truncation of the 2PI effective action, and a Kadanoff-Baym equation for the thermal initial state is derived. This equation can then be renormalized explicitly by transferring the renormalization procedure of the 2PI effective action at finite temperature to the closed real-time contour, which is done in section 7.3.

These renormalized Kadanoff-Baym equations for thermal equilibrium then provide the basis for the transition to renormalized nonequilibrium dynamics.

7.1 Kadanoff-Baym Equations for Non-Gaussian Initial States

A statistical ensemble of physical states in the Hilbert space belonging to the real scalar $\lambda\Phi^4/4!$ quantum field theory is considered, which is described by a density matrix ρ at the time $t_{init} \equiv 0$. The generating functional $Z_\rho[J,K]$ for nonequilibrium correlation functions in the presence of a local external source $J(x)$ and a bilocal external source $K(x,y)$ can be conveniently formulated on the closed real-time path $\mathcal{C}$ (see figure 6.1), and has a path integral representation given in eq. (6.7). The information about the initial state of the system enters via the matrix element of the density matrix with respect to two arbitrary eigenstates $\Phi(0,\boldsymbol{x})|\varphi_\pm,0\rangle = \varphi_\pm(\boldsymbol{x})|\varphi_\pm,0\rangle$ of the quantum field operator evaluated at the initial time.

Non-Gaussian Initial State

The matrix element of the density matrix ρ is a functional of the field configurations $\varphi_+(\boldsymbol{x})$ and $\varphi_-(\boldsymbol{x})$, which can be written as [49]

$$\langle \varphi_+, 0 \,|\rho|\, \varphi_-, 0\rangle = \exp\left(iF[\varphi]\right). \tag{7.1}$$

For a Gaussian initial state, $F[\varphi]$ is a quadratic functional of the field (see eq. (6.8)). For a general initial state, the functional $F[\varphi]$ may be Taylor expanded in the form

$$\begin{aligned} F[\varphi] &= \alpha_0 + \int_{\mathcal{C}} d^4x\, \alpha_1(x)\varphi(x) + \frac{1}{2}\int_{\mathcal{C}} d^4x d^4y\, \alpha_2(x,y)\varphi(x)\varphi(y) \\ &\quad + \frac{1}{3!}\int_{\mathcal{C}} d^4x d^4y d^4z\, \alpha_3(x,y,z)\varphi(x)\varphi(y)\varphi(z) + \dots\,, \end{aligned} \tag{7.2}$$

where the integrals have been written in four dimensions. Since $F[\varphi]$ only depends, by definition, on the field configuration $\varphi_\pm(\boldsymbol{x}) = \varphi(0_\pm, \boldsymbol{x})$ evaluated at the boundaries of the time contour, the kernels $\alpha_n(x_1,\dots,x_n)$ for $n \geq 1$ are only nonzero if all their time arguments lie on the boundaries of the time contour. With the notation $\delta_+(t) = \delta_{\mathcal{C}}(t-0_+)$ and $\delta_-(t) = \delta_{\mathcal{C}}(t-0_-)$, they can be written in the form

$$\alpha_n(x_1,\dots,x_n) = \alpha_n^{\varepsilon_1,\dots,\varepsilon_n}(\boldsymbol{x_1},\dots,\boldsymbol{x_n})\,\delta_{\varepsilon_1}(x_1^0)\cdots\delta_{\varepsilon_n}(x_n^0), \tag{7.3}$$

where $\delta_{\mathcal{C}}$ denotes the Dirac distribution on $\mathcal{C}$ and summation over $\varepsilon_j = +,-$ is implied. In this way, the explicit dependence of the functional $F[\varphi]$ on the field configurations $\varphi_+(\boldsymbol{x})$ and $\varphi_-(\boldsymbol{x})$ may be recovered,

$$F[\varphi] = \alpha_0 + \int d^3x\, \alpha_1^{\varepsilon}(\boldsymbol{x})\varphi_\varepsilon(\boldsymbol{x}) + \frac{1}{2}\int d^3x \int d^3y\, \alpha_2^{\varepsilon_1\varepsilon_2}(\boldsymbol{x},\boldsymbol{y})\varphi_{\varepsilon_1}(\boldsymbol{x})\varphi_{\varepsilon_2}(\boldsymbol{x}) + \dots\,. \tag{7.4}$$

Thus, the kernels α_n contribute only at the initial time. Furthermore, the complete set of kernels α_n for $n \geq 0$ encodes the complete information about the density matrix characterizing the initial state. Not all the kernels are independent. The Hermiticity of the density matrix, $\rho = \rho^\dagger$, implies that

$$i\alpha_n^{\varepsilon_1,\dots,\varepsilon_n}(\boldsymbol{x_1},\dots,\boldsymbol{x_n}) = \left(i\alpha_n^{(-\varepsilon_1),\dots,(-\varepsilon_n)}(\boldsymbol{x_1},\dots,\boldsymbol{x_n})\right)^*. \tag{7.5}$$

If the initial state is invariant under some symmetries, there are further constraints. For example, for an initial state which is invariant under the Z_2-symmetry $\Phi \to -\Phi$, all kernels $\alpha_n(x_1,\dots,x_n)$ with odd n vanish. If the initial state is homogeneous in space, the initial correlations $\alpha_n(x_1,\dots,x_n)$ are invariant under space-translations $\boldsymbol{x_i} \to \boldsymbol{x_i} + \boldsymbol{a}$ of all arguments for any real three-vector $\boldsymbol{a}$, and can be conveniently expressed in spatial momentum space,

$$\begin{aligned} i\alpha_n^{\varepsilon_1,\dots,\varepsilon_n}(\boldsymbol{x_1},\dots,\boldsymbol{x_n}) &= \int\frac{d^3\boldsymbol{k_1}}{(2\pi)^3}\cdots\int\frac{d^3\boldsymbol{k_n}}{(2\pi)^3}\, e^{i(\boldsymbol{k_1}\boldsymbol{x_1}+\dots+\boldsymbol{k_n}\boldsymbol{x_n})} \\ &\quad (2\pi)^3\delta^3(\boldsymbol{k_1}+\dots+\boldsymbol{k_n})\, i\alpha_n^{\varepsilon_1,\dots,\varepsilon_n}(\boldsymbol{k_1},\dots,\boldsymbol{k_n}). \end{aligned} \tag{7.6}$$

Altogether, the generating functional for a statistical ensemble is given by

$$Z_\rho[J,K] = \int\mathcal{D}\varphi\, \exp\left(i\left\{S[\varphi] + J\varphi + \frac{1}{2}\varphi K\varphi + F_3[\varphi;\alpha_3,\alpha_4,\dots]\right\}\right),$$

where the kernels α_0, α_1 and α_2 have been absorbed into the measure $\mathcal{D}\varphi$ and into the sources J and K, respectively. The functional $F_3[\varphi;\alpha_3,\alpha_4,\dots]$ contains the contributions of third, fourth and higher orders of the Taylor expansion (7.2). It vanishes for a Gaussian initial state.

7.1.1 2PI Effective Action for Non-Gaussian Initial States

The 2PI effective action in the presence of non-Gaussian correlations is obtained from the standard parameterization [66] of the 2PI effective action applied to a theory described by the modified classical action $\tilde{S}[\phi;\alpha_3,\alpha_4,\ldots] \equiv S[\phi]+F_3[\phi,\alpha_3,\alpha_4,\ldots]$,

$$\Gamma[\phi,G] = \tilde{S}[\phi] + \frac{i}{2}\mathrm{Tr}\ln G^{-1} + \frac{i}{2}\mathrm{Tr}\left(\tilde{\mathcal{G}}_0^{-1}G-1\right)+\tilde{\Gamma}_2[\phi,G]\,, \tag{7.7}$$

where $i\tilde{\mathcal{G}}_0^{-1} \equiv \frac{\delta^2\tilde{S}[\phi]}{\delta\phi(x)\delta\phi(y)}$. This parameterization may be rewritten by splitting it into a part which contains the contributions from non-Gaussian initial correlations and one which resembles the parameterization obtained in the Gaussian case (D.31),

$$\Gamma[\phi,G] = S[\phi] + \frac{i}{2}\mathrm{Tr}\ln G^{-1} + \frac{i}{2}\mathrm{Tr}\left(\mathcal{G}_0^{-1}G-1\right)+\Gamma_2[\phi,G]+\Gamma_{nG}[\phi,G;\alpha_3,\alpha_4,\ldots]\,, \tag{7.8}$$

where $i\mathcal{G}_0^{-1} \equiv \frac{\delta^2 S[\phi]}{\delta\phi(x)\delta\phi(y)}$ is the classical inverse propagator (D.32) and the non-Gaussian contribution is obtained by comparing eq. (7.8) and eq. (7.7),

$$\Gamma_{nG}[\phi,G;\alpha_3,\alpha_4,\ldots] = F_3[\phi;\alpha_3,\alpha_4,\ldots] + \frac{1}{2}\mathrm{Tr}\left(\frac{\delta^2 F_3}{\delta\phi\delta\phi}G\right)+\Gamma_{2,nG}[\phi,G;\alpha_3,\alpha_4,\ldots]\,. \tag{7.9}$$

The 2PI functional

$$i\tilde{\Gamma}_2[\phi,G;\alpha_3,\alpha_4,\ldots] \equiv i\Gamma_2[\phi,G]+i\Gamma_{2,nG}[\phi,G;\alpha_3,\alpha_4,\ldots] \tag{7.10}$$

is equal to the sum of all 2PI Feynman diagrams with lines given by the full propagator $G(x,y)$ and with vertices given by the derivatives of the modified classical action $\tilde{S}[\phi;\alpha_3,\alpha_4,\ldots]$. Apart from the classical three- and four-point vertices given by eq. (D.33), for a general non-Gaussian initial state, the initial n-point correlations (with $n\geq 3$) lead to additional effective non-local vertices connecting n lines (see figure 7.1). They result from the contribution of the corresponding sources $\alpha_m(x_1,\ldots,x_m)$, $m\geq n$, contained in the contribution $F_3[\phi;\alpha_3,\alpha_4,\ldots]$ to the generating functional (7.7), and are given by

$$\begin{aligned} i\frac{\delta^n F_3[\phi;\alpha_3,\alpha_4,\ldots]}{\delta\phi(x_1)\ldots\delta\phi(x_n)} &= i\alpha_n(x_1,\ldots,x_n)+\int_{\mathcal{C}} d^4x_{n+1}\, i\alpha_{n+1}(x_1,\ldots,x_{n+1})\phi(x_{n+1}) \\ &\quad +\frac{1}{2}\int_{\mathcal{C}} d^4x_{n+1}d^4x_{n+2}\, i\alpha_{n+2}(x_1,\ldots,x_{n+2})\phi(x_{n+1})\phi(x_{n+2})+\ldots \\ &\equiv i\bar{\alpha}_n(x_1,\ldots,x_n)\,. \end{aligned} \tag{7.11}$$

Note that, since the sources $\alpha_m(x_1,\ldots,x_m)$ are only supported at the initial time, all the upper integrals along the time contour $\mathcal{C}$ just depend on powers of the initial value of the field expectation value $\phi(x)|_{x^0=0}$. Therefore, the effective non-local n-point vertex $i\bar{\alpha}_n(x_1,\ldots,x_n)$ indeed encodes information about the initial state and is in particular independent of the subsequent time-evolution of $\phi(x)$. Analogously,

$$i\bar{\alpha}_2(x,y) \equiv i\alpha_2(x,y)+i\frac{\delta^2 F_3[\phi;\alpha_3,\alpha_4,\ldots]}{\delta\phi(x)\delta\phi(y)}\,, \tag{7.12}$$

is defined. For a Z_2-symmetric initial state, the field expectation value vanishes, $\phi(x)|_{x^0=0}=0$, such that $\bar{\alpha}_n(x_1,\ldots,x_n)=\alpha_n(x_1,\ldots,x_n)$. From eq. (7.3) it can be seen that the effective non-local vertices are supported at the initial time similarly to the sources $i\alpha_n(x_1,\ldots,x_n)$,

$$i\bar{\alpha}_n(x_1,\ldots,x_n) = i\bar{\alpha}_n^{\varepsilon_1,\ldots,\varepsilon_n}(\boldsymbol{x_1},\ldots,\boldsymbol{x_n})\,\delta_{\varepsilon_1}(x_1^0)\cdots\delta_{\varepsilon_n}(x_n^0)\,. \tag{7.13}$$

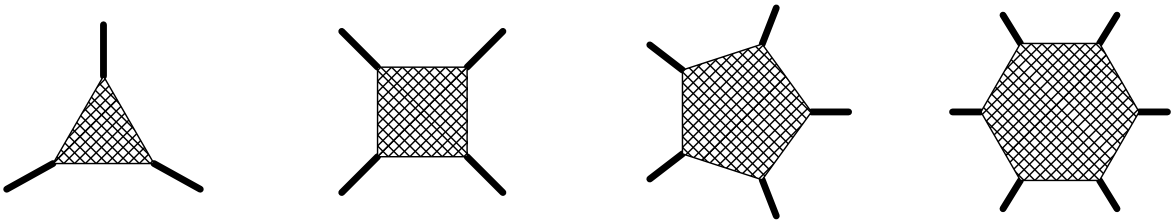

Figure 7.1: *Non-local effective vertices* $i\bar{\alpha}_n(x_1,\ldots,x_n)$ *connecting n lines for* $n = 3,4,5,6$ *encoding the non-Gaussian three-, four-, five-, six-, . . . -point correlations of the initial state.*

Thus, the contribution of these effective non-local vertices will be most important in the first moments of the nonequilibrium evolution. In particular, e.g. the four-point source $\alpha_4(x_1,\ldots,x_4)$ can lead to a non-vanishing value of the connected four-point correlation function at the initial time, which is impossible for a Gaussian initial state.
The 2PI functional (7.10) is thus equal to the sum of all 2PI Feynman diagrams with lines given by the full propagator $G(x,y)$, and with n-point vertices ($n \geq 3$) given by eq. (7.11) as well as classical three- and four-point vertices given by eq. (D.33). Note that those 2PI diagrams which contain exclusively the classical vertices given in eq. (D.33) by definition contribute to the functional $i\Gamma_2[\phi,G]$. Therefore, the diagrams contributing to the non-Gaussian part $i\Gamma_{2,nG}[\phi,G,\alpha_3,\alpha_4,\ldots]$ contain at least one effective vertex from eq. (7.11) involving a source $\alpha_n(x_1,\ldots,x_n)$ ($n \geq 3$). Thus, the non-Gaussian contribution to the 2PI effective action defined in eq. (7.8) indeed vanishes for Gaussian initial conditions (D.24),

$$\Gamma_{nG}[\phi,G;\alpha_3=0,\alpha_4=0,\ldots]=0\,. \tag{7.14}$$

As an example, an initial 4-point correlation is considered for an initial state which is Z_2-symmetric such that $\phi(x)=0$. Then the 2PI functional $\tilde{\Gamma}_2[G;\alpha_4] \equiv \tilde{\Gamma}_2[\phi=0,G;\alpha_3=0,\alpha_4,\alpha_5=\alpha_6=\ldots=0]$ in "naïve"[1] three loop approximation reads (see figure 7.2)

$$\begin{aligned} i\tilde{\Gamma}_2[G;\alpha_4] \;=\; & \frac{1}{8}\int_{\mathcal{C}} d^4x_{1234}\left[-i\lambda\,\delta_{12}\delta_{23}\delta_{34}+i\alpha_4(x_1,\ldots,x_4)\right]G(x_1,x_2)G(x_3,x_4) \\ & +\frac{1}{48}\int_{\mathcal{C}} d^4x_{1234}d^4x_{5678}\left[-i\lambda\,\delta_{12}\delta_{23}\delta_{34}+i\alpha_4(x_1,\ldots,x_4)\right]G(x_1,x_5)\times \\ & \times G(x_2,x_6)G(x_3,x_7)G(x_4,x_8)\left[-i\lambda\,\delta_{56}\delta_{57}\delta_{58}+i\alpha_4(x_5,\ldots,x_8)\right], \end{aligned} \tag{7.15}$$

where a compact notation $\delta_{12}=\delta_{\mathcal{C}}(x_1-x_2)$ and $d^4x_{1234}=d^4x_1\cdots d^4x_4$ has been used. Note that the contribution to the mixed "basketball" diagram in the second and third line with one classical and one effective vertex appears twice, which accounts for the symmetry factor $1/24$. This truncation of the 2PI functional is also referred to as setting-sun approximation in the following.

7.1.2 Self-Energy for Non-Gaussian Initial States

The equation of motion for the full propagator is obtained from the stationarity condition of the 2PI effective action in the presence of the source $\alpha_2(x,y)$, $\delta\Gamma[G]/\delta G(y,x) = -\alpha_2(x,y)/2$. Using the parameterization (7.7) and eq. (7.12),

$$G^{-1}(x,y)=\mathcal{G}_0^{-1}(x,y)-\Pi(x,y)-i\bar{\alpha}_2(x,y)\,, \tag{7.16}$$

[1] This means no difference is made between diagrams with or without non-local effective vertices when counting loops.

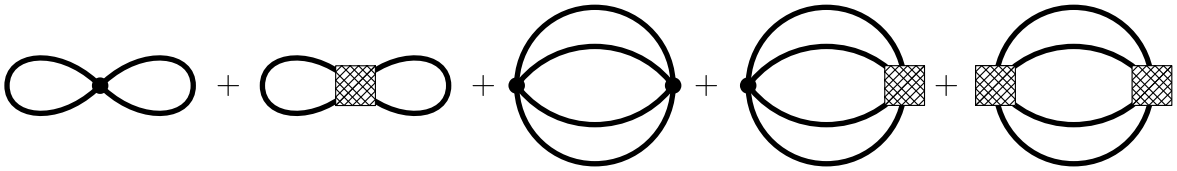

Figure 7.2: *Diagrams contributing to the three-loop truncation of the 2PI effective action in the symmetric phase (setting-sun approximation) in the presence of an effective non-local four-point vertex.*

is obtained, where the self-energy $\Pi(x,y)$ is given by

$$\Pi(x,y) = \frac{2i\delta\tilde{\Gamma}_2[\phi,G;\alpha_4,\alpha_6,\ldots]}{\delta G(y,x)} = \frac{2i\delta\Gamma_2[\phi,G]}{\delta G(y,x)} + \frac{2i\delta\Gamma_{2,nG}[\phi,G;\alpha_4,\alpha_6,\ldots]}{\delta G(y,x)}\,. \tag{7.17}$$

For the non-Gaussian case, the self-energy can be decomposed as

$$\begin{aligned} \Pi(x,y) &= \Pi^{G}(x,y) + \Pi^{nG}(x,y)\,, \\ \Pi^{G}(x,y) &= -i\Pi_{loc}(x)\delta_{\mathcal{C}}(x-y) + \Pi^{G}_{non-loc}(x,y)\,, \\ \Pi^{nG}(x,y) &= \Pi^{nG}_{non-loc}(x,y) + i\Pi^{nG}_{surface}(x,y)\,, \end{aligned} \tag{7.18}$$

where $\Pi^{G} = 2i\delta\Gamma_2/\delta G$ contains the contributions to the self-energy which are also present for a Gaussian initial state, and $\Pi^{nG} = 2i\delta\Gamma_{2,nG}/\delta G$ contains all contributions which contain at least one non-Gaussian initial correlation. The latter can be further decomposed into a non-Gaussian non-local part $\Pi^{nG}_{non-loc}(x,y)$, which contains diagrams where both external lines are attached to a local standard vertex, and a part $i\Pi^{nG}_{surface}(x,y)$, which contains all non-Gaussian contributions which are supported only at the initial time surface where $x^0 = 0$ *or* $y^0 = 0$. In general, such contributions can arise in the following ways:

1. From diagrams where both external lines are connected to an effective non-local vertex as given in eq. (7.11). They are supported at $x^0 = y^0 = 0$.

2. From diagrams where one of the two external lines is connected to an effective non-local vertex, while the other one is connected to a classical local vertex as given in eq. (D.33). They are supported at $x^0 = 0, y^0 \geq 0$ or vice-versa.

3. Via the contribution $i\bar{\alpha}_2(x,y)$ of the initial two-point source which is supported at $x^0 = y^0 = 0$. This is the *only* Gaussian surface-contribution.

Accordingly, the contributions to the self-energy which are supported at the initial time surface can be further decomposed as

$$\Pi_{surface}(x,y) = \Pi^{nG}_{surface}(x,y) + \bar{\alpha}_2(x,y) = \Pi_{\alpha\alpha}(x,y) + \Pi_{\lambda\alpha}(x,y) + \Pi_{\alpha\lambda}(x,y), \tag{7.19}$$

where

$$\begin{aligned} \Pi_{\alpha\alpha}(x,y) &= \delta_{\varepsilon_1}(x_0)\Pi^{\varepsilon_1,\varepsilon_2}_{\alpha\alpha}(\boldsymbol{x},\boldsymbol{y})\delta_{\varepsilon_2}(y_0)\,, \\ \Pi_{\lambda\alpha}(x,y) &= \Pi^{\varepsilon}_{\lambda\alpha}(x^0,\boldsymbol{x},\boldsymbol{y})\delta_{\varepsilon}(y_0)\,, \\ \Pi_{\alpha\lambda}(x,y) &= \delta_{\varepsilon}(x_0)\Pi^{\varepsilon}_{\alpha\lambda}(\boldsymbol{x},y^0,\boldsymbol{y}) \;=\; \Pi_{\lambda\alpha}(y,x)\,. \end{aligned} \tag{7.20}$$

$\Pi_{\alpha\alpha}$ contains all contributions of type (1.) and (3.). Diagrams of type (2.) contribute to $\Pi_{\lambda\alpha}$ or $\Pi_{\alpha\lambda}$ depending which external line is attached to the effective non-local vertex and which to the classical

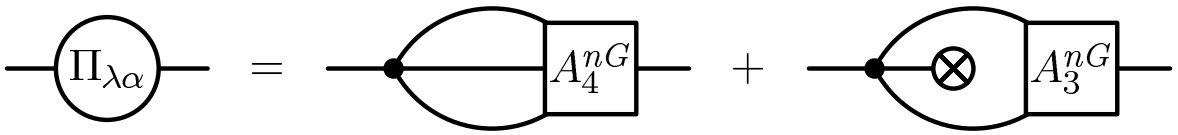

Figure 7.3: *Contribution $\Pi_{\lambda\alpha}(x,y)$ to the self-energy $\Pi(x,y)$ where the left line is connected to a classical vertex, and the right line to an effective non-local vertex.*

local vertex. Thus, for all diagrams contributing to $\Pi_{\lambda\alpha}$ the left line is connected to the classical four- or three-point vertex, which means that it can always be written in the form (see figure 7.3)

$$\begin{aligned} i\Pi_{\lambda\alpha}(x,y) &= \frac{-i\lambda}{6}\int_{\mathcal{C}} d^4x_{123}G(x,x_1)G(x,x_2)G(x,x_3)iA_4^{nG}(x_1,x_2,x_3,y) \\ &\quad + \frac{-i\lambda\phi(x)}{2}\int_{\mathcal{C}} d^4x_{12}G(x,x_1)G(x,x_2)iA_3^{nG}(x_1,x_2,y)\,. \end{aligned} \tag{7.21}$$

The non-local part contains all diagrams where both external lines are attached to a classical local vertex as given in eq. (D.33). It can be split into statistical and spectral components, similarly to the Gaussian case,

$$\Pi_{non-loc}(x,y) = \Pi^G_{non-loc}(x,y) + \Pi^{nG}_{non-loc}(x,y) = \Pi_F(x,y) - \frac{i}{2}\,\mathrm{sgn}_{\mathcal{C}}(x^0-y^0)\,\Pi_\rho(x,y)\,. \tag{7.22}$$

The local part does not receive any changes in the non-Gaussian case and is included in an effective, time-dependent mass term

$$M(x)^2 = m^2 + \frac{\lambda}{2}\phi^2(x) + \Pi_{loc}(x) = m_B^2 + \frac{\lambda}{2}\phi^2(x) + \frac{\lambda}{2}G(x,x)\,. \tag{7.23}$$

For the setting-sun approximation from eq. (7.15), the self-energy is given by (see figure 7.4)

$$\begin{aligned} \Pi^G_{non-loc}(x,y) &= \frac{(-i\lambda)^2}{6}G(x,y)^3\,, \qquad M(x)^2 = m^2 + \frac{\lambda}{2}G(x,x)\,, \\ \Pi^{nG}_{non-loc}(x,y) &= 0\,, \\ i\Pi_{\lambda\alpha}(x,y) &= \frac{-i\lambda}{6}\int d^4x_{123}\,G(x,x_1)G(x,x_2)G(x,x_3)\,i\alpha_4(x_1,x_2,x_3,y)\,, \\ i\Pi_{\alpha\alpha}(x,y) &= i\alpha_2(x,y) + \frac{1}{2}\int d^4x_{34}\,i\alpha_4(x,y,x_3,x_4)G(x_3,x_4) \\ &\quad + \frac{1}{6}\int d^4x_{234567}\,i\alpha_4(x,x_2,x_3,x_4)G(x_2,x_5)G(x_3,x_6)G(x_4,x_7)\,i\alpha_4(x_5,x_6,x_7,y)\,. \end{aligned} \tag{7.24}$$

A comparison with eq. (7.21) yields that

$$iA_4^{nG}(x_1,x_2,x_3,x_4) = i\alpha_4(x_1,x_2,x_3,x_4)\,, \qquad iA_3^{nG}(x_1,x_2,x_3) = 0\,,$$

for the upper approximation.

7.1.3 Kadanoff-Baym Equations for Non-Gaussian Initial States

Multiplying eq. (7.16) with the propagator and integrating yields

$$\begin{aligned} \left(\Box_x + M^2(x)\right)G(x,y) &= -i\delta_{\mathcal{C}}(x-y) - i\int_{\mathcal{C}} d^4z\,\left[\Pi(x,z) + i\bar{\alpha}_2(x,y)\right]G(z,y) \\ &= -i\delta_{\mathcal{C}}(x-y) - i\int_{\mathcal{C}} d^4z\,\left[\Pi^G_{non-loc}(x,z) + \Pi^{nG}_{non-loc}(x,z) + i\Pi_{\lambda\alpha}(x,z)\right]G(z,y)\,. \end{aligned} \tag{7.25}$$

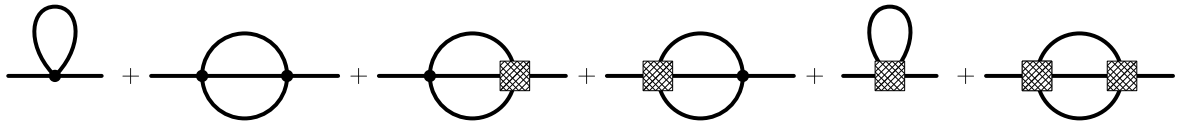

Figure 7.4: *Diagrams contributing to the self-energy* $\Pi(x,y)$ *in setting-sun approximation in the presence of an effective non-local four-point vertex. From left to right, the diagrams contribute to* Π_{loc}, $\Pi^{G}_{non-loc}$, $\Pi_{\lambda\alpha}$, $\Pi_{\alpha\lambda}$ *and the last two both contribute to* $\Pi_{\alpha\alpha}$.

The second line follows from using the parameterization (7.18) of the self-energy, and assuming $x^0 > 0$ and $y^0 > 0$. Using eqs. (7.20,7.22) yields the Kadanoff-Baym equations for $G_F(x^0,y^0,\boldsymbol{k})$ and $G_\rho(x^0,y^0,\boldsymbol{k})$ for an (arbitrary) non-Gaussian initial state,

$$\begin{aligned}
\left(\partial_{x^0}^2+\boldsymbol{k}^2+M^2(x^0)\right)G_F(x^0,y^0,\boldsymbol{k}) &= \int_0^{y^0} dz^0\,\Pi_F(x^0,z^0,\boldsymbol{k})G_\rho(z^0,y^0,\boldsymbol{k}) \\
&\quad -\int_0^{x^0} dz^0\,\Pi_\rho(x^0,z^0,\boldsymbol{k})G_F(z^0,y^0,\boldsymbol{k}) \\
&\quad +\Pi_{\lambda\alpha,F}(x^0,\boldsymbol{k})G_F(0,y^0,\boldsymbol{k}) \\
&\quad +\frac{1}{4}\Pi_{\lambda\alpha,\rho}(x^0,\boldsymbol{k})G_\rho(0,y^0,\boldsymbol{k})\,, \\
\left(\partial_{x^0}^2+\boldsymbol{k}^2+M^2(x^0)\right)G_\rho(x,y) &= \int_{x_0}^{y^0} dz^0\,\Pi_\rho(x^0,z^0,\boldsymbol{k})G_\rho(z^0,y^0,\boldsymbol{k})\,,
\end{aligned} \tag{7.26}$$

where

$$\begin{aligned}
\Pi_{\lambda\alpha,F}(x^0,\boldsymbol{k}) &= \Pi^+_{\lambda\alpha}(x^0,\boldsymbol{k})+\Pi^-_{\lambda\alpha}(x^0,\boldsymbol{k})\,, \\
\Pi_{\lambda\alpha,\rho}(x^0,\boldsymbol{k}) &= 2i\left(\Pi^+_{\lambda\alpha}(x^0,\boldsymbol{k})-\Pi^-_{\lambda\alpha}(x^0,\boldsymbol{k})\right)\,.
\end{aligned} \tag{7.27}$$

Using eq. (7.21) yields an equivalent formulation,

$$\begin{aligned}
\left(\Box_x+M^2(x)\right)G_F(x,y) &= \int_0^{y^0} d^4z\,\Pi_F(x,z)G_\rho(z,y) \\
&\quad -\int_0^{x^0} d^4z\,\Pi_\rho(x,z)G_F(z,y) \\
&\quad -\frac{\lambda}{6}V_4^{nG}(x,x,x,y)-\frac{\lambda\phi(x)}{2}V_3^{nG}(x,x,y)\,, \\
\left(\Box_x+M^2(x)\right)G_\rho(x,y) &= \int_{x_0}^{y^0} d^4z\,\Pi_\rho(x,z)G_\rho(z,y)\,,
\end{aligned} \tag{7.28}$$

where

$$\begin{aligned}
V_4^{nG}(x_1,x_2,x_3,x_4) &\equiv \int_{\mathcal{C}} d^4y_{1234}\,G(x_1,y_1)G(x_2,y_2)G(x_3,y_3)G(x_4,y_4)\,iA_4^{nG}(y_1,y_2,y_3,y_4)\,, \\
V_3^{nG}(x_1,x_2,x_3) &\equiv \int_{\mathcal{C}} d^4y_{123}\,G(x_1,y_1)G(x_2,y_2)G(x_3,y_3)\,iA_3^{nG}(y_1,y_2,y_3)\,,
\end{aligned} \tag{7.29}$$

denote the four- and three-point functions constructed from the kernels A_4^{nG} and A_3^{nG} appearing in the initial-time-surface contribution $\Pi_{\lambda\alpha}(x,y)$ to the self-energy, respectively (see eq. (7.21) and figure 7.3). Note that these new contributions on the right hand side of the Kadanoff-Baym equations

do *not* have to vanish in the limit $x^0, y^0 \to 0$, unlike the memory integrals. This is due to the fact that the higher non-Gaussian correlations of the initial state can lead to a non-vanishing value of the connected four- and three-point correlation functions at the initial time. In contrast to this, for a Gaussian initial state all higher correlations vanish at the initial time by definition.

7.2 Kadanoff-Baym Equations with Nonperturbative Thermal Initial Correlations

The Kadanoff-Baym equations discussed in section 7.1 are in principle capable to describe the time-evolution of the full two-point correlation function for a statistical ensemble which is described by an *arbitrary* state at some initial time $t_{init} = 0$. Since the nonperturbative renormalization is established at finite temperature, it is an important step to show that the full equilibrium propagator is indeed a solution of the nonperturbatively renormalized Kadanoff-Baym equations for a thermal initial state. This requires the incorporation of appropriate thermal initial correlations into the Kadanoff-Baym equations. However, since the underlying approximation based on the truncation of the 2PI effective action is highly non-perturbative, the choice of appropriate thermal initial correlations is not straightforward. For example, for the three-loop truncation of the 2PI effective action, the thermal n-point correlation functions for all $n = 2,4,6,\ldots$ are non-zero, although only two diagrams have been kept in the 2PI effective action. Therefore, one has to expect that non-Gaussian initial n-point correlations for all $n = 2,4,6,\ldots$ are required to describe thermal equilibrium with Kadanoff-Baym equations. In the following, it is shown how to construct the thermal initial correlations required for a given truncation of the 2PI effective action explicitly. This is accomplished by matching the nonperturbative equation of motion for the propagator formulated on the thermal time path with the Kadanoff-Baym equation for a non-Gaussian initial state formulated on the closed real-time path.
Thus, it is necessary to relate the following two equivalent descriptions of thermal equilibrium:

1. Via the thermal time contour ("$\mathcal{C}+\mathcal{I}$").

2. Via the closed real-time contour $\mathcal{C}$ and a thermal initial state, characterized by thermal initial correlations $\alpha_n^{th}(x_1,\ldots,x_n)$ ("$\mathcal{C}+\alpha$").

The first formulation exploits the explicit structure of the thermal density matrix, whereas the second one can easily be generalized to a nonequilibrium ensemble.

The thermal value of any (nonperturbative) Feynman diagram can directly be computed via the thermal time contour $\mathcal{C}+\mathcal{I}$, if the thermal (nonperturbative) propagator for real and imaginary times is available. For the computation of the corresponding (nonperturbative) Feynman diagram via the closed real-time contour $\mathcal{C}$, only real times appear. However, it requires the knowledge of the thermal initial correlations $\alpha_n^{th}(x_1,\ldots,x_n)$ which are appropriate for the considered approximation.

Since nonequilibrium Kadanoff-Baym equations are formulated on the closed real-time path $\mathcal{C}$, it is required to use the second approach. In the following, it is shown how to construct the thermal correlations $\alpha_n^{th}(x_1,\ldots,x_n)$ explicitly for a given truncation of the 2PI effective action. Before turning to the nonperturbative case, the relation between the two descriptions of thermal equilibrium will be discussed within perturbation theory.

7.2.1 Thermal Initial Correlations — Perturbation Theory

Thermal time contour $\mathcal{C}+\mathcal{I}$

The free thermal propagator defined on $\mathcal{C}+\mathcal{I}$ is (see also eq. (D.10))

$$iG^{-1}_{0,th}(x,y) = \left(-\Box_x - m^2\right)\delta_{\mathcal{C}+\mathcal{I}}(x-y) \qquad \text{for } x^0, y^0 \in \mathcal{C}+\mathcal{I}\,, \tag{7.30}$$

which may be decomposed into the free thermal statistical propagator and the free thermal spectral function

$$G_{0,th}(x,y) \;=\; G_{0,F}(x,y) - \frac{i}{2}\mathrm{sgn}_{\mathcal{C}+\mathcal{I}}(x^0-y^0)G_{0,\rho}(x,y)\,.$$

The explicit solution of the equation of motion is

$$\begin{aligned} G_{0,F}(x^0,y^0,\boldsymbol{k}) &= \frac{n_{BE}(\omega_k)+\frac{1}{2}}{\omega_k}\cos\left(\omega_k(x^0-y^0)\right)\,, \\ G_{0,\rho}(x^0,y^0,\boldsymbol{k}) &= \frac{1}{\omega_k}\sin\left(\omega_k(x^0-y^0)\right) \qquad\qquad \text{for } x^0, y^0 \in \mathcal{C}+\mathcal{I}\,, \end{aligned} \tag{7.31}$$

where $n_{BE}(\omega_k)$ is the Bose-Einstein distribution function,

$$n_{BE}(\omega_k) = \frac{1}{e^{\beta\omega_k}-1}, \qquad \omega_k = \sqrt{m^2+\boldsymbol{k}^2}\,.$$

Each of the two time arguments of the propagator can either be real or imaginary, which yields four combinations $G^{\mathcal{C}\mathcal{C}}_{0,th}$, $G^{\mathcal{C}\mathcal{I}}_{0,th}$, $G^{\mathcal{I}\mathcal{C}}_{0,th}$, $G^{\mathcal{I}\mathcal{I}}_{0,th}$. These appear in perturbative Feynman diagrams which are constructed with the free propagator $G_{0,th}$ and the classical vertices. In position space, each internal vertex of a Feynman diagram is integrated over the thermal time contour $\mathcal{C}+\mathcal{I}$. In order to disentangle the contributions from the real and the imaginary branch of the time contour, the following Feynman rules are defined,

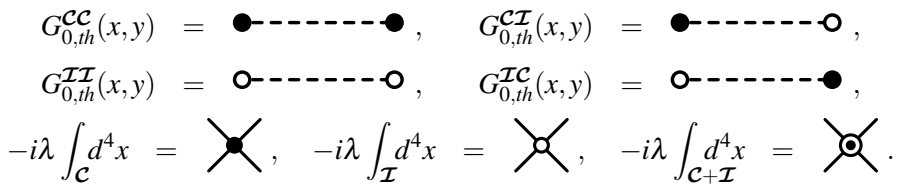

(7.32)

The filled circles denote a real time, and the empty circles denote an imaginary time. As an example, the perturbative setting-sun diagram is considered with propagators attached to both external lines, and evaluated for real external times $x^0, y^0 \in \mathcal{C}$. Both internal vertices are integrated over the two branches $\mathcal{C}$ and $\mathcal{I}$, respectively. Using the upper Feynman rules, the resulting four contributions can be depicted as

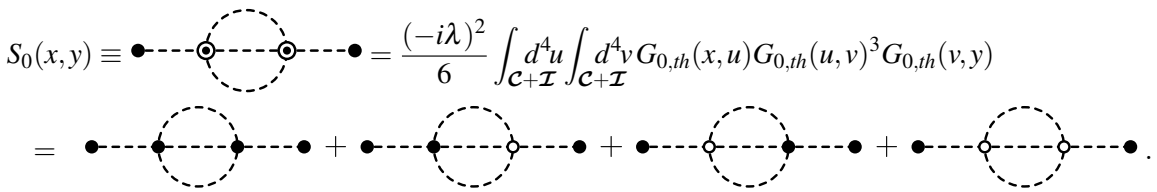

Closed real-time contour with thermal initial correlations $\mathcal{C}+\alpha$

In this paragraph, it will be shown how to explicitly construct the perturbative setting-sun $S_0(x,y)$ (or any other perturbative diagram) from corresponding perturbative Feynman diagrams which just involve *real* times which lie on the closed real-time contour $\mathcal{C}$ as well as the appropriate thermal initial correlations $\alpha_n^{th}(x_1,\ldots,x_n)$. As discussed in section 7.1, initial correlations appear in Feynman diagrams as additional effective, non-local vertices, which are supported only at the initial time $t_{init} \equiv 0$, at which the closed contour $\mathcal{C}$ starts ($t = 0_+$) and ends ($t = 0_-$).
Starting from the diagram on the thermal time contour $\mathcal{C}+\mathcal{I}$, one would like to obtain the function $S_0(x,y)$ without reference to imaginary times. The parts with imaginary and those with real times are connected by the free propagator evaluated with one imaginary and one real time. Using the explicit solution (7.31) together with elementary trigonometric addition theorems, it can be written as

$$G_{0,th}^{\mathcal{IC}}(-i\tau,y^0,\boldsymbol{k}) = \frac{G_{0,th}^{\mathcal{II}}(-i\tau,0,\boldsymbol{k})}{G_{0,th}(0,0,\boldsymbol{k})}\, G_{0,F}^{\mathcal{CC}}(0,y^0,\boldsymbol{k}) + i\partial_\tau G_{0,th}^{\mathcal{II}}(-i\tau,0,\boldsymbol{k})\, G_{0,\rho}^{\mathcal{CC}}(0,y^0,\boldsymbol{k})\,.$$

Next, the unequal-time statistical propagator and the spectral function are rewritten as

$$\begin{aligned} G_{0,F}^{\mathcal{CC}}(0,y^0,\boldsymbol{k}) &= \int_{\mathcal{C}} dz^0\, \delta_s(z^0) G_{0,th}^{\mathcal{CC}}(z^0,y^0,\boldsymbol{k})\,, && (7.33)\\ G_{0,\rho}^{\mathcal{CC}}(0,y^0,\boldsymbol{k}) &= -2i\int_{\mathcal{C}} dz^0\, \delta_a(z^0) G_{0,th}^{\mathcal{CC}}(z^0,y^0,\boldsymbol{k})\,, && (7.34)\end{aligned}$$

where

$$\begin{aligned} \delta_s(z^0) &= \frac{1}{2}\left(\delta_{\mathcal{C}}(z^0-0_+)+\delta_{\mathcal{C}}(z^0-0_-)\right),\\ \delta_a(z^0) &= \frac{1}{2}\left(\delta_{\mathcal{C}}(z^0-0_+)-\delta_{\mathcal{C}}(z^0-0_-)\right). && (7.35)\end{aligned}$$

Combining the upper equations, a helpful expression for the free propagator evaluated with one imaginary and one real time is obtained,

$$\begin{aligned} G_{0,th}^{\mathcal{IC}}(-i\tau,y^0,\boldsymbol{k}) &= \int_{\mathcal{C}} dz^0\, \Delta_0(-i\tau,z^0,\boldsymbol{k}) G_{0,th}^{\mathcal{CC}}(z^0,y^0,\boldsymbol{k})\,, && (7.36)\\ &= \end{aligned}$$

where the free "connection" defined in eq. (D.7) was inserted. In terms of the symmetric and anti-symmetric Dirac-distributions $\delta_{s,a}(z^0)$, the free connection reads

$$\begin{aligned} \Delta_0(-i\tau,z^0,\boldsymbol{k}) &= \Delta_0^s(-i\tau,\boldsymbol{k})\,\delta_s(z^0) + \Delta_0^a(-i\tau,\boldsymbol{k})\,\delta_a(z^0) && (7.37)\\ &= \left(\frac{G_{0,th}^{\mathcal{II}}(-i\tau,0,\boldsymbol{k})}{G_{0,th}(0,0,\boldsymbol{k})}\right)\delta_s(z^0) + \left(2\partial_\tau G_{0,th}^{\mathcal{II}}(-i\tau,0,\boldsymbol{k})\right)\delta_a(z^0)\\ &= \end{aligned}$$

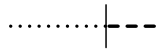

Analogously, the free propagator evaluated with one real and one imaginary time can be written as

$$\begin{aligned} G_{0,th}^{\mathcal{CI}}(y^0,-i\tau,\boldsymbol{k}) &= \int_{\mathcal{C}} dz^0\, G_{0,th}^{\mathcal{CC}}(x^0,z^0,\boldsymbol{k}) \Delta_0^T(z^0,-i\tau,\boldsymbol{k})\,, && (7.39)\\ &= \end{aligned}$$

where $\Delta_0^T(z^0,-i\tau,\boldsymbol{k}) = \Delta_0(-i\tau,z^0,\boldsymbol{k}) =$ 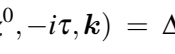 .

The connections Δ_0 and Δ_0^T are attached to an imaginary and a real vertex on the left and right sides, respectively. Their Fourier transform into position space is

$$\Delta_0(v,z) = \int\frac{d^3\boldsymbol{k}}{(2\pi)^3}\,e^{+i\boldsymbol{k}(\boldsymbol{v}-\boldsymbol{z})}\,\Delta_0(v^0,z^0,\boldsymbol{k}) \qquad \text{for } v^0\in\boldsymbol{\mathcal{I}}, z^0\in\boldsymbol{\mathcal{C}}\,,$$

as well as $\Delta_0^T(z,v)=\Delta_0(v,z)$. Conversely, the Fourier transform of the connection with respect to the imaginary time is a function of one Matsubara frequency $\omega_n = 2\pi\beta n$ and one real time $z^0\in\boldsymbol{\mathcal{C}}$,

$$\Delta_0(\omega_n,z^0,\boldsymbol{k}) = \left(\frac{G^{\boldsymbol{\mathcal{I}\mathcal{I}}}_{0,th}(\omega_n,\boldsymbol{k})}{G_{0,th}(0,0,\boldsymbol{k})}\right)\delta_s(z^0) + \left(2i\omega_n G^{\boldsymbol{\mathcal{I}\mathcal{I}}}_{0,th}(\omega_n,\boldsymbol{k})\right)\delta_a(z^0)\,, \tag{7.40}$$

and $\Delta_0^T(z^0,\omega_n,\boldsymbol{k})=\Delta_0(\omega_n,z^0,\boldsymbol{k})$. Eq. (7.36) for the free propagator with one imaginary and one real time then becomes

$$G^{\boldsymbol{\mathcal{I}\mathcal{C}}}_{0,th}(\omega_n,y^0,\boldsymbol{k}) \;=\; \int_{\boldsymbol{\mathcal{C}}} dz^0\,\Delta_0(\omega_n,z^0,\boldsymbol{k})G^{\boldsymbol{\mathcal{C}\mathcal{C}}}_{0,th}(z^0,y^0,\boldsymbol{k})\,. \tag{7.41}$$

By replacing all free propagators which connect an imaginary and a real time inside a perturbative Feynman diagram via the convolution of the connection and the real-real propagator, it is possible to encapsulate the parts of the diagram which involve "imaginary" vertices represented by empty circles. For example, the setting-sun diagram with one real and one imaginary vertex can be rewritten as

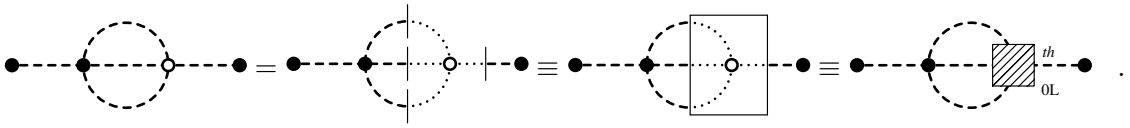

According to the symbolic notation employed here, the subdiagram containing the imaginary vertex, marked by the box, can be encapsulated into an effective non-local 4-point vertex. Its structure is determined by the connections Δ_0 and Δ_0^T, as can be seen by rewriting the above diagrams in terms of the corresponding formal expressions,

$$\begin{aligned}
&\frac{(-i\lambda)^2}{6}\int_{\boldsymbol{\mathcal{C}}}d^4u\int_{\boldsymbol{\mathcal{I}}}d^4v\,G_{0,th}(x,u)G_{0,th}(u,v)^3G_{0,th}(v,y)\\
&\quad= \frac{(-i\lambda)^2}{6}\int_{\boldsymbol{\mathcal{C}}}d^4u\int_{\boldsymbol{\mathcal{C}}}d^4z_1\int_{\boldsymbol{\mathcal{C}}}d^4z_2\int_{\boldsymbol{\mathcal{C}}}d^4z_3\int_{\boldsymbol{\mathcal{C}}}d^4z_4\,G_{0,th}(x,u)G_{0,th}(u,z_1)G_{0,th}(u,z_2)G_{0,th}(u,z_3)\\
&\qquad\qquad\left[\int_{\boldsymbol{\mathcal{I}}}d^4v\,\Delta_0^T(z_1,v)\Delta_0^T(z_2,v)\Delta_0^T(z_3,v)\Delta_0(v,z_4)\right]G_{0,th}(z_4,y)\\
&\quad\equiv \frac{-i\lambda}{6}\int_{\boldsymbol{\mathcal{C}}}d^4u\int_{\boldsymbol{\mathcal{C}}}d^4z_1\int_{\boldsymbol{\mathcal{C}}}d^4z_2\int_{\boldsymbol{\mathcal{C}}}d^4z_3\int_{\boldsymbol{\mathcal{C}}}d^4z_4\,G_{0,th}(x,u)G_{0,th}(u,z_1)G_{0,th}(u,z_2)G_{0,th}(u,z_3)\\
&\qquad\qquad\left[\alpha^{th}_{4,0L}(z_1,z_2,z_3,z_4)\right]G_{0,th}(z_4,y)\,.
\end{aligned}$$

In the last line, the thermal effective 4-point vertex has been introduced,

$$\alpha^{th}_{4,0L}(z_1,z_2,z_3,z_4) \;=\; -i\lambda\int_{\boldsymbol{\mathcal{I}}}d^4v\,\Delta_0(v,z_1)\Delta_0(v,z_2)\Delta_0(v,z_3)\Delta_0(v,z_4)$$

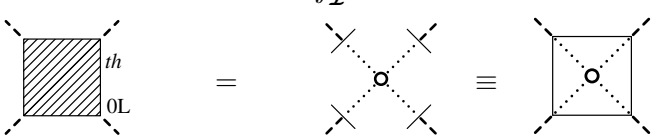

Since the connection $\Delta_0(v,z_i)$ is only supported at the initial time $z_i^0 = 0_\pm$, the effective 4-point vertex vanishes as soon as one of the four real times $z_1^0,\dots,z_0^4$ lies beyond the initial time. Thus, the effective 4-point vertex has precisely the same structure as the non-local effective vertices describing the initial correlations for arbitrary initial states (see section 7.1). Within the perturbative framework treated here, the above 4-point vertex constitutes the leading order contribution to the loop expansion of the thermal initial 4-point correlation function (see section D.1.1),

$$\alpha_4^{th}(z_1,z_2,z_3,z_4) \;=\; \alpha_{4,0L}^{th}(z_1,z_2,z_3,z_4) \;+\; \alpha_{4,1L}^{th}(z_1,z_2,z_3,z_4) \;+\dots$$

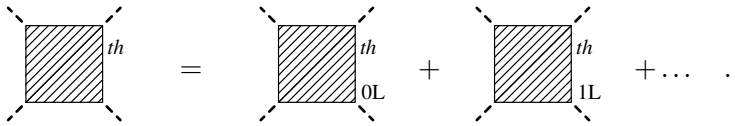

In general, for any thermal diagram on $\mathcal{C}+\mathcal{I}$ with $\mathcal{V}$ vertices, there are $2^\mathcal{V}$ possibilities to combine the integration over $\mathcal{C}$ or $\mathcal{I}$ at each vertex. For each of these $2^\mathcal{V}$ contributions, all lines connecting a real and an imaginary vertex are replaced using relation (7.36). Thereby the parts containing $\mathcal{I}$-integrations are encapsulated into non-local effective vertices. Thus, any thermal diagram on $\mathcal{C}+\mathcal{I}$ can be equivalently represented by $2^\mathcal{V}$ diagrams on $\mathcal{C}$, which contain the classical vertex along with appropriate non-local effective vertices.

These non-local effective vertices indeed match the thermal initial correlations α_n^{th} discussed in section D.1.1. This has been demonstrated above for the setting-sun diagram which contains a single imaginary vertex. For diagrams which contain internal lines which connect *two* imaginary vertices, representing the propagator $G_{0,th}^{\mathcal{I}\mathcal{I}}(-i\tau,-i\tau',\boldsymbol{k})$, the following relation can be employed

$$\begin{aligned} G_{0,th}^{\mathcal{I}\mathcal{I}}(-i\tau,-i\tau',\boldsymbol{k}) &= D_0(-i\tau,-i\tau',\boldsymbol{k}) \\ &\quad + \int_\mathcal{C} dw^0 \int_\mathcal{C} dz^0\, \Delta_0(-i\tau,w^0,\boldsymbol{k}) G_{0,th}^{\mathcal{C}\mathcal{C}}(w^0,z^0,\boldsymbol{k}) \Delta_0^T(z^0,-i\tau',\boldsymbol{k}) \\ &= D_0(-i\tau,-i\tau',\boldsymbol{k}) + \Delta_0^s(-i\tau,\boldsymbol{k}) G_{0,th}(0,0,\boldsymbol{k}) \Delta_0^s(-i\tau',\boldsymbol{k}) \end{aligned} \tag{7.42}$$

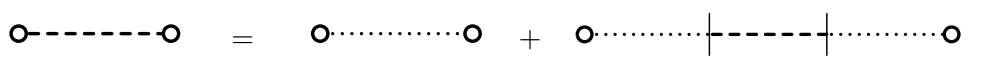

which can be verified by explicit calculation from eqs. (D.6, 7.31, 7.37). Hereby the propagator $D_0(-i\tau,-i\tau',\boldsymbol{k})$, which is defined in eq. (D.6), is represented by the dotted line which connects two imaginary times. It furnishes the perturbative expansion of the thermal initial correlations (see section D.1.1). By applying the upper relation to the setting-sun diagram with two imaginary vertices, it can be rewritten as

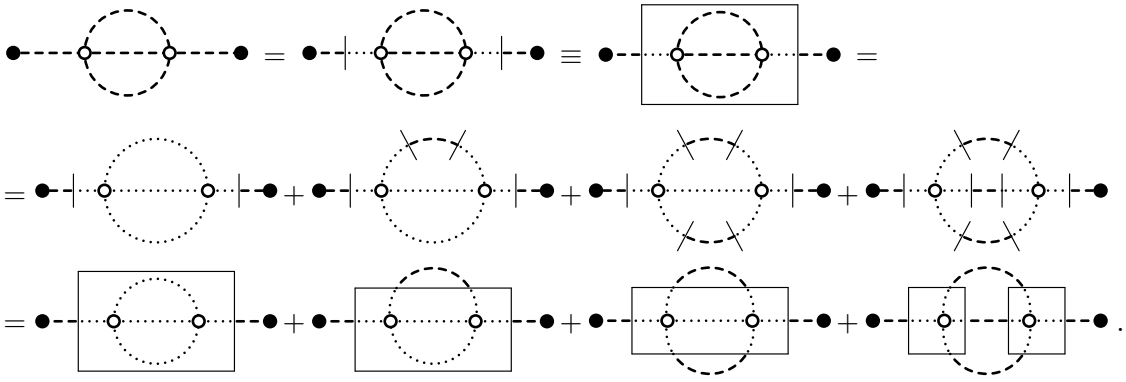

In the first step, the propagators connecting real and imaginary vertices were replaced by the convolution of the connection and the real-real propagator. This already yields an effective non-local two-vertex, as indicated in the third diagram in the first line. In order to check that this effective non-local

two-vertex is indeed composed from the thermal initial correlations, the three propagators connecting the two imaginary vertices are replaced using relation (7.42), such that it falls apart into eight terms, which combine to the four inequivalent contributions shown in the second line[2]. Finally, the parts which contain imaginary vertices and dotted lines can be identified with the corresponding contributions to the perturbative expansion of the thermal initial correlations discussed in section D.1.1, which is represented graphically by encapsulating the subdiagrams inside the boxes. In the third line, the first diagram thus contains a thermal effective two-point vertex, which itself appears at two-loop order in the perturbative expansion of the thermal initial correlations. Similarly, the thermal effective four- and six-point vertices contained in the second and third diagram, respectively, appear at one- and zero-loop order in the perturbative expansion of the thermal initial correlations. The two effective four-point vertices contained in the fourth diagram are identical to those already encountered above.

Thus, using the representation (7.36) of the free propagator connecting a real and an imaginary time, any perturbative thermal Feynman diagram formulated on the thermal time contour $\mathcal{C}+\mathcal{I}$ can be related with a set of perturbative Feynman diagrams formulated on the closed real-time contour $\mathcal{C}$, and the required approximation to the full thermal initial correlations α_n^{th} can be explicitly constructed with the help of the formalism introduced here. For example, for the perturbative setting sun diagram, the equivalence between $\mathcal{C}+\mathcal{I}$ and $\mathcal{C}+\alpha$ can, in summary, be written as

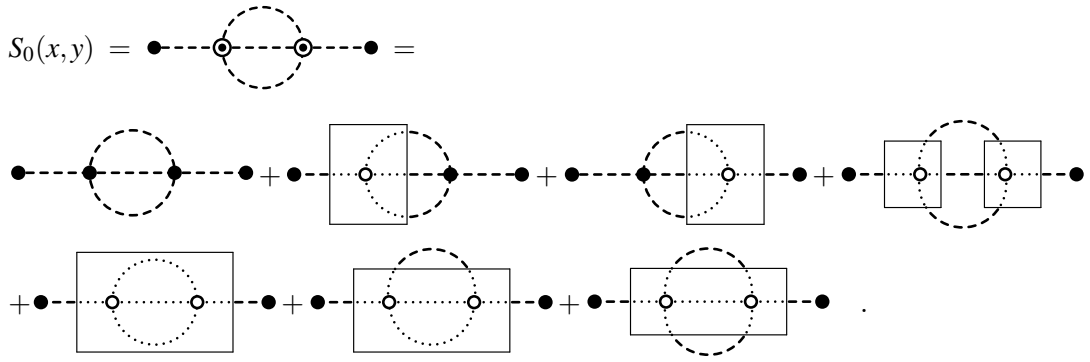

Within perturbation theory, the dotted and dashed propagators as well as the connection are known explicitly. They are given in terms of elementary functions, such that the upper equivalence can be cross-checked by an explicit calculation of both types of diagrams. After this reassuring exercise, one can proceed to the nonperturbative case.

7.2.2 Thermal Initial Correlations — 2PI

Thermal time contour $\mathcal{C}+\mathcal{I}$

The full thermal propagator defined on $\mathcal{C}+\mathcal{I}$ fulfills the nonperturbative Schwinger-Dyson equation derived from the 2PI effective action (see also eq. (6.22))

$$G_{th}^{-1}(x,y) = i(\Box_x + m^2)\delta_{\mathcal{C}+\mathcal{I}}(x-y) - \Pi_{th}(x,y) \qquad \text{for } x^0, y^0 \in \mathcal{C}+\mathcal{I}\,. \tag{7.43}$$

[2]Note that the symmetry factors are taken into account properly. For example, the symmetry factor of the second diagram in the second line is one third times the symmetry factor of the original diagram in the first line. Since there are three possibilities to obtain this diagram from the first one, it is obtained with the correct prefactor.

It furnished the expansion of the 2PI effective action in terms of 2PI Feynman diagrams. Similar to the perturbative case, the following Feynman rules are defined,

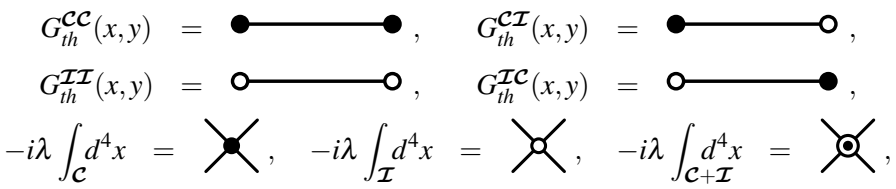

(7.44)

in order to disentangle the contributions from the real and the imaginary branch of the thermal time contour. In order to derive a nonperturbative generalization of eq. (7.36), it is helpful to define a "mixed propagator" which coincides with the full propagator on the imaginary branch $\mathcal{I}$ of the thermal time contour, and obeys the free equation of motion on the real branch $\mathcal{C}$.

Mixed thermal propagator

It is helpful to define projections on the parts $\mathcal{C}$ and $\mathcal{I}$ of the thermal time contour,

$$\mathbf{1}_{\mathcal{I}}(x^0) = \begin{cases} 0 & \text{if} \quad x^0 \in \mathcal{C} \\ 1 & \text{if} \quad x^0 \in \mathcal{I} \end{cases}, \qquad \mathbf{1}_{\mathcal{C}}(x^0) = \begin{cases} 1 & \text{if} \quad x^0 \in \mathcal{C} \\ 0 & \text{if} \quad x^0 \in \mathcal{I} \end{cases}, \tag{7.45}$$

which fulfill the relation

$$\mathbf{1}_{\mathcal{I}}(x^0) + \mathbf{1}_{\mathcal{C}}(x^0) = 1 \qquad \text{for all } x^0 \in \mathcal{C}+\mathcal{I}\,. \tag{7.46}$$

The mixed thermal propagator is defined by the following equation of motion,

$$G^{-1}_{m,th}(x,y) = i(\Box_x + m_B^2)\delta_{\mathcal{C}+\mathcal{I}}(x-y) - \mathbf{1}_{\mathcal{I}}(x^0)\mathbf{1}_{\mathcal{I}}(y^0)\Pi_{th}(x,y) \qquad \text{for } x^0, y^0 \in \mathcal{C}+\mathcal{I}\,, \tag{7.47}$$

where $\Pi_{th}(x,y)$ is the full thermal self-energy. It can be decomposed into statistical and spectral components,

$$G_{m,th}(x,y) = G_{m,F}(x,y) - \frac{i}{2}\mathrm{sgn}_{\mathcal{C}+\mathcal{I}}(x^0-y^0)G_{m,\rho}(x,y)\,.$$

The equation of motion for the mixed propagator can equivalently be written as

$$\left(\Box_x + m^2\right) G_{m,th}(x,y) = -i\delta_{\mathcal{C}+\mathcal{I}}(x-y) - i\mathbf{1}_{\mathcal{I}}(x^0)\int_{\mathcal{I}} d^4z\,\Pi_{m,th}(x,z)G_{m,th}(z,y)\,. \tag{7.48}$$

Each of the two time arguments of the propagator can either be real or imaginary, which yields four combinations $G^{\mathcal{CC}}_{m,th}$, $G^{\mathcal{CI}}_{m,th}$, $G^{\mathcal{IC}}_{m,th}$, $G^{\mathcal{II}}_{m,th}$. The mixed propagator evaluated with two imaginary time arguments is identical to the full thermal 2PI propagator,

$$G^{\mathcal{II}}_{m,th}(x,y) = G^{\mathcal{II}}_{th}(x,y) \qquad \text{for } x^0, y^0 \in \mathcal{I}, \tag{7.49}$$

whereas the mixed propagators evaluated with two real time arguments $G^{\mathcal{CC}}_{m,th}(x,y)$ as well as $G^{\mathcal{CI}}_{m,th}(x,y)$ (where $x^0 \in \mathcal{C}, y^0 \in \mathcal{I}$) fulfill the equation of motion of the free propagator,

$$\left(\Box_x + m_B^2\right) G^{\mathcal{CI}}_{m,th}(x,y) = \left(\Box_x + m_B^2\right) G^{\mathcal{CC}}_{m,F}(x,y) = \left(\Box_x + m_B^2\right) G^{\mathcal{CC}}_{m,\rho}(x,y) = 0\,. \tag{7.50}$$

At the initial time $x^0 = y^0 = 0$, the propagators on all branches of the thermal time path agree,

$$G^{\mathcal{CC}}_{m,th}(x,y)|_{x^0=y^0=0} = G^{\mathcal{CI}}_{m,th}(x,y)|_{x^0=y^0=0} = G^{\mathcal{IC}}_{m,th}(x,y)|_{x^0=y^0=0} = G^{\mathcal{II}}_{m,th}(x,y)|_{x^0=y^0=0} = G_{th}(x,y)|_{x^0=y^0=0}\,.$$

Thus, the initial value of the mixed propagator at $x^0 = y^0 = 0$ is given by the full thermal propagator. For the mixed propagator with one imaginary and one real time, $G^{\mathcal{IC}}_{m,th}(x,y)$ ($x^0 \in \mathcal{I}, y^0 \in \mathcal{C}$), the equation of motion, transformed to spatial momentum space, reads

$$\left(-\partial_\tau^2 + \boldsymbol{k}^2 + M_{th}^2\right) G^{\mathcal{IC}}_{m,th}(-i\tau, y^0, \boldsymbol{k}) \; = -\int_0^\beta d\tau' \, \Pi^{\mathcal{II}}_{th}(-i\tau, -i\tau', \boldsymbol{k}) G^{\mathcal{IC}}_{m,th}(-i\tau', y^0, \boldsymbol{k}) \,.$$

Compared to the corresponding equation (D.17) for the full thermal propagator, the memory integral along the real axis is absent. Next, a Fourier transformation with respect to the imaginary time is performed, using in particular

$$\int_0^\beta d\tau \, e^{-i\omega_n \tau} \, \partial_\tau^2 G^{\mathcal{IC}}_{m,th}(-i\tau, y^0, \boldsymbol{k}) \; = -\omega_n^2 G^{\mathcal{IC}}_{m,th}(\omega_n, y^0, \boldsymbol{k}) + \mathrm{disc}(i\omega_n \, G^{\mathcal{IC}}_{m,th} + \partial_\tau G^{\mathcal{IC}}_{m,th})(y^0, \boldsymbol{k}) \,,$$

where a possible contribution from boundary terms has to be taken into account,

$$\mathrm{disc}(i\omega_n \, G^{\mathcal{IC}}_{m,th} + \partial_\tau G^{\mathcal{IC}}_{m,th})(y^0, \boldsymbol{k}) = \left[(i\omega_n \, G^{\mathcal{IC}}_{m,th} + \partial_\tau G^{\mathcal{IC}}_{m,th})(-i\tau, y^0, \boldsymbol{k})\right]_{\tau=0}^{\tau=\beta} .$$

The Fourier transformed equation for the mixed propagator reads

$$\begin{aligned} &\left(\omega_n^2 + \boldsymbol{k}^2 + M_{th}^2\right) G^{\mathcal{IC}}_{m,th}(\omega_n, y^0, \boldsymbol{k}) \; = \\ &\quad = -\Pi^{\mathcal{II}}_{th}(\omega_n, \boldsymbol{k}) G^{\mathcal{IC}}_{m,th}(\omega_n, y^0, \boldsymbol{k}) + \mathrm{disc}(i\omega_n \, G^{\mathcal{IC}}_{m,th} + \partial_\tau G^{\mathcal{IC}}_{m,th})(y^0, \boldsymbol{k}) \,. \end{aligned} \tag{7.51}$$

The boundary terms have to fulfill the equation of motion

$$\left(\partial_{y^0}^2 + \boldsymbol{k}^2 + m_B^2\right) \mathrm{disc}(G^{\mathcal{IC}}_{m,th})(y^0, \boldsymbol{k}) = \left(\partial_{y^0}^2 + \boldsymbol{k}^2 + m_B^2\right) \mathrm{disc}(\partial_\tau G^{\mathcal{IC}}_{m,th})(y^0, \boldsymbol{k}) = 0 \,,$$

which follows from using $G^{\mathcal{IC}}_{m,th}(\omega_n, y^0, \boldsymbol{k}) = G^{\mathcal{CI}}_{m,th}(y^0, \omega_n, \boldsymbol{k})$ and the equation of motion (7.50) for $G^{\mathcal{CI}}_{m,th}$. Furthermore, the initial conditions at $y^0 = 0$ are fixed by the periodicity relation of the thermal propagator as well as the equal-time commutation relations,

$$\begin{aligned} \mathrm{disc}(G^{\mathcal{IC}}_{m,th})(0, \boldsymbol{k}) &= G_{th}(0,0,\boldsymbol{k}) - G_{th}(-i\beta, 0, \boldsymbol{k}) = 0 \,, \\ \partial_{y^0} \mathrm{disc}(G^{\mathcal{IC}}_{m,th})(0, \boldsymbol{k}) &= \partial_{y^0} G_{th}(0,0,\boldsymbol{k}) - \partial_{y^0} G_{th}(-i\beta, 0, \boldsymbol{k}) \\ &= \partial_{y^0} G_{th}(0,0,\boldsymbol{k}) - \partial_{x^0} G_{th}(0,0,\boldsymbol{k}) = i \,, \\ \mathrm{disc}(\partial_\tau G^{\mathcal{IC}}_{m,th})(0, \boldsymbol{k}) &= \partial_\tau G_{th}(0,0,\boldsymbol{k}) - \partial_\tau G_{th}(-i\beta, 0, \boldsymbol{k}) = 1 \,, \\ \partial_{y^0} \mathrm{disc}(\partial_\tau G^{\mathcal{IC}}_{m,th})(0, \boldsymbol{k}) &= \partial_{y^0} \partial_\tau G_{th}(0,0,\boldsymbol{k}) - \partial_{y^0} \partial_\tau G_{th}(-i\beta, 0, \boldsymbol{k}) = 0 \,. \end{aligned}$$

The statistical and spectral components $G^{\mathcal{CC}}_{m,F}(0, y^0, \boldsymbol{k})$ and $G^{\mathcal{CC}}_{m,\rho}(0, y^0, \boldsymbol{k})$ of the mixed propagator are two linearly independent solutions of the free equation of motion. Since it is a second order differential equation, any solution can be expressed as a linear combination, especially

$$\begin{aligned} \mathrm{disc}(G^{\mathcal{IC}}_{m,th})(y^0, \boldsymbol{k}) &= G^{\mathcal{IC}}_{m,th}(-i\tau, y^0, \boldsymbol{k})\big|_{\tau=0}^{\tau=\beta} = -iG^{\mathcal{CC}}_{m,\rho}(0, y^0, \boldsymbol{k}) \,, \\ \mathrm{disc}(\partial_\tau G^{\mathcal{IC}}_{m,th})(y^0, \boldsymbol{k}) &= \partial_\tau G^{\mathcal{IC}}_{m,th}(-i\tau, y^0, \boldsymbol{k})\big|_{\tau=0}^{\tau=\beta} = \frac{G^{\mathcal{CC}}_{m,F}(0, y^0, \boldsymbol{k})}{G_{th}(0,0,\boldsymbol{k})} \,. \end{aligned} \tag{7.52}$$

Inserting this result together with the self-consistent Schwinger-Dyson equation (D.20) for the full thermal propagator into eq. (7.51) finally yields

$$\begin{aligned} G^{\mathcal{IC}}_{m,th}(\omega_n, y^0, \boldsymbol{k}) &= \left(\frac{G^{\mathcal{II}}_{th}(\omega_n, \boldsymbol{k})}{G_{th}(0,0,\boldsymbol{k})}\right) G^{\mathcal{CC}}_{m,F}(0, y^0, \boldsymbol{k}) - \left(i\omega_n G^{\mathcal{II}}_{th}(\omega_n, \boldsymbol{k})\right) G^{\mathcal{CC}}_{m,\rho}(0, y^0, \boldsymbol{k}) \\ &= \int_{\mathcal{C}} dz^0 \, \Delta_m(\omega_n, z^0, \boldsymbol{k}) G^{\mathcal{CC}}_{m,th}(z^0, y^0, \boldsymbol{k}) \,, \end{aligned} \tag{7.53}$$

where, in the second line, an integration over the closed real-time path $\mathcal{C}$ was inserted, as well as the "mixed connection"

$$\begin{aligned}\Delta_m(\omega_n,z^0,\boldsymbol{k}) &= \left(\frac{G_{th}^{\mathcal{II}}(\omega_n,\boldsymbol{k})}{G_{th}(0,0,\boldsymbol{k})}\right)\delta_s(z^0)+\left(2i\omega_n G_{th}^{\mathcal{II}}(\omega_n,\boldsymbol{k})\right)\delta_a(z^0)\\ &= \Delta_m^s(\omega_n,\boldsymbol{k})\delta_s(z^0)+\Delta_m^a(\omega_n,\boldsymbol{k})\delta_a(z^0)\,, \qquad (7.54)\\ &= \quad ,\end{aligned}$$

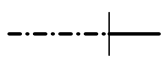

which is only supported at the initial time $z^0=0_\pm$. Furthermore, the transposed connection is defined as $\Delta_m^T(z^0,\omega_n,\boldsymbol{k})=\Delta_m(\omega_n,z^0,\boldsymbol{k})$. Eq. (7.53) for the mixed propagator is the extension of eq. (7.36) for the free propagator. Thus, the mixed propagator evaluated with one real and one imaginary time is decomposed into the convolution of the mixed connection, which involves the full 2PI propagator, and the real-real mixed propagator which obeys the free equation of motion.

Full thermal propagator

Using the equation of motion (7.47) of the mixed propagator, the self-consistent equation of motion (7.43) of the full propagator can be rewritten as

$$G_{th}^{-1}(x,y)=G_{m,th}^{-1}(x,y)-\left[1-\mathbf{1}_{\mathcal{I}}(x^0)\mathbf{1}_{\mathcal{I}}(y^0)\right]\Pi_{th}(x,y)\qquad \text{for } x^0,y^0\in\mathcal{C}+\mathcal{I}\,.$$

By convolving this equation with G_{th} from the left and with $G_{m,th}$ from the right, the integrated Schwinger-Dyson equation is obtained,

$$G_{th}(x,y)=G_{m,th}(x,y)+\int_{\mathcal{C}+\mathcal{I}}d^4u\int_{\mathcal{C}+\mathcal{I}}d^4v\,G_{th}(x,u)\left[1-\mathbf{1}_{\mathcal{I}}(u^0)\mathbf{1}_{\mathcal{I}}(v^0)\right]\Pi_{th}(u,v)G_{m,th}(v,y)\,. \qquad (7.55)$$

Evaluating it for $x^0\in\mathcal{C}$ and $y^0\in\mathcal{I}$, and performing a Fourier transformation with respect to the relative spatial coordinate $\boldsymbol{x}-\boldsymbol{y}$ as well as the imaginary time y^0 gives

$$\begin{aligned}G_{th}^{\mathcal{CI}}(x^0,\omega_n,\boldsymbol{k}) &= G_{m,th}^{\mathcal{CI}}(x^0,\omega_n,\boldsymbol{k})+\int_{\mathcal{C}+\mathcal{I}}du^0\int_{\mathcal{C}}dv^0\left(G_{th}(x^0,u^0,\boldsymbol{k})\Pi_{th}(u^0,v^0,\boldsymbol{k})G_{m,th}^{\mathcal{CI}}(v^0,\omega_n,\boldsymbol{k})\right)\\ &\quad -i\int_{\mathcal{C}}du^0\,G_{th}^{\mathcal{CC}}(x^0,u^0,\boldsymbol{k})\Pi_{th}(u^0,\omega_n,\boldsymbol{k})G_{m,th}^{\mathcal{II}}(\omega_n,\boldsymbol{k})\,.\end{aligned}$$

Next, $G_{m,th}^{\mathcal{CI}}(x^0,\omega_n,\boldsymbol{k})$ and $G_{m,th}^{\mathcal{CI}}(v^0,\omega_n,\boldsymbol{k})$ are replaced using eq. (7.53) with interchanged arguments,

$$\begin{aligned}&G_{th}^{\mathcal{CI}}(x^0,\omega_n,\boldsymbol{k})\\ &=\int_{\mathcal{C}}dz^0\left[G_{m,th}^{\mathcal{CC}}(x^0,z^0,\boldsymbol{k})+\int_{\mathcal{C}+\mathcal{I}}du^0\int_{\mathcal{C}}dv^0\left(G_{th}(x^0,u^0,\boldsymbol{k})\Pi_{th}(u^0,v^0,\boldsymbol{k})\;G_{m,th}^{\mathcal{CC}}(v^0,z^0,\boldsymbol{k})\right)\right]\Delta_m^T(z^0,\omega_n,\boldsymbol{k})\\ &\quad -i\int_{\mathcal{C}}du^0\,G_{th}^{\mathcal{CC}}(x^0,u^0,\boldsymbol{k})\Pi_{th}(u^0,\omega_n,\boldsymbol{k})G_{th}^{\mathcal{II}}(\omega_n,\boldsymbol{k})\\ &=\int_{\mathcal{C}}dz^0\left[G_{th}^{\mathcal{CC}}(x^0,z^0,\boldsymbol{k})-\int_{\mathcal{C}}du^0\int_{\mathcal{I}}dv^0\left(G_{th}^{\mathcal{CC}}(x^0,u^0,\boldsymbol{k})\Pi_{th}(u^0,v^0,\boldsymbol{k})\;G_{m,th}^{\mathcal{IC}}(v^0,z^0,\boldsymbol{k})\right)\right]\Delta_m^T(z^0,\omega_n,\boldsymbol{k})\\ &\quad -i\int_{\mathcal{C}}du^0\,G_{th}^{\mathcal{CC}}(x^0,u^0,\boldsymbol{k})\Pi_{th}(u^0,\omega_n,\boldsymbol{k})G_{th}^{\mathcal{II}}(\omega_n,\boldsymbol{k})\\ &=\int_{\mathcal{C}}dz^0\,G_{th}^{\mathcal{CC}}(x^0,z^0,\boldsymbol{k})\left\{\Delta_m^T(z^0,\omega_n,\boldsymbol{k})-i\Pi_{th}(z^0,\omega_n,\boldsymbol{k})G_{th}^{\mathcal{II}}(\omega_n,\boldsymbol{k})\right.\\ &\qquad\left.-\int_{\mathcal{C}}du^0\int_{\mathcal{I}}dv^0\,\Pi_{th}(z^0,v^0,\boldsymbol{k})G_{m,th}^{\mathcal{IC}}(v^0,u^0,\boldsymbol{k})\Delta_m^T(u^0,\omega_n,\boldsymbol{k})\right\},\end{aligned}$$

where $G^{\mathcal{I}\mathcal{I}}_{m,th}(\omega_n,\boldsymbol{k}) = G^{\mathcal{I}\mathcal{I}}_{th}(\omega_n,\boldsymbol{k})$ has been used (see eq. (7.49)). In the second step, the Schwinger-Dyson equation (7.55) evaluated for $x^0, z^0 \in \mathcal{C}$ was used again. In the third step the full real-real propagator was factored out by interchanging the integration variables $u^0 \leftrightarrow z^0$ in the second and third term. The last line can be simplified by Fourier transforming the imaginary time v^0, and performing the integral over $\mathcal{C}$ using eq. (7.54),

$$\begin{aligned}
&\int_{\mathcal{C}} du^0 \int_{\mathcal{I}} dv^0\, \Pi_{th}(z^0,v^0,\boldsymbol{k}) G^{\mathcal{I}\mathcal{C}}_{m,th}(v^0,u^0,\boldsymbol{k}) \Delta^T_m(u^0,\omega_n,\boldsymbol{k}) \;= \\
&\quad = \; -iT \sum_l \int_{\mathcal{C}} du^0\, \Pi_{th}(z^0,\omega_l,\boldsymbol{k}) G^{\mathcal{I}\mathcal{C}}_{m,th}(\omega_l,u^0,\boldsymbol{k}) \Delta^T_m(u^0,\omega_n,\boldsymbol{k}) \\
&\quad = \; -iT \sum_l \Pi_{th}(z^0,\omega_l,\boldsymbol{k}) G^{\mathcal{I}\mathcal{C}}_{m,th}(\omega_l,0,\boldsymbol{k}) \Delta^s_m(\omega_n,\boldsymbol{k}) \\
&\quad = \; -iT \sum_l \Pi_{th}(z^0,\omega_l,\boldsymbol{k}) G^{\mathcal{I}\mathcal{I}}_{th}(\omega_l,\boldsymbol{k}) \frac{G^{\mathcal{I}\mathcal{I}}_{th}(\omega_n,\boldsymbol{k})}{G_{th}(0,0,\boldsymbol{k})} .
\end{aligned}$$

Finally, a decomposition of the full thermal 2PI propagator evaluated with one real time and one Matsubara frequency is obtained,

$$\begin{aligned}
G^{\mathcal{C}\mathcal{I}}_{th}(x^0,\omega_n,\boldsymbol{k}) \;&=\; \int_{\mathcal{C}} dz^0\, G^{\mathcal{C}\mathcal{C}}_{th}(x^0,z^0,\boldsymbol{k}) \Bigg\{ \Delta^T_m(z^0,\omega_n,\boldsymbol{k}) - i\Pi_{th}(z^0,\omega_n,\boldsymbol{k}) G^{\mathcal{I}\mathcal{I}}_{th}(\omega_n,\boldsymbol{k}) \\
&\qquad\qquad - iT \sum_m \Pi_{th}(z^0,\omega_m,\boldsymbol{k}) G^{\mathcal{I}\mathcal{I}}_{th}(\omega_m,\boldsymbol{k}) \frac{G^{\mathcal{I}\mathcal{I}}_{th}(\omega_n,\boldsymbol{k})}{G_{th}(0,0,\boldsymbol{k})} \Bigg\} \\
&=\; \int_{\mathcal{C}} dz^0\, G^{\mathcal{C}\mathcal{C}}_{th}(x^0,z^0,\boldsymbol{k}) \Delta^T(z^0,\omega_n,\boldsymbol{k}) . \qquad (7.56)
\end{aligned}$$

In the last line, the "full connection" was introduced,

$$\begin{aligned}
\Delta^T(z^0,\omega_n,\boldsymbol{k}) \;&=\; \Delta^T_m(z^0,\omega_n,\boldsymbol{k}) - iT \sum_m \Pi_{th}(z^0,\omega_m,\boldsymbol{k}) \left[\frac{\delta_{n,m}}{T} G^{\mathcal{I}\mathcal{I}}_{th}(\omega_n,\boldsymbol{k}) - \frac{G^{\mathcal{I}\mathcal{I}}_{th}(\omega_m,\boldsymbol{k}) G^{\mathcal{I}\mathcal{I}}_{th}(\omega_n,\boldsymbol{k})}{G_{th}(0,0,\boldsymbol{k})} \right] \\
&\equiv\; \Delta^T_m(z^0,\omega_n,\boldsymbol{k}) - iT \sum_m \Pi_{th}(z^0,\omega_m,\boldsymbol{k}) D(\omega_m,\omega_n,\boldsymbol{k}) , \qquad (7.57)
\end{aligned}$$

with $\Delta(\omega_n,z^0,\boldsymbol{k}) = \Delta^T(z^0,\omega_n,\boldsymbol{k})$. Compared to the mixed connection, the full connection contains an additional term, which is the convolution of the thermal self-energy, evaluated with one real time and one Matsubara frequency, with the propagator $D(\omega_m,\omega_n,\boldsymbol{k})$ defined in the last line. This propagator can be rewritten as

$$\begin{aligned}
D(\omega_n,\omega_m,\boldsymbol{k}) \;&=\; \frac{\delta_{n,m}}{T} G^{\mathcal{I}\mathcal{I}}_{th}(\omega_n,\boldsymbol{k}) - \frac{G^{\mathcal{I}\mathcal{I}}_{th}(\omega_n,\boldsymbol{k}) G^{\mathcal{I}\mathcal{I}}_{th}(\omega_m,\boldsymbol{k})}{G_{th}(0,0,\boldsymbol{k})} \qquad (7.58) \\
&=\; \frac{\delta_{n,m}}{T} G^{\mathcal{I}\mathcal{I}}_{th}(\omega_n,\boldsymbol{k}) - \Delta^s_m(\omega_n,\boldsymbol{k}) G_{th}(0,0,\boldsymbol{k}) \Delta^s_m(\omega_m,\boldsymbol{k}) \\
&=\; \frac{\delta_{n,m}}{T} G^{\mathcal{I}\mathcal{I}}_{th}(\omega_n,\boldsymbol{k}) - \int_{\mathcal{C}} dw^0 \int_{\mathcal{C}} dz^0\, \Delta_m(\omega_n,w^0,\boldsymbol{k}) G_{th}(w^0,z^0,\boldsymbol{k}) \Delta^T_m(z^0,\omega_m,\boldsymbol{k}) \\
&=\; \frac{\delta_{n,m}}{T} G^{\mathcal{I}\mathcal{I}}_{th}(\omega_n,\boldsymbol{k}) - \int_{\mathcal{C}} dw^0 \int_{\mathcal{C}} dz^0\, \Delta(\omega_n,w^0,\boldsymbol{k}) G_{th}(w^0,z^0,\boldsymbol{k}) \Delta^T(z^0,\omega_m,\boldsymbol{k}) .
\end{aligned}$$

In the last line $\int_{\mathcal{C}} dw^0 \int_{\mathcal{C}} dz^0 X(\omega_n,w^0,\boldsymbol{k}) G_{th}(w^0,z^0,\boldsymbol{k}) \Pi_{th}(z^0,\omega_m,\boldsymbol{k}) = 0$ was used, where $X \in \{\Delta,\Pi_{th}\}$. The propagator D has the properties

$$D(\omega_n,\omega_m,\boldsymbol{k}) = D(\omega_m,\omega_n,\boldsymbol{k}), \quad T\sum_m D(\omega_n,\omega_m,\boldsymbol{k}) = 0 . \qquad (7.59)$$

From the last property it can be inferred that only the non-local part of the thermal self-energy $\Pi_{th}(z^0,\omega_m,\boldsymbol{k}) = \Pi^{loc}_{th} + \Pi^{nl}_{th}(z^0,\omega_m,\boldsymbol{k})$ contributes in eq. (7.57), since the local part is independent of the Matsubara frequency (see eq. D.13),

$$T\sum_m \Pi_{th}(z^0,\omega_m,\boldsymbol{k})D(\omega_m,\omega_n,\boldsymbol{k}) = T\sum_m \Pi^{nl}_{th}(z^0,\omega_m,\boldsymbol{k})D(\omega_m,\omega_n,\boldsymbol{k})\,.$$

By applying the inverse Fourier transformation with respect to imaginary time, using in particular

$$D(-i\tau,-i\tau',\boldsymbol{k}) = T^2\sum_{nm} e^{i\omega_n\tau - i\omega_m\tau'}D(\omega_n,\omega_m,\boldsymbol{k})\,,$$

the full thermal 2PI propagator with one imaginary and one real time can be decomposed as

$$\begin{aligned} G^{\mathcal{CI}}_{th}(x^0,-i\tau,\boldsymbol{k}) &= \int_{\mathcal{C}} dz^0\, G^{\mathcal{CC}}_{th}(x^0,z^0,\boldsymbol{k})\Delta^T(z^0,-i\tau,\boldsymbol{k})\,, \\ &= \end{aligned}$$

$$\begin{aligned} G^{\mathcal{IC}}_{th}(-i\tau,y^0,\boldsymbol{k}) &= \int_{\mathcal{C}} dz^0\,\Delta(-i\tau,z^0,\boldsymbol{k})G^{\mathcal{CC}}_{th}(z^0,y^0,\boldsymbol{k})\,, \qquad (7.60) \\ &= \end{aligned}$$

where the full connection is given by

$$\begin{aligned} \Delta(-i\tau,z^0,\boldsymbol{k}) &= \Delta_m(-i\tau,z^0,\boldsymbol{k}) + \int_{\mathcal{I}} dv^0\, D(-i\tau,v^0,\boldsymbol{k})\Pi^{nl}_{th}(v^0,z^0,\boldsymbol{k}) \qquad (7.61) \\ &= \Delta^s(-i\tau,\boldsymbol{k})\delta_s(z^0) + \Delta^a(-i\tau,\boldsymbol{k})\delta_a(z^0) + \int_{\mathcal{I}} dv^0\, D(-i\tau,v^0,\boldsymbol{k})\Pi^{nl}_{th}(v^0,z^0,\boldsymbol{k}) \\ &= \end{aligned}$$

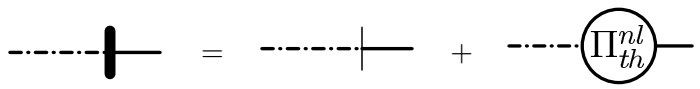

$$\Delta^T(z^0,-i\tau,\boldsymbol{k}) = \Delta(-i\tau,z^0,\boldsymbol{k}) =$$

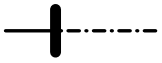

$$. \qquad (7.62)$$

The coefficients $\Delta^{s,a}(-i\tau,\boldsymbol{k})$ are derived from eq. (7.53). They are given in terms of the full thermal 2PI propagator evaluated on the imaginary contour $\mathcal{I}$,

$$\begin{aligned} \Delta^s(-i\tau,\boldsymbol{k}) &= \Delta^s_m(-i\tau,\boldsymbol{k}) = \frac{G^{\mathcal{II}}_{th}(-i\tau,0,\boldsymbol{k})}{G_{th}(0,0,\boldsymbol{k})}\,, \\ \Delta^a(-i\tau,\boldsymbol{k}) &= \Delta^a_m(-i\tau,\boldsymbol{k}) = 2\partial_\tau G^{\mathcal{II}}_{th}(-i\tau,0,\boldsymbol{k})\,. \qquad (7.63) \end{aligned}$$

Eqs. (7.60,7.61,7.63) constitute the nonperturbative generalizations of eqs. (7.36,7.37). The nonperturbative generalization of eq. (7.42) is obtained from eq. (7.58) using eq. (D.19),

$$\begin{aligned} G^{\mathcal{II}}_{th}(-i\tau,-i\tau',\boldsymbol{k}) &= D(-i\tau,-i\tau',\boldsymbol{k}) + \int_{\mathcal{C}} dw^0 \int_{\mathcal{C}} dz^0\, \Delta(-i\tau,w^0,\boldsymbol{k})G_{th}(w^0,z^0,\boldsymbol{k})\Delta^T(z^0,-i\tau',\boldsymbol{k}) \\ &= D(-i\tau,-i\tau',\boldsymbol{k}) + \Delta^s_m(-i\tau,\boldsymbol{k})G_{th}(0,0,\boldsymbol{k})\Delta^s_m(-i\tau',\boldsymbol{k})\,. \qquad (7.64) \end{aligned}$$

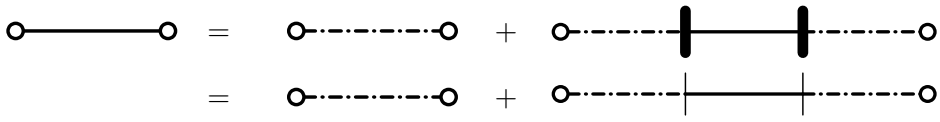

Note that only the parts of the connections which are proportional to $\delta_{s,a}(w^0)$ and $\delta_{s,a}(z^0)$ contribute to the integrals in the first line. The parts involving Π^{nl}_{th} do not contribute since the integrals over the closed real-time path in the first line vanish for them. This is due to the fact that $G^{\mathcal{II}}_{th}$ and D purely depend on imaginary time arguments.

Closed real-time contour with thermal initial correlations $\mathcal{C}+\alpha$

Similar to the free propagator, the full propagator connecting imaginary and real times can be decomposed into a convolution of the full "connection" $\Delta(-i\tau,z^0,\boldsymbol{k})$ and the full real-real propagator. However, equation (7.61) for the full connection is an implicit equation due to the extra contribution of the non-local part of the full thermal self-energy. For example, for the 2PI three loop approximation in the Z_2-symmetric phase, the thermal self-energy is given by the tadpole- and the setting-sun diagrams, which itself contain the full propagator. Only the latter contributes to the non-local part, such that eq. (7.61) takes the form,

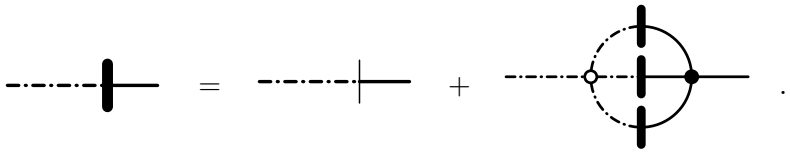

The full connection within a given 2PI truncation is the exact solution of equation (7.61). Formally, it can be expanded in an infinite series obtained from iteratively inserting the mixed connection for the full connection,

$$\begin{aligned}\Delta^{(0)}(-i\tau,z^0,\boldsymbol{k}) &= \Delta_m(-i\tau,z^0,\boldsymbol{k})\,,\\ \Delta^{(k+1)}(-i\tau,z^0,\boldsymbol{k}) &= \Delta_m(-i\tau,z^0,\boldsymbol{k})+\int_{\mathcal{I}} dv^0\, D(-i\tau,v^0,\boldsymbol{k})\,\Pi^{nl}_{th}(v^0,z^0,\boldsymbol{k})\big|_{G^{\mathcal{I}\mathcal{C}}_{th}\to\Delta^{(k)}*G^{\mathcal{C}\mathcal{C}}_{th}}\,.\end{aligned} \tag{7.65}$$

For example, for the 2PI three loop approximation in the Z_2-symmetric phase, the first steps of this iteration can be depicted as

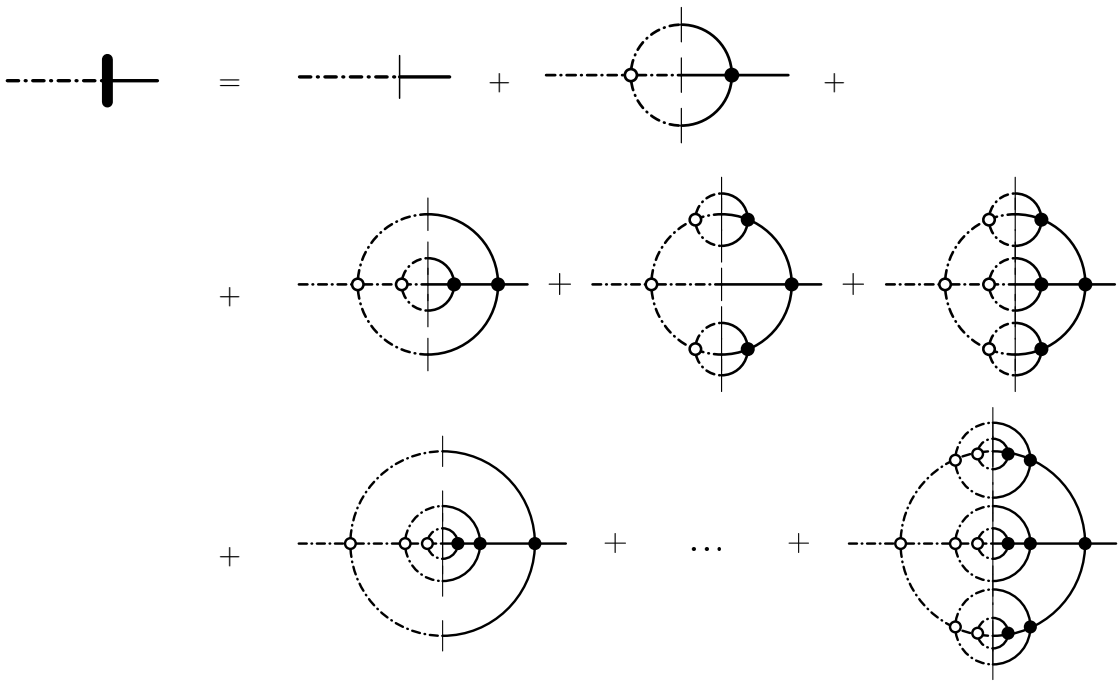

where the first line represents the zeroth step and the first step, and the second line shows all diagrams contributing at the second step. The diagrams in the third line appear at the third step. The diagrams are generated with the correct symmetry factors (see footnote 2 on p. 91). Obviously, the expansion can be re-organized as an expansion in the number of mixed connections contained in each diagram.

Similar to the perturbative case, the formalism established above can be used to relate any Feynman diagram formulated on the thermal time path ("$\mathcal{C}+\mathcal{I}$"), the lines of which are given by the full propagator, with a set of Feynman diagrams formulated on the closed real-time path containing non-local effective vertices representing the thermal initial correlations ("$\mathcal{C}+\alpha$"). This is accomplished by three steps:

1. First, the contour integrations over the thermal time path $\mathcal{C}+\mathcal{I}$ associated with interaction vertices are split into two integrations over $\mathcal{C}$ and $\mathcal{I}$. A diagram with $\mathcal{V}$ vertices is thus decomposed into $2^{\mathcal{V}}$ contributions.

2. Second, all internal propagator lines connecting a real and an imaginary time are replaced by the convolution of the full connection with the real-real propagator according to eq. (7.61). Additionally, the internal propagator lines connecting two imaginary times are replaced according to eq. (7.64). The parts containing imaginary times are encapsulated, which can be visualized by joining the full "connections" to boxes surrounding the imaginary vertices.

3. Third, the series expansion of the full connection in terms of the mixed connection is inserted. Each resulting contribution can be identified as a diagram formulated on the closed real-time path $\mathcal{C}$ containing non-local effective vertices $\boldsymbol{\alpha_n}$. The latter are constructed explicitly, as appropriate for the underlying 2PI approximation.

The first two steps are analogous to the perturbative case, with full propagators and connections instead of free ones. The third step is special for the nonperturbative case. It results in contributions which contain non-local effective vertices α_n^{th} of arbitrarily high order n. These take into account thermal initial n-point correlations, which are present for all n due to the underlying nonperturbative approximation. For example, for the full setting sun diagram, step one and two can be written as

$$S(x,y) = = \frac{(-i\lambda)^2}{6}\int_{\mathcal{C}+\mathcal{I}} d^4u \int_{\mathcal{C}+\mathcal{I}} d^4v\, G_{th}(x,u)G_{th}(u,v)^3 G_{th}(v,y)$$

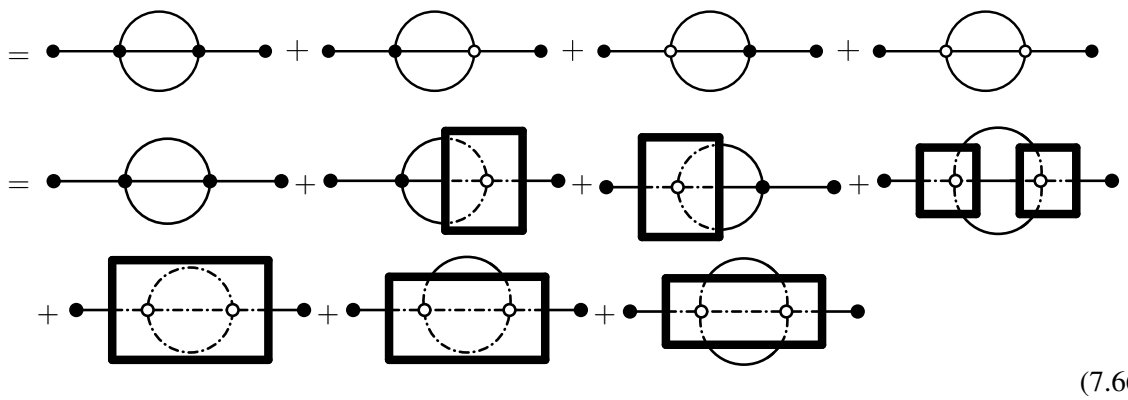

(7.66)

The symmetry factors of all diagrams are taken into account properly (see footnote 2 on page 91).

For the setting-sun diagram with one real and one imaginary vertex, the third step can be written as

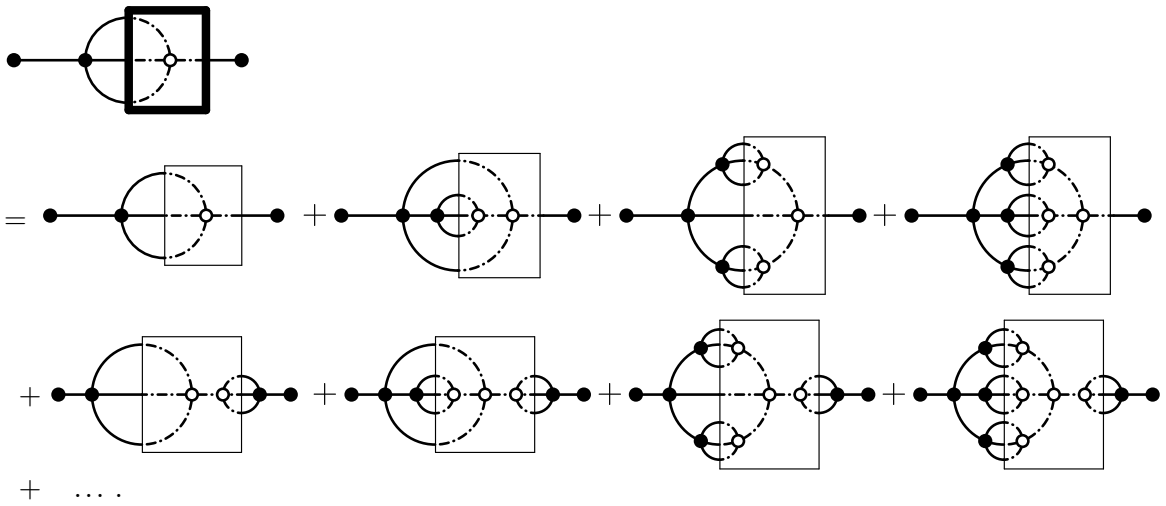

The first diagram in the second line is obtained by inserting the zeroth iteration for the four full connections, $\Delta \to \Delta^{(0)} = \Delta_m$. The other diagrams are obtained by inserting the first iteration $\Delta \to \Delta^{(1)}$. The ellipsis stand for the contributions obtained by inserting the second and higher iterations of the full connection. All diagrams shown above are generated with the correct symmetry factor.

Each of the boxes with thin lines represents a non-local effective vertex, encoding the correlations of the initial state. Accordingly, a thin box which is attached to n propagator lines represents a contribution to the initial correlation α_n.

The thermal initial correlations are determined by the matrix element of the thermal density matrix. As has been shown in section D.1.1, the thermal initial correlations can be expanded in a series of connected Feynman diagrams with propagator $D_0(-i\tau,-i\tau',\boldsymbol{k})$ (see eq. (D.6)) and "imaginary" vertices within perturbation theory. Moreover, in section 7.2.1 it has been shown that these appear as sub-diagrams inside the perturbative non-local effective vertices denoted by the thin boxes.

Within the 2PI framework, the thermal effective non-local vertices are also given by subdiagrams inside the thin boxes, however with lines representing the propagator $D(-i\tau,-i\tau',\boldsymbol{k})$ which is determined by the full thermal propagator (see eq. (7.64)). These subdiagrams represent the approximation of the full thermal initial correlations which are appropriate in the nonperturbative case. Within the formalism established above, these can be constructed explicitly. For example, the lowest order nonperturbative thermal 4-point and 6-point initial correlations are given by

$$\alpha^{th}_{4,0L,2PI}(z_1,z_2,z_3,z_4) = -i\lambda\int_{\mathcal{I}} d^4v\,\Delta_m(v,z_1)\Delta_m(v,z_2)\Delta_m(v,z_3)\Delta_m(v,z_4)$$

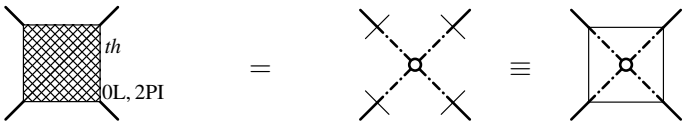

(7.67)

$$\alpha^{th}_{6,0L,2PI}(z_1,z_2,\ldots,z_6) = (-i\lambda)^2\int_{\mathcal{I}} d^4v\int_{\mathcal{I}} d^4w\,\Delta^T_m(z_1,v)\Delta^T_m(z_2,v)\Delta^T_m(z_3,v)D(v,w)$$
$$\Delta_m(w,z_4)\Delta_m(w,z_5)\Delta_m(w,z_6)$$

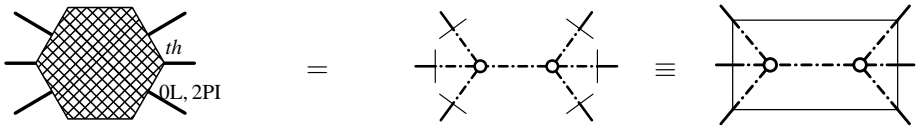

(7.68)

7.2.3 Kadanoff-Baym Equation for the Thermal Initial State

On the one hand, the equation of motion for the full thermal propagator defined on the closed real-time contour $\mathcal{C}$ is given by the Kadanoff-Baym equation for a thermal initial state, represented by thermal initial correlations α_n^{th} ("$\mathcal{C}+\alpha$"). The latter is a special case of the Kadanoff-Baym equation for a non-Gaussian initial state (see eq. (7.25)), which has the form

$$\begin{aligned}\left(\partial_{x^0}^2+\boldsymbol{k}^2+M_{th}^2\right)G_{th}(x^0,y^0,\boldsymbol{k}) &= -i\delta_{\mathcal{C}}(x^0-y^0) \\ &\quad -i\int_{\mathcal{C}}dz^0\left[\Pi^G_{th,nl}(x^0,z^0,\boldsymbol{k})+\Pi^{nG}_{th,nl}(x^0,z^0,\boldsymbol{k})+i\Pi_{th,\lambda\alpha}(x^0,z^0,\boldsymbol{k})\right]G_{th}(z^0,y^0,\boldsymbol{k})\,,\end{aligned} \tag{7.69}$$

where $\Pi^G_{th,nl}(x^0,z^0,\boldsymbol{k})$ and $\Pi^{nG}_{th,nl}(x^0,z^0,\boldsymbol{k})$ denote the Gaussian- and non-Gaussian parts of the non-local self-energy, respectively, and

$$\Pi_{th,\lambda\alpha}(x^0,z^0,\boldsymbol{k}) = \Pi_{th,\lambda\alpha,F}(x^0,\boldsymbol{k})\delta_s(z^0)-\frac{i}{2}\Pi_{th,\lambda\alpha,\rho}(x^0,\boldsymbol{k})\delta_a(z^0)$$

denotes the contribution from the non-Gaussian initial correlations which is only supported at the initial time surface $z^0=0$ (see section 7.1).
On the other hand, the equation of motion of the full thermal propagator based on the thermal time contour ("$\mathcal{C}+\mathcal{I}$") evaluated for $x^0,y^0\in\mathcal{C}$ (see eq. D.14) is

$$\left(\partial_{x^0}^2+\boldsymbol{k}^2+M_{th}^2\right)G_{th}(x^0,y^0,\boldsymbol{k}) = -i\delta_{\mathcal{C}}(x^0-y^0)-i\int_{\mathcal{C}+\mathcal{I}}dz^0\,\Pi^{nl}_{th}(x^0,z^0,\boldsymbol{k})G_{th}(z^0,y^0,\boldsymbol{k})\,.$$

For example, for the three-loop truncation of the 2PI effective action in the Z_2-symmetric phase (setting-sun approximation), the convolution of the thermal non-local self energy and the full thermal propagator is

$$\int_{\mathcal{C}+\mathcal{I}}dz^0\,\Pi^{nl}_{th}(x^0,z^0,\boldsymbol{k})G_{th}(z^0,y^0,\boldsymbol{k}) \quad =$$

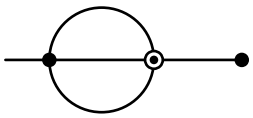

.

Using the full connection (7.61), the integral over the imaginary contour $\mathcal{I}$ can be rewritten as

$$\begin{aligned}&\int_{\mathcal{I}}dz^0\,\Pi^{nl}_{th}(x^0,z^0,\boldsymbol{k})G_{th}(z^0,y^0,\boldsymbol{k}) = \int_{\mathcal{I}}dv^0\,\Pi^{nl}_{th}(x^0,v^0,\boldsymbol{k})\int_C dz^0\,\Delta(v^0,z^0,\boldsymbol{k})G_{th}(z^0,y^0,\boldsymbol{k}) \\ &= \int_C dz^0\left[\int_{\mathcal{I}}dv^0\,\Pi^{nl}_{th}(x^0,v^0,\boldsymbol{k})\left(\Delta_m(v^0,z^0,\boldsymbol{k})+\int_{\mathcal{I}}dw^0\,D(v^0,w^0,\boldsymbol{k})\Pi^{nl}_{th}(w^0,z^0,\boldsymbol{k})\right)\right]G_{th}(z^0,y^0,\boldsymbol{k})\,.\end{aligned}$$

Inserting this into the upper equation of motion, it takes precisely the form of the Kadanoff-Baym equation for a non-Gaussian initial state. By comparison, the non-Gaussian contributions to the self-energy for the thermal initial state can be inferred,

$$\begin{aligned}\Pi^G_{th,nl}(x^0,z^0,\boldsymbol{k}) &= \Pi^{nl}_{th}(x^0,z^0,\boldsymbol{k})\big|_{x^0,z^0\in\mathcal{C}}\,, \\ \Pi^{nG}_{th,nl}(x^0,z^0,\boldsymbol{k}) &= \int_{\mathcal{I}}dv^0\int_{\mathcal{I}}dw^0\,\Pi^{nl}_{th}(x^0,v^0,\boldsymbol{k})D(v^0,w^0,\boldsymbol{k})\Pi^{nl}_{th}(w^0,z^0,\boldsymbol{k})\Big|_{x^0,z^0\in\mathcal{C}}\,, \\ i\Pi_{th,\lambda\alpha}(x^0,z^0,\boldsymbol{k}) &= \int_{\mathcal{I}}dv^0\,\Pi^{nl}_{th}(x^0,v^0,\boldsymbol{k})\Delta_m(v^0,z^0,\boldsymbol{k})\Big|_{x^0,z^0\in\mathcal{C}}\,.\end{aligned} \tag{7.70}$$

For the setting-sun approximation, the steps listed above leading from the formulation of the Kadanoff-Baym equation on the thermal time path ("$\mathcal{C}+\mathcal{I}$") to the formulation on the closed real-time

path with thermal initial correlations ("$\mathcal{C}+\alpha$") are

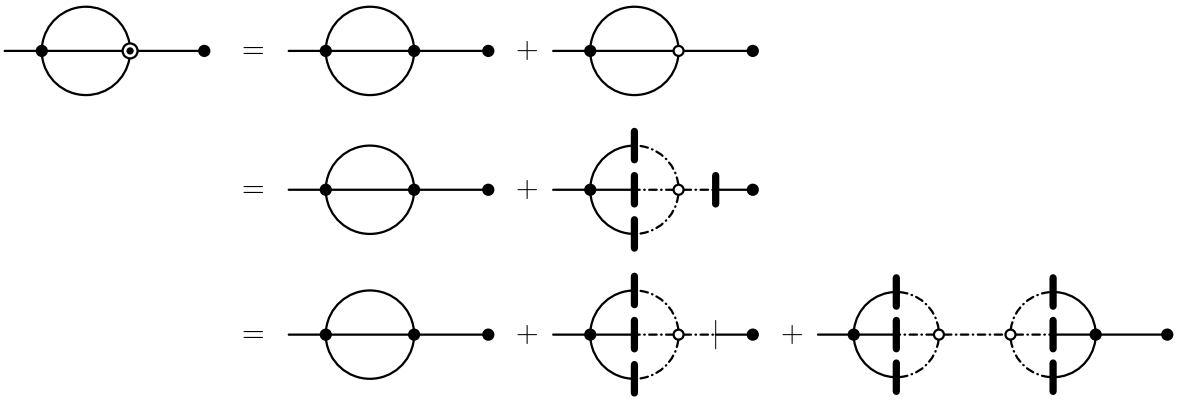

Thus, the Gaussian and non-Gaussian contributions to the self-energy in setting-sun approximation for a thermal initial state are

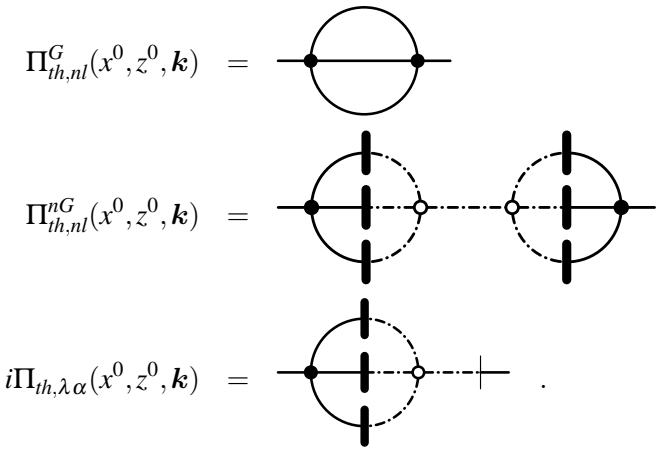

(7.71)

In order to explicitly obtain the thermal initial correlations which are appropriate for a specific 2PI approximation, the iterative expansion (7.65) of the full connection in terms of the mixed connection has to be inserted. This yields a series expansion of the non-Gaussian self-energies,

$$\Pi_{th,\lambda\alpha} = \sum_{k=0}^{\infty} \Pi^{(k)}_{th,\lambda\alpha}, \qquad \Pi^{nG}_{th,nl} = \sum_{k=0}^{\infty} \Pi^{(k),nG}_{th,nl}, \tag{7.72}$$

where

$$\begin{aligned}
\Pi^{(0)}_{th,\lambda\alpha}(x^0,z^0,\boldsymbol{k}) &= \Pi_{th,\lambda\alpha}(x^0,z^0,\boldsymbol{k})\Big|_{G^{\mathcal{TC}}_{th}\to\Delta^{(0)}*G^{\mathcal{CC}}_{th}}, \\
\Pi^{(k)}_{th,\lambda\alpha}(x^0,z^0,\boldsymbol{k}) &= \Pi_{th,\lambda\alpha}(x^0,z^0,\boldsymbol{k})\Big|_{G^{\mathcal{TC}}_{th}\to\Delta^{(k)}*G^{\mathcal{CC}}_{th}} - \Pi^{(k-1)}_{th,\lambda\alpha}(x^0,z^0,\boldsymbol{k}),
\end{aligned}$$

and analogously for $\Pi^{(k),nG}_{th,nl}$. For example, in setting-sun approximation, the thermal initial correlations obtained from inserting the zeroth, first and second iteration of the full connection are

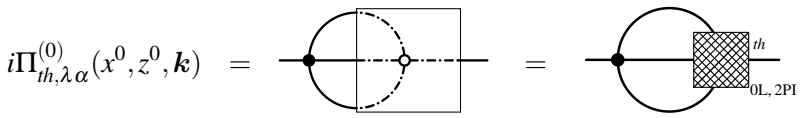

(7.73)

$$i\Pi^{(1)}_{th,\lambda\alpha}(x^0,z^0,\boldsymbol{k}) \;=\;$$

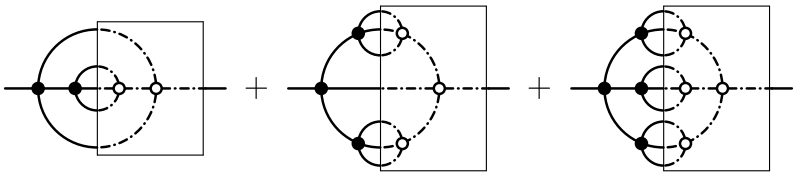

$$i\Pi^{(2)}_{th,\lambda\alpha}(x^0,z^0,\boldsymbol{k}) \;=\;$$

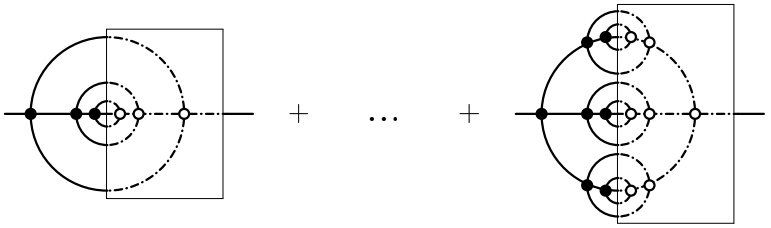

The zeroth contribution contains the thermal non-local effective 4-point vertex (7.67). The first contribution contains three diagrams with thermal effective 6-, 8-, and 10-point vertices, and the second iteration yields six contributions with thermal effective 8-, 10-, 12- (two diagrams), 14-, and 16-point vertices, the smallest and largest of which are depicted in the last line of (7.73). The expansion of $\Pi^{nG}_{th,nl}$ contains thermal non-local effective vertices of order six and higher,

$$\Pi^{(0),nG}_{th,nl}(x^0,z^0,\boldsymbol{k}) \;=\;$$

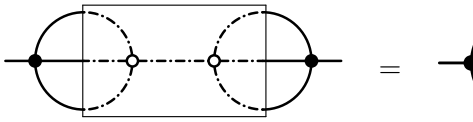

$$\Pi^{(1),nG}_{th,nl}(x^0,z^0,\boldsymbol{k}) \;=\;$$

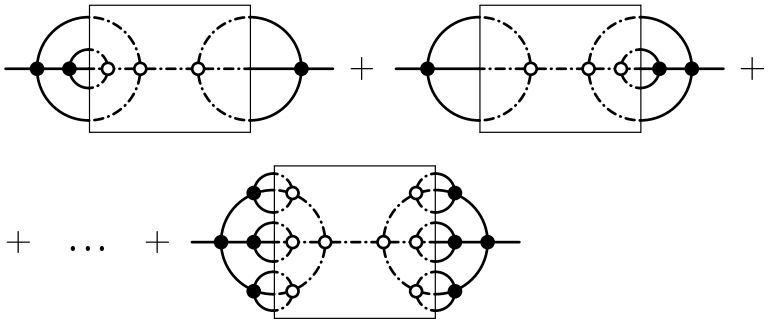

The zeroth contribution contains the thermal non-local effective 6-point vertex (7.68). The first contribution contains 15 diagrams with thermal effective vertices of order 8 to 18.

The order of the thermal initial correlations appearing up to the fifth contribution in setting-sun approximation are shown in table 7.1. Only a single term contains an initial 4-point correlation, which is given in the first line of eq. (7.73),

$$i\Pi^{(0)}_{th,\lambda\alpha}(x,z) = \frac{-i\lambda}{6}\int_{\mathcal{C}} d^4x_{123}\, G_{th}(x,x_1)G_{th}(x,x_2)G_{th}(x,x_3)\, i\alpha^{th}_{4,0L,2PI}(x_1,x_2,x_3,z)\,. \tag{7.74}$$

Furthermore, the upper term yields the only contribution to the Kadanoff-Baym equation (7.69) for the thermal initial state which does *not* contain an internal "real" vertex. Thus, all other contributions contain at least one contour integral over the closed real-time path $\mathcal{C}$ associated to internal real vertices. These integrals have to vanish when all external times approach the initial time, since the integrations over the two branches of the closed real-time contour yield identical contributions with opposite sign. Therefore, in the limit $x^0, y^0 \to 0$, only the diagram containing the initial 4-point correlation given in the first line of eq. (7.73) contributes to the right hand side of the Kadanoff-Baym equation (7.69) for the thermal initial state in setting-sun approximation,

$$\begin{aligned}
\left(\partial^2_{x^0} + \boldsymbol{k}^2 + M^2_{th}\right) G_{th,F}(x^0,y^0,\boldsymbol{k})\big|_{x^0=y^0=0} &= \Pi^{(0)}_{th,\lambda\alpha,F}(x^0,\boldsymbol{k})G_{th,F}(0,y^0,\boldsymbol{k})\Big|_{x^0=y^0=0}\,,\\
\left(\partial^2_{x^0} + \boldsymbol{k}^2 + M^2_{th}\right) G_{th,\rho}(x^0,y^0,\boldsymbol{k})\big|_{x^0=y^0=0} &= 0\,.
\end{aligned} \tag{7.75}$$

$\Pi_{th,\lambda\alpha}(x^0,z^0,\boldsymbol{k})$

	4	6	8	10	12	14	16	⋯	22	⋯	28	⋯	34	⋯
0	×													
1		×	×	×										
2			×	×	×	×	×							
3				×	×	×	×	⋯	×					
4					×	×	×	⋯	×	⋯	×			
5						×	×	⋯	×	⋯	×	⋯	×	
⋮														

$\Pi^{nG}_{th,nl}(x^0,z^0,\boldsymbol{k})$

	4	6	8	10	12	14	16	18	⋯	30	⋯	42	⋯	54	⋯	66	⋯
0		×															
1			×	×	×	×	×	×									
2				×	×	×	×	×	⋯	×							
3					×	×	×	×	⋯	×	⋯	×					
4						×	×	×	⋯	×	⋯	×	⋯	×			
5							×	×	⋯	×	⋯	×	⋯	×	⋯	×	
⋮																	

Table 7.1: *Thermal initial correlations in 2PI setting-sun approximation. The column number is the order $n = 4,6,\ldots$ of the thermal initial n-point correlation. The row number $k = 0,1,\ldots$ shows which initial correlations contribute to $\Pi^{(k)}_{th,\lambda\alpha}$ (upper table) and $\Pi^{(k),nG}_{th,nl}$ (lower table), respectively. Due to the Z_2-symmetry, only even correlations are non-zero.*

In summary, the formulation of the equation of motion for the thermal propagator derived from the 2PI effective action on the closed real-time path can now serve as the link required to combine the nonperturbative 2PI renormalization with Kadanoff-Baym equations.

7.3 Renormalized Kadanoff-Baym Equation for the Thermal Initial State

On the one hand, the nonperturbative renormalization procedure of the 2PI effective action described in section 6.2 renders the thermal propagator defined on the thermal time path finite. On the other hand, the Schwinger-Keldysh propagator which is the solution of the Kadanoff-Baym equations for the thermal initial state coincides with the thermal propagator on the real time axis. Therefore, the nonperturbative renormalization procedure of the 2PI effective action also renders the Kadanoff-Baym equations for the thermal initial state finite. The corresponding renormalized thermal initial correlations

$$\alpha_{n,R}(x_1,\ldots,x_n) = Z^{n/2}\,\alpha_n(x_1,\ldots,x_n) \tag{7.76}$$

are obtained by transferring the renormalized Schwinger-Dyson (6.22) equation formulated on the thermal time path $\mathcal{C}+\mathcal{I}$ to the formulation on the closed real-time path with initial correlations $(\mathcal{C}+\alpha)$ as described above.

The renormalized Kadanoff-Baym equation for the thermal initial state thus reads

$$\left(\Box_x + \delta Z_0 \Box_x + m_R^2 + \delta m_0^2 + \frac{\lambda_R + \delta\lambda_0}{2} G_{th,R}(x,x)\right) G_{th,R}(x,y) = -i\delta^4_{\mathcal{C}}(x-y) \qquad (7.77)$$
$$- i\int_{\mathcal{C}} d^4z \left[\Pi^G_{th,nl,R}(x,z) + \Pi^{nG}_{th,nl,R}(x,z) + i\Pi_{th,\lambda\alpha,R}(x,z)\right] G_{th,R}(z,y)\,,$$

where δZ_0, δm_0^2, and $\delta\lambda_0$ are the 2PI vacuum counterterms as determined by the nonperturbative renormalization procedure of the 2PI effective action at finite temperature, and $G_{th,R}(x,y) = Z^{-1}G_{th}(x,y)$. The renormalized self-energies for the thermal initial state are obtained from eq. (7.70),

$$\begin{aligned}
\Pi^G_{th,nl,R}(x,z) &= Z\Pi^G_{th,nl}(x,z) = \Pi^{nl}_{th,R}(x,z)\big|_{x^0,z^0\in\mathcal{C}}\,, \qquad (7.78)\\
\Pi^{nG}_{th,nl,R}(x,z) &= Z\Pi^{nG}_{th,nl}(x,z) = \int_{\mathcal{I}} d^4v \int_{\mathcal{I}} d^4w\, \Pi^{nl}_{th,R}(x,v) D_R(v,w) \Pi^{nl}_{th,R}(w,z)\Big|_{x^0,z^0\in\mathcal{C}}\,,\\
i\Pi_{th,\lambda\alpha,R}(x,z) &= Z\, i\Pi_{th,\lambda\alpha}(x,z) = \int_{\mathcal{I}} d^4v\, \Pi^{nl}_{th,R}(x,v)\Delta_m(v,z)\Big|_{x^0,z^0\in\mathcal{C}}\,,
\end{aligned}$$

where $D_R(x,y) = Z^{-1}D(x,y)$ is the renormalized propagator from which the thermal initial correlations are constructed via the iterative expansion (7.72).
In the three-loop approximation of the 2PI effective action, the non-local part of the renormalized thermal self-energy, which is given by the setting-sun diagram,

$$\Pi^{nl}_{th,R}(x,y) = \frac{(-i\lambda_R)^2}{6} G_{th,R}(x,y)^3\,,$$

contains the renormalized coupling. Therefore, all thermal initial correlations which are generated via the iterative expansion (7.72) also contain the renormalized coupling. For example, the contribution of the zeroth iteration (which is the only one containing an initial 4-point correlation) is given by

$$i\Pi^{(0)}_{th,\lambda\alpha,R}(x,z) = \frac{-i\lambda_R}{6}\int_{\mathcal{C}} d^4x_{123} G_{th,R}(x,x_1) G_{th,R}(x,x_2) G_{th,R}(x,x_3)\, i\alpha^{th}_{4,0L,2PI,R}(x_1,x_2,x_3,z)\,, \qquad (7.79)$$

where the renormalized thermal initial 4-point correlation is given by

$$i\alpha^{th}_{4,0L,2PI,R}(z_1,z_2,z_3,z_4) = -i\lambda_R\int_{\mathcal{I}} d^4v\, \Delta_m(v,z_1)\Delta_m(v,z_2)\Delta_m(v,z_3)\Delta_m(v,z_4)\,. \qquad (7.80)$$

Altogether, it has been possible to explicitly construct a class of renormalized solutions of Kadanoff-Baym equations (namely those for thermal initial states), which can serve as the basis to derive renormalized Kadanoff-Baym equations for nonequilibrium initial states.

Chapter 8

Renormalization of Kadanoff-Baym Equations

In recent years it turned out that the 2PI effective action [66] defined on the closed real-time path [68, 126, 166] is an excellent starting point to study quantum fields out of thermal equilibrium [1, 2, 25, 32]. So far, however, in this highly nonperturbative context the issue of renormalization has not been addressed properly.

As mentioned in the introduction, there are several reasons why a proper renormalization of Kadanoff-Baym equations derived from the 2PI effective action is desirable. Most important, it is required for a quantitative comparison with semi-classical approximations, like Boltzmann equations. Furthermore, renormalization can have an important quantitative impact on solutions of Kadanoff-Baym equations, is crucial in order to identify physical initial states, and enhances the robustness of the computational algorithm [147].

In this chapter, nonperturbatively renormalized Kadanoff-Baym equations are proposed, and their finiteness is verified analytically for a special case. The relevance of renormalization for Kadanoff-Baym equations is illustrated by means of numerical solutions.

In section 8.1, it is shown that it is necessary to extend the Kadanoff-Baym equations (6.15) (which have been the basis for numerical investigations so far) in order to be compatible with renormalization. Then, the tools derived in chapter 7 are used in order to tackle the nonperturbative renormalization of Kadanoff-Baym equations, which is done in section 8.2 by including an initial 4-point correlation. An important reference value for the latter is the thermal value, for which the connection to the nonperturbative renormalization procedure of the 2PI effective action is demonstrated explicitly. Finally, the relevance of nonperturbative counterterms as well as non-Gaussian initial correlations for numerical solutions of Kadanoff-Baym equations is demonstrated in section 8.3.

8.1 Kadanoff-Baym Equations and 2PI Counterterms

On the one hand, it has been shown [28] that nonperturbative 2PI vacuum counterterms render all n-point functions derived from the 2PI effective action finite in thermal equilibrium. In particular, this means that these 2PI counterterms can be chosen independent of the temperature.

On the other hand, it has been shown [32] that Kadanoff-Baym equations respect late-time universality, meaning that the late-time behavior depends only on conserved quantities like average energy density and global charges, but not on the details of the initial conditions, and that the solutions asymptotically approach a stationary state for which the effective particle number distribution converges towards a thermal Bose-Einstein distribution.

Altogether, this suggests that the 2PI vacuum counterterms are adequate to renormalize the solutions of Kadanoff-Baym equations for late times for any appropriate initial condition. However, as will be shown below, inserting the 2PI counterterms into the Kadanoff-Baym equations (6.15) is not sufficient for their renormalization. Instead, it is additionally required to remove the restriction to a Gaussian initial state.

By splitting the bare mass- and coupling appearing in the bare classical action (6.24) into renormalized parts and counterterms (see eq. 6.25), and rescaling the field value, the self-consistent Schwinger-Dyson equation (6.11) derived from the 2PI effective action (6.9) for a Gaussian initial state formulated on the closed real-time path can be written as,

$$\begin{aligned} G_R^{-1}(x,y) &= i\left(\Box_x + m_R^2\right)\delta_{\mathcal{C}}^4(x-y) - \Pi_R(x,y) \\ \Pi_R(x,y) &= -i\left(\delta Z_0 \Box_x + \delta m_0^2 + \frac{\lambda_R + \delta\lambda_0}{2} G_R(x,x)\right)\delta_{\mathcal{C}}^4(x-y) + \frac{(-i\lambda_R)^2}{6} G_R(x,y)^3 . \end{aligned} \tag{8.1}$$

It is equivalent to the Kadanoff-Baym equations (6.15). The full connected Schwinger-Keldysh propagator $G_R(x,y) \equiv Z^{-1}G(x,y)$ also appears in the self-energy $\Pi_R(x,y)$, which is given in "setting-sun approximation" (see section 6.1) here. It contains counterterms parameterized analogously to the corresponding Schwinger-Dyson equation (6.26) in thermal equilibrium.

One peculiarity of the Kadanoff-Baym equations (6.15) is that, at the initial time, only the local part of the self-energy (which is proportional to $\delta_{\mathcal{C}}^4(x-y)$) contributes, while the non-local part is suppressed due to the memory integrals which vanish at the initial time. Since both parts of the self-energy contain divergences, it is thus impossible to choose the counterterms such that the Kadanoff-Baym equations for a Gaussian initial state are finite at $t = 0$ and $t > 0$ simultaneously.

So far, an approximate perturbative renormalization prescription has been used by default [17]. This prescription is designed such that it is appropriate at the initial time $t = 0$, while it misses divergences occurring at $t > 0$. In contrast to this, the nonperturbative renormalization procedure (see section 6.2), which can, as explained above, be expected to be correct for $t \to \infty$, fails at $t = 0$ for a Gaussian initial state, since the divergence contained in the setting-sun diagram, which is to be canceled by the coupling counterterm, vanishes at the initial time. The reason for this are the missing higher correlations at the initial time. Therefore, it is necessary to extend the Kadanoff-Baym equations (6.15) to non-Gaussian initial states.

8.2 Renormalizable Kadanoff-Baym Equations from the 4PI Effective Action

In thermal equilibrium, the full thermal 4-point correlation function carries logarithmic divergences which are accounted for by the 2PI renormalization prescription. However, for a Gaussian initial state the connected 4-point correlation function vanishes at the initial time by construction. In order to transfer the 2PI renormalization prescription to Kadanoff-Baym equations, it is therefore important to take a 4-point correlation into account from the beginning on.

The 4PI effective action provides an efficient framework to derive Kadanoff-Baym equations for initial states featuring a non-Gaussian 4-point correlation, for which reason its three-loop truncation is employed below[1].

[1] Note however that it is also possible to derive these equations without reference to the 4PI effective action. This has the advantage that completely general initial states (featuring also initial n-point correlations for $n > 4$) as well as truncations of the 2PI effective action, which cannot be obtained via the 4PI effective action [26], can also be incorporated on the same footing. The general formalism can be found in section 7.1.

8.2.1 4PI Effective Action with Initial 4-Point Correlation

The generating functional for nonequilibrium correlation functions describing an ensemble characterized by the density matrix ρ at an initial time $t_{init} \equiv 0$ in the presence of classical external 2- and 4-point sources can be represented by the path integral (see section 6.1)

$$Z_\rho[K,L] = \int \mathcal{D}\varphi \, \langle \varphi_+, 0 \,|\rho|\, \varphi_-, 0 \rangle \, \exp\left(iS[\varphi] + \frac{i}{2}\varphi K \varphi + \frac{i}{4!} L_{1234}\varphi_1\varphi_2\varphi_3\varphi_4 \right) . \tag{8.2}$$

The density matrix element for an initial state featuring a non-Gaussian 4-point correlation can be parameterized as

$$\langle \varphi_+, 0 \,|\rho|\, \varphi_-, 0 \rangle = \exp\left(i\alpha_0 + \frac{i}{2}\varphi\alpha_2\varphi + \frac{i}{4!}(\alpha_4)_{1234}\varphi_1\varphi_2\varphi_3\varphi_4 \right) , \tag{8.3}$$

where the short-hand notations (3.21, 3.34) apply (with $\int \to \int_{\mathcal{C}}$). Here only the Z_2-symmetric case where all odd correlation functions vanish at all times is covered for simplicity. The generalization can be found in section 7.1. The kernels characterizing the initial correlations are supported at the initial time only (i.e. for $t = 0_+$ and $t = 0_-$ on $\mathcal{C}$),

$$\alpha_n(x_1,\ldots,x_n) = \sum_{\varepsilon_1=\pm} \cdots \sum_{\varepsilon_n=\pm} \alpha_n^{\varepsilon_1,\ldots,\varepsilon_n}(\boldsymbol{x_1},\ldots,\boldsymbol{x_n}) \, \delta_{\mathcal{C}}(x_1^0 - 0_{\varepsilon_1}) \cdots \delta_{\mathcal{C}}(x_n^0 - 0_{\varepsilon_n}) . \tag{8.4}$$

In this case, the contribution of the density matrix to the generating functional can be absorbed into the external sources, $K + \alpha_2 \to K$ and $L + \alpha_4 \to L$ (the constant α_0 can be absorbed into the normalization of the path integral measure).
The 4PI effective action $\Gamma[G, V_4]$ is the double Legendre transform of the generating functional (8.2) with respect to the external sources. The latter has the same structure as the corresponding generating functional (3.33) with 2- and 4-point sources in vacuum, except that all time-integrations are performed over the closed real-time path. Consequently, the 4PI effective action for the initial state (8.3) is obtained from the parameterization given in eq. (3.37) by replacing the time-integrations $\int \to \int_{\mathcal{C}}$.

8.2.2 Kadanoff-Baym Equation with Initial 4-Point Correlation

The equation of motion for the connected 4-point function derived from the 4PI effective action is

$$\frac{\delta}{\delta V_4(x,y,z,w)} \Gamma[G, V_4] = -\frac{1}{4!} L(x,y,z,w) , \tag{8.5}$$

and the equation of motion for the Schwinger-Keldysh propagator reads

$$\frac{\delta}{\delta G(x,y)} \Gamma^L[G] = -\frac{1}{2} K(x,y) . \tag{8.6}$$

Here, the external sources are formally not zero for the physical situation, but $K(x,y) = \alpha_2(x,y)$ and $L(x,y,z,w) = \alpha_4(x,y,z,w)$, due to the density matrix element (8.3). Furthermore, $\Gamma^L[G]$ denotes the 2PI effective action obtained from inserting the solution $\bar{V}_4$ of eq. (8.5) into the 4PI effective action and performing the inverse Legendre transform with respect to the 4-point source (where $d^4x_{1234} = d^4x_1 \cdots d^4x_4$ and $G_{12} = G(x_1, x_2)$),

$$\Gamma^L[G] = \Gamma[G, \bar{V}_4] + \frac{1}{4!} \int_{\mathcal{C}} d^4x_{1234} \, L(x_1,x_2,x_3,x_4) \, [\bar{V}_4(x_1,x_2,x_3,x_4) + G_{12}G_{34} + G_{13}G_{24} + G_{14}G_{23}] .$$

In the following, the three-loop approximation (setting-sun approximation) of the 4PI effective action (see section 3.3) is considered for concreteness. Although the three-loop 2PI and three-loop 4PI approximations agree in the absence of sources, this is not the case here due to the initial 4-point correlation $L = \alpha_4 \neq 0$. Instead, the solution of eq. (8.5) obtained from eq. (3.37) is

$$\frac{\delta\Gamma}{\delta V_4} = -\frac{\alpha_4}{4!} \quad \Leftrightarrow \quad iA_4(x_1,x_2,x_3,x_4) = -i\lambda\,\delta_{\mathcal{C}}^4(x_1-x_2)\delta_{\mathcal{C}}^4(x_1-x_3)\delta_{\mathcal{C}}^4(x_1-x_4) + i\alpha_4(x_1,x_2,x_3,x_4)\,.$$

Thus the kernel $iA_4 \equiv iA_4^G + iA_4^{nG}$ is given by the sum of the classical vertex, which is also present in the Gaussian case, and the non-Gaussian initial 4-point correlation $A_4^{nG} \equiv \alpha_4$. Accordingly, the 4-point function has two contributions given by

$$\begin{aligned}\bar{V}_4(x_1,x_2,x_3,x_4) &= \int_{\mathcal{C}} d^4y_{1234}\, G(x_1,y_1)G(x_2,y_2)G(x_3,y_3)G(x_4,y_4)[(iA_4^G + iA_4^{nG})(y_1,y_2,y_3,y_4)] \\ &\equiv V_4^G(x_1,x_2,x_3,x_4) + V_4^{nG}(x_1,x_2,x_3,x_4)\,. \end{aligned} \tag{8.7}$$

The corresponding 2PI effective action $\Gamma^L[G]$ is obtained by inserting $\bar{V}_4$ into the 4PI effective action and setting $L = \alpha_4$. The result coincides with the 2PI effective action (7.15) considered in section 7.1. Therefore, the Kadanoff-Baym equations are

$$\begin{aligned}\big(\Box_x + M^2(x)\big)\,G_F(x,y) &= \int_0^{y^0} d^4z\,\Pi_F(x,z)G_\rho(z,y) - \int_0^{x^0} d^4z\,\Pi_\rho(x,z)G_F(z,y) \\ &\quad - \frac{\lambda}{6}\,V_4^{nG}(x,x,x,y)\,, \\ \big(\Box_x + M^2(x)\big)\,G_\rho(x,y) &= \int_{x_0}^{y^0} d^4z\,\Pi_\rho(x,z)G_\rho(z,y)\,. \end{aligned} \tag{8.8}$$

They constitute an extension of the Kadanoff-Baym equations (6.15) incorporating a non-Gaussian initial 4-point correlation, which leads to the additional contribution in the second line. It has to be emphasized that, in contrast to the memory integrals, this contribution does *not* have to vanish when $x^0, y^0 \to 0$. The effective mass $M^2(x)$ and the non-local self-energies $\Pi_{F/\rho}(x,y)$ are identical to those in the Gaussian case (see eq. (6.16)).

8.2.3 Renormalization

Motivated by the parameterization (6.26) of the renormalized 2PI effective action at finite temperature, as well as the renormalized Kadanoff-Baym equation (7.77) for the thermal initial state, the following ansatz for the Kadanoff-Baym equation determining the renormalized Schwinger-Keldysh propagator $G_R(x,y) = Z^{-1}G(x,y)$ is proposed,

$$\left(\Box_x + \delta Z_0 \Box_x + m_R^2 + \delta m_0^2 + \frac{\lambda_R + \delta\lambda_0}{2} G_R(x,x)\right) G_{F,R}(x,y)$$
$$= \int_0^{y^0} d^4z \,\Pi_{F,R}(x,z) G_{\rho,R}(z,y) - \int_0^{x^0} d^4z \,\Pi_{\rho,R}(x,z) G_{F,R}(z,y)$$
$$- \frac{\lambda_R}{6} V_{4,R}^{nG}(x,x,x,y)\,, \tag{8.9a}$$

$$\left(\Box_x + \delta Z_0 \Box_x + m_R^2 + \delta m_0^2 + \frac{\lambda_R + \delta\lambda_0}{2} G_R(x,x)\right) G_{\rho,R}(x,y)$$
$$= \int_{x_0}^{y^0} d^4z \,\Pi_{\rho,R}(x,z) G_{\rho,R}(z,y)\,. \tag{8.9b}$$

Here δZ_0, δm_0^2 and $\delta\lambda_0$ denote the 2PI vacuum counterterms determined by the nonperturbative renormalization procedure. The non-local part of the renormalized self-energy $\Pi_R(x,y) = Z\Pi(x,y)$ is given by the setting-sun diagram with renormalized couplings,

$$\Pi_{non-local,R}(x,y) = \Pi_{F,R}(x,y) - \frac{i}{2}\,\mathrm{sgn}_{\mathcal{C}}(x^0 - y^0)\,\Pi_{\rho,R}(x,y) = \frac{(-i\lambda_R)^2}{6} G_R(x,y)^3\,,$$

and $V_{4,R}^{nG} = Z^{-2} V_4^{nG}$ is given by the renormalized initial 4-point correlation $\alpha_{4,R} = Z^2\alpha_4$,

$$V_{4,R}^{nG}(x,x,x,y) = \int_{\mathcal{C}} d^4y_{1234}\, G_R(x,y_1) G_R(x,y_2) G_R(x,y_3) [i\alpha_{4,R}(y_1,y_2,y_3,y_4)] G_R(y_4,y)\,.$$

Although the initial 4-point correlation $\alpha_{4,R}$ is only supported at the initial time, it does lead to a non-zero contribution to the Kadanoff-Baym equations for non-zero times $x^0, y^0 \geq 0$. This can be seen by inserting the parameterization (8.4) into the upper equation,

$$V_{4,R}^{nG}(x,x,x,y) = \int d^3y_{1234}\, G_R(x,y_{\varepsilon_1}) G_R(x,y_{\varepsilon_2}) G_R(x,y_{\varepsilon_3}) [i\alpha_{4,R}^{\varepsilon_1\varepsilon_2\varepsilon_3\varepsilon_4}(\boldsymbol{y_1},\boldsymbol{y_2},\boldsymbol{y_3},\boldsymbol{y_4})] G_R(y_{\varepsilon_4},y)\,.$$

The four time integrations over the closed contour are annihilated by the four Dirac distributions of the initial correlation. Above, summation over $\varepsilon_i = \pm$ is implied, and

$$G_R(x,y_\varepsilon) = G_R(x^0,\boldsymbol{x};0_\varepsilon,\boldsymbol{y}) = G_{F,R}(x^0,\boldsymbol{x};0,\boldsymbol{y}) - \frac{i\varepsilon}{2} G_{\rho,R}(x^0,\boldsymbol{x};0,\boldsymbol{y}) \qquad \text{for} \quad \varepsilon \in \{+,-\}\,.$$

The non-Gaussian contribution to the Kadanoff-Baym equations (8.9) may also be understood as a contribution to the self-energy which is only supported at the initial time surface $y^0 = 0_\pm$,

$$-\frac{\lambda_R}{6} V_{4,R}^{nG}(x,x,x,y) \equiv \int_{\mathcal{C}} d^4y_4\, \Pi_{\lambda\alpha,R}(x,y_4) G_R(y_4,y)\,, \tag{8.10}$$

where

$$\begin{aligned} i\Pi_{\lambda\alpha,R}(x,y) &= \frac{1}{6}\int_{\mathcal{C}} d^4y_{123}\,[-i\lambda_R] G_R(x,y_1) G_R(x,y_2) G_R(x,y_3) [i\alpha_{4,R}(y_1,y_2,y_3,y)] \\ &\equiv i\Pi_{\lambda\alpha,F,R}(x^0,\boldsymbol{x},\boldsymbol{y})\delta_s(y^0) - \frac{i}{2} i\Pi_{\lambda\alpha,\rho,R}(x^0,\boldsymbol{x},\boldsymbol{y})\delta_a(y^0)\,, \end{aligned} \tag{8.11}$$

with $\delta_{s/a}(y^0) \equiv \left[\delta_{\mathcal{C}}(y^0 - 0_+) \pm \delta_{\mathcal{C}}(y^0 - 0_-)\right]/2$. Due to the structure of the initial correlation, the three propagators appearing in the non-Gaussian contribution $\Pi_{\lambda\alpha,R}(x,y)$ to the self-energy are evaluated at the times $t = x^0$ and $t_{init} = 0$. For sufficiently dense and strongly coupled systems, the unequal-time propagators $G_{F/\rho,R}(x^0,0,\boldsymbol{k})$ are damped exponentially for each momentum mode $\boldsymbol{k}$ (see left part

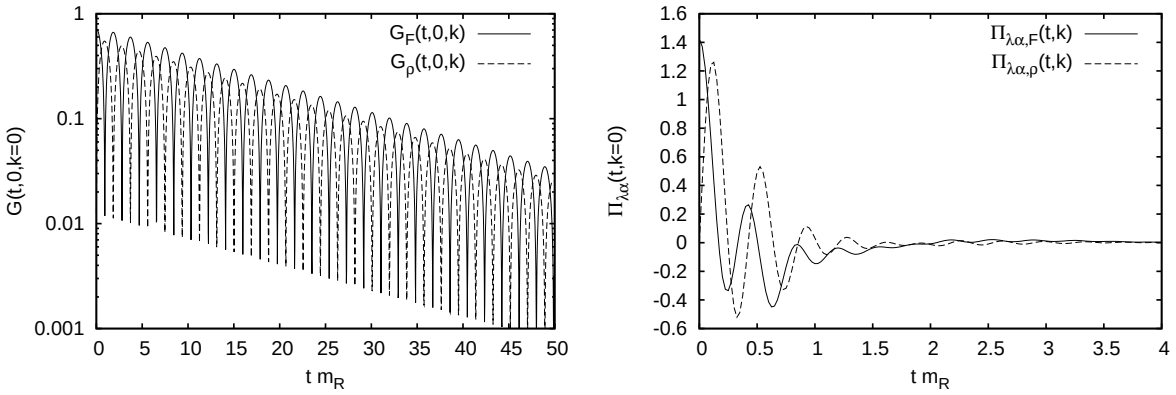

Figure 8.1: ***Left:*** *The unequal-time propagator is damped exponentially. The damping rate increases with the density and the coupling strength of the system.* ***Right:*** *The non-Gaussian contribution to the self-energy is strongly damped. Thus, the contribution of the initial* 4*-point correlation is most relevant close to the initial time* $t = 0$*.*

of figure 8.1). Therefore, also $\Pi_{\lambda\alpha,F/\rho,R}(x^0,\boldsymbol{k}) = \int d^3x\, e^{-i\boldsymbol{k}(\boldsymbol{x}-\boldsymbol{y})}\,\Pi_{\lambda\alpha,F/\rho,R}(x^0,\boldsymbol{x},\boldsymbol{y})$ is damped exponentially with respect to x^0 (see right part of figure 8.1). Hence, the contribution of the initial 4-point correlation to the Kadanoff-Baym equation is suppressed for times much larger than the characteristic damping time-scale. This means in particular that all properties of solutions of Kadanoff-Baym equations at late times, including universality and thermalization, are not changed. Instead, the influence of the initial 4-point correlation is maximal near the initial time. Additionally, the memory integrals vanish for $x^0, y^0 \to t_{init} = 0$, such that the non-Gaussian contribution $-\lambda_R V^{nG}_{4,R}(x,x,x,y)/6$ makes up the only non-zero term on the right-hand side of the Kadanoff-Baym equations in this limit.
In section 8.1 it was observed that the 2PI vacuum counterterms renormalizing the 2PI effective action in equilibrium, which can be expected to be correct at late times, fail for $x^0, y^0 \to 0$ for a Gaussian initial state. The reason was that the divergence contained in the memory integral, which is to be canceled by the coupling counterterm, vanishes at the initial time. Now, however, it is possible to investigate whether the non-Gaussian initial 4-point correlation can be chosen such as to remedy this shortcoming of the Gaussian initial state.

8.2.4 Finiteness for Renormalized Initial States

In order to verify the ansatz (8.9) for renormalized Kadanoff-Baym equations it will be shown in the following (as a first step) that the 2PI vacuum counterterms determined via the nonperturbative renormalization procedure indeed render the Kadanoff-Baym equations finite in the limit $x^0, y^0 \to 0$ for the special case where both the initial 2- and 4-point correlations take their thermal values.
Note that, nevertheless, this initial state corresponds to a nonequilibrium situation, since all higher correlations are omitted. However, it represents the choice for which the deviation from thermal equilibrium is minimal within the class of initial states characterized by a density matrix of the form (8.3).
In setting-sun approximation, the renormalized thermal initial 4-point correlation is given by (see eq. (7.80))

$$i\alpha^{th}_{4,R}(z_1,z_2,z_3,z_4) = -i\lambda_R \int_{\mathcal{I}} d^4v\, \Delta_m(v,z_1)\Delta_m(v,z_2)\Delta_m(v,z_3)\Delta_m(v,z_4)\,, \tag{8.12}$$

where $\Delta_m(v,z) = \int \frac{d^3k}{(2\pi)^3} e^{i\boldsymbol{k}(\boldsymbol{v}-\boldsymbol{z})}\, T\sum_n e^{i\omega_n\tau}\Delta_m(\omega_n,z^0,\boldsymbol{k})$ for $v = (-i\tau,\boldsymbol{v})$ denotes the Fourier transformed "mixed connection" defined in eq. (7.54). For thermal initial 2- and 4-point correlations, the

2- and 4-point functions in the limit $x^0, y^0 \to 0$ are thus given by (see chapter 7)

$$\begin{aligned} G_{F,R}(x,y)|_{x^0,y^0=0} &= G_{th,R}(x,y)|_{x^0,y^0=0}\,, \\ V^{nG}_{4,R}(x_1,x_2,x_3,x_4)|_{x_i^0=0} &= -i\lambda_R \int_{\mathcal{I}} d^4v\, G_{th,R}(x_1,v) G_{th,R}(x_2,v) G_{th,R}(x_3,v) G_{th,R}(x_4,v)|_{x_i^0=0}\,, \end{aligned} \tag{8.13}$$

where $G_{th,R}$ is the solution of the renormalized Schwinger-Dyson equation (6.26) obtained from the three-loop truncation of the 2PI effective action at finite temperature. Inserting this into the Kadanoff-Baym equation (8.9) for the statistical propagator evaluated at $x^0 = y^0 = 0$ yields (after dividing by $Z = 1 + \delta Z_0$)

$$\begin{aligned} \partial^2_{x^0} G_{F,R}(x,y)|_{x^0,y^0=0} &= -\left[-\boldsymbol{\nabla}^2 + Z^{-1}\left(\delta m_0^2 + m_R^2 + \frac{\lambda_R + \delta\lambda_0}{2} G_{th,R}(x,x)\right)\right] G_{th,R}(x,y)|_{x^0,y^0=0} \\ &\quad - Z^{-1}\frac{\lambda_R}{6}(-i\lambda_R)\int_{\mathcal{I}} d^4v\, G_{th,R}(x,v)^3 G_{th,R}(v,y)|_{x^0,y^0=0}\,. \end{aligned}$$

After Fourier transforming with respect to $(\boldsymbol{x} - \boldsymbol{y})$ as well as inserting the Fourier transformation of the thermal propagator with respect to the 4-momentum $k = (\omega_n, \boldsymbol{k})$, the upper equation becomes

$$\begin{aligned} \partial^2_{x^0} G_{F,R}(x^0,y^0,\boldsymbol{k})|_{x^0,y^0=0} &= -T\sum_n e^{i\omega_n\tau}\left[\boldsymbol{k}^2 + Z^{-1}\left(\delta m_0^2 + m_R^2 + \frac{\lambda_R + \delta\lambda_0}{2}\int_q G_{th,R}(q)\right.\right. \\ &\quad \left.\left. - \frac{\lambda_R^2}{6}\int_{pq} G_{th,R}(p) G_{th,R}(q) G_{th,R}(k-q-p)\right)\right] G_{th,R}(\omega_n,\boldsymbol{k})|_{\tau\to 0} \\ &= -T\sum_n e^{i\omega_n\tau}\left[\boldsymbol{k}^2 + Z^{-1}\left(m_R^2 + \Pi_{th,R}(k) - \delta Z_0 k^2\right)\right] G_{th,R}(\omega_n,\boldsymbol{k})|_{\tau\to 0}\,. \end{aligned}$$

The combination of the thermal tadpole- and setting-sun contributions in the inner brackets of the first line is precisely the same as for the renormalized thermal self-energy (6.26), which has been inserted in the second line. The nonperturbative renormalization procedure is designed such that $\Pi_{th,R}(k)$ is finite. Therefore, the thermal setting-sun contribution, which stems from the contribution of the initial 4-point correlation, is crucial for renormalization. Next, it is used that the thermal 2PI propagator fulfills the self-consistent Schwinger-Dyson equation (6.26),

$$\begin{aligned} \partial^2_{x^0} G_{F,R}(x^0,y^0,\boldsymbol{k})|_{x^0,y^0=0} &= -T\sum_n e^{i\omega_n\tau}\left[\boldsymbol{k}^2 + Z^{-1}\left(G^{-1}_{th,R}(\omega_n,\boldsymbol{k}) - Zk^2\right)\right] G_{th,R}(\omega_n,\boldsymbol{k})|_{\tau\to 0} \\ &= -T\sum_n e^{i\omega_n\tau}\left[Z^{-1} - \omega_n^2 G_{th,R}(\omega_n,\boldsymbol{k})\right]_{\tau\to 0} \\ &= -\partial^2_\tau G_{th,R}(-i\tau,0,\boldsymbol{k})|_{\tau\to 0}\,, \end{aligned}$$

where $k^2 = \omega_n^2 + \boldsymbol{k}^2$ and $T\sum_n e^{i\omega_n\tau} = 0$ for $\tau \neq 0$ has been used. The last expression is manifestly finite, since the full renormalized thermal propagator $G_{th,R}(-i\tau,0,\boldsymbol{k})$ is finite for $0 \leq \tau \leq \beta$. The Kadanoff-Baym equation for the spectral function does not involve any divergences for $x^0, y^0 \to 0$.

Outlook

It has been shown that the Kadanoff-Baym equations (8.9) supplied with 2PI vacuum counterterms derived from the three-loop truncation of the 2PI effective action with thermal initial 2- and 4-point correlation are rendered finite in the limit $x^0, y^0 \to 0$. As discussed above, in the opposite limit $x^0, y^0 \to \infty$, where thermal equilibrium is approached, the nonperturbative renormalization procedure of the 2PI effective action at finite temperature can also be expected to be appropriate. In order to

show that the Kadanoff-Baym equations with thermal initial 2- and 4-point correlation are also rendered finite at intermediate times, it is required to show that the truncation of the higher thermal n-point correlations for $n \geq 6$ does not introduce any divergences. Furthermore, if the initial 2-point correlation deviates from its thermal value, it can be expected that the initial 4-point correlation also has to be modified such that the Kadanoff-Baym equations stay finite. In order to investigate this question, it is necessary to expand the Kadanoff-Baym equations with nonequilibrium initial conditions around the renormalized Kadanoff-Baym equations for thermal equilibrium, which have been derived in chapter 7. Therefore, it is required to formulate the Bethe-Salpeter equation encountered in section 6.2 on the closed real-time path. In this way, it should be possible to derive criteria which the nonequilibrium initial state of the ensemble has to fulfill in order to be compatible with renormalization. Only these "renormalized initial states" may occur as real physical states of the ensemble. Above, already one class of renormalized initial states could be identified, namely those with thermal initial 2- and 4-point correlation functions.

8.3 Impact of 2PI Renormalization on Solutions of Kadanoff-Baym Equations

The Kadanoff-Baym equations (8.9) for the renormalized Schwinger-Keldysh propagator contain counterterms determined according to the nonperturbative renormalization procedure of the 2PI effective action and take into account a non-Gaussian initial state featuring an initial 4-point correlation. In this section, the relevance of nonperturbative 2PI counterterms as well as the initial 4-point correlation is investigated by means of numerical solutions of Kadanoff-Baym equations.
In order to compare the nonperturbatively renormalized Kadanoff-Baym equations to the conventionally used Kadanoff-Baym equations, which contain approximate perturbative counterterms and Gaussian initial correlations, both sets of equations are given in section 8.3.1. Next, the numerical computation of the 2PI counterterms is discussed in section 8.3.2.
The impact of the non-Gaussian initial 4-point correlation is investigated in section 8.3.3. Therefore, solutions of Kadanoff-Baym equations with Gaussian and non-Gaussian initial states, but with identical (2PI) counterterms, are compared.
The impact of the renormalization prescription is investigated in section 8.3.4, by comparing solutions of Kadanoff-Baym equations with approximate perturbative counterterms and with nonperturbative 2PI counterterms, but with identical (Gaussian) initial state.
Finally, in section 8.3.5, it is shown that the nonequilibrium time-evolution of the renormalized Schwinger-Keldysh propagator is compatible with time-independent counterterms.
The nonperturbative 2PI counterterms were determined with the `renormalize` program, which was developed following the lines of Ref. [29]. Furthermore, the numerical solutions of the Kadanoff-Baym equations are based on an extended version of the `kadanoffBaymmm` program [146, 147].

8.3.1 Kadanoff-Baym Equations with Nonperturbative 2PI Counterterms and Initial Four-Point Correlation Function

The general form of the evolution equation for the full connected Schwinger-Keldysh two-point function (Kadanoff-Baym equation) for a space-translation invariant system, without further approximations, is

$$\left(\partial_{x^0}^2 + \boldsymbol{k}^2 + M^2(x^0)\right) G_F(x^0, y^0, \boldsymbol{k}) = \int_0^{y^0} dz^0 \, \Pi_F(x^0, z^0, \boldsymbol{k}) G_\rho(z^0, y^0, \boldsymbol{k})$$

$$-\int_0^{x^0} dz^0\,\Pi_\rho(x^0,z^0,\boldsymbol{k})G_F(z^0,y^0,\boldsymbol{k})+\Pi_{\lambda\alpha,F}(x^0,\boldsymbol{k})G_F(0,y^0,\boldsymbol{k})+\frac{1}{4}\Pi_{\lambda\alpha,\rho}(x^0,\boldsymbol{k})G_\rho(0,y^0,\boldsymbol{k})\,,$$

complemented by a similar equation for the spectral function (see eq. (7.26)). The information about the underlying 2PI (loop) approximation and renormalization prescription is encoded in the expressions for the self-energies, which will be given below for the cases of interest. In particular, non-Gaussian initial correlations enter via the contributions $\Pi_{\lambda\alpha,F/\rho}$, which vanish for a Gaussian initial state.

The Kadanoff-Baym equations (8.9) can be brought into the upper form by Fourier transforming with respect to the relative spatial coordinate and parameterizing it in terms of "bare" propagators $G = ZG_R$ and self-energies $\Pi = Z^{-1}\Pi_R$ (where $Z = 1+\delta Z_0$). Furthermore, the parameterization of the initial 4-point correlation described in eqs. (8.10, 8.11) is used. Before presenting the resulting expressions for the self-energies corresponding to the full nonperturbative renormalization procedure, those for the approximate perturbative renormalization prescription are given for comparison.

Approximate perturbative renormalization

So far, when solving Kadanoff-Baym equations, an approximate perturbative renormalization prescription has been used by default [17]. Here, only the mass is renormalized at one-loop order of standard perturbation theory, while the coupling remains unchanged. The bare mass is then given by

$$m_B^2 = m_R^2 - \frac{\lambda}{2}\left(\int\frac{d^3p}{(2\pi)^3}\,\frac{1}{2\sqrt{m_R^2+\boldsymbol{p}^2}}\right)_{reg},$$

where the momentum integral is calculated employing a regulator (which is provided by the lattice discretization in the case of numerical calculations). As the coupling constant is unchanged the effective mass and the nonlocal self-energies are given by

$$\begin{aligned}
M^2(x^0) &= m_B^2+\frac{\lambda}{2}\int\frac{d^3p}{(2\pi)^3}\,G_F(x^0,x^0,\boldsymbol{p})\,,\\
\Pi_F(x^0,y^0,\boldsymbol{k}) &= -\frac{\lambda^2}{6}\left([G_F*G_F*G_F](x^0,y^0,\boldsymbol{k})-\frac{3}{4}[G_\rho*G_\rho*G_F](x^0,y^0,\boldsymbol{k})\right),\\
\Pi_\rho(x^0,y^0,\boldsymbol{k}) &= -\frac{\lambda^2}{6}\left(3[G_F*G_F*G_\rho](x^0,y^0,\boldsymbol{k})-\frac{1}{4}[G_\rho*G_\rho*G_\rho](x^0,y^0,\boldsymbol{k})\right).
\end{aligned}$$

The non-local parts contain the double convolutions

$$[G_F*G_F*G_F](x^0,y^0,\boldsymbol{k}) = \int\frac{d^3p}{(2\pi)^3}\frac{d^3q}{(2\pi)^3}\,G_F(x^0,y^0,\boldsymbol{p})G_F(x^0,y^0,\boldsymbol{q})G_F(x^0,y^0,\boldsymbol{k}-\boldsymbol{p}-\boldsymbol{q})\,,$$

with similar expressions involving G_ρ. The approximate perturbative renormalization prescription is designed for a Gaussian initial state, for which

$$\Pi_{\lambda\alpha,F}(x^0,\boldsymbol{k}) \;=\; \Pi_{\lambda\alpha,\rho}(x^0,\boldsymbol{k}) \;=\; 0\,.$$

It is important to note that this perturbative renormalization prescription suffers from several shortcomings. First, it neglects the renormalization of the coupling. Second, it does not take into account contributions from higher loop orders. And third, it ignores the nonperturbative nature of the underlying 2PI formalism.

Full nonperturbative renormalization

The Kadanoff-Baym equations for the renormalized Schwinger-Keldysh propagator, which have been proposed in eq. (8.9), contain mass and coupling counterterms determined according to the full nonperturbative renormalization procedure of the 2PI effective action, as well as an initial 4-point correlation function.

Nonperturbative counterterms: The Kadanoff-Baym equations (8.9) contain the full 2PI counterterms. Their determination requires the solution of a self-consistent Schwinger-Dyson equation for the full thermal propagator together with a Bethe-Salpeter equation for the appropriate 4-point kernel (see section 6.2). Evaluated for the 3-loop truncation of the 2PI effective action both equations read:

$$\begin{aligned} G^{-1}(k) &= k^2 + m_B^2 + \frac{\lambda_B}{2}\int_q G(q) - \frac{\lambda_R^2}{6Z^4}\int_{pq} G(p)G(q)G(k-p-q)\,, \\ V(k) &= \lambda_B - \frac{\lambda_B}{2}\int_q G^2(q)V(q) \\ &\quad - \frac{\lambda_R^2}{Z^4}\int_q G(q)G(k-q) + \frac{\lambda_R^2}{2Z^4}\int_{pq} G(p)G(k-q-p)G^2(q)V(q)\,, \end{aligned} \tag{8.14}$$

where $G(k) \equiv ZG_{th,R}(k)$, $V(k) \equiv ZV_R(k, q=0)$, $Z = 1 + \delta Z_0$, $m_B^2 = (m_R^2 + \delta m_0^2)/Z$ and $\lambda_B = (\lambda_R + \delta\lambda_0)/Z^2$. For given bare mass m_B^2 and bare coupling λ_B the renormalized mass m_R^2, the renormalized coupling λ_R, and the field renormalization Z are determined by the renormalization conditions

$$\begin{aligned} Z\frac{d}{dk^2}G_{vac}^{-1}(k=0) &= +1\,, \\ Z\,G_{vac}^{-1}(k=0) &= m_R^2\,, \\ Z^2 V_{vac}(k=0) &= \lambda_R\,, \end{aligned} \tag{8.15}$$

where $G_{vac}(k)$ and $V_{vac}(k)$ denote the solutions of eqs. (8.14) obtained at zero temperature. Desired values for the renormalized mass and coupling can be achieved by an appropriate choice of the bare mass and coupling (see section 8.3.2).

Initial 4-point correlation: It is convenient to expand the initial 4-point correlation in terms of the symmetric and antisymmetric Dirac distributions $\delta_{s/a}(t)$ defined below eq. (8.11),

$$\alpha_4(x,y,z,w) = \sum_{ijkl\in\{s,a\}} \alpha_4^{ijkl}(\boldsymbol{x},\boldsymbol{y},\boldsymbol{z},\boldsymbol{w})\delta_i(x^0)\delta_j(y^0)\delta_k(z^0)\delta_l(w^0)\,,$$

which is equivalent to the expansion (8.4). The possible combinations of the upper indices together with the Hermiticity condition (7.5) imply that it is parameterized by 16 real functions of four spatial points. However, only five of them are independent, namely α_4^{ssss}, α_4^{aaaa}, α_4^{ssaa}, α_4^{sssa} and α_4^{saaa}, while the other components are obtained by permutation of the four arguments. If, in addition, the contribution of the 4-point correlation to the density matrix (8.3) is real (which turns out to be true for all cases considered below) the latter two vanish, such that only three independent functions remain.

Self-energy: The nonperturbatively renormalized effective mass and non-local self-energies are given by

$$M^2\left(x^0\right) = m_B^2 + \frac{\lambda_B}{2}\int\frac{d^3p}{(2\pi)^3}\,G_F(x^0,x^0,\boldsymbol{p})\,, \tag{8.16}$$

$$\Pi_F(x^0,y^0,\boldsymbol{k}) = -\frac{\lambda_R^2}{6Z^4}\left([G_F*G_F*G_F](x^0,y^0,\boldsymbol{k}) - \frac{3}{4}[G_\rho*G_\rho*G_F](x^0,y^0,\boldsymbol{k})\right),$$
$$\Pi_\rho(x^0,y^0,\boldsymbol{k}) = -\frac{\lambda_R^2}{6Z^4}\left(3[G_F*G_F*G_\rho](x^0,y^0,\boldsymbol{k}) - \frac{1}{4}[G_\rho*G_\rho*G_\rho](x^0,y^0,\boldsymbol{k})\right).$$

In addition, a real initial 4-point correlation can be incorporated in the non-Gaussian self-energies given by

$$\Pi_{\lambda\alpha,F}(x^0,\boldsymbol{k}) = -\frac{\lambda_R}{6Z^2}\left([G_F\cdot G_F\cdot G_F\cdot i\alpha_4^{ssss}](x^0,0,\boldsymbol{k}) - \frac{3}{4}\left[G_\rho\cdot G_\rho\cdot G_F\cdot i\alpha_4^{aass}\right](x^0,0,\boldsymbol{k})\right),$$
$$\Pi_{\lambda\alpha,\rho}(x^0,\boldsymbol{k}) = -\frac{\lambda_R}{6Z^2}\left(3\left[G_F\cdot G_F\cdot G_\rho\cdot i\alpha_4^{ssaa}\right](x^0,0,\boldsymbol{k}) - \frac{1}{4}\left[G_\rho\cdot G_\rho\cdot G_\rho\cdot i\alpha_4^{aaaa}\right](x^0,0,\boldsymbol{k})\right).$$

Here, the spatial Fourier transform of the initial 4-point correlation enters according to

$$[G_F\cdot G_F\cdot G_F\cdot i\alpha_4^{ssss}](x^0,0,\boldsymbol{k}) =$$
$$= \int\frac{d^3p}{(2\pi)^3}\frac{d^3q}{(2\pi)^3}G_F(x^0,0,\boldsymbol{p})G_F(x^0,0,\boldsymbol{q})G_F(x^0,0,\boldsymbol{k}-\boldsymbol{p}-\boldsymbol{q})\,i\alpha_4^{ssss}(\boldsymbol{p},\boldsymbol{q},\boldsymbol{k}-\boldsymbol{p}-\boldsymbol{q},-\boldsymbol{k}),$$

with similar expressions involving G_ρ.

8.3.2 Numerical Computation of Nonperturbative Counterterms

In order to be able to solve Kadanoff-Baym equations containing 2PI counterterms, it is necessary to compute the latter according to the nonperturbative renormalization procedure of the 2PI effective action [28,29]. This has to be done numerically, for two reasons: First, it is required to compute these counterterms with the identical regulator as for the Kadanoff-Baym equations, which is provided by the lattice discretization. Second, the Schwinger-Dyson and Bethe-Salpeter equations cannot be solved analytically. Accordingly, these equations are solved numerically on a lattice with the same size N_s^3 and lattice spacing a_s for the spatial coordinates as is used for the solution of the Kadanoff-Baym equations (typical values are $N_s = 32$ and $a_s m_R = 0.5$), in order to obtain the 2PI counterterms for the same regulator.

The discretization of the temporal direction determines the temperature according to $T = 1/(N_t a_t)$. The temporal lattice spacing a_t is chosen small enough such that the continuum limit is approached[2]. If appropriate, a_t may be chosen to coincide with the time-step used for the solution of the Kadanoff-Baym equations. The lattice cutoff is then determined by the spatial spacing, $\Lambda \sim \pi/a_s$.

The 2PI counterterms are determined by solving eqs. (8.14, 8.15) at a reference temperature $T_0 \ll m_R$ which is sufficiently close to the zero-temperature (infinite volume) limit by choosing $N_t \gg 10/(m_R a_t)$. Using the counterterms determined at the reference temperature, the thermal propagator at some temperature $T \neq T_0$ is determined by solving eqs. (8.14) on a lattice where $N_t = 1/(T a_t)$ while a_t, a_s and N_s remain fixed.

In the course of this work, the numerical computation of 2PI counterterms has been achieved following the lines of Ref. [29]. Starting from some initial values of the bare parameters, the Schwinger-Dyson and Bethe-Salpeter equations are solved iteratively (see figure 8.2) simultaneously for all momentum modes, and the renormalized quantities are then extracted from the renormalization conditions. Then, the values of the bare parameters are adjusted, and the upper iteration is repeated, until

[2] The discretization required to solve Kadanoff-Baym equations apparently breaks Lorentz invariance, as does the nonequilibrium ensemble itself. This singles out a preferred frame where the expectation value of the total momentum of the ensemble vanishes (center of mass frame). The field renormalization can be obtained by evaluating the 4-momentum derivative in eq. (8.15) via spatial (Z_s) or temporal (Z_t) lattice points. It has been checked that both possibilities lead to negligible differences in the results.

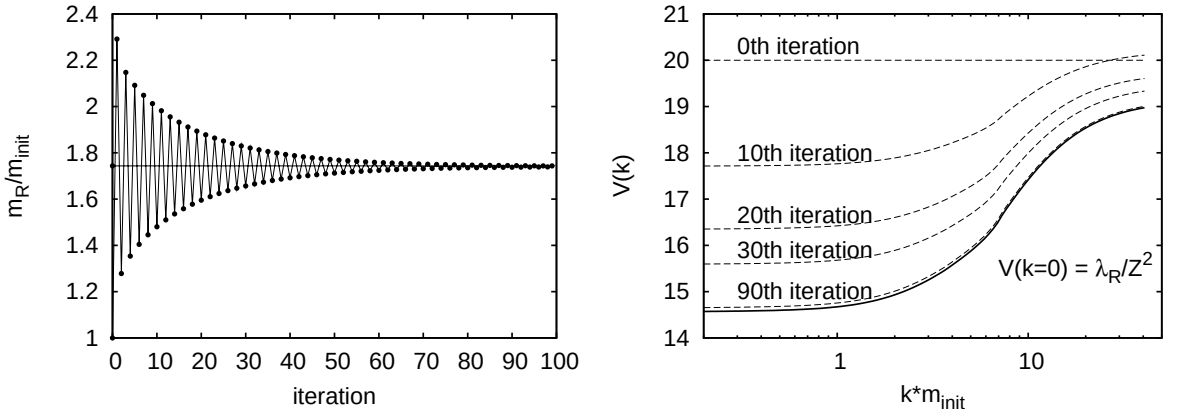

Figure 8.2: ***Left:*** *Renormalized mass extracted from the iterative solution of the Schwinger-Dyson equation for the propagator $G(k)$ according to the renormalization condition (8.15).* ***Right:*** *Iterative solution of the Bethe-Salpeter equation for the kernel $V(k)$.*

the result yields the desired values of the renormalized mass and coupling. The renormalized vacuum mass m_R is used to set the scale for all simulations. The dependence of the 2PI counterterms on the coupling λ_R is shown in figure 8.3.
For the subsequent calculation of the thermal propagator at some temperature $T \gg T_0$, it is only necessary to perform the iteration once since the bare parameters are fixed to those determined at the reference temperature. The thermal mass can then be extracted via the zero-mode of the thermal propagator,

$$m_{th}^2 = Z\, G_{th}^{-1}(k=0)\,. \tag{8.17}$$

8.3.3 Gaussian versus Non-Gaussian Initial State

In order to verify the full nonperturbative renormalization procedure of Kadanoff-Baym equations, it is instructive to investigate solutions which minimally deviate from thermal equilibrium, for several reasons. First, it permits a detailed comparison with renormalized equilibrium quantities. The latter can independently be computed within thermal quantum field theory, for which the renormalization of the 2PI effective action is known. Second, it provides the possibility to show the importance of the non-Gaussian 4-point correlation of the initial state for renormalization. Furthermore, the thermal limit is valuable in order to investigate the dependence on the cutoff provided by the (lattice) regulator, the elimination of which is the ultimate goal of renormalization. Finally, a reasonable description of the thermal limit within Kadanoff-Baym equations is the basis for a controlled transition to nonequilibrium.
The reason for the existence of a minimal deviation of solutions of Kadanoff-Baym equations from thermal equilibrium is the following. Describing thermal equilibrium requires to incorporate thermal initial n-point correlation functions for all $n \in \mathbb{N}$ into Kadanoff-Baym equations, as has been shown in chapter 7. Therefore, for Kadanoff-Baym equations incorporating initial n-point correlations for finite n, the thermal propagator is *no* "fixed-point" solution[3]. Since numerical investigations are confined to finite n (actually, already the inclusion of $n = 4$ requires a sophisticated algorithm), it is a non-trivial question how large the unavoidable deviations from thermal equilibrium are for a given truncation of the thermal initial correlations.

[3] In contrast to this, standard (classical) Boltzmann equations do possess a "fixed-point" solution for thermal one-particle distribution functions.

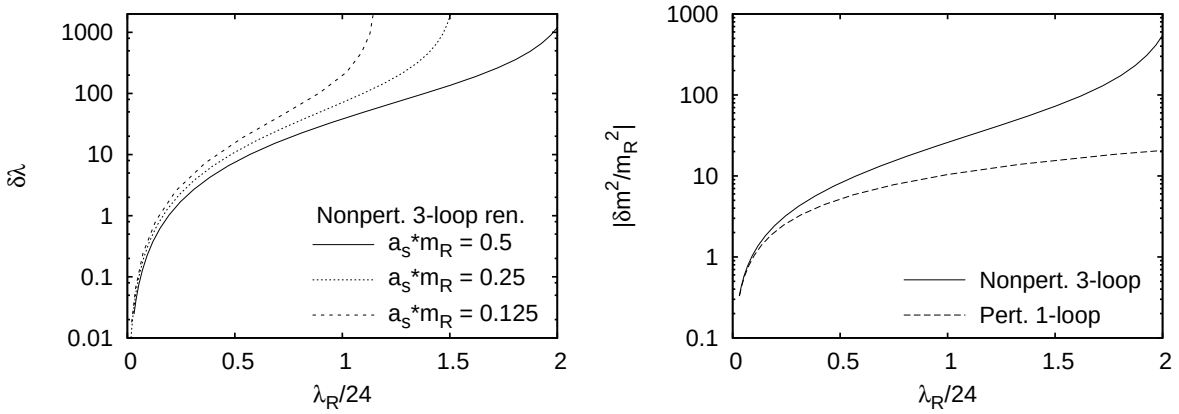

Figure 8.3: ***Left:*** *Dependence of the nonperturbative 2PI coupling counterterm on the renormalized coupling for three different lattice spacings a_s. For a given regulator, the coupling counterterm diverges at some maximal value of the renormalized coupling. This maximal value becomes smaller when decreasing a_s, i.e. when increasing the cutoff (triviality).* ***Right:*** *Comparison of the nonperturbative 2PI mass counterterm and the approximate perturbative mass counterterm for $a_s m_R = 0.5$.*

In the case of Kadanoff-Baym equations for Gaussian initial states, only the initial 2-point correlation is retained. Since the 4-point function carries logarithmic divergences, this means that Gaussian initial states feature an unavoidable, cutoff-dependent offset from thermal equilibrium.
In contrast to this, Kadanoff-Baym equations incorporating a thermal initial 2- and 4-point correlation coincide with those for thermal equilibrium in the limit $x^0, y^0 \to 0$ (see section 7.2). In particular, this means that the initial values of thermal masses or energy densities coincide with those in thermal equilibrium, which are renormalized by the 2PI counterterms.
The thermal n-point correlations for $n \geq 6$ are suppressed due to two reasons: First, since the effective non-local n-point vertices describing the initial n-point correlations are supported only at the initial time, they would enter the Kadanoff-Baym equations accompanied by n propagators $G_R(t,0,\boldsymbol{k})$ evaluated at $t = x^0, y^0$, which are damped exponentially for $t \gg m_R^{-1}$ (see figure 8.1). Thus, the memory to n-point correlations of the initial state is lost the more rapidly the higher n. Second, for Φ^4-theory, the contribution of initial correlations higher than 4 is also suppressed when approaching the initial time, as has been shown in section 7.2.3.
In the following, a detailed comparison between the Kadanoff-Baym equations with and without thermal initial 4-point correlation is presented. In both cases, the full nonperturbative renormalization procedure is employed. For the first set of solutions, however, a Gaussian initial state is used. For the second set of solutions, the non-Gaussian thermal initial 4-point correlation is added. The 2PI counterterms and the initial conditions for the thermal 2-point correlation are identical for both sets. The solutions with initial 4-point correlation are used to show the relevance of non-Gaussian correlations for renormalization. Finally, the cutoff dependence is investigated.

Renormalized thermal initial 2- and 4-point correlation

2-point correlation: The thermal initial 2-point correlation is encoded in the initial conditions for the statistical propagator. For the thermal case, they are given by

$$\begin{aligned} G_F(x^0,y^0,\boldsymbol{k})\big|_{x^0=y^0=0} &= G_{th}(\boldsymbol{k}), \\ \partial_{x^0} G_F(x^0,y^0,\boldsymbol{k})\big|_{x^0=y^0=0} &= 0, \end{aligned} \tag{8.18}$$

$$\partial_{x^0}\partial_{y^0} G_F(x^0,y^0,\boldsymbol{k})\big|_{x^0=y^0=0} \;=\; \omega_{th}(\boldsymbol{k})\, G_{th}(\boldsymbol{k})\,,$$

where

$$\begin{aligned} G_{th}(\boldsymbol{k}) &= G_{th}(-i\tau,0,\boldsymbol{k})|_{\tau=0} = T\sum_n G_{th}(\omega_n,\boldsymbol{k})\,, \\ \omega_{th}(\boldsymbol{k})^2 &= \left(\frac{\partial_\tau^2 G_{th}(-i\tau,0,\boldsymbol{k})}{G_{th}(-i\tau,0,\boldsymbol{k})}\right)\Big|_{\tau\to 0} = \frac{T\sum_n \left(1-\omega_n^2 G_{th}(\omega_n,\boldsymbol{k})\right)}{G_{th}(\boldsymbol{k})}\,, \end{aligned} \tag{8.19}$$

and $G_{th}(\omega_n,\boldsymbol{k})$ is a solution of the thermal self-consistent Schwinger-Dyson equation (8.14) at temperature $T=1/\beta$.

4-point correlation: The full thermal initial 4-point correlation appearing in the in setting-sun approximation is derived in chapter 7. It is given by (see eqs. 7.74, 7.67)

$$i\alpha_{4,th}^{ijkl}(\boldsymbol{k_1},\boldsymbol{k_2},\boldsymbol{k_3},\boldsymbol{k_4}) \;=\; -\frac{\lambda_R}{Z^2}\int_0^\beta d\tau\, \Delta^i(-i\tau,\boldsymbol{k_1})\Delta^j(-i\tau,\boldsymbol{k_2})\Delta^k(-i\tau,\boldsymbol{k_3})\Delta^l(-i\tau,\boldsymbol{k_4}),$$

where $ijkl\in\{s,a\}$, and

$$\begin{aligned} \Delta^s(-i\tau,\boldsymbol{k}) &= \Delta^s(-i(\beta-\tau),\boldsymbol{k}) &&= \frac{G_{th}(-i\tau,0,\boldsymbol{k})}{G_{th}(\boldsymbol{k})} = \frac{T\sum_n e^{i\omega_n\tau} G_{th}(\omega_n,\boldsymbol{k})}{G_{th}(\boldsymbol{k})}, \\ \Delta^a(-i\tau,\boldsymbol{k}) &= -\Delta^a(-i(\beta-\tau),\boldsymbol{k}) &&= 2\partial_\tau G_{th}(-i\tau,0,\boldsymbol{k}) = T\sum_n e^{i\omega_n\tau}\, 2i\omega_n G_{th}(\omega_n,\boldsymbol{k})\,. \end{aligned}$$

Using the (anti-)symmetry relations which follow from the periodicity of the thermal propagator, one can rewrite the upper integral according to $\int_0^\beta \to 2\int_0^{\beta/2}$. Furthermore, the anti-symmetry of $\Delta^a(-i\tau,\boldsymbol{k})$ implies that the correlations $\alpha_{4,th}^{sssa}$ and $\alpha_{4,th}^{saaa}$ indeed vanish.

Comparison of solutions with and without thermal initial 4-point correlation function

The comparison is based on two sets of numerical solutions [146] of Kadanoff-Baym equations, one with and one without thermal initial 4-point correlation, on a lattice with $32^3\times 2000^2$ lattice sites and lattice spacings of $a_s m_R = 0.5$ and $a_t m_R \in \{0.01, 0.025\}$ (the latter was used for solutions covering a total time range $t\cdot m_R > 10^3$ in order to reduce computational costs). For both sets, the 2PI counterterms and the thermal propagator, which is required for the computation of the thermal initial correlations, were obtained by independently solving the Schwinger-Dyson and Bethe-Salpeter equations (8.14) on a lattice of the same spatial size and with identical spatial lattice spacing. For the temporal lattice spacing, $a_t m_R = 0.01$ was used throughout in order to minimize numerical errors. For the computation of the 2PI counterterms, a number $N_t = 1024$ of sites along the time direction was used, while $N_t = 1/(Ta_t)$ for the thermal propagator at temperature T.

Energy conservation: One of the most attractive properties of approximations derived from *nPI* effective actions is their compatibility with conserved charges of the underlying theory [24]. In the case of real scalar Φ^4-theory in Minkowski space-time, this means that total energy and momentum are conserved by solutions of Kadanoff-Baym equations. Extending the derivation in Ref. [147] of

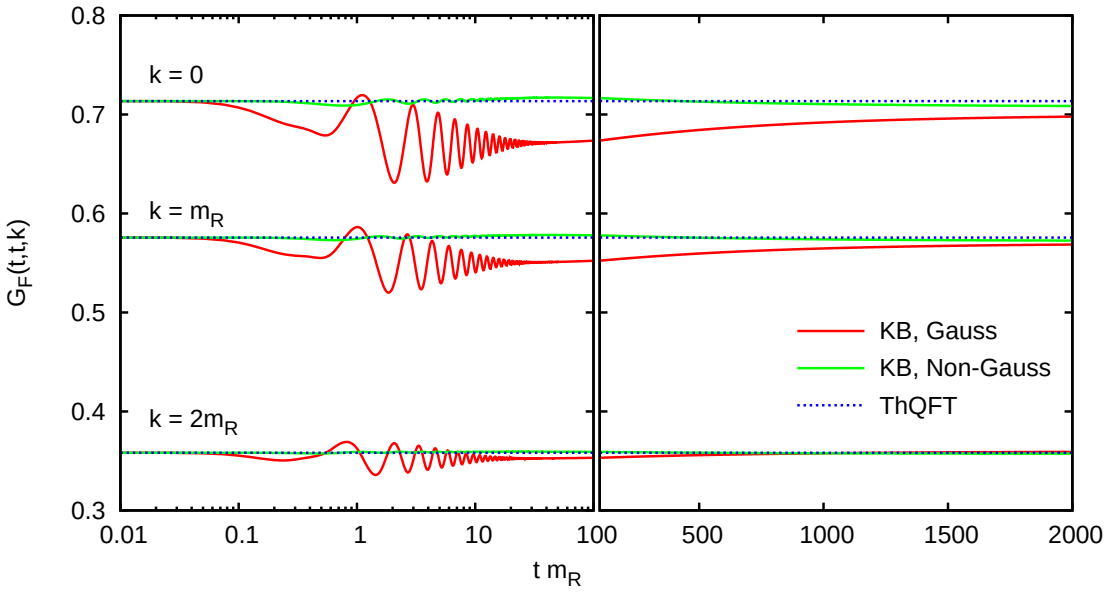

Figure 8.4: *Time evolution of the equal-time propagator $G_F(t,t,\boldsymbol{k})$ obtained from Kadanoff-Baym equations with thermal initial 2-point correlation function (red lines) as well as thermal initial 2- and 4-point correlation functions (green lines), for three momentum modes, respectively. The blue horizontal lines show the renormalized thermal propagator $G_{th}(\boldsymbol{k})$ which serves as initial condition at $t = 0$.*

the energy-momentum tensor from the 2PI effective action defined on the closed real-time contour to non-Gaussian initial states yields for the total renormalized energy density

$$\begin{aligned} E_{total}(t) \;=\; & \int\frac{d^3k}{(2\pi)^3}\left[\frac{1}{2}\left(\partial_{x^0}\partial_{y^0}+\boldsymbol{k}^2+m_B^2+\frac{\lambda_B}{4}\int\frac{d^3q}{(2\pi)^3}G_F(t,t,\boldsymbol{q})\right)G_F(x^0,y^0,\boldsymbol{k})|_{x^0=y^0=t}\right. \\ & -\frac{1}{4}\int_0^t dz^0\,\left(\Pi_F(t,z^0,\boldsymbol{k})G_\rho(z^0,t,\boldsymbol{k})-\Pi_\rho(t,z^0,\boldsymbol{k})G_F(z^0,t,\boldsymbol{k})\right) \\ & \left.-\frac{1}{4}\left(\Pi_{\lambda\alpha,F}(t,\boldsymbol{k})G_F(0,t,\boldsymbol{k})+\frac{1}{4}\Pi_{\lambda\alpha,\rho}(t,\boldsymbol{k})G_\rho(0,t,\boldsymbol{k})\right)\right]+\text{const.} \end{aligned} \tag{8.20}$$

It has been checked that the total energy density is conserved by the numerical solutions used below to an accuracy of $< 10^{-3}$ for Gaussian initial conditions and $< 10^{-4}$ for non-Gaussian initial conditions. Furthermore, similar to the Kadanoff-Baym equations, it is possible to show that the total energy density is formally finite in the limit $t \to 0$ and for thermal 2- and 4-point initial correlation functions (up to a time- and temperature-independent constant), provided the self-energies are chosen according to the full nonperturbative renormalization procedure.

Minimal offset from thermal equilibrium: In thermal equilibrium, the propagator $G_{th}(x^0,y^0,\boldsymbol{k})$ depends only on the difference x^0-y^0 of its two time arguments. Therefore, the thermal equal-time propagator $G_{th}(t,t,\boldsymbol{k}) = G_{th}(\boldsymbol{k})$ is given by a time-independent constant for all momentum modes. The Schwinger-Keldysh propagator $G(x^0,y^0,\boldsymbol{k})$ obtained from solving Kadanoff-Baym equations with nonequilibrium initial conditions approaches thermal equilibrium at late times, such that $G(t,t,\boldsymbol{k}) = G_F(t,t,\boldsymbol{k})$ evolves with time, but converges towards a constant value for $t \to \infty$. However, even in the case where the initial conditions of the Schwinger-Keldysh propagator are chosen

to coincide with the thermal propagator, $G(t,t,\boldsymbol{k})$ *does* depend on time since all higher thermal correlations have been truncated at the initial time due to the restriction to Gaussian initial conditions. Thus, this unavoidable time-dependence of the equal-time propagator is a measure of the impact of the truncation of higher correlations. It reveals the minimal deviation of solutions of Kadanoff-Baym equations from thermal equilibrium. For the extended Kadanoff-Baym equations, which take into account an initial 4-point correlation function, both the propagator and the non-Gaussian 4-point correlation function can be chosen to coincide with their respective values in thermal equilibrium at the initial time. Therefore, one expects that the time-dependence of the equal-time propagator, and therefore the minimal deviation from thermal equilibrium, is smaller compared to the case without initial 4-point correlation function.

In figure 8.4, the time-evolution of the equal-time propagator is shown for two solutions which represent the minimal deviation from thermal equilibrium for Gaussian Kadanoff-Baym equations as well as non-Gaussian Kadanoff-Baym equations including a thermal initial 4-point correlation function. For both solutions, the initial values of the propagator are chosen to coincide with the thermal propagator at temperature $T = 2m_R$. For the Gaussian case, the equal-time propagator immediately starts to oscillate for times $t \cdot m_R \gtrsim 1$ and then drifts towards a stationary value, which is slightly displaced from the initial value. For the non-Gaussian case, the time-dependence is indeed considerably reduced, and the Schwinger-Keldysh propagator always remains close to the renormalized thermal propagator. The residual time-dependence can be attributed to the truncation of the higher thermal n-point correlation functions for $n > 4$, as well as to numerical errors (the latter can be reduced by choosing a smaller time-step a_t). Qualitatively, a similar behaviour is found when varying the initial temperature and the lattice cutoff $\Lambda \propto a_s^{-1}$.

Offset between initial and final Temperature: Due to the truncation of higher correlations, the Kadanoff-Baym equations for Gaussian initial states as well as those incorporating an initial 4-point correlation function cannot describe thermal equilibrium exactly. However, the minimal offset from thermal equilibrium is considerably reduced when taking a thermal initial 4-point correlation into account.

Apart from that, a qualitative difference between both types of equations exists, which has the following reason. As has been shown in section 7.2.3, the 4-point correlation of the initial state contributes to the Kadanoff-Baym equations in the limit $x^0, y^0 \to 0$, whereas the contributions from even higher thermal correlations are suppressed, since these enter Kadanoff-Baym equations exclusively via memory integrals within Φ^4-theory. The same is true for the total energy density (8.20). Therefore, the total energy density $E_{init} \equiv E_{total}(t=0)$ computed at the initial time using thermal initial 2- and 4-point correlation functions corresponding to a temperature T_{init} coincides with the total energy $E_{eq}(T)$ of an ensemble in complete thermal equilibrium at the same temperature, i.e. $E_{init} = E_{eq}(T_{init})$. For $t \to \infty$, solutions of Kadanoff-Baym equations asymptotically approach thermal equilibrium. Due to universality [32], the final temperature T_{final} is uniquely characterized by the value of the total energy density, i.e. $E_{final} = E_{eq}(T_{final})$. Furthermore, the initial and final total energy agree, since the total energy is conserved. Therefore, also the initial and final temperatures have to agree, i.e. $T_{init} = T_{final}$.

In contrast to this, if only a Gaussian thermal 2-point correlation at temperature T_{init} is used, the resulting total energy does *not* coincide with the corresponding value in thermal equilibrium, i.e. $E_{init} \neq E_{eq}(T_{init})$, due to the missing contribution from the thermal 4-point correlation function. Nevertheless, for $t \to \infty$ complete thermal equilibrium is approached asymptotically, i.e. $E_{final} = E_{eq}(T_{final})$ for some final value of the temperature T_{final}. Since the total energy is also conserved, the initial and final temperatures can *not* agree, i.e. one expects that $T_{init} \neq T_{final}$ for a Gaussian initial state.

For solutions of Kadanoff-Baym equations which minimally deviate from thermal equilibrium, an

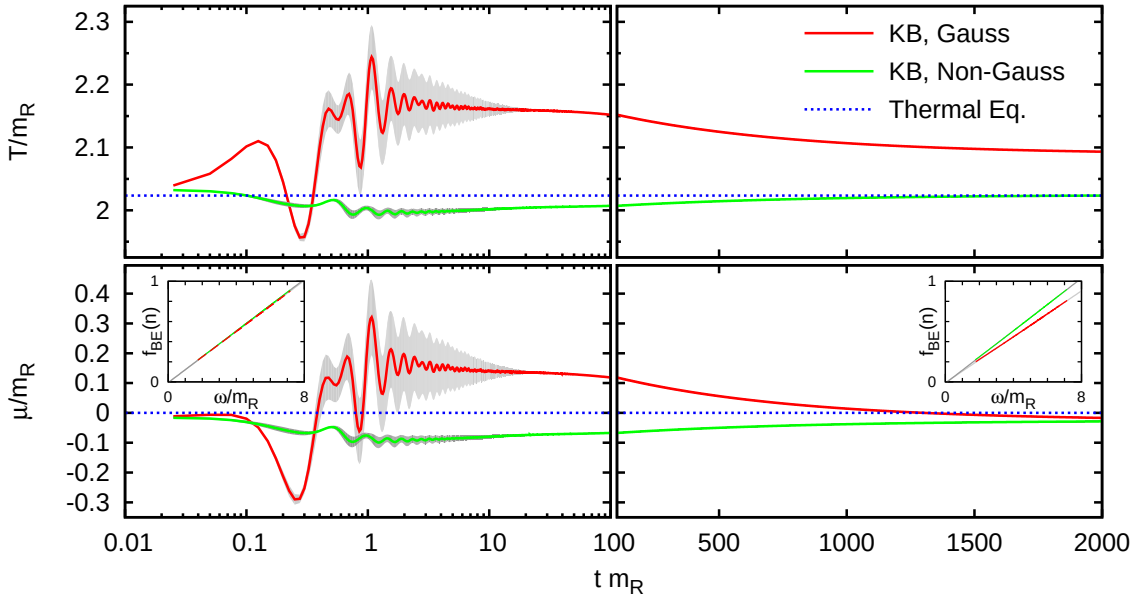

Figure 8.5: *Time evolution of the temperature and chemical potential obtained from a fit of the effective particle number density $n(t,\boldsymbol{k})$ to a Bose-Einstein distribution, for Kadanoff-Baym equations with thermal initial 2-point correlation function (red lines) as well as thermal initial 2- and 4-point correlation functions (green lines). The shaded areas illustrate qualitatively the deviation of the momentum dependence of $n(t,\boldsymbol{k})$ from the Bose-Einstein distribution function. They are obtained from the asymptotic standard error of the fit (via least-square method) magnified by a factor 10, for better visibility. Nevertheless, the errors become invisibly small at times $t \cdot m_R \gg 10$. The insets show a function $f_{BE}(n)$ of the effective particle number density $n(t,\boldsymbol{k})$ plotted over the effective energy density $\omega(t,\boldsymbol{k})$. The function is chosen such that a Bose-Einstein distribution corresponds to a straight line, the slope and y-axis intercept of which determine the temperature and the chemical potential (here, $f_{BE}(n) = \ln(1/n+1) - \omega/T_{ref}$ was used with $T_{ref} = 2.75 m_R$). At the initial time (left inset) the particle number densities of both solutions agree with a Bose-Einstein distribution with the same temperature and therefore lie on top of each other. At the largest time (right inset), the slope of the red line is smaller, which corresponds to an increase in temperature. Inside the insets, the underlying grey lines show the best-fit Bose-Einstein distribution function.*

effective time-dependent temperature $T(t)$ and chemical potential $\mu(t)$ may be obtained by fitting the effective particle number density $n(t,\boldsymbol{k})$ (see eq. (6.17)) to a Bose-Einstein distribution function for each time t,

$$n_{fit}(t,\boldsymbol{k}) = \left[\exp\left(\frac{\omega(t,\boldsymbol{k})+\mu(t)}{T(t)}\right) - 1\right]^{-1} .$$

The time evolution of the effective temperature and chemical potential obtained from numerical solutions of Gaussian Kadanoff-Baym equations with thermal initial 2-point correlation function as well as non-Gaussian Kadanoff-Baym equations with thermal initial 2- and 4-point correlation functions are shown in figure 8.5. Due to the thermal initial 2-point correlation function, the effective particle number densities agree with a Bose-Einstein distribution at the initial time, with identical initial temperature for both types of equations. For $t \to \infty$, the effective particle number densities also agree with a Bose-Einstein distribution very well, as expected. However, for the solution without initial 4-point

correlation, the final temperature has increased compared to the initial value. In contrast to this, the initial and final values of the temperature agree up to 0.5% for the solution with thermal initial 4-point correlation function.
The offset between the initial and final temperature is a quantitative measure of the unavoidable offset from thermal equilibrium which occurs for a Gaussian initial state. Equivalently, it may be parameterized by the energy difference

$$\begin{aligned}\Delta E &= E_{eq}(T_{final}) - E_{eq}(T_{init}) = E_{final} - E_{eq}(T_{init}) = E_{init} - E_{eq}(T_{init}) \\ &= \frac{1}{4}\int \frac{d^3k}{(2\pi)^3}\, \Pi_{\lambda\alpha,F}(t,\boldsymbol{k}) G_F(0,t,\boldsymbol{k})\big|_{t=0} = -\frac{\lambda_R}{24Z^2}\, V_4^{nG}(x,x,x,x)\big|_{x^0=0} \\ &= \frac{\lambda_R^2}{24}\int_{kpq} G_{th,R}(p) G_{th,R}(q) G_{th,R}(k-p-q) G_{th,R}(-k)\,,\end{aligned}$$

which is equal to the contribution of the initial thermal 4-point correlation function to the total energy. This contribution contains a (quadratic and quartic) UV divergence, and therefore the Kadanoff-Baym equations for a Gaussian initial state feature a divergent offset from thermal equilibrium. Since the 2PI counterterms renormalize the divergences in thermal equilibrium, they cannot do so for a Gaussian initial state as well. On the other hand, if a thermal 4-point correlation of the initial state is taken into account, then $\Delta E = 0$, and no (divergent) offset occurs.
The temperature-offset implies that also all quantities derived from the Schwinger-Keldysh propagator, like the total number density $N(t) \equiv \int d^3k/(2\pi)^3\, n(t,\boldsymbol{k})$ or the effective thermal mass $m_{th}(t) \equiv \omega(t,\boldsymbol{k}=0)$, feature an offset between their initial values and their late-time asymptotic values for a Gaussian initial state (see figure 8.6).

Thermalization: For a real scalar quantum field, the chemical potential vanishes in thermal equilibrium, due to the absence of global conserved charges apart from energy and momentum. In figure 8.5, it can be seen that the effective chemical potential $\mu(t)$ is indeed very close to zero at the initial time, which shows that the initial thermal propagator indeed yields a thermal effective number density distribution. Furthermore, $\mu(t)$ also approaches zero in the late-time limit, which means that thermal equilibrium has effectively been reached for times $t \cdot m_R > 2000$ for both types of equation. For the solution with thermal initial 4-point correlation function, the effective particle number density remains very close to a Bose-Einstein distribution also at intermediate times, and the time-variation of the corresponding effective temperature and chemical potential is significantly smaller compared to the solution without initial 4-point correlation function. Furthermore, for the latter also the deviation from the Bose-Einstein distribution is larger at intermediate times, which is illustrated by the shaded areas in figure 8.5. It is interesting to note that, for a Gaussian initial state, the solution which minimally deviates from thermal equilibrium resembles a typical non-equilibrium solution. The quantum thermalization process is characterized by a phase of kinetic equilibration, after which the effective particle number is already close to a Bose-Einstein distribution, however with non-zero chemical potential (prethermalization [31]). In figure 8.5, this corresponds to the phase when the shaded area becomes invisibly small. Subsequently, the chemical potential approaches its equilibrium value (zero) on a much longer time-scale, as can be seen on the right part of figure 8.5. Altogether, it is concluded that a controlled transition from equilibrium to nonequilibrium cannot be achieved for a Gaussian initial state.

Matching of Kadanoff-Baym equations with thermal quantum field theory: In order to quantitatively compare solutions of Kadanoff-Baym equations, which are formulated on the closed real-time path, with numerical solutions of the Schwinger-Dyson equation at finite temperature, which are

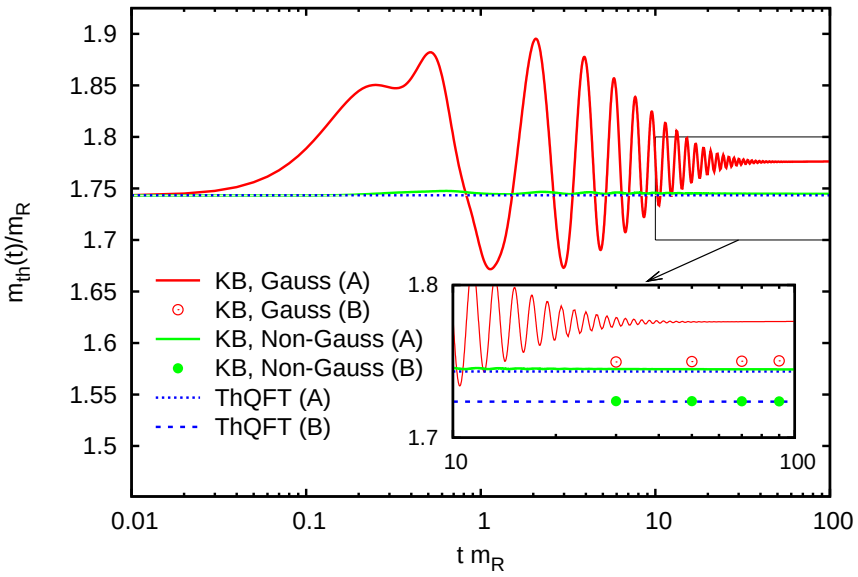

Figure 8.6: *Time evolution of the effective thermal mass* $m_{th}(t) = \omega(t, \boldsymbol{k} = 0)$ *obtained from Kadanoff-Baym equations with (green) and without (red) a thermal initial* 4*-point correlation function. The horizontal line (blue) shows the value obtained from thermal quantum field theory within 2PI 3-loop approximation according to definition (A) in table 8.1. In the inset, also the thermal mass according to definition (B) is shown. The red and green circles give the values of the thermal mass obtained from evaluating definition (B) for Gaussian and non-Gaussian Kadanoff-Baym equations, respectively.*

	Kadanoff-Baym	Thermal QFT
m_{th}^A	$\omega(t, \boldsymbol{k} = 0) = \sqrt{\frac{\partial_{x^0}\partial_{y^0} G_{F,R}(x^0, y^0, \boldsymbol{k})}{G_{F,R}(x^0, y^0, \boldsymbol{k})}}\Big\|_{x^0 = y^0 = t}$	$\omega_{th}(\boldsymbol{k} = 0) = \sqrt{\frac{\partial_\tau^2 G_{th,R}(-i\tau, 0, \boldsymbol{k})}{G_{th,R}(-i\tau, 0, \boldsymbol{k})}}\Big\|_{\tau = 0}$
m_{th}^B	$\left(\lim_{s\to\infty} \int_0^s ds' G_{\rho,R}(t + \frac{s'}{2}, t - \frac{s'}{2}, \boldsymbol{k})\right)^{-1/2}$	$\left(G_{th,R}(\omega_n = \boldsymbol{k} = 0)\right)^{-1/2}$

Table 8.1: *The two rows show two definitions of the effective thermal mass as observed at different energy scales. Both definitions can be evaluated on the real time path (left column) or the imaginary time path (right column), and coincide in thermal equilibrium. The expressions in the left column can also be evaluated in a nonequilibrium situation.*

solved on the imaginary time path, it is necessary to identify quantities which can be computed in both cases. One such quantity is the two-point function evaluated for coincident time arguments, as has been discussed above (see figure 8.4). The effective thermal mass $m_{th}(t) = \omega(t, \boldsymbol{k} = 0)$ obtained from the zero-mode of the effective energy density for Kadanoff-Baym equations, corresponds within thermal quantum field theory to the zero-mode of the thermal effective energy density $\omega_{th}(\boldsymbol{k} = 0)$ defined in eq. (8.19). However, the thermal mass $m_{th} = G_{th,R}(\omega_n = \boldsymbol{k} = 0)^{-1/2}$ defined in eq. (8.17) constitutes an inequivalent definition for non-zero coupling. The latter corresponds to the infrared-limit of the two-point correlation function while the former is related to its oscillation frequency, and therefore their difference is a manifestation of the scale-dependence of physical observables. The thermal mass according to both definitions can be computed for solutions of Kadanoff-Baym equations as well as

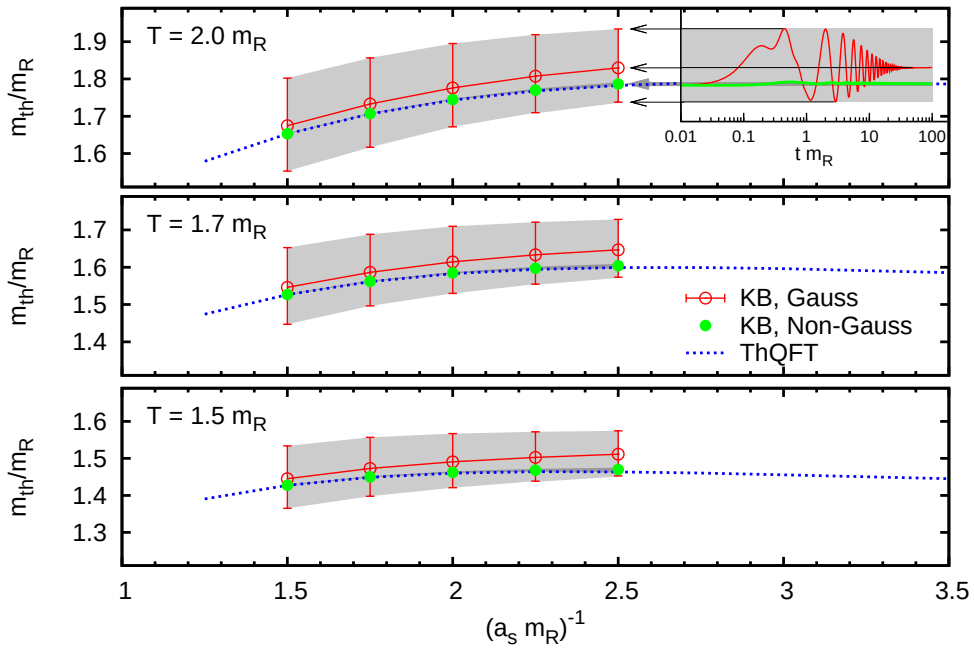

Figure 8.7: *Cutoff dependence of the effective thermal mass* $m_{th}(t) = \omega(t, \boldsymbol{k} = 0)$ *obtained from Kadanoff-Baym equations with (green) and without (red) a thermal initial* 4*-point correlation function for three different initial temperatures. The areas shaded light and dark grey (as well as the errorbars in the Gaussian case) show the maximal and the minimal values of the thermal mass in the interval* $0 \leq t \cdot m_R \leq 100$*, and the circles show the value of the thermal mass which is approached at the largest time. For one exemplary case, the determination of these values is shown in the inset in the upper right corner. In the non-Gaussian case, the time-variation of the thermal mass is very small, such that it remains close to the thermal mass computed within thermal quantum field theory (blue) at all times.*

for the full thermal propagator parameterized by imaginary times (see table 8.1).
In figure 8.6, the time-evolution of the effective mass according to definition (A) for Kadanoff-Baym equations is shown. For the solution with thermal initial 2- and 4-point correlation function, the thermal mass is nearly constant and therefore agrees with the initial equilibrium value very well. The second definition (B) of the thermal mass provides an independent consistency check. Its computation for Kadanoff-Baym equations amounts to the limiting value of the integral of the spectral function over the relative time, which is obtained by extrapolating the value of the integral with definite upper boundary for the available times. Since the spectral function is damped exponentially with respect to the relative time, good convergence is achieved provided the maximal relative time is large compared to the inverse damping rate. As shown in the inset of figure 8.6, the thermal masses computed according to definition (B) also agree very well with the equilibrium value for the non-Gaussian case. Below, definition (A) is used throughout, unless otherwise stated.

Cutoff dependence: Figure 8.7 displays the thermal masses obtained from solutions of Kadanoff-Baym equations solved on five different lattice configurations corresponding to five values of the UV cutoff (with constant IR cutoff), as well as three different values of the initial temperature, respectively. Additionally, the renormalized thermal mass computed within thermal quantum field theory

employing the nonperturbative renormalization of the 2PI effective action is shown, which indeed becomes independent of the cutoff when $a_s^{-1} \gg T$. For lower values of the cutoff, a residual cutoff dependence occurs, which can be attributed to the Boltzmann-tail of the thermal particle number distribution. Since the Boltzmann-tail is exponentially suppressed for smaller temperatures, also the residual cutoff dependence decreases for smaller temperatures, as can bee seen in figure 8.7.
For the solutions of the Gaussian Kadanoff-Baym equations with thermal initial 2-point correlation function, the errorbars in figure 8.7 represent the maximal, the minimal, and the final value[4] of the effective thermal mass $m_{th}(t)$ in the time interval $0 \leq t \cdot m_R \leq 100$, while the initial value is given by the renormalized thermal mass computed within thermal quantum field theory at the initial temperature. For the solutions of the non-Gaussian Kadanoff-Baym equations with thermal initial 2- and 4-point correlation functions, the effective thermal mass always remains very close to the renormalized thermal mass, for all values of the cutoff and of the initial temperature.
For the Gaussian case, an offset between the initial and the final value of the thermal mass occurs. This offset is equivalent to the temperature-offset discussed above. It is a measure for the influence of the higher correlations which have been neglected in the Gaussian case. Since the non-Gaussian 4-point correlation function contains divergences, one expects that the offset increases with the cutoff. In figure 8.7, the offset corresponds to the difference between the dashed and the dotted lines. It indeed increases with the cutoff for the considered parameters.

8.3.4 Approximate Perturbative versus Nonperturbative Counterterms

In this section, the impact of the renormalization prescription on nonequilibrium solutions of Kadanoff-Baym equations is investigated. Therefore, two distinct prescriptions are used in order to determine the mass and coupling counterterms appearing in the Kadanoff-Baym equations. First, the mass is renormalized using the approximate perturbative prescription at one-loop order, while leaving the coupling unchanged [17]. Second, the full nonperturbative 2PI renormalization procedure [28,29] is employed to determine the mass and coupling counterterms in vacuum. Then, solutions of the Kadanoff-Baym equations for both renormalization procedures are compared. For this comparison, a Gaussian initial state is used in both cases, in order to guarantee an identical initial state.
It is emphasized that, even for a Gaussian initial state, the approximately renormalized and the nonperturbatively renormalized Kadanoff-Baym equations are genuinely inequivalent for two reasons. First, for the approximate perturbative renormalization prescription the coupling constants which appear in front of the tadpole and setting-sun contributions in the self-energy are identical, whereas the bare coupling appears in front of the tadpole and the renormalized coupling appears in front of the setting-sun diagram of the nonperturbatively renormalized Kadanoff-Baym equations. Second, the ratio of the bare and the renormalized masses are different, and in particular also the ratio of the bare and the renormalized coupling are specific for the renormalization prescription.
The Kadanoff-Baym equations were solved [146] for both renormalization procedures and two values of the (renormalized) coupling, respectively, on a lattice with $32^3 \times 1000^2$ lattice sites and lattice spacings of $a_s m_R = 0.5$ and $a_t m_R = 0.05$. For the approximate perturbative renormalization prescription, the corresponding value of the bare mass is given in the left column of table 8.2. The bare mass and coupling obtained by the full nonperturbative renormalization procedure are given in the right column of table 8.2. The initial conditions for the propagator are determined in accordance with Ref. [25, 142], and correspond to an initial effective particle number distribution which is peaked around the momentum $|\boldsymbol{k}| = 3m_R$. In Figure 8.8 the time evolution of the statistical equal-time propagator for the four parameter sets introduced above and identical initial conditions is shown. For

[4] It has been checked that the effective thermal mass has indeed reached its final value already for times $t \cdot m_R \lesssim 100$, in contrast to the effective temperature and chemical potential.

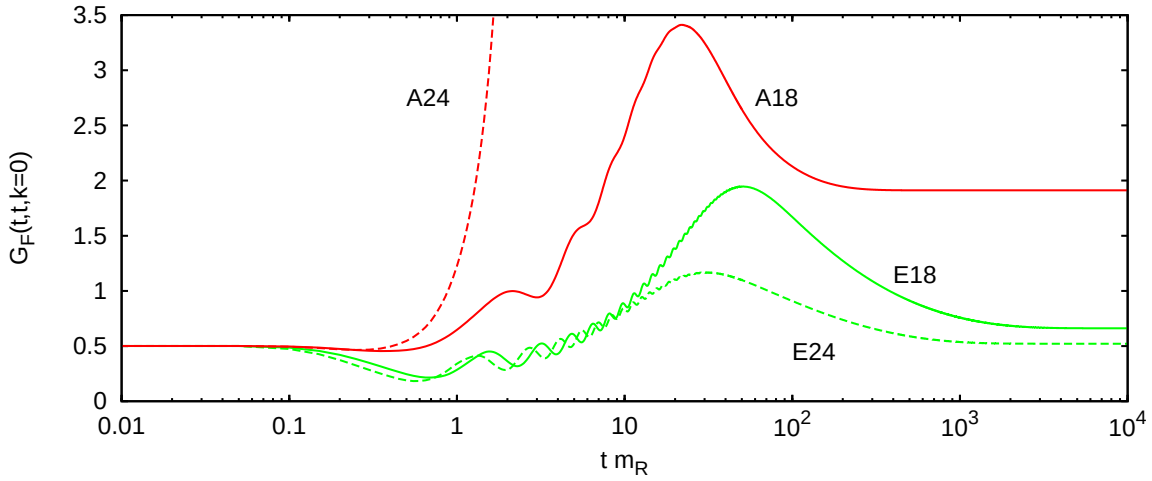

Figure 8.8: *Statistical equal-time propagator over time for the four different parameter sets shown in table 8.2.*

parameter set A24 the Kadanoff-Baym numerics is very unstable and breaks down already for very early times. Decreasing the coupling, the numerics can be stabilized, as can be seen for parameter set A18. The curve for parameter set E24 shows two features: First, the numerics is stable although both, the bare and the renormalized coupling, are greater or equal to the value used for parameter set A24. Second, although both couplings are strictly greater than the value chosen for parameter set A18 the thermalization time is dramatically larger. Thus, the exact nonperturbative renormalization procedure indeed has a stabilizing virtue for the computational algorithm and also has a significant quantitative impact on the numerical solutions of Kadanoff-Baym equations. Furthermore, it is important to note that qualitative features of Kadanoff-Baym equations like late-time universality and prethermalization are independent of the renormalization procedure.

8.3.5 Renormalized Nonequilibrium Dynamics

Above, it has been shown that extended Kadanoff-Baym equations, which take into account an initial state featuring a 4-point correlation function, possess solutions which come very close to the renormalized thermal state as obtained from the three-loop truncation of the 2PI effective action at finite temperature. This provides the possibility for a controlled transition to a nonequilibrium situation by distorting the thermal initial 2- and 4-point correlation functions. However, these distortions cannot be chosen arbitrarily, if one demands that the nonequilibrium state should also be renormalized by the identical 2PI counterterms. One of these restrictions is that the nonequilibrium initial correla-

A18: $\lambda = 18\,, m_B^2 = -6.87\, m_R^2\,.$	**E18:** $\lambda_R = 18\,, \lambda_B = 37.18\,, m_B^2 = -14.39\, m_R^2\,.$
A24: $\lambda = 24\,, m_B^2 = -9.49\, m_R^2\,.$	**E24:** $\lambda_R = 24\,, \lambda_B = 63.43\,, m_B^2 = -25.14\, m_R^2\,.$

Table 8.2: *Counterterms for the two sets of couplings and the approximate perturbative renormalization prescription (left column) as well as the exact nonperturbative renormalization procedure (right column).*

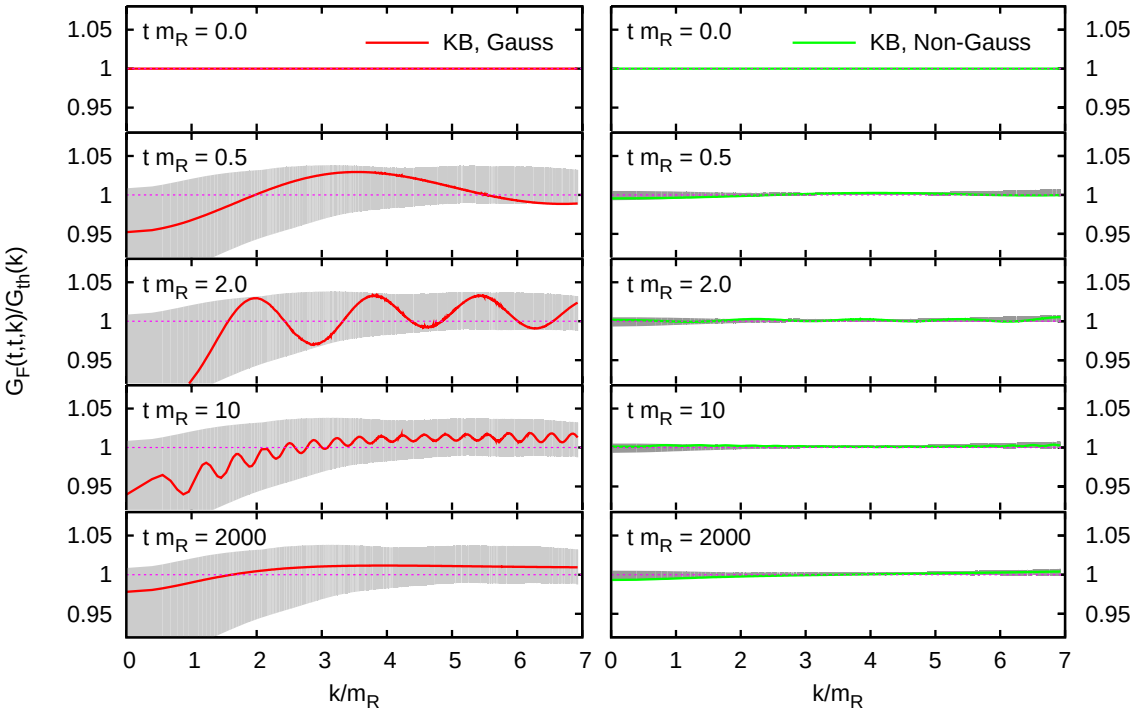

Figure 8.9: *Momentum dependence of the equal-time propagator for five different times* $t \cdot m_R = 0.0, 0.5, 2.0, 10, 2000$ *obtained from Kadanoff-Baym equations with (green lines, right side) and without (red lines, left side) thermal initial* 4*-point correlation function, respectively. The shaded areas show the maximum and minimum values of* $G_F(t,t,\boldsymbol{k})/G_{th}(\boldsymbol{k})$ *for all times.*

tion functions coincide with the thermal values asymptotically for large spatial momenta, since this asymptotic behaviour determines the divergences which are to be canceled by the counterterms. Furthermore, one may expect that the distortions of the 2- and the 4-point correlations cannot be chosen completely independently, but have to be related in such a way that the Kadanoff-Baym equations remain finite.

Additionally, since the counterterms are given by fixed, time-independent numbers, a necessary condition for the finiteness of Kadanoff-Baym equations at all times is that the divergences are also time-independent. Since the divergences are related to the asymptotic behaviour of the full propagator at large momenta, this can only be the case if this asymptotic behaviour does not change with time.

In figures 8.9 and 8.10 the ratio of the equal-time propagator over the thermal propagator is plotted over the absolute spatial momentum for five different times. The largest spatial momentum is determined by the size of the spatial lattice spacing, providing the UV cutoff.

For the solutions shown in figure 8.9, a thermal initial 2-point correlation function has been used. Therefore, at the initial time, the ratio of the equal-time propagator and the thermal propagator is unity. However, for the solution without initial 4-point correlation function, all momentum modes of the propagator are excited as soon as $t \cdot m_R \gtrsim 1$ (see left part of figure 8.9). This indicates that renormalization with time-independent counterterms is impossible in this case. In contrast to this, the solution with thermal initial 4-point correlation function always remains close to the renormalized thermal propagator for all momentum modes (see right part of figure 8.9). It has been checked that

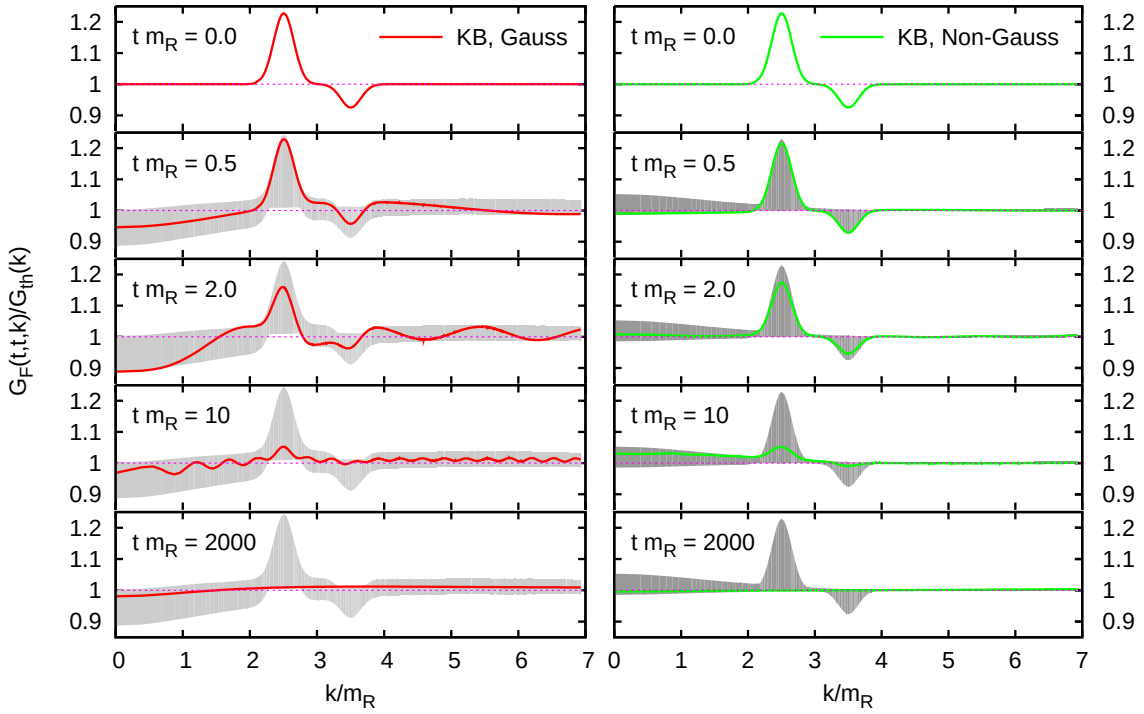

Figure 8.10: *Momentum dependence of the ratio of the equal-time propagator and the thermal propagator for five different times* $t \cdot m_R = 0.0, 0.5, 2.0, 10, 2000$ *obtained from Kadanoff-Baym equations with (green lines, right side) and without (red lines, left side) thermal initial* 4*-point correlation function as well as identical nonequilibrium initial conditions for the* 2*-point function, respectively. The shaded areas show the maximum and minimum values of* $G_F(t,t,\boldsymbol{k})/G_{th}(\boldsymbol{k})$ *for all times.*

this behaviour stays the same when the cutoff is varied.

For the solutions shown in figure 8.10, the initial 2-point correlation function has been distorted such that it corresponds to a nonequilibrium initial condition. At large values of the momentum, it coincides with the thermal propagator, as required for renormalizability. Furthermore, the nonequilibrium initial condition has been chosen such that the energy density is identical to the case with thermal initial correlation. For the solution without initial 4-point correlation function, it is found again that all momentum modes of the propagator are excited as soon as $t \cdot m_R \gtrsim 1$, up to the highest momentum (see left part of figure 8.10). In contrast to this, when employing a thermal initial 4-point correlation function, the high momentum modes of the propagator are not excited considerably. Instead, the nonequilibrium correlation relaxes by exciting the low momentum modes of the two-point function (see right part of figure 8.10). This is precisely the property required for renormalization with time-independent counterterms. It is an indication that the renormalization of Kadanoff-Baym equations is indeed possible within the framework presented here.

When going to initial conditions which deviate more strongly from equilibrium, it may be expected that also the initial 4-point correlation function has to be modified accordingly in order to preserve the renormalization. However, this is beyond of the scope of the present work.

Altogether, it is concluded that the Kadanoff-Baym equations (8.9) are a good candidate to describe renormalized nonequilibrium dynamics. Furthermore, they provide the possibility for a controlled transition from renormalized thermal equilibrium to nonequilibrium quantum dynamics.

8.4 Summary

In this and the previous chapter, a framework appropriate for the nonperturbative renormalization of Kadanoff-Baym equations has been developed, and an ansatz for renormalized Kadanoff-Baym equations has been proposed. For the three-loop truncation of the 2PI effective action, it has been shown analytically that these Kadanoff-Baym equations are indeed finite for one special class of renormalized initial conditions and close to the initial time. Additionally, it has been demonstrated that their numerical solutions possess properties which are expected from renormalized Kadanoff-Baym equations.

The renormalization of Kadanoff-Baym equations is based on the nonperturbative renormalization procedure of the 2PI effective action, which has been formulated recently at finite temperature [28, 29, 37, 173–175].

In chapter 7 the nonperturbative renormalization procedure of the 2PI effective action at finite temperature has been transferred to the closed real-time path. In order to do so it is necessary to explicitly specify all thermal correlation functions characterizing the thermal state, which plays the role of the "initial" state on the closed real-time path. It has been shown that thermal n-point correlation functions have to be taken into account for all $n \geq 0$ within the nonperturbative 2PI formalism. Furthermore, an iterative computation prescription for the nonperturbative thermal initial correlations which are appropriate for a given truncation of the 2PI effective action has been developed, and applied to the three-loop truncation. Finally, renormalized Kadanoff-Baym equations which describe thermal equilibrium on the closed real-time path have been derived.

In this chapter, an ansatz for renormalized Kadanoff-Baym equations describing nonequilibrium ensembles has been proposed. These contain mass and coupling counterterms determined according to the nonperturbative renormalization prescription of the 2PI effective action [28, 29], and take into account a non-Gaussian 4-point correlation function of the initial state [32, 49, 57]. They can be conveniently derived from the 4PI effective action. For the three-loop truncation, it has been verified analytically that these Kadanoff-Baym equations are rendered finite close to the initial time and for initial conditions which correspond to the minimal deviation from thermal equilibrium. In contrast to this, Kadanoff-Baym equations for a Gaussian initial state feature a divergent offset from renormalized thermal equilibrium, which means that they cannot be renormalized with time-independent counterterms. This qualitative difference could also be demonstrated by means of numerical solutions. It has been found that the Kadanoff-Baym equations containing nonperturbative 2PI counterterms and a non-Gaussian initial 4-point correlation possess particular solutions which remain close to the renormalized thermal propagator for all times. For Gaussian Kadanoff-Baym equations, it was found that the offset from thermal equilibrium, which was mentioned above, indeed increases when the cutoff is increased.
So far approximate perturbative counterterms have been used when solving Kadanoff-Baym equations [17]. It has been demonstrated that numerical instabilities which occur when the coupling is increased can be alleviated if nonperturbative 2PI counterterms are used instead.

A necessary requirement for the renormalizability of Kadanoff-Baym equations with time-independent counterterms is that the divergences are also time-independent. Therefore, it is required that the asymptotic behaviour of the Schwinger-Keldysh propagator at large momenta is universal, i.e. time-independent. It was demonstrated that this is indeed the case for nonequilibrium solutions of Kadanoff-Baym equations containing nonperturbative 2PI counterterms and a non-Gaussian initial 4-point correlation function. In contrast to this, all momentum modes are excited when Gaussian Kadanoff-Baym equations are employed.

Chapter 9

Conclusions

In this work, the quantum dynamics of time-evolving scalar fields has been studied in a cosmological context. In particular, the robustness of quintessence tracker potentials with respect to quantum corrections has been investigated, and nonequilibrium renormalization techniques for Kadanoff-Baym equations have been developed.

The classical dynamics of the quintessence field is described by its self-interaction potential. Quintessence potentials featuring tracking solutions avoid some of the problems connected to the cosmological constant. Therefore, it is important to investigate quantum corrections for these exceptional potentials.

Quantum field theory together with classical gravity determines the effective quintessence potential only up to a constant. Therefore, it was assumed here that the freedom to shift the potential by an arbitrary constant is used in such a way that the quintessence energy density matches the observed value for dark energy in the present cosmological epoch. However, even with this assumption there remain quantum corrections to the dynamics of the quintessence field, which can be addressed by quantum field theory. These quantum corrections arise from the self-interactions of the scalar field, couplings to Standard Model particles and couplings to gravity.

Quantum corrections induced from self-interactions have been investigated for two classes of prototype tracker potentials, namely exponential and inverse power law potentials. In particular, the robustness of the shape of the potential was analyzed within the framework of effective field theory. Therefore, a suitable Hartree-Fock approximation scheme has been developed, which resums all relevant contributions. Its validity has been verified by applying it to Liouville quantum field theory. Furthermore, it has been shown that corrections to the Hartree-Fock approximation are suppressed by powers of the ratio of the Hubble parameter and the Planck scale for typical tracker potentials.

Remarkably, for a classical exponential potential, the Hartree-Fock approximation yields an effective potential which also features an exponential dependence on the field value. This extends the one-loop result of Ref. [83]. For the inverse power law potential, the one-loop approximation breaks down near the singularity of the classical potential [83]. In contrast to this, it could be shown that the Hartree-Fock effective potential does not have a singularity, but instead approaches a finite maximum value, and thus is applicable in the whole range of admissible field values. Furthermore, it was shown that the effective potential leads to a modification of the tracking solution compared to the classical case. If the ultraviolet embedding scale of the effective theory is close to the Planck scale, the prediction for the dark energy equation of state differs significantly from the classical value.

Quantum corrections induced from couplings of the quintessence field to Standard Model particles have been investigated employing the low-energy effective action obtained from integrating out the

Standard Model degrees of freedom. If the couplings are too large, these quantum corrections would destroy the desired properties of the tracker potential. An upper bound for the couplings was obtained under the assumption of minimal quantum vacuum backreaction. These indirect bounds were compared to direct observational bounds. The latter result for example from tests of a time-variation of the electron-proton mass ratio and of the equivalence principle.

Quantum corrections induced by the gravitational coupling of the quintessence field have been investigated using the one-loop renormalization group improved effective action in curved space-time. They have been found to be negligibly small for tracker potentials.

Quintessence fields can also be important in the early universe, in contrast to the cosmological constant. In this work, this has been demonstrated by presenting an explicit model, where baryogenesis and the present-day acceleration are both driven by a complex quintessence field, which carries lepton number. The introduction of new interactions, which violate baryon or lepton number, is not necessary. Instead, a lepton asymmetry is stored in the quintessence field. It has been shown that the observed baryon asymmetry can be explained quantitatively by the semi-classical dynamics resulting from the considered model.

The nonequilibrium processes that occur in the early universe until now, e.g. baryogenesis, (p)reheating, or a rolling quintessence field, are typically described by semi-classical approximations like Boltzmann equations, or by effective equations of motion for a coherent scalar field expectation value. In order to assess the validity of these approximations a quantitative comparison with the evolution equations for the full quantum dynamics is necessary. The latter is provided by Kadanoff-Baym equations. For this purpose, a proper renormalization of Kadanoff-Baym equations is an indispensable precondition.

In this thesis, a framework for the nonperturbative renormalization of Kadanoff-Baym equations has been developed. In particular, the nonperturbative renormalization procedure of the 2PI effective action at finite temperature has been transferred to the closed real-time path, which is the starting point for nonequilibrium quantum field theory.

Furthermore, an ansatz for renormalized Kadanoff-Baym equations has been proposed within $\lambda\Phi^4$-theory. These equations contain mass and coupling counterterms determined according to the nonperturbative renormalization procedure of the 2PI effective action in vacuum. Additionally, it has been shown that renormalization requires the extension of Kadanoff-Baym equations to non-Gaussian initial states. Such an extension has been derived from the 4PI effective action. It features a non-Gaussian initial 4-point correlation function. The ansatz for renormalized Kadanoff-Baym equations could be verified analytically for the three-loop (setting-sun) approximation for a special class of renormalized initial conditions and close to the initial time.

Finally, it has been demonstrated that the Kadanoff-Baym equations containing nonperturbative 2PI counterterms and a non-Gaussian initial 4-point correlation function possess solutions with properties which are expected from renormalized Kadanoff-Baym equations.

Thus, it could be shown that the methods used for describing the nonequilibrium quantum dynamics of scalar fields are indeed considerably improved by the renormalization techniques developed in this work. Applying these techniques is essential for a *quantitative* description of quantum fields far from thermal equilibrium.

Therefore, the renormalization of Kadanoff-Baym equations is an important step towards realistic applications within astro-particle and high-energy physics. In particular, renormalized Kadanoff-Baym equations provide the basis for describing time-evolving scalar fields beyond the limitations of the derivative expansion of the effective action. The derivative expansion is used for example to

describe cosmic inflation, and has also been used for the quintessence field above. Within inflationary models, predictions like the spectral index are directly tested by CMB measurements. Since these predictions rely on the underlying derivative expansion, it is important to assess its validity.
Furthermore, renormalized Kadanoff-Baym equations can also be applied to study the quantum dynamics of other nonequilibrium processes, like for example for preheating, baryogenesis, or heavy ion collisions. In view of these applications, it is important to note that the renormalization of Kadanoff-Baym equations presented above can be transferred to quantum field theories including fermions and gauge fields. In particular, renormalized Kadanoff-Baym equations provide a quantum field theoretical generalization of semi-classical Boltzmann equations. The latter are used for example to describe the formation of a lepton asymmetry within the leptogenesis framework. However, for specific realizations of leptogenesis, quantum corrections may play an important role. In this context, the renormalization techniques developed above are required in order to describe leptogenesis within nonequilibrium quantum field theory.

Appendix A

Conventions

The Minkowski metric sign convention $(+1,-1,-1,-1)$ is used. In General Relativity the sign convention according to the classification of Misner-Thorne-Wheeler [144] is $(-,+,+)$. In this convention the curvature tensor is

$$R^{\alpha}{}_{\mu\nu\lambda} = +\left(\partial_\nu \Gamma^{\alpha}_{\mu\lambda} - \partial_\lambda \Gamma^{\alpha}_{\mu\nu} + \Gamma^{\eta}_{\mu\lambda}\Gamma^{\alpha}_{\eta\nu} - \Gamma^{\eta}_{\mu\nu}\Gamma^{\alpha}_{\eta\lambda}\right),$$

with the Christoffel symbols

$$\Gamma^{\alpha}_{\mu\nu} = \frac{1}{2} g^{\alpha\beta}\left(\partial_\mu g_{\beta\nu} + \partial_\nu g_{\mu\beta} - \partial_\beta g_{\mu\nu}\right),$$

and the Ricci tensor is given by

$$R_{\mu\lambda} = +R^{\alpha}{}_{\mu\alpha\lambda}\,.$$

The curvature scalar is

$$R = g^{\mu\lambda} R_{\mu\lambda} = R^{\mu}{}_{\mu}\,.$$

Throughout, energy, momentum, frequency, time, length and temperature are all measured in natural units, for which $\hbar = c = k = 1$.

Appendix B

Effective Action Techniques

B.1 Low-Energy Effective Action

The contribution to the effective action for a scalar field from quantum fluctuations of degrees of freedom much heavier than the scalar field is discussed in this section. This is the typical situation for an extremely light quintessence field ϕ coupled to Standard Model fields[1] ψ_j, described by the action

$$S[\phi,\psi_j] = \int d^4x \left(\frac{1}{2}(\partial\phi)^2 - V_{cl}(\phi) + \mathcal{L}(\phi,\psi_j) \right) , \tag{B.1}$$

where $\mathcal{L}(\phi,\psi_j)$ contains the Standard Model Lagrangian as well as couplings between operators $\mathcal{O}_k^{SM}$ composed from the fields ψ_j and the scalar field ϕ,

$$\mathcal{L}(\phi,\psi_j) = \mathcal{L}_{SM}(\psi_j) + \sum_k f_k(\phi)\mathcal{O}_k^{SM} . \tag{B.2}$$

As before, the effective action $\Gamma[\phi]$ is the Legendre transform of the generating functional,

$$\exp\left(iW[J]\right) = \int \mathcal{D}\varphi \int \left(\prod_j \mathcal{D}\psi_j \right) \exp\left(iS[\varphi,\psi_j] + i\int d^4x J(x)\varphi(x) \right) . \tag{B.3}$$

In order to obtain the impact of the fluctuations of the fields ψ_j on the evolution of the field ϕ, it is convenient to perform the path integrals in two steps. In the first step, the path integral over the heavy fields ψ_j yields the semi-classical low-energy effective action $S_{\mathit{eff}}[\phi]$,

$$\exp\left(iS_{\mathit{eff}}[\phi]\right) \equiv \int \left(\prod_j \mathcal{D}\psi_j \right) \exp\left(iS[\varphi,\psi_j]\right) , \tag{B.4}$$

where the fields ψ_j are "integrated out" and the scalar field is treated as a classical background field. The complete effective action is obtained in the second step from the path integral over φ,

$$\begin{aligned} \exp\left(i\Gamma[\phi]\right) &= \exp\left(iW[J] - i\int d^4x J(x)\phi(x) \right) \\ &= \int \mathcal{D}\varphi \, \exp\left(iS_{\mathit{eff}}[\varphi] + i\int d^4x \, J(x)(\varphi(x)-\phi(x)) \right) , \end{aligned}$$

[1] A coupling of the field ϕ to particles beyond the Standard Model, like dark matter, can easily be included here.

which can be recognized as the effective action for an uncoupled scalar field ϕ described by the low-energy effective action $S_{eff}[\phi]$. Thus, $S_{eff}[\phi]$ is the leading contribution to the effective action from quantum fluctuations of degrees of freedom much heavier than the scalar field. As for the effective action, the low-energy effective potential $V_{eff}(\phi)$ can be defined as the lowest-order contribution to the derivative expansion of $S_{eff}[\phi]$ defined analogously to eq. (3.18). For non-derivative couplings between ϕ and ψ_j the low-energy effective potential in one-loop approximation is given by eq. (4.51) [60, 105].

Note that the one-loop low-energy effective action is analogous to the Heisenberg-Euler effective action [90] which describes the impact of quantum (vacuum) fluctuations of the Standard Model fermions, predominantly the electron being the lightest charged particle, on a classical electromagnetic background field.

In the context of a rolling quintessence field, quantum (vacuum) fluctuations of the Standard Model fields lead to quantum corrections to the equation of motion of the scalar field. In other words, standard-model couplings of the quintessence field lead to a quantum backreaction on its dynamics (see [96] for a discussion of the classical backreaction of Standard Model particles and dark matter). It should be emphasized that the quantum corrections to the equation of motion of the scalar field ϕ captured by the low-energy effective action $S_{eff}[\phi]$ have their origin in the quantum fluctuations of the degrees of freedom ψ_j. For a quintessence field ϕ coupled to standard-model particles, these "heavy" degrees of freedom are well-known. In fact, for typical quintessence masses of the order of the Hubble parameter, $m_\phi \sim H$, even masses at the neutrino energy scale $\sim$meV are "heavy".

B.2 Effective Action in Curved Background

In this section the calculation of the one-loop effective action in a non-trivial background geometry given by the metric $g_{\mu\nu}$ using Heat Kernel Expansion [35] and zeta-function regularization [91, 110] is briefly reviewed. Similarly to dimensional regularization, zeta-function regularization exploits the analyticity properties of Feynman integrals, but is more convenient in curved space-time [110]. The one-loop higher derivative contributions to the effective action, see eq. (3.18), can be obtained by the same formalism. A generalization of the classical action (3.1) to curved space-time is considered, using the covariant integration measure $d^4x\sqrt{-g}$,

$$S[\phi, g_{\mu\nu}] = \int d^4x\sqrt{-g}\left(\frac{1}{2}(\partial\phi)^2 - V(\phi,R) + \varepsilon_1 C + \varepsilon_2 G + \Box B(\phi,R)\right). \tag{B.5}$$

$V(\phi,R)$ is a generalized potential which depends on ϕ and the curvature scalar R, and terms proportional to the square of the Weyl tensor $C = R_{\mu\nu\rho\sigma}R^{\mu\nu\rho\sigma} - 2R_{\mu\nu}R^{\mu\nu} + \frac{1}{3}R^2$, and proportional to the Gauss-Bonnet invariant $G = R_{\mu\nu\rho\sigma}R^{\mu\nu\rho\sigma} - 4R_{\mu\nu}R^{\mu\nu} + R^2$, have been added. Furthermore, an additional term $\Box B(\phi,R)$ is included, where $B(\phi,R)$ is a (so far arbitrary) function of ϕ and R and $\Box$ is the covariant D'Alembert operator. The form of the action is chosen in anticipation of the result that it includes all terms needed for the cancellation of divergences [35]. The latter two terms are total derivatives and thus not relevant for the dynamics, but are also required for the cancellation of divergences [35] and do appear in the dynamics if their running is considered [92]. Note that the Einstein-Hilbert term $-R/(16\pi G)$ as well as a possible cosmological constant have been absorbed into the generalized potential $V(\phi,R)$. Minimal coupling between R and ϕ in the classical action is realized for the choice $V(\phi,R) = V_{cl}(\phi) + f(R)$. Standard General Relativity is then recovered for $f(R) = -R/(16\pi G)$ and $\varepsilon_1 = 0$.

The effective action can be calculated analogously to flat space by an expansion in 1PI Feynman

diagrams with the classical propagator[2]

$$\mathcal{G}_0^{-1}(x,y) = \frac{-i\delta^2 S[\phi, g_{\mu\nu}]}{\delta\phi(x)\delta\phi(y)} = i\left(\Box_x + \left.\frac{\delta^2 V(\phi,R)}{\delta\phi^2}\right|_{\phi(x),R(x)}\right)\delta^4(x-y)\,, \tag{B.6}$$

and interaction vertices given by the third and higher derivatives $i\delta^k S[\phi]/\delta\phi(x_1)\cdots\delta\phi(x_k)$ $(k\geq 3)$ of the classical action. In one-loop approximation, the effective action is (see eq. (3.14))

$$\Gamma[\phi, g_{\mu\nu}] = S[\phi, g_{\mu\nu}] + \frac{i}{2}\mathrm{Tr}\ln\mathcal{G}_0^{-1}. \tag{B.7}$$

Rewriting the trace of a logarithm as the logarithm of the determinant, the one-loop contribution to the effective action for the action (B.5) is

$$\Gamma[\phi, g_{\mu\nu}]_{1L} = \frac{i}{2}\ln\det\hat{A}, \tag{B.8}$$

with the operator

$$\hat{A} \equiv \Box_x + X(x), \qquad X(x) = \left.\frac{\delta^2 V(\phi,R)}{\delta\phi^2}\right|_{\phi(x),R(x)}. \tag{B.9}$$

The generalized zeta-function for $\hat{A}$ is $\zeta_A(\nu) \equiv \sum_m \lambda_m^{-\nu}$ where λ_m are the eigenvalues of $\hat{A}$. Using zeta-function regularization (see e.g. [35, 110]) the determinant can be written as

$$\Gamma[\phi, g_{\mu\nu}]_{1L} = \frac{i}{2}\sum_m \ln\frac{\lambda_m}{\mu^2} = \frac{1}{2i}(\zeta_A'(0) + \zeta_A(0)\ln\mu^2), \tag{B.10}$$

where $\zeta_A' = d\zeta_A/d\nu$ and an arbitrary renormalization scale μ was introduced in order to obtain dimensionless quantities in the logarithm by shifting the effective action by a field-independent constant. The zeta-function can also be expressed via the heat kernel $K(x,y,s)$ fulfilling the heat equation

$$i\frac{\partial}{\partial s}K(x,y,s) = \hat{A}(x)K(x,y,s)\,,$$

with boundary condition $K(x,y,0) = \delta^4(x-y)$. The name of the "heat equation" originates from the Helmholtz equation with a "proper time" "$i\cdot$s" and the Laplace operator $\hat{A} = \triangle$. In terms of a complete set of normalized eigenfunctions $\hat{A}\phi_m(x) = \lambda_m\phi_m(x)$, the solution of the heat equation is[3]

$$K(x,y,s) = \sum_m e^{-\lambda_m is}\,\phi_m(x)\phi_m^*(y)\,,$$

such that the zeta-function has the representation

$$\zeta_A(\nu) = \sum_m \frac{i}{\Gamma(\nu)}\int_0^\infty ds\,(is)^{\nu-1}\,e^{-\lambda_m is} = \frac{i}{\Gamma(\nu)}\int_0^\infty ds\,(is)^{\nu-1}\int d^4x\,K(x,x,s), \tag{B.11}$$

where the integral representation $\Gamma(\nu) = i\lambda^\nu\int_0^\infty ds\,(is)^{\nu-1}e^{-\lambda is}$ of the Γ-function and the normalization of the eigenfunctions has been used. The ansatz for the solution $K(x,y,s)$ of the heat equation of Refs. [121, 153] is

$$K(x,y,s) = \frac{i\Delta_{VM}^{1/2}(x,y)}{(4\pi is)^2}\,\bar{G}(x,y,s)\exp\left(-\frac{\sigma(x,y)}{2is} - is\left(X(y) - \frac{R(y)}{6}\right)\right), \tag{B.12}$$

[2] The Dirac δ-distribution in curved space-time is defined through the requirement that $\int d^4x\sqrt{-g(x)}\,\delta^4(x-y)f(x) = f(y)$ for test functions $f(x)$ [121].

[3] The boundary condition $K(x,y,0) = \delta^4(x-y)$ follows directly from the completeness relation of the eigenfunctions.

where $\sigma(x,y)$ is the proper arclength along the geodesic from x to y and Δ_{VM} the van Vleck-Morette determinant [35]

$$\Delta_{\rm VM}(x,y) = -\frac{1}{\sqrt{g(x)g(y)}}\det\left[\frac{-\partial^2\sigma(x,y)}{\partial x^\mu \partial y^\nu}\right], \tag{B.13}$$

fulfilling $\Delta_{VM}(x,x) = -g(x)$. After inserting this ansatz together with the expansion $\bar{G}(x,y,s) = \sum_{j=0}^{\infty}(is)^j \bar{g}_j(x,y)$ of the Heat Kernel into eq. (B.11), the integration over s can be performed using again the integral representation of the Γ-function,

$$\begin{aligned}
\zeta_A(\nu) &= \frac{i}{\Gamma(\nu)}\int\frac{d^4x}{16\pi^2}\sqrt{-g}\sum_{j=0}^{\infty}\bar{g}_j(x,x)\frac{\Gamma(\nu+j-2)}{(X-R/6)^{\nu+j-2}} \\
&= i\int\frac{d^4x}{16\pi^2}\sqrt{-g}\left(\bar{g}_0(x,x)\frac{(X-R/6)^{2-\nu}}{(\nu-1)(\nu-2)} + \bar{g}_1(x,x)\frac{(X-R/6)^{1-\nu}}{\nu-1}\right. \\
&\quad \left. + \bar{g}_2(x,x)(X-R/6)^{-\nu} + \sum_{j=3}^{\infty}\bar{g}_j(x,x)\frac{\Gamma(\nu+j-2)}{\Gamma(\nu)(X-R/6)^{\nu+j-2}}\right),
\end{aligned}$$

where $\Gamma(\alpha+1) = \alpha\Gamma(\alpha)$ was used to rewrite the first three terms of the Heat Kernel Expansion explicitly. From the previous relation, it can be inferred that $\Gamma(\nu+j-2)/\Gamma(\nu) = (\nu+j-3)(\nu+j-4)\cdots\nu$ for $j \geq 3$. Therefore, the limit $\nu \to 0$ for $\zeta_A(\nu)$ and $\zeta_A'(\nu)$ can be performed, and eq. (B.10) finally yields for the one-loop contribution to the effective action

$$\begin{aligned}
\Gamma[\phi, g_{\mu\nu}]_{1L} &= \int\frac{d^4x}{32\pi^2}\sqrt{-g}\left[-\bar{g}_0(x,x)\frac{\tilde{X}^2}{2}\left(\ln\frac{\tilde{X}}{\mu^2} - \frac{3}{2}\right) + \bar{g}_1(x,x)\tilde{X}\left(\ln\frac{\tilde{X}}{\mu^2} - 1\right)\right. \\
&\quad \left. - \bar{g}_2(x,x)\ln\frac{\tilde{X}}{\mu^2} + \sum_{j=3}^{\infty}\bar{g}_j(x,x)\frac{(j-3)!}{\tilde{X}^{j-2}}\right],
\end{aligned} \tag{B.14}$$

where $\tilde{X} \equiv X - R/6$. The coincidence limits $y \to x$ of the coefficients $\bar{g}_j(x,y)$ of the Heat Kernel Expansion can be calculated recursively. The results for the lowest orders from Ref. [121] are,

$$\begin{aligned}
\bar{g}_0(x,x) &= 1, \\
\bar{g}_1(x,x) &= 0, \\
\bar{g}_2(x,x) &= \frac{1}{180}(R_{\mu\nu\rho\sigma}R^{\mu\nu\rho\sigma} - R_{\mu\nu}R^{\mu\nu}) - \frac{1}{30}\Box R + \frac{1}{6}\Box X \\
&= \frac{1}{120}C - \frac{1}{360}G - \frac{1}{30}\Box R + \frac{1}{6}\Box X,
\end{aligned} \tag{B.15}$$

where C and G are the Weyl- and Gauss-Bonnet terms as given above. The coefficients $\bar{g}_j(x,x)$ with $j \geq 3$ contain higher-order curvature scalars built from the curvature- and Ricci tensors and space-time derivatives of R and X. They correspond to finite contributions to the one-loop effective action (B.14), whereas the $j = 0,1,2$-contributions come along with divergences proportional to $\bar{g}_0\tilde{X}^2$, $\bar{g}_1\tilde{X}$ and $\bar{g}_2$. Using eq. (B.15) one can see that it is necessary to introduce counterterms proportional to $\tilde{X}^2 = (\partial^2 V/\partial\phi^2 - R/6)^2$, $\Box(X - R/5) = \Box(\partial^2 V/\partial\phi^2 - R/5)$, C and G in order to cancel these divergences, which is already done implicitly in the result (B.14) for the effective action through the zeta-function regularization [110]. Nevertheless, all operators contained in the counterterms should be already present in the tree level action [90].

B.3 Renormalization Group Equations

Callan-Symanzik Equation

Within the renormalization scheme provided e.g. by the zeta-function regularization [110], the renormalized one-loop effective action explicitly depends on a renormalization scale μ. In contrast to this, the exact effective action is by construction independent of the renormalization scale. It can be equivalently written either entirely in terms of bare parameters, which are manifestly scale-independent, or in terms of scale-dependent renormalized parameters. In the latter case, the vanishing total μ-derivative of the effective action yields the Callan-Symanzik equation for the effective action,

$$0 = \frac{d}{d\ln\mu^2}\Gamma[\phi_i] = \left(\frac{\partial}{\partial\ln\mu^2} + \sum_N \beta_N \frac{\partial}{\partial c_N} + \sum_i \int d^4x\, \gamma_i \phi_i(x) \frac{\delta}{\delta\phi_i(x)}\right)\Gamma[\phi_i]\,,$$

where all parameters of the theory are denoted collectively by c_N and all fields by $\phi_i(x)$. For a scalar field in curved space, $\{\phi_i(x)\} = \{\phi(x), g_{\mu\nu}(x)\}$. Furthermore, for example for ϕ^4-theory, $\{c_N\} \supset \{\Lambda, m^2, \lambda, \xi, G, \varepsilon_0, \ldots, \varepsilon_4\}$. The coefficients β_N (β-functions) and γ_i (anomalous dimensions) are functions of these parameters. The Callan-Symanzik equation is a partial differential equation which possesses characteristic solutions given by trajectories in parameter space, $c_N(\mu)$, and field space, $\phi_i(x;\mu)$, parameterized by the renormalization scale μ, along which the effective action is constant. These trajectories are determined by definition by the renormalization-group equations

$$\frac{d}{d\ln\mu^2}\, c_N(\mu) = \beta_N(\{c_N(\mu)\}), \quad \text{and} \qquad \frac{d}{d\ln\mu^2}\, \phi_i(x;\mu) = \gamma_i(\{c_N(\mu)\})\phi_i(x;\mu)\,.$$

Renormalization Group Improved Effective Action

If the exact β-functions and anomalous dimensions were known, as well as the exact effective action for one set of parameters $\{c_N(\mu_0)\}$ and one field configuration $\{\phi_i(x;\mu_0)\}$, the renormalization group equations yield the effective action along the complete trajectory for all scales μ. The effective action at $\mu = \mu_0$ then yields the initial conditions for the renormalization group equations. In practice, only approximations to the effective action are known. Using the one-loop β-functions and anomalous dimensions, as well as the classical (zero-loop) action $S[\phi_i]$ for one set of parameters $\{c_N(\mu_0)\}$ and one field configuration $\{\phi_i(x;\mu_0)\}$ as initial condition at the scale $\mu = \mu_0$, the renormalization group equations yield an improved approximation ("leading logarithm approximation") $\Gamma_{LL}[\phi_i;\mu]$ to the effective action for all scales μ. This renormalization-group improved effective action is determined by the partial differential equation

$$\begin{aligned} \frac{\partial}{\partial t}\Gamma_{LL}[\phi_i;\mu] &= -\left(\sum_N \beta_N(\mu)\frac{\partial}{\partial c_N} + \sum_i \int d^4x\, \gamma_i(\mu)\phi_i(x;\mu)\frac{\delta}{\delta\phi_i(x)}\right)\Gamma_{LL}[\phi_i;\mu], \\ \Gamma_{LL}[\phi_i;\mu_0] &= S[\phi_i]\,, \end{aligned} \tag{B.16}$$

where $t = \ln(\mu^2/\mu_0^2)$. The solutions of the one-loop renormalization group equations have to be inserted for $\beta_N(\mu) \equiv \beta_{N,1L}(\{c_N(\mu)\})$ and $\gamma_i(\mu) \equiv \gamma_{i,1L}(\{c_N(\mu)\})$.

One-Loop Renormalization Group Equations

The one-loop β-functions and the one-loop anomalous dimensions are obtained by matching the partial differential equation (B.16) at $\mu = \mu_0$ with the one-loop effective action (4.71). The one-loop β-functions will now be derived in this way for the action (4.66) of a scalar field in curved space with

generalized potential $V(\phi,R)$ and $B(\phi,R)$ from eq. (4.70). On the one hand, the classical action (4.66) can be inserted into the partial differential eq. (B.16) evaluated at $\mu=\mu_0$,

$$\begin{aligned}\frac{\partial}{\partial t}\Gamma_{LL}[\phi,g_{\mu\nu};\mu]\Big|_{\mu=\mu_0} &= -\left(\sum_N \beta_N \frac{\partial}{\partial c_N}+\sum_i\int d^4x\,\gamma_i\phi_i(x)\frac{\delta}{\delta\phi_i(x)}\right)S[\phi_i]\\ &= -\int d^4x\sqrt{-g}\left[\sum_{nm}\beta_{nm}\phi^n R^m+\beta_{\varepsilon_1}C+\beta_{\varepsilon_2}G+\sum_{nm}\overline{\beta}_{nm}\Box(\phi^n R^m)\right.\\ &\quad\left.+\gamma_\phi\,\phi\left(\Box\phi-\frac{\partial V(\phi,R)}{\partial\phi}\right)+\gamma_{g_{\mu\nu}}g_{\mu\nu}\left(\frac{1}{2}g^{\mu\nu}\mathcal{L}(\phi,g_{\mu\nu})+\frac{\delta\mathcal{L}(\phi,g_{\mu\nu})}{\delta g_{\mu\nu}}\right)\right],\end{aligned}$$

where the β-functions β_{nm} and $\overline{\beta}_{nm}$ control the running of the coefficients c_{nm} and $\overline{c}_{nm}$, respectively. On the other hand, it can be used that the first derivative with respect to $t=\ln(\mu^2/\mu_0^2)$ of the renormalization-group improved effective action and of the one-loop effective action coincide at the reference scale $\mu=\mu_0$ [60]. For the one-loop effective action (4.71), the following is obtained

$$\begin{aligned}\frac{\partial}{\partial t}\Gamma_{LL}[\phi,g_{\mu\nu};\mu]\Big|_{\mu=\mu_0} &= -\frac{\partial}{\partial\ln\mu_0^2}\Gamma_{1L}[\phi,g_{\mu\nu};\mu_0]\\ &= \int\frac{d^4x}{32\pi^2}\sqrt{-g}\left[-\frac{(X-R/6)^2}{2}-\frac{1}{120}C-\frac{1}{360}G-\frac{1}{30}\Box R+\frac{1}{6}\Box X\right]\\ &= -\int\frac{d^4x}{32\pi^2}\sqrt{-g}\left[\frac{1}{2}\sum_{nm}\left(\sum_{k=0}^{n}\sum_{l=0}^{m}d_{kl}d_{n-k,m-l}\right)\phi^n R^m-\frac{1}{120}C-\frac{1}{360}G\right.\\ &\quad\left.+\frac{1}{6}\sum_{nm}\left((n+2)(n+1)c_{n+2,m}-\frac{1}{5}\delta_{n0}\delta_{m1}\right)\Box(\phi^n R^m)\right],\end{aligned}$$

where the parameterizations (4.70) were inserted for $X=\partial V(\phi,R)/\partial\phi^2$ with $d_{nm}\equiv(n+2)(n+1)c_{n+2,m}-\delta_{n0}\delta_{m1}/6$, where $\delta_{nm}=1$ if $n=m$ and zero otherwise. The one-loop β-functions are obtained by comparing the coefficients of both upper expressions,

$$\begin{aligned}\beta_{nm} &= \frac{1}{64\pi^2}\sum_{k=0}^{n}\sum_{l=0}^{m}d_{kl}d_{n-k,m-l}\,,\\ \overline{\beta}_{nm} &= \frac{1}{192\pi^2}\left((n+2)(n+1)c_{n+2,m}-\frac{1}{5}\delta_{n0}\delta_{m1}\right),\\ \beta_{\varepsilon_1} &= -\frac{1}{32\pi^2}\frac{1}{120},\quad \beta_{\varepsilon_2}=-\frac{1}{32\pi^2}\frac{1}{360},\quad \gamma_\phi=0,\quad \gamma_{g_{\mu\nu}}=0.\end{aligned}\tag{B.17}$$

It is convenient to define a renormalization-group improved generalized potential $V_{LL}(\phi,R;\mu)$ and a renormalization-group improved function $B_{LL}(\phi,R;\mu)$,

$$V_{LL}(\phi,R;\mu)=\sum_{nm}c_{nm}(\mu)\phi^n R^m,\quad B_{LL}(\phi,R;\mu)=\sum_{nm}\overline{c}_{nm}(\mu)\phi^n R^m,\tag{B.18}$$

where the coefficients are solutions of the one-loop renormalization group equations $dc_{nm}/dt=\beta_{nm}$ and $d\overline{c}_{nm}/dt=\overline{\beta}_{nm}$. Using the one-loop β-functions (B.17) gives

$$\begin{aligned}\frac{\partial}{\partial t}V_{LL}(\phi,R;\mu) &= \frac{1}{64\pi^2}\left(\frac{\partial^2 V_{LL}(\phi,R;\mu)}{\partial\phi^2}-\frac{R}{6}\right)^2,\\ \frac{\partial}{\partial t}B_{LL}(\phi,R;\mu) &= \frac{1}{192\pi^2}\left(\frac{\partial^2 V_{LL}(\phi,R;\mu)}{\partial\phi^2}-\frac{R}{5}\right).\end{aligned}\tag{B.19}$$

Thus, the solution of the partial differential equation (B.16) for the renormalization-group improved effective action can be rewritten as

$$\Gamma_{LL}[\phi, g_{\mu\nu}; \mu] = \int d^4x \sqrt{-g} \left(\frac{1}{2} g^{\mu\nu} \partial_\mu \phi \partial_\nu \phi - V_{LL}(\phi, R; \mu) \varepsilon_1(\mu) C + \varepsilon_2(\mu) G + \Box B_{LL}(\phi, R; \mu) \right) .$$

The initial condition at $\mu = \mu_0$ in eq. (B.16) yields the initial conditions

$$V_{LL}(\phi, R; \mu_0) = V(\phi, R), \qquad B_{LL}(\phi, R; \mu_0) = 0 .$$

In the second equation, it was used that the initial condition for $B_{LL}(\phi, R; \mu)$ can be chosen arbitrarily, since it appears as a total derivative in the action[4].

Sliding Renormalization Scale

The renormalization-group improved effective action $\Gamma_{LL}[\phi, g_{\mu\nu}; \mu]$ yields an approximation to the effective action which is applicable around the scale μ. It is desirable to have one approximation $\Gamma_{CW}[\phi, g_{\mu\nu}]$ available which simultaneously describes the dynamics for a certain range of scales. For a single scalar field, this is accomplished by exploiting the fact that the choice of the scale μ in $\Gamma_{LL}[\phi, g_{\mu\nu}; \mu]$ is free. In fact, so far no assumptions have been made which would restrict μ to a constant (see footnote 4). Evaluating the renormalization-group improved effective action with a field-dependent scale parameter $t = \ln(\mu^2/\mu_0^2)$ yields [60]

$$\Gamma_{CW}[\phi, g_{\mu\nu}] = \Gamma_{LL}[\phi, g_{\mu\nu}; \mu] \Big|_{t = \ln\left(\frac{\partial^2 V / \partial \phi^2 - R/6}{\mu_0^2} \right)} + \Gamma_{1L,HD}[\phi, g_{\mu\nu}] ,$$

where the second term denotes the scale-independent part of the one-loop effective action (4.71). The choice for the field-dependent scale is obtained from requiring that $\Gamma_{CW}[\phi, g_{\mu\nu}] \to S[\phi, g_{\mu\nu}] + \Gamma_{1L}[\phi, g_{\mu\nu}; \mu_0]$ for $t \to 0$ [60].

[4] In fact, $\sqrt{-g} \cdot \Box B_{LL}(\phi, R; \mu)$ is *not* a total derivative if a field-dependent scale $\mu = \mu(\phi(x), \ldots)$ is chosen, and therefore it contributes to the effective action in this case. However, since the reference scale μ_0 is a constant, $\sqrt{-g} \cdot \Box B_{LL}(\phi, R; \mu_0)$ is a total derivative (recall that $\sqrt{-g} \cdot \Box = \partial^\mu \sqrt{-g} \cdot \partial_\mu$ when applied to a Lorentz scalar).

Appendix C

Resummation Techniques and Perturbation Theory

C.1 Relation between 2PI and 1PI

The equation of motion for the full connected two-point correlation function $G(x,y)$ derived from the 2PI effective action has the form of a self-consistent Schwinger-Dyson equation [66],

$$G^{-1}(x,y) = \mathcal{G}_0^{-1}(x,y) - \Pi[\phi,G](x,y)\,, \qquad \text{where} \quad \Pi[\phi,G](x,y) = \frac{2i\delta\Gamma_2[\phi,G]}{\delta G(y,x)}\,. \tag{C.1}$$

It is an inherently nonperturbative equation, since the self-energy $\Pi[\phi,G]$ is given by an expression which also involves the full propagator $G(x,y)$. As explained in section 3.2, approximations within the 2PI formalism are achieved by truncating the 2PI functional $\Gamma_2[\phi,G]$, which is equal to the sum of all 2PI diagrams with lines representing the *full* propagator and without external lines. The full propagator is the solution of the self-consistent Schwinger-Dyson equation (C.1), where the expression for the self-energy is obtained from the functional derivative of the truncated 2PI functional $\Gamma_2[\phi,G]$. Equivalently, the full propagator $G(x,y)$ can also be expressed in terms of perturbative Feynman diagrams involving the classical propagator $\mathcal{G}_0(x,y)$. In section 3.2 it has been mentioned that, even if only a very limited number of 2PI diagrams is retained in the truncated 2PI functional $\Gamma_2[\phi,G]$, the resulting full propagator corresponds to an infinite set of perturbative Feynman diagrams. In this section, the construction of this infinite set is reviewed following Refs. [37, 147]. By convolving eq. (C.1) with the classical propagator from the left and with the full propagator from the right, the integrated form of the Schwinger-Dyson equation is obtained,

$$G(x,y) = \mathcal{G}_0(x,y) + \int d^4u \int d^4v\, \mathcal{G}_0(x,u)\Pi[\phi,G](u,v)G(v,y)\,. \tag{C.2}$$

This equation permits an iterative solution, starting from the classical propagator,

$$\begin{aligned}
G^{(0)}(x,y) &= \mathcal{G}_0(x,y)\,, \\
G^{(k+1)}(x,y) &= \mathcal{G}_0(x,y) + \int d^4u \int d^4v\, \mathcal{G}_0(x,u)\Pi^{(k)}(u,v)G^{(k+1)}(v,y) \\
&= \mathcal{G}_0(x,y) + \int d^4u \int d^4v\, \mathcal{G}_0(x,u)\Pi^{(k)}(u,v)\mathcal{G}_0(x,u)(v,y) + \\
&\quad + \int d^4u \int d^4v \int d^4z \int d^4w\, \mathcal{G}_0(x,u)\Pi^{(k)}(u,v)\mathcal{G}_0(v,z)\Pi^{(k)}(z,w)\mathcal{G}_0(w,y) + \dots\,.
\end{aligned}$$

The self-energy appearing in the kth step is obtained by inserting the propagator $G^{(k)}(x,y)$ into the expression $\Pi[\phi,G]$ for the self-energy derived from the (truncated) 2PI functional,

$$\Pi^{(k)}(u,v) = \Pi[\phi, G^{(k)}](u,v)\,.$$

The propagator $G^{(k)}(x,y)$ is itself given by the Schwinger-Dyson series involving the self-energy $\Pi^{(k-1)}(u,v)$. Employing a compact notation by suppressing the space-time integrations yields

$$\begin{aligned}\Pi^{(0)} &= \Pi[\phi, \mathcal{G}_0]\,,\\ \Pi^{(k)} &= \Pi[\phi, G^{(k)}] = \Pi[\phi, \mathcal{G}_0 \sum_{n=0}^{\infty} (\Pi^{(k-1)}\mathcal{G}_0)^n]\,.\end{aligned}$$

Thus, $\Pi^{(k)}$ is obtained from attaching self-energy insertions given by $\Pi^{(k-1)}$ to the internal lines of the "skeleton" diagrams contained in $\Pi[\phi,G]$. Therefore, for $k\to\infty$, this leads to an infinite hierarchy of Feynman diagrams each of which is composed from nested skeleton diagrams, with lines representing the classical propagator $\mathcal{G}_0$. Since

$$\Pi[\phi, \bar{G}[\phi]] = \lim_{k\to\infty} \Pi^{(k)}\,,$$

where $\bar{G}[\phi]$ is the solution of the self-consistent Schwinger-Dyson equation (C.1), the full propagator obtained from the 2PI effective action indeed corresponds to an infinite summation of perturbative diagrams.

If the self-energy $\Pi[\phi,G]$ is derived from the *exact* 2PI functional $\Gamma_2[\phi,G]$, the self-energy $\Pi[\phi,\bar{G}[\phi]]$ equals the sum of *all* perturbative 1PI self-energy diagrams. Furthermore, these are obtained from the iterative procedure described above with the correct symmetry factors [37]. If the self-energy $\Pi[\phi,G]$ is derived from a *truncation* of the 2PI functional $\Gamma_2[\phi,G]$, then $\Pi[\phi,\bar{G}[\phi]]$ corresponds to an infinite *subset* of all perturbative 1PI self-energy diagrams. This subset is characterized by restrictions on the topology of the perturbative diagrams, since only a restricted set of skeletons is used for their construction. Even if only a single 2PI diagram is retained in the 2PI functional, the corresponding infinite subset contains perturbative diagrams of arbitrarily high loop order.

An approximation of the effective action can be obtained by inserting the full propagator $\bar{G}[\phi]$ into the truncated 2PI effective action (see section 3.2).

C.2 Resummed Perturbation Theory

Effective action from the 2PI Hartree-Fock approximation

For the extended Hartree-Fock approximation of the 2PI effective action derived in section 4.1.2, the solution of the self-consistent Schwinger-Dyson equation can be written in the form

$$G_{hf}^{-1}(x,y) = i(\Box_x + M^2_{eff}(x;\phi))\delta^d(x-y)\,, \tag{C.3}$$

where $G_{hf}\equiv\bar{G}[\phi]$ is the full propagator in Hartree-Fock approximation. The effective mass is determined by the Hartree-Fock gap equation

$$M^2_{eff}(x;\phi) = \exp\left[\frac{1}{2}G(x,x)\frac{d^2}{d\phi^2}\right] V''_{cl}(\phi(x))\Big|_{G(x,x)=G\left(x,x;M^2_{eff}(\cdot;\phi)\right)}\,, \tag{C.4}$$

where, for any function $M^2(x)$, $G\left(x,y;M^2(\cdot)\right)$ is the solution of the equation

$$\left(\Box_x + M^2(x)\right) G\left(x,y;M^2(\cdot)\right) = -i\delta^d(x-y)\,.$$

An approximation of the effective action is obtained by inserting the full propagator in Hartree-Fock approximation into the 2PI effective action,

$$\begin{aligned}\Gamma_{hf}[\phi] &= \Gamma[\phi,\bar{G}[\phi]] \\ &= \int d^dx\left(\frac{1}{2}(\partial\phi)^2 - V_{hf}(\phi)\right) + \frac{i}{2}\mathrm{Tr}\left[\ln\left(\Box_x + M^2_{eff}(x;\phi)\right) - iM^2_{eff}(x;\phi)\bar{G}[\phi]\right],\end{aligned} \tag{C.5}$$

where

$$V_{hf}(\phi(x)) \equiv \exp\left[\frac{1}{2}\bar{G}(x,x;\phi)\frac{d^2}{d\phi^2}\right] V_{cl}(\phi(x)), \tag{C.6}$$

has been defined. Furthermore, it is convenient to define an auxiliary potential

$$\overline{V}(\phi(x);M^2(\cdot)) \equiv \exp\left[\frac{1}{2}G\left(x,x;M^2(\cdot)\right)\frac{d^2}{d\phi^2}\right] V_{cl}(\phi(x)), \tag{C.7}$$

in terms of which the effective mass and $V_{hf}(\phi(x))$ can be written as

$$\begin{aligned}M^2_{eff}(x;\phi) &= \left.\frac{\partial^2\overline{V}(\phi;M^2(\cdot))}{\partial\phi^2}\right|_{\phi=\phi(x),M^2(\cdot)=M^2_{eff}(\cdot;\phi)}, \\ V_{hf}(\phi(x)) &= \left.\overline{V}(\phi;M^2(\cdot))\right|_{\phi=\phi(x),M^2(\cdot)=M^2_{eff}(\cdot;\phi)}.\end{aligned} \tag{C.8}$$

Expansion of the exact effective action in terms of 1PI Feynman diagrams without tadpoles

It is possible to expand the exact effective action around the Hartree-Fock approximation (C.5),

$$\begin{aligned}\Gamma_{exact}[\phi] &= \Gamma_{hf}[\phi] + \Gamma_{notad}[\phi], \\ i\Gamma_{notad}[\phi] &= \\ &= \frac{1}{12}\int d^dx \int d^dy\,[-i\overline{V}^{(3)}(\phi(x))]G_{hf}(x,y)^3[-i\overline{V}^{(3)}(\phi(y))] + \ldots,\end{aligned} \tag{C.9}$$

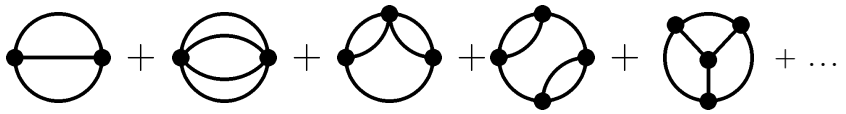

where $i\Gamma_{notad}[\phi]$ is equal to the sum of all 1PI Feynman diagrams *without tadpoles* with lines representing the field-dependent dressed propagator

$$G^{-1}_{hf}(x,y) = i(\Box_x + \overline{V}^{(2)}(\phi(x)))\delta^d(x-y),$$

determined self-consistently by the solution of the gap equation (C.4), and field-dependent dressed vertices given by the derivatives of the auxiliary potential,

$$-i\overline{V}^{(k)}(\phi(x)) \equiv \left.\frac{-i\partial^k\overline{V}(\phi;M^2(\cdot))}{\partial\phi^k}\right|_{\phi=\phi(x),M^2(\cdot)=M^2_{eff}(\cdot;\phi)},$$

for $k \geq 3$. The gap equation (C.4) can be rewritten as $M^2_{eff}(x;\phi) = \overline{V}^{(2)}(\phi(x))$, which has already been used above. A Feynman diagram contains a "tadpole" if it contains at least one line which begins and ends at the same vertex. The effective action expanded in terms of the dressed propagator and vertices defined above only contains Feynman diagrams which have no "tadpoles".

Derivation

The upper expansion of the effective action can be derived in two steps. In the first step, an expansion of the exact propagator around the full Hartree-Fock propagator is performed. Subtracting the equation of motion of the exact propagator from the equation of motion of the full Hartree-Fock propagator yields

$$G^{-1}(x,y) - G_{hf}^{-1}(x,y) = -\Pi[\phi, G](x,y) + \Pi_{hf}[\phi, G_{hf}](x,y) \equiv -\Pi_{notad}(x,y)\,,$$

where Π_{hf} denotes the expression for the self-energy derived from the Hartree-Fock truncation (4.8) of the 2PI effective action. An expansion of the self-energy Π_{notad} defined above in terms of 1PI diagrams with lines representing the Hartree-Fock propagator and vertices given by the derivatives of the classical potential can be obtained by an iterative expansion similar to the one discussed in section C.1,

$$\begin{aligned} \Pi_{notad}^{(0)} &= \Pi[\phi, G_{hf}] - \Pi_{hf}[\phi, G_{hf}]\,, \\ \Pi_{notad}^{(k)} &= \Pi[\phi, G_{hf} \sum_{n=0}^{\infty} (\Pi_{notad}^{(k-1)} G_{hf})^n] - \Pi_{hf}[\phi, G_{hf}]\,. \end{aligned} \tag{C.10}$$

According to Ref. [37], any 1PI Feynman diagram with two external lines ("self-energy diagram") can be decomposed into a unique *skeleton diagram* (obtained from opening one line of a 2PI diagram without external lines), and a set of self-energy sub-diagrams which are attached to the internal lines of the skeleton as *insertions*. The Hartree-Fock self-energy $\Pi_{hf}[\phi, G_{hf}]$ consists of the sum of all tadpole self-energy diagrams, which are called *tadpole-skeletons* or *tadpole-insertions* in the following.
The 0th iteration $\Pi_{notad}^{(0)}$ consists of all possible skeleton diagrams evaluated with the propagator G_{hf} *except* those contained in $\Pi_{hf}[\phi, G_{hf}]$, i.e. except tadpole-skeletons. Furthermore, the skeleton diagrams themselves do by definition not contain any insertions, and therefore especially no tadpole-insertions. Thus, $\Pi_{notad}^{(k)}$ for $k = 0$ does not contain any tadpole-skeletons or diagrams carrying tadpole-insertions. It can be proven by induction that this is also true for all $k \geq 0$, and therefore for Π_{notad} itself. The tadpole-skeletons are explicitly subtracted at each step of the iteration (C.10). Furthermore, the diagrams contained in $\Pi_{notad}^{(k-1)}$ are the insertions of the diagrams contributing to $\Pi_{notad}^{(k)}$. Since the former contain no tadpole-skeletons, the latter contain no tadpole-insertions.
The fact that Π_{notad} does neither contain tadpole-skeletons nor diagrams carrying tadpole-insertions can also be formulated in the following way: When all tadpoles appearing in any self-energy diagram contributing to Π_{notad} are removed, the remaining diagram is still 1PI. All contributions to Π_{notad} that *do* contain tadpoles can be generated from such diagrams by adding tadpoles at the vertices. Summing over the number of tadpoles attached to each vertex is equivalent to replacing the vertices according to

$$-iV^{(k)}(\phi(x)) \to -i \exp\left(\frac{1}{2} G_{hf}(x,x) \frac{d^2}{d\phi^2}\right) V^{(k)}(\phi(x)) = -i\overline{V}^{(k)}(\phi(x))\,, \tag{C.11}$$

which can be seen from a Taylor expansion of the exponential. The term of order L corresponds to L tadpoles. It remains to be shown that the diagrams are generated with the correct symmetry factors. Let $\mathcal{F}$ be a Feynman diagram contributing to Π_{notad} and let $\mathcal{F}/\gamma$ be the unique diagram obtained by removing all tadpoles from $\mathcal{F}$ with $\gamma = \{\gamma_1, \ldots, \gamma_l\}$, $l \geq 2$, the unique set of tadpoles contained at the vertices $1, \ldots, l$ of $\mathcal{F}$. Then $\mathcal{F}/\gamma \in \Pi_{NoTad}$ and $\mathcal{F}/\gamma$ has the same number of vertices as $\mathcal{F}$ since $\mathcal{F}$ does not contain any tadpole-insertions. Due to the exponential in eq. (C.11) the tadpoles γ_i are generated with correct symmetry factors $N(\gamma_i)$. Furthermore, $\mathcal{F}/\gamma \in \Pi_{NoTad}$ has the correct symmetry

factor $N(\mathcal{F}/\gamma)$. However, there can be several possibilities how to attach the tadpoles in γ to $\mathcal{F}/\gamma$ leading to the same diagram $\mathcal{F}$. Let $K(\mathcal{F})$ be the number of these possibilities. Then it is to be shown that

$$K(\mathcal{F}) \cdot \frac{1}{N(\mathcal{F}/\gamma)\prod_{i=1}^{l} N(\gamma_i)}\,\overline{\mathcal{F}} = \frac{1}{N(\mathcal{F})}\,\overline{\mathcal{F}}\,, \tag{C.12}$$

where $\overline{\mathcal{F}}$ denotes the diagram $\mathcal{F}$ without symmetry factor, and $N(\cdot) \equiv |S(\cdot)|$ denotes the symmetry factor equal to the order of the symmetry group $S(\cdot)$ of a given diagram. Thus eq. (C.12) is equivalent to

$$K(\mathcal{F}) = \left| S(\mathcal{F}/\gamma) \otimes \prod_{i=1}^{l} S(\gamma_i) \right| / \left| S(\mathcal{F}) \right| . \tag{C.13}$$

Since $S(\mathcal{F})$ is a subgroup of $S(\mathcal{F}/\gamma) \otimes \prod_{i=1}^{l} S(\gamma_i)$ the expression on the right-hand side of eq. (C.13) is an integer and equal to the order of the set of co-sets $S(\mathcal{F}/\gamma) \otimes \prod_{i=1}^{l} S(\gamma_i)/S(\mathcal{F})$. Each co-set corresponds to one of the possible attachments counted by $K(\mathcal{F})$ [61].
Altogether, it is found that $\Pi_{no\,tad}(x,y)$ is equal to the sum of all 1PI Feynman diagrams with two external lines, internal lines representing the Hartree-Fock propagator $G_{hf}(x,y)$, dressed vertices $-i\overline{V}^{(k)}(\phi(x))$ obtained from the derivatives of the auxiliary potential, and without any tadpoles.

In the second step, it is shown that $\Gamma_{no\,tad}[\phi] \equiv \Gamma_{exact}[\phi] - \Gamma_{tad}[\phi]$ can analogously be expressed in terms of 1PI Feynman diagrams with propagator $G_{hf}(x,y)$, dressed vertices $-i\overline{V}^{(k)}(\phi(x))$, without external lines and *without any tadpoles*. Therefore, it will first be shown that the Feynman diagrams contributing to $\Gamma_{no\,tad}[\phi]$ are neither "multi-bubble" diagrams (see section 4.1.2) nor carry tadpole-insertions when formulated in terms of the propagator $G_{hf}(x,y)$ and *classical* vertices $-iV^{(k)}(\phi(x))$. Second, the remaining tadpoles are resummed by replacing the classical vertices by the dressed vertices according to the rule (C.11).
Using the parameterization (3.26) of the exact 2PI effective action, and eq. (C.9) for $\Gamma_{tad}[\phi]$, one finds

$$\Gamma_{no\,tad}[\phi] = \frac{i}{2}\mathrm{Tr}\,\ln(1 - \Pi_{no\,tad}G_{hf}) + \frac{i}{2}\mathrm{Tr}\,\Pi_{no\,tad}G + \tilde{\Gamma}_2[\phi, G_{hf}]\,, \tag{C.14}$$

where

$$\tilde{\Gamma}_2[\phi, G_{hf}] = \Gamma_2[\phi, G] - \Gamma_{2,hf}[\phi, G_{hf}] - \mathrm{Tr}\,\frac{\delta\Gamma_{2,hf}[\phi, G_{hf}]}{\delta G_{hf}}\left(G - G_{hf}\right) . \tag{C.15}$$

Here, $\Gamma_2[\phi, G]$ denotes the exact 2PI functional evaluated with the exact propagator, and $\Gamma_{2,hf}[\phi, G_{hf}]$ denotes the Hartree-Fock truncation (4.8) of the 2PI functional, which resums the multi-bubble diagrams, evaluated with the Hartree-Fock propagator.
An expansion of $\Gamma_{no\,tad}[\phi]$ in terms of 1PI Feynman diagrams with propagator $G_{hf}(x,y)$ and classical vertices $-iV^{(k)}(\phi(x))$ is obtained from eq. (C.14) by Taylor expanding the logarithm in the first term on the right-hand side in powers of $\Pi_{no\,tad}G_{hf}$ and by inserting the Schwinger-Dyson sum

$$G = G_{hf}\sum_{n=0}^{\infty}(\Pi_{no\,tad}G_{hf})^n \equiv G_{hf} + \Delta G\,, \tag{C.16}$$

for the exact propagator. Then multi-bubble diagrams or diagrams carrying tadpole-insertions could arise in eq. (C.14) from the following terms:

(*i*) The linear term in the expansion of $\frac{i}{2}\mathrm{Tr}\,\ln(1 - \Pi_{no\,tad}G_{hf})$ in powers of $\Pi_{no\,tad}G_{hf}$.

(*ii*) The linear term in the expansion of $\frac{i}{2}\mathrm{Tr}\,\Pi_{no\,tad}G$ in powers of $\Pi_{no\,tad}G_{hf}$.

(*iii*) Diagrams contributing to Π_{notad} which carry tadpole-insertions.

(*iv*) Diagrams contributing to $\tilde{\Gamma}_2[\phi, G_{hf}]$.

The contributions from (*i*) and (*ii*) cancel, and (*iii*) cannot occur as was shown in the first step of the derivation. In order to investigate (*iv*), the 2PI functional $\Gamma_2[\phi, G] \equiv \Gamma_{2,hf}[\phi, G] + \Gamma_{2,notad}[\phi, G]$ is split into a Hartree-Fock part containing (local) multi-bubble diagrams evaluated with the exact propagator and a non-local part. Inserting eq. (C.16) into the former yields

$$\Gamma_{2,hf}[\phi, G] \;=\; \Gamma_{2,hf}[\phi, G_{hf}] \;+\; \mathrm{Tr}\,\frac{\delta\Gamma_{2,hf}[\phi, G_{hf}]}{\delta G_{hf}}\,\Delta G \;+\; \mathcal{O}\,(\Delta G)^2\,.$$

Multi-bubble diagrams arise from the first term on the right-hand side and diagrams carrying tadpole insertions from the second. However, precisely those are cancelled in the expression for $\tilde{\Gamma}_2[\phi, G_{hf}]$, which can be seen from eq. (C.15). Thus $\Gamma_{notad}[\phi]$ does not contain multi-bubble diagrams or diagrams carrying tadpole-insertions when formulated in terms of the propagator $G_{hf}(x, y)$ and classical vertices $-iV^{(k)}(\phi(x))$.

Similar to self-energy diagrams, any 1PI Feynman diagram *without external lines* can be decomposed into a 2PI *skeleton diagram* without external lines and a set of self-energy sub-diagrams which are attached to the internal lines of the skeleton as insertions. However, in contrast to the self-energy diagrams, this decomposition is not unique. Therefore, it is important to check that every 1PI Feynman diagram without tadpole-insertions contributes exactly *once* to $\Gamma_{notad}[\phi]$, i.e. that no over-counting occurs. The argument is analogous to the expansion of the 2PI effective action in terms of perturbative Feynman diagrams [37]. The three contributions on the right-hand side of eq. (C.14) count every diagram with a multiplicity factor n_c, $-n_l$, and n_s respectively, where n_c is the number of circles, n_l the number of lines in circles and n_s the number of skeletons of a given 1PI diagram without external lines, as defined in Ref. [37]. Due to the relation $n_c - n_l + n_s = 1$ [37] every diagram is counted once. Any diagram $\mathcal{F}$ contributing to $\Gamma_{notad}[\phi]$ can be composed from a unique 1PI diagram without *any* tadpoles $\mathcal{F}/\gamma$ by attaching tadpoles $\gamma = \{\gamma_1, \ldots, \gamma_l\}$, $l \geq 2$, at the l vertices of $\mathcal{F}/\gamma$. Thus, it follows analogously to the first step of the derivation that $\mathcal{F}$ can be generated with correct symmetry factor from the diagram $\mathcal{F}/\gamma$ formulated with dressed vertices $-\overline{V}^{(k)}(\phi)$, by expanding the exponential in eq. (C.11). Due to the uniqueness of $\mathcal{F}/\gamma$ for any $\mathcal{F} \in \Gamma_{notad}[\phi]$ no over-counting can occur here. Since also $\mathcal{F}/\gamma \in \Gamma_{notad}[\phi]$, *all* 1PI diagrams without any tadpoles are included in $\Gamma_{notad}[\phi]$.

Finally, it is found that $i\Gamma_{notad}[\phi]$ is equal to the sum of all 1PI Feynman diagrams with internal lines representing the Hartree-Fock propagator $G_{hf}(x, y)$, with no external lines, with dressed vertices $-\overline{V}^{(k)}(\phi)$ derived from the auxiliary potential (C.7), and without any tadpoles.

Appendix D

Quantum Fields in and out of Equilibrium

D.1 Thermal Quantum Field Theory

Thermal quantum field theory describes quantum fields in thermal equilibrium. In section D.1.1, two alternative representations of the density matrix element of the thermal density matrix within perturbation theory are reviewed. Furthermore, in section D.1.2 an equation of motion for the full thermal propagator is derived from the 2PI effective action formulated on the thermal time path.

D.1.1 Thermal State

A statistical ensemble in a thermal state at temperature $T = 1/\beta$ is described by the density matrix

$$\rho = \frac{1}{Z} \exp\left(-\beta H\right),$$

where the partition function Z is chosen such that $\mathrm{Tr}\rho = 1$ [124, 135, 136]. The interaction terms contained in the full Hamiltonian H lead to the presence of higher correlations and make the thermal state a highly non-Gaussian state. In contrast to any generic nonequilibrium density matrix, the thermal density matrix has the property to lead to correlation functions which are invariant under time translations [104,136]. This means that the thermal state indeed describes an ensemble in equilibrium. The exponential appearing in the thermal density matrix can be interpreted as the full time-evolution operator $\exp\left(-itH\right)$ evaluated for the imaginary time $t = -i\beta$. Accordingly, the matrix element of the thermal density matrix (see eq. (6.7)) can be written as a path integral over field configurations $\varphi(x)$ with time argument on a time contour $\mathcal{I}$ running along the imaginary axis from $t = 0$ to $t = -i\beta$ [49]. Alternatively, the matrix element can be represented by a Taylor expansion in terms of thermal correlation functions $\alpha_n^{th}(x_1, \ldots, x_n)$ as in eqs. (7.1,7.2).

$$\left\langle \varphi_+, 0 \left| \rho \right| \varphi_-, 0 \right\rangle = \begin{cases} \displaystyle\int_{\varphi(0,\boldsymbol{x})=\varphi_-(\boldsymbol{x})}^{\varphi(-i\beta,\boldsymbol{x})=\varphi_+(\boldsymbol{x})} \mathcal{D}\varphi \, \exp\left(i \int_{\mathcal{I}} d^4x \, \mathcal{L}(x)\right) & \mathcal{C}+\mathcal{I}\,, \\ \exp\left(i \displaystyle\sum_{n=0}^{\infty} \alpha_{12\cdots n}^{th} \varphi_1 \varphi_2 \cdots \varphi_n\right) & \mathcal{C}+\alpha\,, \end{cases} \tag{D.1}$$

where the short-hand notation from eq. (3.34) applies. Thus, for the thermal state, there exist two possibilities how to calculate thermal correlation functions: Either by extending the closed real-time

path $\mathcal{C}$ in the generating functional (6.7) by the imaginary path $\mathcal{I}$ ("$\mathcal{C}+\mathcal{I}$"), or by keeping the closed real-time contour $\mathcal{C}$ in the generating functional (6.7) and inserting the thermal initial correlations $\alpha_n^{th}(x_1,\ldots,x_n)$ ("$\mathcal{C}+\alpha$"). Within perturbation theory, the latter can be obtained from a perturbative expansion of the thermal density matrix element. Since extensive use of both formulations is made, both are reviewed here.

Thermal time contour $\mathcal{C}+\mathcal{I}$

By using the path integral representation of the thermal density matrix, a path integral representation of the generating functional for the thermal state can be obtained by concatenating the time contours $\mathcal{C}$ and $\mathcal{I}$ (the derivation is analogous to the steps leading from eq. (6.7) to eq. (6.19)),

$$Z_\beta[J] = \mathrm{Tr}\left(\rho\, T_{\mathcal{C}+\mathcal{I}}\left[\exp\left(i\int_{\mathcal{C}+\mathcal{I}} d^4x J(x)\Phi(x)\right)\right]\right) = \int \mathcal{D}\varphi \exp\left(i\int_{\mathcal{C}+\mathcal{I}} d^4x\,\{\mathcal{L}(x)+J(x)\varphi(x)\}\right).$$

The part of the time path along the imaginary axis prepares the system in a thermal state at the initial time $t_{init}=0$ and is characteristic for thermal equilibrium, whereas the part of the time path along the real axis yields the time-evolution of the system. For calculations in thermal equilibrium, it is sometimes convenient to use a pure imaginary time formalism by setting $t_{max}=0$ such that only the path $\mathcal{I}$ contributes. However, here the real-time evolution of correlation functions (with a finite initial time) is of interest, in which case the full thermal time path is required.
The time arguments of the thermal propagator can also be attached to the thermal time path, and, using the time-ordering operator $T_{\mathcal{C}+\mathcal{I}}$, it reads

$$G_{th}(x,y) \;=\; \langle T_{\mathcal{C}+\mathcal{I}}\Phi(x)\Phi(y)\rangle - \langle\Phi(x)\rangle\langle\Phi(y)\rangle \;=\; -\left.\frac{\delta^2 \ln Z_\beta[J]}{\delta J(x)\delta J(y)}\right|_{J=0}. \tag{D.2}$$

The thermal propagator evaluated with imaginary time arguments fulfills the relation

$$G_{th}(-i\tau,\boldsymbol{x},0,\boldsymbol{y}) = G_{th}(0,\boldsymbol{x},-i(\beta-\tau),\boldsymbol{y}) \qquad \text{for } 0\le\tau\le\beta\,,$$

i.e. it is periodic with period β, which can be seen using cyclic invariance of the trace,

$$\begin{aligned}\mathrm{Tr}\left(e^{-\beta H}\Phi(-i\tau,\boldsymbol{x})\Phi(0,\boldsymbol{y})\right) &= \mathrm{Tr}\left(e^{-\beta H}e^{\tau H}\Phi(0,\boldsymbol{x})e^{-\tau H}\Phi(0,\boldsymbol{y})\right)\\ &= \mathrm{Tr}\left(e^{-\tau H}\Phi(0,\boldsymbol{y})e^{-(\beta-\tau)H}\Phi(0,\boldsymbol{x})\right) = \mathrm{Tr}\left(e^{-\beta H}\Phi(-i(\beta-\tau),\boldsymbol{y})\Phi(0,\boldsymbol{x})\right).\end{aligned}$$

Due to time-translation invariance, the thermal field expectation value is constant in time. Thermal n-point correlation functions can be calculated by taking the nth derivative of the generating functional $Z_\beta[J]$ with respect to the external source $J(x)$.

Closed real-time contour with thermal initial correlations $\mathcal{C}+\alpha$

Alternatively, one can describe the generating functional for thermal correlation functions without reference to imaginary times by inserting the representation of the thermal density matrix element in the second line of eq. (D.1) into the generating functional (6.7). For this approach, it is required to calculate the thermal correlation functions $\alpha_n^{th}(x_1,\ldots,x_n)$ explicitly. This requires to match the two formulations of the thermal density matrix element in eq. (D.1).
For an interacting theory, the thermal density matrix element cannot be calculated exactly. However, it can be expanded perturbatively [49], starting from the density matrix $\rho_0 = \frac{1}{Z_0}\exp(-\beta H_0)$ containing

the free Hamiltonian H_0, which is quadratic in the field, such that the path integral in eq. (D.1) can be performed,

$$\langle \varphi_+, 0 \,|\rho_0|\, \varphi_-, 0\rangle = \mathcal{N}_0 \exp\left[iS_0[\phi_0]\right] = \mathcal{N}_0 \exp\left[i\int_{\mathcal{I}} d^4x \left(\frac{1}{2}(\partial\phi_0)^2 - \frac{1}{2}m^2\phi_0^2\right)\right].$$

Here $\mathcal{N}_0$ is a normalization factor which is independent of $\varphi_\pm$, and $\phi_0(x)$ is the solution of the free equation of motion $\delta S_0/\delta\phi = (-\Box - m^2)\phi_0 = 0$ on $\mathcal{I}$ subject to the boundary conditions

$$\phi_0(0,\boldsymbol{x}) = \phi_0(0_-,\boldsymbol{x}) = \varphi_-(\boldsymbol{x}) \quad \text{and} \quad \phi_0(-i\beta,\boldsymbol{x}) = \phi_0(0_+,\boldsymbol{x}) = \varphi_+(\boldsymbol{x}).$$

The solution is uniquely determined, and, in spatial momentum space, given by

$$\phi_0(-i\tau,\boldsymbol{k}) = \frac{\sinh(\omega_{\boldsymbol{k}}\tau)}{\sinh(\omega_{\boldsymbol{k}}\beta)}\varphi_+(\boldsymbol{k}) + \frac{\sinh(\omega_{\boldsymbol{k}}(\beta-\tau))}{\sinh(\omega_{\boldsymbol{k}}\beta)}\varphi_-(\boldsymbol{k}), \tag{D.3}$$

where $\omega_{\boldsymbol{k}}^2 = m^2 + \boldsymbol{k}^2$. The exponent of the free thermal density matrix element is quadratic in ϕ_0. Therefore, it describes a Gaussian initial state. Using the explicit form of $\phi_0(-i\tau,\boldsymbol{k})$, it can be written as in eq. (D.25) with

$$\xi_{\boldsymbol{k}}^2 = \frac{n_{BE}(\omega_{\boldsymbol{k}}) + \frac{1}{2}}{\omega_{\boldsymbol{k}}}, \quad \eta_{\boldsymbol{k}} = 0, \quad \frac{\sigma_{\boldsymbol{k}}^2}{4\xi_{\boldsymbol{k}}^4} = \omega_{\boldsymbol{k}}^2 \qquad \text{where} \quad n_{BE}(\omega_k) = \frac{1}{e^{\beta\omega_k} - 1}. \tag{D.4}$$

The full thermal initial correlations can be obtained by perturbing the full Hamiltonian H around H_0,

$$\langle \varphi_+, 0 \,|\rho|\, \varphi_-, 0\rangle = \exp\left[iF[\phi_0]\right], \qquad iF[\phi_0] = \ln\mathcal{N} + iS_0[\phi_0] + iF_{int}[\phi_0],$$

where $\mathcal{N}$ is a normalization factor, $iS_0[\phi_0]$ is the free contribution and $iF_{int}[\phi_0]$ is the sum of all connected Feynman diagrams with vertices

$$i\delta^4 S_{int}/\delta\phi^4 = -i\lambda\,\delta_{\mathcal{I}}(x_1-x_2)\delta_{\mathcal{I}}(x_1-x_3)\delta_{\mathcal{I}}(x_1-x_4) \;=$$

which are integrated over the imaginary contour $\mathcal{I}$, denoted by the empty circle. The boundary conditions of the path integral (D.1) are formally taken into account by the field "expectation" value

$$\phi_0(-i\tau,\boldsymbol{k}) \;=$$

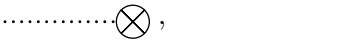

(D.5)

along the imaginary contour $\mathcal{I}$, as well as the propagator

$$D_0(-i\tau,-i\tau',\boldsymbol{k}) \;=$$

(D.6)

$$= \frac{\sinh(\omega_{\boldsymbol{k}}\tau)\sinh(\omega_{\boldsymbol{k}}(\beta-\tau'))\Theta(\tau'-\tau) + \sinh(\omega_{\boldsymbol{k}}\tau')\sinh(\omega_{\boldsymbol{k}}(\beta-\tau))\Theta(\tau-\tau')}{\omega_{\boldsymbol{k}}\sinh(\omega_{\boldsymbol{k}}\beta)},$$

which is the Greens function for solutions of the free equation of motion that vanish at the boundaries $\tau = 0, \beta$, denoted by the dotted line. To first order in λ, $iF_{int}[\phi_0]$ is given by

$$iF_{int}[\phi_0] \;=$$

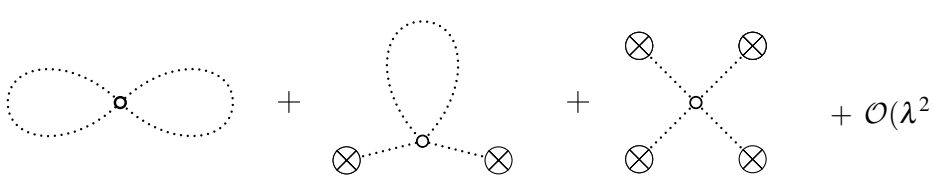

$$+ \mathcal{O}(\lambda^2)$$

$$= \frac{-i\lambda}{4!}\int_{\mathcal{I}} d^4x \left\{3D_0(x,x)^2 + 6\phi_0(x)^2 D_0(x,x) + \phi_0(x)^4\right\} + \mathcal{O}(\lambda^2).$$

The field-independent diagrams, like the first one above, can be absorbed into the normalization $\mathcal{N}$. The perturbative expansions of the thermal initial correlations α_n^{th} are obtained by the n-th functional derivative with respect to the field,

$$i\alpha_n^{th}(x_1,\ldots,x_n) = \left(\frac{\delta iF[\phi_0]}{\delta\varphi_{\varepsilon_1}(\boldsymbol{x_1})\cdots\delta\varphi_{\varepsilon_n}(\boldsymbol{x_n})}\bigg|_{\phi_0=0} \right) \delta_{\mathcal{C}}(x_1^0-0_{\varepsilon_1})\cdots\delta_{\mathcal{C}}(x_n^0-0_{\varepsilon_n}),$$

to which all diagrams with n insertions of ϕ_0 contribute. Here, it can explicitly be seen that the initial correlations are supported only at the initial time, as required. Formally, the functional derivative corresponds to replacing the field insertions by (distinguishable) external lines in the diagrammatic expansion of $iF_{int}[\phi_0]$ according to

$$\begin{aligned} \phi_0(-i\tau,\boldsymbol{k}) \quad &\mapsto \quad \Delta_0(-i\tau,x^0,\boldsymbol{k}) \equiv \frac{\sinh(\omega_{\boldsymbol{k}}\tau)}{\sinh(\omega_{\boldsymbol{k}}\beta)}\,\delta_{\mathcal{C}}(x^0-0_+) + \frac{\sinh(\omega_{\boldsymbol{k}}(\beta-\tau))}{\sinh(\omega_{\boldsymbol{k}}\beta)}\,\delta_{\mathcal{C}}(x^0-0_-) \\ &\equiv \Delta_0^+(-i\tau,\boldsymbol{k})\,\delta_{\mathcal{C}}(x^0-0_+) + \Delta_0^-(-i\tau,\boldsymbol{k})\,\delta_{\mathcal{C}}(x^0-0_-) \end{aligned}$$

(D.7)

For example, the thermal four-point initial correlation function obtained from the fourth derivative of $iF_{int}[\phi_0]$ is

$$\begin{aligned} i\alpha_4^{th}(x_1,x_2,x_3,x_4) &= -i\lambda\int_{\mathcal{I}} d^4v\,\Delta_0(v,x_1)\Delta_0(v,x_2)\Delta_0(v,x_3)\Delta_0(v,x_4) + \mathcal{O}(\lambda^2) \\ &= \end{aligned}$$

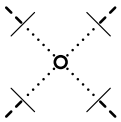

$$+\ \mathcal{O}(\lambda^2), \qquad (D.8)$$

where $\Delta_0(v,x) = \int\frac{d^3\boldsymbol{k}}{(2\pi)^3}\,e^{+i\boldsymbol{k}(\boldsymbol{v}-\boldsymbol{x})}\,\Delta_0(v^0,x^0,\boldsymbol{k})$ for $v^0\in\mathcal{I}, z^0\in\mathcal{C}$. Switching again to momentum space, an explicit expression for the leading contribution to the perturbative thermal initial four-point correlation function is obtained,

$$\begin{aligned} &i\alpha_4^{th,\varepsilon_1,\varepsilon_2,\varepsilon_3,\varepsilon_4}(\boldsymbol{k_1},\boldsymbol{k_2},\boldsymbol{k_3},\boldsymbol{k_4}) = \\ &\quad = -\lambda\int_0^\beta d\tau\,\Delta_0^{\varepsilon_1}(-i\tau,\boldsymbol{k_1})\Delta_0^{\varepsilon_2}(-i\tau,\boldsymbol{k_2})\Delta_0^{\varepsilon_3}(-i\tau,\boldsymbol{k_3})\Delta_0^{\varepsilon_4}(-i\tau,\boldsymbol{k_4}) \qquad + \mathcal{O}(\lambda^2). \end{aligned}$$

For example, for $\varepsilon_1=\varepsilon_2=\varepsilon_3=\varepsilon_4 = +$ or $-$,

$$\begin{aligned} &i\alpha_4^{th,++++}(\boldsymbol{k_1},\boldsymbol{k_2},\boldsymbol{k_3},\boldsymbol{k_4}) = i\alpha_4^{th,----}(\boldsymbol{k_1},\boldsymbol{k_2},\boldsymbol{k_3},\boldsymbol{k_4}) = \\ &\quad = -\lambda\int_0^\beta d\tau\,\frac{\sinh(\omega_{\boldsymbol{k}_1}\tau)}{\sinh(\omega_{\boldsymbol{k}_1}\beta)}\frac{\sinh(\omega_{\boldsymbol{k}_2}\tau)}{\sinh(\omega_{\boldsymbol{k}_2}\beta)}\frac{\sinh(\omega_{\boldsymbol{k}_3}\tau)}{\sinh(\omega_{\boldsymbol{k}_3}\beta)}\frac{\sinh(\omega_{\boldsymbol{k}_4}\tau)}{\sinh(\omega_{\boldsymbol{k}_4}\beta)} \qquad + \mathcal{O}(\lambda^2) \\ &\quad \to \quad \frac{-\lambda}{\omega_{\boldsymbol{k}_1}+\omega_{\boldsymbol{k}_2}+\omega_{\boldsymbol{k}_3}+\omega_{\boldsymbol{k}_4}} \quad + \mathcal{O}(\lambda^2) \qquad \text{for } \beta\to\infty. \end{aligned} \qquad (D.9)$$

The last line represents the zero-temperature limit. The correlations with mixed upper indices vanish in the zero-temperature limit, as required for a pure initial state. Altogether, a diagrammatic expansion of the matrix element of the thermal density matrix in terms of perturbative Feynman diagrams has been developed as suggested in Ref. [49]. This allows to explicitly calculate thermal correlation functions order by order in the quartic coupling constant. The lowest-order perturbative result (D.8) may be compared to the nonperturbative 2PI result (7.67).

D.1.2 Nonperturbative Thermal 2PI Propagator on the Thermal Time Path

In this section an equation of motion for the full thermal propagator is derived from the stationarity condition of the 2PI effective action formulated on the thermal time path $\mathcal{C}+\mathcal{I}$. This self-consistent equation of motion is the analogon of the Kadanoff-Baym equation on the closed real-time path $\mathcal{C}$. The classical thermal propagator defined on $\mathcal{C}+\mathcal{I}$ is ($\phi(x)\equiv\phi=$ const. in equilibrium)

$$i\mathcal{G}^{-1}_{0,th}(x,y)=\left(-\Box_x-m^2-\frac{\lambda}{2}\phi^2\right)\delta_{\mathcal{C}+\mathcal{I}}(x-y)\qquad\text{for } x^0,y^0\in\mathcal{C}+\mathcal{I}\,. \tag{D.10}$$

The full thermal propagator is determined by the equation of motion derived from the 2PI effective action defined on the thermal time contour $\mathcal{C}+\mathcal{I}$, which is given by the self-consistent Schwinger-Dyson equation

$$G^{-1}_{th}(x,y)=\mathcal{G}^{-1}_{0,th}(x,y)-\Pi_{th}(x,y)\qquad\text{for } x^0,y^0\in\mathcal{C}+\mathcal{I}\,. \tag{D.11}$$

The thermal propagator can be decomposed into the statistical propagator and the spectral function,

$$G_{th}(x,y)=G_F(x,y)-\frac{i}{2}\,\mathrm{sgn}_{\mathcal{C}+\mathcal{I}}(x^0-y^0)\,G_\rho(x,y)\qquad\text{for } x^0,y^0\in\mathcal{C}+\mathcal{I}\,, \tag{D.12}$$

where $\mathrm{sgn}_{\mathcal{C}+\mathcal{I}}(x^0-y^0)$ is the signum function defined on the path $\mathcal{C}+\mathcal{I}$. It is equal to $+1$ if x^0 corresponds to a "later" time than y^0 along the time path, where "later" refers to the time-ordering operator $T_{\mathcal{C}+\mathcal{I}}$. In particular, all times on the imaginary branch $\mathcal{I}$ are "later" than all times on the antichronological branch $\mathcal{C}_-$, and these are "later" than all times on the chronological branch $\mathcal{C}_+$. The thermal self-energy can be decomposed similarly as in eqs. (D.42, D.44),

$$\begin{aligned}
\Pi_{th}(x,y) &= -i\Pi^{loc}_{th}(x)\,\delta_{\mathcal{C}+\mathcal{I}}(x-y)+\Pi^{nl}_{th}(x,y)\,,\\
\Pi^{nl}_{th}(x,y) &= \Pi_F(x,y)-\frac{i}{2}\,\mathrm{sgn}_{\mathcal{C}+\mathcal{I}}(x^0-y^0)\,\Pi_\rho(x,y)\,,\\
&= \frac{(-i\lambda)^2}{2}\phi^2 G_{th}(x,y)^2+\frac{(-i\lambda)^2}{6}G_{th}(x,y)^3\\
M^2_{th} &= m^2+\frac{\lambda}{2}\phi^2+\Pi^{loc}_{th}(x)\;=\;m^2+\frac{\lambda}{2}\phi^2+\frac{\lambda}{2}G_{th}(x,x)\,,
\end{aligned} \tag{D.13}$$

where in the third line, as an example, the 2PI-$\mathcal{O}(\lambda^2)$ approximation is given (see section D.2). This approximation coincides with the setting-sun approximation for vanishing field expectation value. The thermal effective mass M^2_{th} is time-independent in equilibrium. Convolving the thermal Schwinger-Dyson equation with G^{-1}_{th} yields an equation of motion for the thermal propagator on the thermal time path $\mathcal{C}+\mathcal{I}$

$$\left(\Box_x+M^2_{th}\right)G_{th}(x,y)=-i\delta_{\mathcal{C}+\mathcal{I}}(x-y)-i\int_{\mathcal{C}+\mathcal{I}}d^4z\,\Pi^{nl}_{th}(x,z)G_{th}(z,y)\,. \tag{D.14}$$

Each of the two time arguments of the propagator can either be real or imaginary, which yields four combinations $G^{\mathcal{C}\mathcal{C}}_{th}$, $G^{\mathcal{C}\mathcal{I}}_{th}$, $G^{\mathcal{I}\mathcal{C}}_{th}$, $G^{\mathcal{I}\mathcal{I}}_{th}$. The equation of motion evaluated for two real arguments yields an equation for $G^{\mathcal{C}\mathcal{C}}_{th}$, etc. The four equations of motion for $G^{\mathcal{C}\mathcal{C}}_{th}$, $G^{\mathcal{C}\mathcal{I}}_{th}$, $G^{\mathcal{I}\mathcal{C}}_{th}$ and $G^{\mathcal{I}\mathcal{I}}_{th}$ are coupled due to the contour integral on the right hand side. For example, the equation for $G^{\mathcal{C}\mathcal{C}}_{th}$ is,

$$\begin{aligned}
\left(\Box_x+M^2_{th}\right)G^{\mathcal{C}\mathcal{C}}_{th}(x,y) &= -i\delta_{\mathcal{C}}(x-y)-i\int_{\mathcal{C}}d^4z\,\Pi^{\mathcal{C}\mathcal{C}}_{th}(x,z)G^{\mathcal{C}\mathcal{C}}_{th}(z,y)\\
&\quad -i\int_{\mathcal{I}}d^4z\,\Pi^{\mathcal{C}\mathcal{I}}_{th}(x,z)G^{\mathcal{I}\mathcal{C}}_{th}(z,y)\,.
\end{aligned} \tag{D.15}$$

Similar to the Kadanoff-Baym equations on the closed real-time contour, the upper equation can be decomposed into an equation for the thermal statistical propagator $G_F^{\mathcal{CC}}$ and the thermal spectral function $G_\rho^{\mathcal{CC}}$,

$$\begin{aligned}
\left(\Box_x + M_{th}^2\right) G_F^{\mathcal{CC}}(x,y) &= \int_0^{y^0} d^4z\, \Pi_F^{\mathcal{CC}}(x,z) G_\rho^{\mathcal{CC}}(z,y) \\
&\quad - \int_0^{x^0} d^4z\, \Pi_\rho^{\mathcal{CC}}(x,z) G_F^{\mathcal{CC}}(z,y) \\
&\quad - \int_0^\beta d\tau \int d^3\boldsymbol{z}\, \Pi_{th}^{\mathcal{CI}}(x,(-i\tau,\boldsymbol{z})) G_{th}^{\mathcal{IC}}((-i\tau,\boldsymbol{z}),y)\,, \\
\left(\Box_x + M_{th}^2\right) G_\rho^{\mathcal{CC}}(x,y) &= \int_{x_0}^{y^0} d^4z\, \Pi_\rho^{\mathcal{CC}}(x,z) G_\rho^{\mathcal{CC}}(z,y)\,.
\end{aligned} \tag{D.16}$$

For the propagators $G_{th}^{\mathcal{IC}}$, $G_{th}^{\mathcal{CI}}$ and $G_{th}^{\mathcal{II}}$ one finds analogously

$$\begin{aligned}
\left(\Box_x + M_{th}^2\right) G_{th}^{\mathcal{IC}}(x,y) &= \int_0^{y^0} d^4z\, \Pi_{th}^{\mathcal{IC}}(x,z) G_\rho^{\mathcal{CC}}(z,y) \\
&\quad - \int_0^\beta d\tau \int d^3\boldsymbol{z}\, \Pi_{th}^{\mathcal{II}}(x,(-i\tau,\boldsymbol{z})) G_{th}^{\mathcal{IC}}((-i\tau,\boldsymbol{z}),y)\,, \\
\left(\Box_x + M_{th}^2\right) G_{th}^{\mathcal{CI}}(x,y) &= -\int_0^{x^0} d^4z\, \Pi_\rho^{\mathcal{CC}}(x,z) G_{th}^{\mathcal{CI}}(z,y) \\
&\quad - \int_0^\beta d\tau \int d^3\boldsymbol{z}\, \Pi_{th}^{\mathcal{CI}}(x,(-i\tau,\boldsymbol{z})) G_{th}^{\mathcal{II}}((-i\tau,\boldsymbol{z}),y)\,, \\
\left(\Box_x + M_{th}^2\right) G_{th}^{\mathcal{II}}(x,y) &= -i\delta_{\mathcal{I}}(x-y) \\
&\quad - \int_0^\beta d\tau \int d^3\boldsymbol{z}\, \Pi_{th}^{\mathcal{II}}(x,(-i\tau,\boldsymbol{z})) G_{th}^{\mathcal{II}}((-i\tau,\boldsymbol{z}),y)\,.
\end{aligned} \tag{D.17}$$

The equation of motion for the purely imaginary-time propagator is independent of the other equations, which is an reflection of causality. Since thermal correlations are invariant under space and time translations, it is convenient to switch to momentum space. In addition to the spatial Fourier transform (D.48), a temporal Fourier transformation can be performed for all times which lie on the imaginary part $\mathcal{I}$ of the thermal time contour,

$$\begin{aligned}
G_{th}(x^0,y^0,\boldsymbol{k}) &= \int d^3\boldsymbol{x}\, e^{-i\boldsymbol{k}(\boldsymbol{x}-\boldsymbol{y})}\, G_{th}(x^0,\boldsymbol{x},y^0,\boldsymbol{y}) \\
G_{th}^{\mathcal{II}}(k_0,\boldsymbol{k}) &= \int_0^\beta d\tau\, e^{-ik_0(\tau-\tau')}\, G_{th}^{\mathcal{II}}(-i\tau,-i\tau',\boldsymbol{k})\,, \\
G_{th}^{\mathcal{IC}}(k_0,y^0,\boldsymbol{k}) &= \int_0^\beta d\tau\, e^{-ik_0\tau}\, G_{th}^{\mathcal{II}}(-i\tau,y^0,\boldsymbol{k})\,,
\end{aligned} \tag{D.18}$$

and analogously for $G_{th}^{\mathcal{CI}}$. Since the thermal propagator is periodic on the finite interval $\mathcal{I}$, it is sufficient to know its Fourier transform for the Matsubara frequencies

$$k_0 = \omega_n = \frac{2\pi}{T} n = 2\pi\beta n, \qquad n = 0, \pm 1, \pm 2, \dots\,.$$

The inverse Fourier transformation with respect to the imaginary time is thus given by the discrete Fourier sum

$$\begin{aligned}
G_{th}^{\mathcal{II}}(-i\tau,-i\tau',\boldsymbol{k}) &= T\sum_n e^{i\omega_n(\tau-\tau')}\, G_{th}^{\mathcal{II}}(\omega_n,\boldsymbol{k})\,, \\
G_{th}^{\mathcal{IC}}(-i\tau,y^0,\boldsymbol{k}) &= T\sum_n e^{i\omega_n\tau}\, G_{th}^{\mathcal{IC}}(\omega_n,y^0,\boldsymbol{k})\,.
\end{aligned} \tag{D.19}$$

By applying the Fourier transformation to the last equation in (D.17), the nonperturbative Schwinger-Dyson equation for the full thermal Matsubara propagator is obtained

$$\left(\omega_n^2 + \boldsymbol{k}^2 + M_{th}^2\right) G_{th}^{\mathcal{I}\mathcal{I}}(\omega_n, \boldsymbol{k}) = 1 - \Pi_{th}^{\mathcal{I}\mathcal{I}}(\omega_n, \boldsymbol{k}) G_{th}^{\mathcal{I}\mathcal{I}}(\omega_n, \boldsymbol{k}) \,, \tag{D.20}$$

where $\int_0^\beta d\tau(-i\delta_{\mathcal{I}}(-i\tau - i\tau')) = 1$ was used.

D.2 Nonequilibrium Quantum Field Theory

Within nonequilibrium quantum field theory, nonperturbative approximations of the full effective action based on the 2PI formalism [66] can be used to describe the quantum equilibration process [27]. In contrast to this, perturbative approximations based on the usual (1PI) effective action cannot describe thermalization even for arbitrarily small couplings λ due to secular behaviour [27]. This means that the perturbative approximation fails for late times $\lambda t \gtrsim 1$. The derivation of the 2PI effective action for ensembles out of equilibrium and the resulting Kadanoff-Baym equations, which describe the time-evolution of the full connected two-point correlation function, is reviewed below for Gaussian initial states. For an introduction to nonequilibrium quantum field theory, it is referred to Ref. [27]. As was shown in section 6.1, the information about the initial state enters via the matrix element of the density matrix describing the statistical ensemble at some initial time $t_{init} \equiv 0$, which can be characterized by an infinite set of initial n-point correlation functions $\alpha_n(x_1, \ldots, x_n)$ according to eqs. (7.1,7.2). In the following, the form of these initial correlations is discussed for two special classes of initial states.

D.2.1 Pure Initial States

If the complete statistical ensemble is in a definite state $|\psi\rangle$ in Hilbert space (pure initial state), the density matrix has the form $\rho = |\psi\rangle\langle\psi|$. In this case, the density matrix element (7.1) is of the form

$$\langle\varphi_+, 0|\rho|\varphi_-, 0\rangle = \langle\varphi_+, 0|\psi\rangle\langle\psi|\varphi_-, 0\rangle \equiv \exp\left(iF_\psi[\varphi_+]\right)\exp\left(-iF_\psi^*[\varphi_-]\right) \,, \tag{D.21}$$

where $\exp\left(iF_\psi[\varphi]\right) \equiv \langle\varphi, 0|\psi\rangle$. Thus, for a pure initial state the functional defined in eq. (7.1) splits up into two separate contributions, where the first one depends only on $\varphi_+(\boldsymbol{x}) = \varphi(0_+, \boldsymbol{x})$ and the second one depends only on $\varphi_-(\boldsymbol{x}) = \varphi(0_-, \boldsymbol{x})$,

$$F[\varphi] = F_\psi[\varphi_+] - iF_\psi^*[\varphi_-] \,. \tag{D.22}$$

The coefficients of the Taylor expansion (7.2) thus cannot contain any mixed terms with respect to the upper indices for a pure initial state,

$$\begin{aligned} \alpha_n(x_1, \ldots, x_n) \;\; = \;\; & \alpha_n^{+\,+\,\cdots\,+}(\boldsymbol{x_1}, \ldots, \boldsymbol{x_n})\, \delta_+(x_1^0) \cdots \delta_+(x_n^0) \\ & + \alpha_n^{-\,-\,\cdots\,-}(\boldsymbol{x_1}, \ldots, \boldsymbol{x_n})\, \delta_-(x_1^0) \cdots \delta_-(x_n^0) \,. \end{aligned} \tag{D.23}$$

D.2.2 Gaussian Initial States

A Gaussian initial state is characterized by the absence of higher correlations,

$$\alpha_n(x_1, \ldots, x_n) = 0 \quad \text{for } n \geq 3 \quad \text{(Gaussian initial state)} \,. \tag{D.24}$$

The most general Gaussian initial state can thus be parameterized as

$$\langle\varphi_+, 0|\rho|\varphi_-, 0\rangle = \exp\left(i\left\{\alpha_0 + \int d^3x\, \alpha_0^\varepsilon(\boldsymbol{x})\varphi_\varepsilon(\boldsymbol{x}) + \frac{1}{2}\int d^3x d^3y\, \varphi_{\varepsilon_1}(\boldsymbol{x})\alpha_2^{\varepsilon_1\varepsilon_2}(\boldsymbol{x}, \boldsymbol{y})\varphi_{\varepsilon_2}(\boldsymbol{y})\right\}\right) .$$

For an initial state which is invariant under spatial translations, it is convenient to switch to spatial momentum space and use $\alpha_1^\varepsilon(\boldsymbol{x}) = \alpha_1^\varepsilon = \text{const}$ and $\alpha_2^{\varepsilon_1\varepsilon_2}(\boldsymbol{x},\boldsymbol{y}) = \int \frac{d^3k}{(2\pi)^3}\, e^{i\boldsymbol{k}(\boldsymbol{x}-\boldsymbol{y})}\, \alpha_2^{\varepsilon_1\varepsilon_2}(\boldsymbol{k})$,

$$\langle \varphi_+, 0\,|\rho|\,\varphi_-, 0\rangle = \exp\left(i\left\{ \alpha_0 + \alpha_0^\varepsilon\, \varphi_\varepsilon(\boldsymbol{0}) + \frac{1}{2}\int \frac{d^3k}{(2\pi)^3}\, \varphi_{\varepsilon_1}(\boldsymbol{k})\alpha_2^{\varepsilon_1\varepsilon_2}(\boldsymbol{k})\varphi_{\varepsilon_2}(-\boldsymbol{k}) \right\}\right). \tag{D.25}$$

Due to the Hermiticity of the density matrix, the initial correlations have to fulfill the relations $\alpha_1^+ = -\alpha_1^{-*}$, $\alpha_2^{++} = -\alpha_2^{--*}$, and $\alpha_2^{+-} = -\alpha_2^{-+*}$. Within real scalar theory, the initial correlations $\alpha_n^{\varepsilon_1,\ldots,\varepsilon_n}$ may additionally be chosen to be totally symmetric in the upper indices. For a Gaussian initial state, this is equivalent to $\alpha_2^{+-} = \alpha_2^{-+}$. Thus, $\alpha_1^\varepsilon(\boldsymbol{x})$ and $\alpha_2^{\varepsilon_1\varepsilon_2}(\boldsymbol{x},\boldsymbol{y})$ can be described by two and three real-valued functions, respectively[1]. One may completely parameterize these independent degrees of freedom of the Gaussian state by the initial expectation values of the field operator and of its conjugate [27],

$$\phi(x)|_{x^0=0} = \text{Tr}\left(\rho\,\Phi(x)\right)\Big|_{x^0=0}, \quad \dot\phi(x)|_{x^0=0} = \text{Tr}\left(\rho\,\partial_{x^0}\Phi(x)\right)\Big|_{x^0=0}, \tag{D.26}$$

together with the initial values of the three real correlation functions

$$\begin{aligned}
G(x,y)|_{x^0=y^0=0} &= \left\{\text{Tr}\left(\rho\,\Phi(x)\Phi(y)\right) - \phi(\boldsymbol{x})\phi(\boldsymbol{y})\right\}\Big|_{x^0=y^0=0}, \\
(\partial_{x^0}+\partial_{y^0})G(x,y)|_{x^0=y^0=0} &= \left\{\text{Tr}\left(\rho\,\left[\Phi(x)\partial_{y^0}\Phi(y) + \partial_{x^0}\Phi(x)\Phi(y)\right]\right)\right. \\
&\quad \left. - \left(\phi(\boldsymbol{x})\dot\phi(\boldsymbol{y}) + \dot\phi(\boldsymbol{x})\phi(\boldsymbol{y})\right)\right\}|_{x^0=y^0=0}, \\
\partial_{x^0}\partial_{y^0}G(x,y)|_{x^0=y^0=0} &= \left\{\text{Tr}\left(\rho\,\partial_{x^0}\Phi(x)\partial_{y^0}\Phi(y)\right) - \dot\phi(\boldsymbol{x})\dot\phi(\boldsymbol{y})\right\}|_{x^0=y^0=0}.
\end{aligned} \tag{D.27}$$

The relations between the upper initial conditions for the one- and two-point function and the density matrix (D.25) are obtained by evaluating the Gaussian integrals [27]. For an initial state which is invariant under spatial translations, one obtains

$$\phi(x)|_{x^0=0} = \int \mathcal{D}\varphi\,\varphi(\boldsymbol{x})\,\langle\varphi,0\,|\rho|\,\varphi,0\rangle = \xi^2_{\boldsymbol{k}=0}\sum_{\varepsilon=\pm} i\alpha_1^\varepsilon, \tag{D.28}$$

$$\dot\phi(x)|_{x^0=0} = \int \mathcal{D}\varphi\,\frac{-i\partial}{\partial\varphi(\boldsymbol{x})}\,\langle\varphi,0\,|\rho|\,\varphi',0\rangle\Big|_{\varphi'=\varphi} = \frac{1}{2i}\left(\sum_{\varepsilon=\pm}\varepsilon\, i\alpha_1^\varepsilon + 2i\,\eta_{\boldsymbol{k}=0}\,\xi_{\boldsymbol{k}=0}\sum_{\varepsilon=\pm} i\alpha_1^\varepsilon\right).$$

Setting $G(x,y) = \int \frac{d^3k}{(2\pi)^3}\, e^{i\boldsymbol{k}(\boldsymbol{x}-\boldsymbol{y})}\, G(x^0,y^0,\boldsymbol{k})$, one obtains similarly

$$\begin{aligned}
G(x^0,y^0,\boldsymbol{k})|_{x^0=y^0=0} &= \xi^2_{\boldsymbol{k}}, \\
(\partial_{x^0}+\partial_{y^0})G(x^0,y^0,\boldsymbol{k})|_{x^0=y^0=0} &= 2\eta_{\boldsymbol{k}}\xi_{\boldsymbol{k}}, \\
\partial_{x^0}\partial_{y^0}G(x^0,y^0,\boldsymbol{k})|_{x^0=y^0=0} &= \eta^2_{\boldsymbol{k}} + \frac{\sigma^2_{\boldsymbol{k}}}{4\xi^2_{\boldsymbol{k}}},
\end{aligned} \tag{D.29}$$

with

$$1/\xi^2_{\boldsymbol{k}} = -\sum_{\varepsilon_j=\pm} i\alpha_2^{\varepsilon_1\varepsilon_2}(\boldsymbol{k}),$$

[1] The constant α_0 is determined by the normalization condition $\text{Tr}\rho = 1$ of the density matrix.

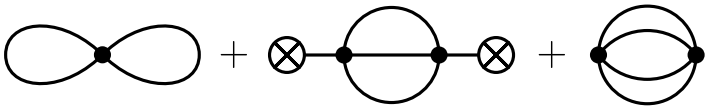

Figure D.1: *Diagrams contributing to $i\Gamma_2[\phi,G]$ at two- and three-loop order with less than three vertices (2PI-$\mathcal{O}(\lambda^2)$-approximation).*

$$\begin{aligned} 2i\eta_{\boldsymbol{k}}/\xi_{\boldsymbol{k}} &= \sum_{\varepsilon_j=\pm} \varepsilon_1 i\alpha_2^{\varepsilon_1\varepsilon_2}(\boldsymbol{k}) = \sum_{\varepsilon_j=\pm} \varepsilon_2 i\alpha_2^{\varepsilon_1\varepsilon_2}(\boldsymbol{k}), \\ \sigma_{\boldsymbol{k}}^2/\xi_{\boldsymbol{k}}^2 &= -\sum_{\varepsilon_j=\pm} \varepsilon_1\varepsilon_2 i\alpha_2^{\varepsilon_1\varepsilon_2}(\boldsymbol{k}). \end{aligned} \tag{D.30}$$

From eq. (D.23) it can be seen that the Gaussian density matrix (D.25) describes a pure initial state if $\eta_{\boldsymbol{k}} = 0$ and $\sigma_{\boldsymbol{k}}^2 = 1$.

D.2.3 2PI Effective Action for Gaussian Initial States

As has been discussed in section 6.1, the 2PI effective action formulated on the closed real-time path $\mathcal{C}$ can be parameterized in the standard form [66]

$$\Gamma[\phi,G] = S[\phi] + \frac{i}{2}\mathrm{Tr}\ln G^{-1} + \frac{i}{2}\mathrm{Tr}\left(\mathcal{G}_0^{-1}G\right) + \Gamma_2[\phi,G], \tag{D.31}$$

for a nonequilibrium ensemble which is characterized by a Gaussian initial state. While the derivation of Kadanoff-Baym equations discussed in section 6.1 has been restricted to the setting-sun approximation, the general derivation is reviewed here. The general form of the Kadanoff-Baym equations includes also a non-vanishing field expectation value $\phi(x)$.
Within $\lambda\Phi^4/4!$-theory, the inverse classical propagator is given by

$$i\mathcal{G}_0^{-1}(x,y) \equiv \frac{\delta^2 S[\phi]}{\delta\phi(x)\delta\phi(y)} = \left(-\Box_x - m^2 - \frac{\lambda}{2}\phi(x)^2\right)\delta_{\mathcal{C}}(x-y). \tag{D.32}$$

The functional $i\Gamma_2[\phi,G]$ is the sum of all two particle irreducible (2PI) Feynman diagrams with lines given by the full propagator $G(x,y)$ and without external lines [66]. The vertices of the graphs contained in $i\Gamma_2[\phi,G]$ are given by the third and fourth derivatives of the classical action $S[\phi]$,

$$\begin{aligned} \times &= \frac{i\delta^4 S[\phi]}{\delta\phi(x_1)\ldots\delta\phi(x_4)} = -i\lambda\,\delta_{\mathcal{C}}(x_1-x_2)\delta_{\mathcal{C}}(x_2-x_3)\delta_{\mathcal{C}}(x_3-x_4), \\ \otimes\!\!-\!\!\bullet\!\!< &= \frac{i\delta^3 S[\phi]}{\delta\phi(x_1)\ldots\delta\phi(x_3)} = -i\lambda\,\phi(x_1)\delta_{\mathcal{C}}(x_1-x_2)\delta_{\mathcal{C}}(x_2-x_3). \end{aligned} \tag{D.33}$$

The initial one- and two-point correlation functions parameterizing the Gaussian initial density matrix (D.25) do not appear explicitly in the 2PI effective action, which is a peculiarity of the Gaussian initial state. Instead, the initial state enters via the initial conditions for the one- and two-point functions $\phi(x)$, $\partial_{x^0}\phi(x)$, $G(x,y)$, $(\partial_{x^0}+\partial_{y^0})G(x,y)$ and $\partial_{x^0}\partial_{y^0}G(x,y)$ at $x^0 = y^0 = 0$ (see eqs. (D.28) and (D.29)).
The two- and three-loop contributions to $i\Gamma_2[\phi,G]$ with less than three vertices are (see figure D.1),

$$\begin{aligned} i\Gamma_2[\phi,G] &= \frac{-i\lambda}{8}\int_{\mathcal{C}} d^4x\, G(x,x)^2 + \frac{(-i\lambda)^2}{12}\int_{\mathcal{C}} d^4x d^4y\, \phi(x)G(x,y)^3\phi(y) \\ &\quad + \frac{(-i\lambda)^2}{48}\int_{\mathcal{C}} d^4x d^4y\, G(x,y)^4 + \mathcal{O}(\lambda^3). \end{aligned} \tag{D.34}$$

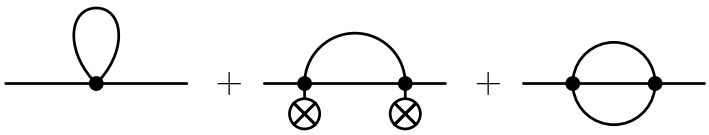

Figure D.2: *Diagrams contributing to the self-energy* $\Pi(x,y)$ *at two- and three-loop order with less than three vertices (2PI-*$\mathcal{O}(\lambda^2)$*-approximation).*

The 2PI-$\mathcal{O}(\lambda^2)$-approximation of $i\Gamma_2[\phi,G]$ coincides with the setting-sun approximation for vanishing field expectation value.

Equation of motion for the full propagator

The equation of motion for the full propagator is obtained from evaluating the functional derivative $\delta\Gamma[\phi,G]/\delta G(x,y) = -K(x,y)/2$ of the 2PI effective action (see eq. (3.24)) using the parameterization (D.31),

$$G^{-1}(x,y) = \mathcal{G}_0^{-1}(x,y) - \Pi(x,y) - iK(x,y)\,, \tag{D.35}$$

where, for generality, the bilocal source $K(x,y)$ was included, and the self-energy $\Pi(x,y)$ was introduced, which is defined as

$$\Pi(x,y) \equiv \frac{2i\delta\Gamma_2[\phi,G]}{\delta G(y,x)}\,. \tag{D.36}$$

In 2PI-$\mathcal{O}(\lambda^2)$-approximation, the self energy can be calculated using eq. (D.34),

$$\Pi(x,y) = \frac{-i\lambda}{2}\,G(x,x)\,\delta_{\mathcal{C}}(x-y) + \frac{(-i\lambda)^2}{2}\,\phi(x)G(x,y)^2\phi(y) + \frac{(-i\lambda)^2}{6}\,G(x,y)^3 + \mathcal{O}(\lambda^3)\,. \tag{D.37}$$

Since the diagrams contributing to the self-energy $\Pi(x,y)$ contain the full propagator $G(x,y)$, the "gap equation" (D.35) is an intrinsically non-perturbative equation for the two-point function. It can be compared to the usual perturbative Schwinger-Dyson equation, which has a similar form as eq. (D.35). However, in the perturbative case, the self-energy is evaluated using the perturbative propagator $\mathcal{G}_0(x,y)$. In contrast to the perturbative case, the gap equation (D.35) which determines the full propagator may be viewed as a self-consistent Schwinger-Dyson equation. It is precisely this self-consistency of the 2PI formalism, which leads to well-behaved nonequilibrium evolution equations for the two-point function, in contrast to perturbative approaches which suffer from the secularity problem [27]. The bilocal source $K(x,y)$ may be split into two parts,

$$K(x,y) = \alpha_2(x,y) + K_{ext}(x,y)\,, \tag{D.38}$$

where the first contribution stems from the initial two-point correlations encoded in the source $\alpha_2(x,y)$, and the second contribution is an additional external bilocal source term. In a physical situation the bilocal external source vanishes, $K_{ext}(x,y) = 0$, such that $K(x,y)$ is only supported at initial times $x^0 = y^0 = 0$. This source term fixes the initial condition for the propagator at $x^0 = y^0 = 0$.

D.2.4 Kadanoff-Baym Equations for Gaussian Initial States

The Kadanoff-Baym equations for the two-point function are obtained by multiplying the equation of motion (D.35), $G^{-1}(x,z) = \mathcal{G}_0^{-1}(x,z) - \Pi(x,z) - i\alpha_2(x,z)$, with $G(z,y)$ and integrating over z,

$$\left(\Box_x + m^2 + \frac{\lambda}{2}\phi(x)^2\right)G(x,y) = -i\delta_{\mathcal{C}}(x-y) - i\int_{\mathcal{C}} d^4z\,(\Pi(x,z) + i\alpha_2(x,z))\,G(z,y)\,, \tag{D.39}$$

where the inverse classical propagator $\mathcal{G}_0^{-1}$ from eq. (D.32) was inserted. It is useful to decompose the two-point function into the statistical propagator $G_F(x,y)$ and the spectral function $G_\rho(x,y)$, which are defined via the anticommutator and commutator of the field operator, respectively,

$$\begin{aligned} G_F(x,y) &= \frac{1}{2}\langle\,[\Phi(x),\Phi(y)]_+\,\rangle - \langle\Phi(x)\rangle\,\langle\Phi(y)\rangle\,, \\ G_\rho(x,y) &= i\langle\,[\Phi(x),\Phi(y)]_-\,\rangle\,, \end{aligned} \tag{D.40}$$

such that the Schwinger-Keldysh propagator can be written in the form

$$G(x,y) = G_F(x,y) - \frac{i}{2}\,\mathrm{sgn}_{\mathcal{C}}(x^0-y^0)\,G_\rho(x,y)\,. \tag{D.41}$$

Furthermore, the self-energy contains local and non-local parts,

$$\Pi(x,y) = -i\Pi_{loc}(x)\delta_{\mathcal{C}}(x-y) + \Pi_{non-loc}(x,y)\,. \tag{D.42}$$

The local part can be included in an effective, time-dependent mass term

$$M(x)^2 = m^2 + \frac{\lambda}{2}\phi^2(x) + \Pi_{loc}(x) = m^2 + \frac{\lambda}{2}\phi^2(x) + \frac{\lambda}{2}G(x,x)\,, \tag{D.43}$$

and the non-local part can be split into statistical and spectral components, similar to the propagator,

$$\Pi_{non-loc}(x,y) = \Pi_F(x,y) - \frac{i}{2}\,\mathrm{sgn}_{\mathcal{C}}(x^0-y^0)\,\Pi_\rho(x,y)\,. \tag{D.44}$$

In 2PI-$\mathcal{O}(\lambda^2)$-approximation, the non-local self-energies are given by

$$\begin{aligned} \Pi_F(x,y) &= \frac{(-i\lambda)^2}{2}\,\phi(x)\left(G_F(x,y)^2 - \frac{1}{4}G_\rho(x,y)^2\right)\phi(y) \\ &\quad + \frac{(-i\lambda)^2}{6}\left(G_F(x,y)^3 - \frac{3}{4}G_F(x,y)G_\rho(x,y)^2\right) + \mathcal{O}(\lambda^3)\,, \\ \Pi_\rho(x,y) &= \frac{(-i\lambda)^2}{2}\,\phi(x)\left(2G_F(x,y)G_\rho(x,y)\right)\phi(y) \\ &\quad + \frac{(-i\lambda)^2}{6}\left(3G_F(x,y)^2G_\rho(x,y) - \frac{1}{4}G_\rho(x,y)^3\right) + \mathcal{O}(\lambda^3)\,. \end{aligned} \tag{D.45}$$

Using the equal-time commutation relations (3.2) of the quantum field gives

$$G_\rho(x,y)\big|_{x^0=y^0} = 0, \quad \partial_{x^0}G_\rho(x,y)\big|_{x^0=y^0} = \delta^{(3)}(\boldsymbol{x}-\boldsymbol{y}). \tag{D.46}$$

With the help of these relations, it is found that

$$\begin{aligned} \partial_{x^0}^2 G(x,y) &= \partial_{x^0}^2 G_F(x,y) - \frac{i}{2}\,\mathrm{sgn}_{\mathcal{C}}(x^0-y^0)\,\partial_{x^0}^2 G_\rho(x,y) \\ &\quad - i\delta_{\mathcal{C}}(x^0-y^0)\partial_{x^0}G_\rho(x,y) - i\partial_{x^0}\left[\delta_{\mathcal{C}}(x^0-y^0)G_\rho(x,y)\right] \\ &= \partial_{x^0}^2 G_F(x,y) - \frac{i}{2}\,\mathrm{sgn}_{\mathcal{C}}(x^0-y^0)\,\partial_{x^0}^2 G_\rho(x,y) - i\delta_{\mathcal{C}}(x^0-y^0)\delta^{(3)}(\boldsymbol{x}-\boldsymbol{y})\,. \end{aligned}$$

Using this relation along with the integration rules on the closed real-time path (see appendix F), the real and causal Kadanoff-Baym equations are finally obtained from inserting the decompositions (D.41, D.42, D.44) of the propagator and the self-energy into the equation of motion (D.39),

$$\begin{aligned} \left(\Box_x + M^2(x)\right)G_F(x,y) &= \int_0^{y^0} d^4z\,\Pi_F(x,z)G_\rho(z,y) - \int_0^{x^0} d^4z\,\Pi_\rho(x,z)G_F(z,y)\,, \\ \left(\Box_x + M^2(x)\right)G_\rho(x,y) &= \int_{x_0}^{y^0} d^4z\,\Pi_\rho(x,z)G_\rho(z,y)\,. \end{aligned} \tag{D.47}$$

The Kadanoff-Baym equations split into two coupled integro-differential equations for $G_F(x,y)$ and $G_\rho(x,y)$. For a system with spatial translation invariance it is convenient to perform a Fourier transformation with respect to the relative spatial coordinate $(\boldsymbol{x}-\boldsymbol{y})$,

$$G(x^0,y^0,\boldsymbol{k}) = \int d^3x\, e^{-i\boldsymbol{k}(\boldsymbol{x}-\boldsymbol{y})}\, G(x,y)\,, \tag{D.48}$$

and similarly for $\Pi(x,y)$. For isotropic systems the propagator $G(x^0,y^0,\boldsymbol{k})$ depends only on the absolute value $|\boldsymbol{k}|$ of the spatial momentum $\boldsymbol{k}$. The Kadanoff-Baym equations in the upper form have been used successfully as a basis to study quantum fields far from equilibrium during the last decade [2, 25, 32, 123, 142] (see also section 6.1). In section 7.1 a generalization of these equations for general initial states which may contain non-Gaussian initial correlations is discussed.
Note that the two-point source $\alpha_2(x,y)$ has been dropped, since it vanishes for $x^0 > 0$. However, it fixes the initial conditions for the statistical propagator $G_F(x,y)$ at $x^0 = y^0 = 0$, see eq. (D.29). The initial conditions for the spectral function $G_\rho(x,y)$ are fixed by eq. (D.46) obtained from the equal-time commutation relations (3.2),

$$\begin{aligned}
G_F(x^0,y^0,\boldsymbol{k})\big|_{x^0=y^0=0} &= \xi_{\boldsymbol{k}}^2\,,\\
\partial_{x^0} G_F(x^0,y^0,\boldsymbol{k})\big|_{x^0=y^0=0} &= \eta_{\boldsymbol{k}}\xi_{\boldsymbol{k}},
\end{aligned} \tag{D.49}$$

$$\begin{aligned}
\partial_{x^0}\partial_{y^0} G_F(x^0,y^0,\boldsymbol{k})\big|_{x^0=y^0=0} &= \eta_{\boldsymbol{k}}^2 + \frac{\sigma_{\boldsymbol{k}}^2}{4\xi_{\boldsymbol{k}}^2}\,,\\
G_\rho(x^0,y^0,\boldsymbol{k})\big|_{x^0=y^0=0} &= 0,\\
\partial_{x^0} G_\rho(x^0,y^0,\boldsymbol{k})\big|_{x^0=y^0=0} &= 1\,,\\
\partial_{x^0}\partial_{y^0} G_\rho(x^0,y^0,\boldsymbol{k})\big|_{x^0=y^0=0} &= 0\,.
\end{aligned} \tag{D.50}$$

The first derivatives with respect to y^0 are related to the first derivatives with respect to x^0 in the second and fifth line due to the symmetry property $G_F(x,y) = G_F(y,x)$ and the antisymmetry property $G_\rho(x,y) = -G_\rho(y,x)$, which follow directly from the definition (D.40). A physical interpretation of the initial conditions for the statistical propagator $G_F(x,y)$ can be obtained by parameterizing it in terms of the initial effective particle- and energy number densities (6.17),

$$\xi_{\boldsymbol{k}}^2 = \frac{n(t=0,\boldsymbol{k})+\frac{1}{2}}{\omega(t=0,\boldsymbol{k})}, \quad \eta_{\boldsymbol{k}} = 0, \quad \frac{\sigma_{\boldsymbol{k}}^2}{4\xi_{\boldsymbol{k}}^4} = \omega^2(t=0,\boldsymbol{k})\,. \tag{D.51}$$

The "memory integrals" on the right hand side of the Kadanoff-Baym equations imply that the time-evolution of $G(x,y)$ near the point (x^0,y^0) in the x^0-y^0-plane depends on the value of the propagator $G(u,v)$ during the entire history $0 < u^0 < x^0$, $0 < v^0 < y^0$ from the initial time $t_{init} = 0$ on. The "memory integrals" turn out to be crucial for the successful description of the quantum thermalization process [32].

Appendix E

Nonperturbative Renormalization Techniques

Truncations of the 2PI effective action yield self-consistent and nonperturbative approximations to the equations of motion for the two-point correlation function. These equations contain ultraviolet divergences, which commonly occurs in relativistic quantum field theory. However, due to their self-consistent structure, the isolation and removal of divergences requires much more sophisticated techniques for these equations compared to perturbative calculations. The proper renormalization requires nonperturbative techniques, which have been formulated recently [28, 29, 37, 174, 175] for systems in thermal equilibrium and at zero temperature. It has been found that approximations based on systematic (e.g. loop) truncations of the 2PI functional are indeed renormalizable, and that the vacuum counterterms are sufficient to remove all divergences at finite temperature. The determination of the vacuum counterterms by solving self-consistent equations for the two- and four-point functions will be discussed in the following based on Refs. [28, 29].

E.1 Renormalization of the 2PI Effective Action

It is convenient to split the action into a free and an interaction part,

$$S_0[\phi] = \int d^4x \left(\frac{1}{2}(\partial\phi)^2 - \frac{1}{2}m_B^2\phi^2 \right), \quad S_{int}[\phi] = -\int d^4x \, \frac{\lambda_B}{4!}\phi(x)^4, \tag{E.1}$$

such that the 2PI Effective Action can be written as

$$\Gamma[\phi, G] = S_0[\phi] + \frac{i}{2}\mathrm{Tr}\ln G^{-1} + \frac{i}{2}\mathrm{Tr}\, G_0^{-1}G + \Gamma_{int}[\phi, G], \tag{E.2}$$

where $iG_0^{-1}(x,y) = (-\Box_x - m_B^2)\delta(x-y)$ is the free perturbative propagator, and

$$\Gamma_{int}[\phi, G] = S_{int}[\phi] + \frac{1}{2}\mathrm{Tr}\frac{\partial^2 S_{int}}{\partial\phi\partial\phi}G + \Gamma_2[\phi, G]. \tag{E.3}$$

Here $i\Gamma_2[\phi, G]$ is the sum of all 2PI vacuum diagrams with lines representing the full propagator $G(x,y)$. The equations of motion for the field expectation value and the full propagator are obtained from the stationarity conditions (3.25) of the 2PI effective action. For the full propagator $G(x,y)$, the equation of motion takes the form of a self-consistent Schwinger-Dyson equation[1],

$$G^{-1}(x,y) = G_0^{-1}(x,y) - \overline{\Pi}(x,y), \tag{E.4}$$

[1] The Schwinger-Dyson equation can equivalently be written in the two forms $G^{-1} = G_0^{-1} - 2i\delta\Gamma_{int}/\delta G = \mathcal{G}_0^{-1} - 2i\delta\Gamma_2/\delta G$. The latter corresponds to eq. (3.29). Here, the first form is more convenient.

where the self-energy is given by $\overline{\Pi}(x,y) = 2i\frac{\delta\Gamma_{int}[\phi,G]}{\delta G(y,x)}$.

Definition of counterterms

For the purpose of renormalization, the action is rewritten by rescaling the field ϕ and splitting the bare mass m_B and coupling λ_B into a renormalized part and a counterterm, respectively,

$$\phi_R = Z^{-1/2}\phi, \quad Zm_B^2 = m_R^2 + \delta m^2, \quad Z^2\lambda_B = \lambda_R + \delta\lambda\,. \tag{E.5}$$

The action expressed in terms of renormalized quantities can be written as

$$S_R[\phi_R] = S[\phi] = S_{0,R}[\phi_R] + S_{int}[\phi_R]_{\lambda_B\to\lambda_R+\delta\lambda} + \frac{1}{2}\int_{xy}\phi_R\, i\delta G_0^{-1}\phi_R\,, \tag{E.6}$$

with the renormalized free action

$$S_{0,R}[\phi_R] = \int d^4x\left(\frac{1}{2}(\partial\phi_R)^2 - \frac{1}{2}m_R^2\phi_R^2\right), \tag{E.7}$$

and a contribution containing the counterterms $\delta Z = Z - 1$ and δm^2 of the form $i\delta G_0^{-1}(x,y) = (-\delta Z\Box_x - \delta m^2)\delta(x-y)$. Similarly, the 2PI effective action can be expressed in terms of the rescaled field expectation value $\phi_R = Z^{-1/2}\phi$ and the rescaled full propagator $G_R = Z^{-1}G$,

$$\Gamma_R[\phi_R, G_R] = \Gamma[\phi, G] = S_{0,R}[\phi_R] + \frac{i}{2}\mathrm{Tr}\ln G_R^{-1} + \frac{i}{2}\mathrm{Tr}\, G_{0,R}^{-1}G_R + \Gamma_{int}^R[\phi_R, G_R]\,, \tag{E.8}$$

where $iG_{0,R}^{-1}(x,y) = (-\Box_x - m_R^2)\delta(x-y)$ is the renormalized free perturbative propagator, and

$$\Gamma_{int}^R[\phi_R, G_R] = \frac{1}{2}\int_{xy}\phi_R\, i\delta G_0^{-1}\phi_R + \frac{i}{2}\mathrm{Tr}\,\delta G_0^{-1}G_R + \Gamma_{int}[\phi_R, G_R]_{\lambda_B\to\lambda_R+\delta\lambda}\,. \tag{E.9}$$

To derive the last relation, $\Gamma_{int}[\phi,G] = \Gamma_{int}[\phi_R, G_R]_{\lambda\to\lambda_R+\delta\lambda}$ was used. For each 2PI vacuum diagram contributing to $\Gamma_{int}[\phi,G]$ this follows from the relation $4V = 2P + E$ between the number of vertices V, the number of propagators P, and the number of field expectation values E.

E.1.1 Divergences and Counterterms in 2PI Kernels

Due to the self-consistent nature of the 2PI formalism the structure of the Schwinger-Dyson equations determining the complete propagator is inherently nonperturbative, and corresponds to the resummation of an infinite set of perturbative diagrams [37]. As a consequence, the renormalization of approximations based on truncations of the 2PI functional is highly nontrivial. It has been shown [28, 37, 174, 175] recently that systematic truncations indeed lead to renormalizable approximations. Besides the divergences which can be identified and subtracted via the BPHZ construction [38, 113, 191], the divergent contributions hidden in the nonperturbative propagator have to be accounted for in a way compatible with the self-consistent structure of the Schwinger-Dyson equations (see section 6.2).

E.1.2 Parameterization of the Renormalized 2PI Effective Action

In order to renormalize the 2PI effective action completely, counterterms which cancel all types of divergences indicated above have to be included. For a given truncation of the 2PI functional, it can be necessary to keep only some parts of the full counterterms which are appropriate for the considered

Figure E.1: *Diagrams containing mass and field counterterms.*

approximation. Thus, the counterterms which appear in different places may be different parts of the full counterterms. Here, a parameterization of the renormalized 2PI effective action is used following Ref. [28],

$$\Gamma^R_{int}[\phi_R, G_R] = \frac{1}{2}\int_{xy} \phi_R\, i\delta G^{-1}_{0,2}\phi_R + \frac{i}{2}\mathrm{Tr}\,\delta G^{-1}_{0,0} G_R + \Gamma_{int}[\phi_R, G_R]_{\lambda_B\to\lambda_R+\delta\lambda_i}\,, \tag{E.10}$$

where the mass- and wavefunction renormalization counterterms are given by (see figure E.1),

$$\begin{aligned} i\delta G^{-1}_{0,2}(x,y) &= (-\delta Z_2\Box_x - \delta m_2^2)\delta(x-y)\,, \\ i\delta G^{-1}_{0,0}(x,y) &= (-\delta Z_0\Box_x - \delta m_0^2)\delta(x-y)\,. \end{aligned} \tag{E.11}$$

The coupling counterterms $\delta\lambda_i$ are chosen in the following way (see figure E.2),

$$\begin{aligned} \Gamma_{int}[\phi_R, G_R]_{\lambda_B\to\lambda_R+\delta\lambda_i} &= -\frac{\lambda_R+\delta\lambda_4}{4!}\int_x \phi_R^4(x) - \frac{\lambda_R+\delta\lambda_2}{4}\int_x \phi_R^2(x) G_R(x,x) \\ &\quad - \frac{\lambda_R+\delta\lambda_0}{8}\int_x G_R^2(x,x) + \gamma_R[\phi_R, G_R]\,, \end{aligned} \tag{E.12}$$

where $\gamma_R[\phi_R, G_R]$ stands for the contributions from nonlocal diagrams, which just contain the BPHZ counterterms to the appropriate order.

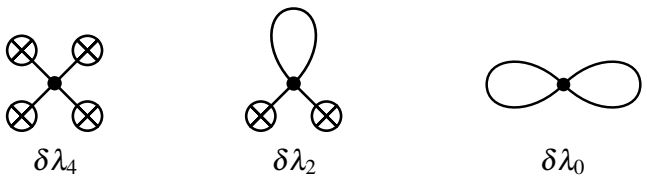

Figure E.2: *Local diagrams containing coupling counterterms.*

E.2 Renormalization of 2PI Kernels

The counterterms are determined by imposing renormalization conditions for the two- and four-point functions. Therefore, the two-point kernels

$$\overline{\Pi}_R(x,y) = \frac{2i\delta\Gamma^R_{int}}{\delta G_R(y,x)}\,, \qquad \Pi_R(x,y) = \frac{i\delta^2\Gamma^R_{int}}{\delta\phi_R(x)\delta\phi_R(y)}\,, \tag{E.13}$$

are defined, in terms of which the renormalized Schwinger-Dyson equation for the full propagator $G_R(x,y)$ can be expressed as

$$G_R^{-1}(x,y) = G^{-1}_{0,R}(x,y) - \overline{\Pi}_R(x,y)\,. \tag{E.14}$$

Furthermore, the four-point kernels

$$\overline{\Lambda}(x,y,u,v) = \frac{4\delta^2\Gamma_{int}}{\delta G(x,y)\delta G(u,v)}\,, \qquad \Lambda(x,y,u,v) = \frac{2\delta^3\Gamma_{int}}{\delta\phi(x)\delta\phi(y)\delta G(u,v)}\,, \tag{E.15}$$

are defined. Due to the self-consistent structure of the 2PI formalism, the four-point kernels $\overline{\Lambda}$ and Λ do only contribute to the complete n-point functions via the resummed kernels $\overline{V}$ and V, which are solutions of the Bethe-Salpeter equations [28],

$$\begin{aligned}
\overline{V}(x,y,u,v) &= \overline{\Lambda}(x,y,u,v) + \frac{i}{2}\int_{abcd} \overline{\Lambda}(x,y,a,b)G(a,c)G(d,b)\overline{V}(c,d,u,v)\,, \\
V(x,y,u,v) &= \Lambda(x,y,u,v) + \frac{i}{2}\int_{abcd} V(x,y,a,b)G(a,c)G(d,b)\overline{\Lambda}(c,d,u,v)\,.
\end{aligned} \tag{E.16}$$

The solutions of the Bethe-Salpeter equations can formally be obtained by an iteration, which yields a resummation of ladder diagrams, where the ladder steps are given by the kernel $\overline{\Lambda}$, and the connections of the steps are given by the complete propagator G. Note that the nonperturbative renormalization of the four-point kernels can formally be understood as being built up of two steps. First, the divergences contained in the diagrammatic contributions to the kernels $\overline{\Lambda}$ and Λ are subtracted via an appropriate choice of BPHZ counterterms $\delta\lambda_0^{BPHZ}$ and $\delta\lambda_2^{BPHZ}$, respectively. Second, the additional divergences appearing in the renormalized solutions $\overline{V}_R \equiv Z^2\overline{V}$ and $V_R \equiv Z^2 V$ of the Bethe-Salpeter equation are removed by additional counterterms $\Delta\lambda_0$ and $\Delta\lambda_2$, such that the complete counterterms are given by the sum, $\delta\lambda_0 = \delta\lambda_0^{BPHZ} + \Delta\lambda_0$ and $\delta\lambda_2 = \delta\lambda_2^{BPHZ} + \Delta\lambda_2$. In practice, the full counterterms $\delta\lambda_0$ and $\delta\lambda_2$ can be determined in one step by imposing a renormalization condition on the kernels $\overline{V}_R$ and V_R.

Renormalization conditions

For the vacuum theory it is most convenient to work in Euclidean momentum space $q^\mu = (iq^0, \boldsymbol{q})$ by performing a Fourier transformation and a Wick rotation along the q^0-axis. The Euclidean propagator is given by

$$G(x,y) = \int_q e^{-iq(x-y)} G(q)\,,$$

and the four-point kernel in momentum space is given by

$$(2\pi)^4\delta^{(4)}(p_1+p_2+p_3+p_4)\overline{\Lambda}(p_1,p_2,p_3,p_4) = \int_{x_1x_2x_3x_4} e^{i\sum_n p_n x_n}\overline{\Lambda}(x_1,x_2,x_3,x_4)\,.$$

An analogous transformation holds for the other four-point functions.
The renormalization conditions can be imposed at an arbitrary subtraction point $\tilde{q}$ in momentum space. However, it is important that the same point is used consistently for all 2PI kernels,

$$\begin{aligned}
\overline{\Pi}_R(q=\tilde{q}) = \Pi_R(q=\tilde{q}) &= 0\,, \\
\frac{d}{dq^2}\overline{\Pi}_R(q=\tilde{q}) = \frac{d}{dq^2}\Pi_R(q=\tilde{q}) &= 0\,, \\
\overline{V}_R(p_i=\tilde{q}) = V_R(p_i=\tilde{q}) = \Gamma_R^{(4)}(p_i=\tilde{q}) &= -\lambda_R\,.
\end{aligned} \tag{E.17}$$

Especially, the renormalization conditions for the kernels $\overline{V}_R$ and V_R coincide with the one for the four-point function $\Gamma_R^{(4)} \equiv Z^2\Gamma^{(4)}$,

$$\Gamma^{(4)}(x,y,u,v) = \frac{d^4\Gamma[\phi,\overline{G}[\phi]]}{d\phi(x)d\phi(y)d\phi(u)d\phi(v)}\,, \tag{E.18}$$

where $\overline{G}[\phi]$ denotes the solution of the Schwinger-Dyson equation (E.4) for a given field configuration $\phi(x)$. The renormalization conditions for $\overline{\Pi}_R$ are equivalent to the conditions

$$G_R^{-1}(q=\tilde{q}) = \tilde{q}^2 + m_R^2\,, \qquad \frac{d}{dq^2} G_R^{-1}(q=\tilde{q}) = +1\,, \tag{E.19}$$

for the complete propagator. The seven conditions (E.17) determine the counterterms δm_0^2, δZ_0, δm_2^2, δZ_2, $\delta\lambda_0$, $\delta\lambda_2$ and $\delta\lambda_4$. A simplification occurs for approximations where all contributions to $\overline{\Pi}_R(x,y)$ and $\Pi_R(x,y)$ are identical. In this case, also the corresponding counterterms agree, $\delta m_0^2 = \delta m_2^2$, $\delta Z_0 = \delta Z_2$ and $\delta\lambda_0 = \delta\lambda_2$. In the following, the subtraction point will be chosen at zero momentum, $\tilde{q}=0$. Another interesting choice is $\tilde{q}^2 = -m_R^2$, which corresponds to the on-shell renormalization scheme.

E.3 Two Loop Approximation

The 2PI two-loop approximation corresponds to a Hartree-Fock approximation, and can be used to check the nonperturbative renormalization procedure explicitly. It corresponds to a truncation of the 2PI functional where only the local two-loop $\mathcal{O}(\lambda)$ contributions are retained, in which case eqs. (E.8), (E.10) and (E.12) with $\gamma_R(\phi_R, G_R) \equiv 0$ define the renormalized 2PI effective action completely. Furthermore, the symmetric phase with vanishing field expectation value $\phi = 0$ is considered. In this case, the 2PI two-point kernels $\overline{\Pi}_R(x,y)$ and $\Pi_R(x,y)$ are given by

$$\begin{aligned}
\overline{\Pi}_R(x,y) &= -i\left(\delta Z_0 \Box_x + \delta m_0^2 + \frac{\lambda_R + \delta\lambda_0}{2} G_R(x,x)\right)\delta(x-y)\,,\\
\Pi_R(x,y) &= -i\left(\delta Z_2 \Box_x + \delta m_2^2 + \frac{\lambda_R + \delta\lambda_2}{2} G_R(x,x)\right)\delta(x-y)\,,
\end{aligned} \tag{E.20}$$

and the 2PI four-point kernels are given by

$$\begin{aligned}
Z^2\overline{\Lambda}(x,y,u,v) &= -(\lambda_R + \delta\lambda_0)\delta(x-y)\delta(x-u)\delta(x-v)\,,\\
Z^2\Lambda(x,y,u,v) &= -(\lambda_R + \delta\lambda_2)\delta(x-y)\delta(x-u)\delta(x-v)\,,\\
Z^2\Gamma^{(4)}(x,y,u,v) &= -(\lambda_R + \delta\lambda_4 - 3\delta\lambda_0)\delta(x-y)\delta(x-u)\delta(x-v)\,.
\end{aligned} \tag{E.21}$$

Since the kernels $\overline{\Pi}_R(x,y)$ and $\Pi_R(x,y)$ have an identical structure, the renormalization conditions (E.17) can be satisfied by identical counterterms, i.e. $\delta m_0^2 = \delta m_2^2$, $\delta Z_0 = \delta Z_2$ and $\delta\lambda_0 = \delta\lambda_2$. From eq. (E.20) the renormalized Schwinger-Dyson equation (E.14) in two-loop approximation in Euclidean momentum space is obtained,

$$G_R^{-1}(k) = k^2 + m_R^2 + \delta Z_0 k^2 + \delta m_0^2 + \frac{\lambda_R + \delta\lambda_0}{2}\int_q G_R(q)\,.$$

Using the renormalization conditions for the propagator (E.19) immediately yields the mass- and field counterterms

$$\delta Z_0 = 0\,, \qquad \delta m_0^2 = -\frac{\lambda_R + \delta\lambda_0}{2}\int_q G_R(q)\,, \tag{E.22}$$

and the complete propagator in two-loop approximation is simply given by

$$G_R^{-1}(k) = G^{-1}(k) = k^2 + m_R^2\,. \tag{E.23}$$

In order to determine the coupling counterterm, the Schwinger-Dyson equation has to be supplemented by the Bethe-Salpeter equation (E.16) in two-loop approximation,

$$\overline{V}_R(p_1,p_2,p_3,p_4) = -(\lambda_R+\delta\lambda_0) - \frac{\lambda_R+\delta\lambda_0}{2}\int_q G_R(q+p_1+p_2)G_R(q)\overline{V}_R(q+p_1+p_2,-q,p_3,p_4)\,,$$

which is obtained by inserting the two-loop 2PI kernel from eq. (E.21) into eq. (E.16), and performing a Fourier transformation. For the determination of the counterterm, it suffices to solve this equation for $V_R(k) \equiv -\overline{V}_R(k,-k,0,0)$,

$$V_R(k) = \lambda_R + \delta\lambda_0 - \frac{\lambda_R+\delta\lambda_0}{2}\int_q G_R^2(q)V_R(q)\,. \tag{E.24}$$

Obviously, this equation has a constant solution $V_R(k) = V_R(0) = \lambda_R$, where the last equality follows from the renormalization condition for $\overline{V}_R$ in eq. (E.17). Thus, the Bethe-Salpeter equation in two-loop approximation reduces to an algebraic equation for the counterterm $\delta\lambda_0$. It is most convenient to rewrite the Bethe-Salpeter equation and eq. (E.22) in terms of $Z = 1+\delta Z_0$ and the bare quantities $\lambda_B = Z^{-2}(\lambda_R+\delta\lambda_0)$ and $m_B^2 = Z^{-1}(m_R^2+\delta m_0^2)$,

$$\begin{aligned} Z &= 1\,, \\ m_B^2 &= m_R^2 - \frac{\lambda_B}{2}\int_q G(q)\,, \\ \lambda_B^{-1} &= \lambda_R^{-1} - \int_q G^2(q)\,. \end{aligned} \tag{E.25}$$

These equations, together with eq. (E.23), form a closed set of equations for the determination of the nonperturbative 2PI counterterms $\delta m_0^2 = \delta m_2^2$, $\delta Z_0 = \delta Z_2$ and $\delta\lambda_0 = \delta\lambda_2$ in two-loop approximation. It is understood that the momentum integrals are suitably regularized, e.g. by dimensional or lattice regularization. Additionally, the counterterm $\delta\lambda_4$ has to be determined by imposing the renormalization condition (E.17) on the four-point function $\Gamma^{(4)}$ from eq. (E.21), yielding

$$\delta\lambda_4 = 3\delta\lambda_0\,. \tag{E.26}$$

E.4 Three Loop Approximation

The 2PI three-loop approximation includes non-local contributions, and therefore yields non-local equations of motion for nonequilibrium initial conditions. This approximation has frequently been used to study quantum dynamics far from equilibrium [1, 2, 25, 32, 142], and therefore the nonperturbative renormalization within this approximation is of interest. Truncating all diagrams which contribute to the 2PI functional to more than $\mathcal{O}(\lambda^2)$, the renormalized 2PI effective action is given by eqs. (E.8), (E.10) and (E.12), where the non-local contributions are given by

$$i\,\gamma_R(\phi_R,G_R) = \frac{(-i\lambda_R)^2}{12}\int_{xy}\phi_R(x)G_R(x,y)^3\phi_R(y) \;+\; \frac{(-i\lambda_R)^2}{48}\int_{xy}G_R(x,y)^4\,. \tag{E.27}$$

Thus, $\gamma_R(\phi_R,G_R)$ contains diagrams up to three-loop order which are shown in figure E.3. Evaluating the 2PI two-point kernels $\overline{\Pi}_R(x,y)$ and $\Pi_R(x,y)$ using the definitions in eq. (E.13) for the symmetric phase, $\phi = 0$, yields

$$\begin{aligned} \overline{\Pi}_R(x,y) &= -i\left(\delta Z_0\Box_x + \delta m_0^2 + \frac{\lambda_R+\delta\lambda_0}{2}G_R(x,x)\right)\delta(x-y) - \frac{\lambda_R^2}{6}G_R^3(x,y)\,, \\ \Pi_R(x,y) &= -i\left(\delta Z_2\Box_x + \delta m_2^2 + \frac{\lambda_R+\delta\lambda_2}{2}G_R(x,x)\right)\delta(x-y) - \frac{\lambda_R^2}{6}G_R^3(x,y)\,. \end{aligned} \tag{E.28}$$

Figure E.3: *Nonlocal diagrams contributing up to three-loop / 2PI-$\mathcal{O}(\lambda^2)$ order.*

The 2PI four-point kernels defined in eqs. (E.15) and the four-point function given by eq. (E.18) in three-loop approximation read,

$$\begin{aligned}
Z^2\overline{\Lambda}(x,y,u,v) &= -(\lambda_R+\delta\lambda_0)\delta(x-y)\delta(x-u)\delta(x-v)+i\lambda_R^2 G_R^2(x,y)\delta(x-z)\delta(y-w)\,,\\
Z^2\Lambda(x,y,u,v) &= -(\lambda_R+\delta\lambda_2)\delta(x-y)\delta(x-u)\delta(x-v)+i\lambda_R^2 G_R^2(x,y)\delta(x-z)\delta(y-w)\,,\\
Z^2\Gamma^{(4)}(x,y,u,v) &= -(\lambda_R+\delta\lambda_4)\delta(x-y)\delta(x-u)\delta(x-v)+\\
&\quad +(\overline{V}_R-Z^2\overline{\Lambda})(x,y,u,v)+(\overline{V}_R-Z^2\overline{\Lambda})(x,u,y,v)+(\overline{V}_R-Z^2\overline{\Lambda})(x,v,u,y)\,.
\end{aligned} \tag{E.29}$$

As for the two-loop approximation, the two-point kernels $\overline{\Pi}_R(x,y)$ and $\Pi_R(x,y)$ have an identical structure, which implies that the renormalization conditions (E.17) can be satisfied by identical counterterms, i.e. $\delta m_0^2=\delta m_2^2$, $\delta Z_0=\delta Z_2$ and $\delta\lambda_0=\delta\lambda_2$, and that the four-point kernels $\overline{\Lambda}$ and Λ as well as $\overline{V}$ and V coincide. From eq. (E.20) the renormalized Schwinger-Dyson equation (E.14) in three-loop approximation in Euclidean momentum space is obtained,

$$\begin{aligned}
G_R^{-1}(k) &= k^2+m_R^2+\delta Z_0 k^2+\delta m_0^2+\frac{\lambda_R+\delta\lambda_0}{2}\int_q G_R(q)\\
&\quad -\frac{\lambda_R^2}{6}\int_{pq} G_R(p)G_R(q)G_R(k-q-p)\,.
\end{aligned} \tag{E.30}$$

The Bethe-Salpeter equation in three-loop approximation is obtained analogously to the two-loop case by inserting the three-loop 2PI kernel from eq. (E.29) into eq. (E.16). After performing a Fourier transformation, the Bethe-Salpeter equation for the kernel $V_R(k)\equiv-\overline{V}_R(k,-k,0,0)$ reads[2]

$$\begin{aligned}
V_R(k) &= \lambda_R+\delta\lambda_0-\lambda_R^2\int_q G_R(q)G_R(k-q)-\frac{\lambda_R+\delta\lambda_0}{2}\int_q G_R^2(q)V_R(q)\\
&\quad +\frac{\lambda_R^2}{2}\int_{pq} G_R(p)G_R(k-q-p)G_R^2(q)V_R(q)\,.
\end{aligned} \tag{E.31}$$

For a numerical solution it is convenient to rewrite the Bethe-Salpeter equation and the Schwinger-Dyson equation in terms of $Z=1+\delta Z_0$ and the bare quantities $\lambda_B=Z^{-2}(\lambda_R+\delta\lambda_0)$ and $m_B^2=Z^{-1}(m_R^2+\delta m_0^2)$,

$$\begin{aligned}
G^{-1}(k) &= k^2+m_B^2+\frac{\lambda_B}{2}\int_q G(q)\\
&\quad -\frac{Z^{-4}\lambda_R^2}{6}\int_{pq} G(p)G(q)G(k-q-p)\,,
\end{aligned} \tag{E.32}$$

$$\begin{aligned}
V(k) &= \lambda_B-Z^{-4}\lambda_R^2\int_q G(q)G(k-q)-\frac{\lambda_B}{2}\int_q G^2(q)V(q)\\
&\quad +\frac{Z^{-4}\lambda_R^2}{2}\int_{pq} G(p)G(k-q-p)G^2(q)V(q)\,.
\end{aligned} \tag{E.33}$$

[2] The kernel $V_R(q,p)$ defined in section 6.2 is related to the 4-point kernel via $V_R(q,p)=\overline{V}_R(q,-q,-p,p)$.

The renormalization conditions (E.17) written in terms of $G(k)$ and $V(k)$ read

$$ZG^{-1}(k=0) = m_R^2\,, \quad Z\frac{d}{dq^2}G^{-1}(k=0) = +1\,, \quad Z^2V(k=0) = \lambda_R\,. \tag{E.34}$$

The Bethe-Salpeter equation (E.33) and the Schwinger-Dyson equation (E.32) together with the upper renormalization conditions form a closed set of equations for the determination of the nonperturbative 2PI counterterms $\delta m_0^2 = \delta m_2^2$, $\delta Z_0 = \delta Z_2$ and $\delta\lambda_0 = \delta\lambda_2$ in three-loop approximation. Finally, the counterterm $\delta\lambda_4$ is determined by imposing the renormalization condition (E.17) on the four-point function $\Gamma^{(4)}$ from eq. (E.29), yielding

$$\delta\lambda_4 = 3\delta\lambda_0 - 3\lambda_R^2\int_q G_R^2(q)\,. \tag{E.35}$$

Appendix F

Integrals on the Closed Real-Time Path

Nonequilibrium as well as thermal correlation functions can conveniently be calculated by attaching the time arguments to the closed real-time contour $\mathcal{C}$ (see figure 6.1) and the imaginary time contour $\mathcal{I}$ (see figure 6.4), respectively. In general, any time contour $\mathcal{P}$ is a complex valued curve, which can be parameterized by a mapping $t_p : [a,b] \to \mathbb{C}$, $u \mapsto t_p(u)$, from a real interval into the complex plane. The integral of a function $f : \mathbb{C} \to \mathbb{C}$ along the time contour $\mathcal{P}$ is given by the curve integral,

$$\int_{\mathcal{P}} dt_p \, f(t_p) = \int_a^b du \, \frac{dt_p(u)}{du} \, f(t_p(u)) \, .$$

Furthermore, for space-time points $x_p^\mu = (x_p^0, \boldsymbol{x})$ with zero-component on the time contour $\mathcal{P}$,

$$\int_{\mathcal{P}} d^4x = \int_{\mathcal{P}} dx_p^0 \int d^3x \, ,$$

is defined. The signum function on a time contour $\mathcal{P}$ is defined as

$$\mathrm{sgn}_{\mathcal{P}}(t_p(u_1) - t_p(u_2)) = \mathrm{sgn}(u_1 - u_2) = \begin{cases} +1 & \text{if} \quad u_1 > u_2 \, , \\ 0 & \text{if} \quad u_1 = u_2 \, , \\ -1 & \text{if} \quad u_1 < u_2 \, , \end{cases}$$

for $u_1, u_2 \in [a,b]$.
Let $f : \mathbb{R} \to \mathbb{C}$ be a continous function with time argument attached to the real axis. Then its integral over the closed real-time path $\mathcal{C}$ vanishes, since the contributions from the chronological and the antichronological parts cancel,

$$\int_{\mathcal{C}} dt_c \, f(t_c) = 0 \, .$$

For the derivation of the Kadanoff-Baym equations (6.15), the following relations, which involve the signum function on the closed real-time path, are required,

$$\begin{aligned} \int_{\mathcal{C}} dt_c \, \mathrm{sgn}_{\mathcal{C}}(t_1 - t_c) \, f(t_c) &= 2 \int_{t_0}^{t_1} dt \, f(t) \, , \\ \int_{\mathcal{C}} dt_c \, \mathrm{sgn}_{\mathcal{C}}(t_1 - t_c) \, \mathrm{sgn}_{\mathcal{C}}(t_c - t_3) \, f(t_c) &= 2 \, \mathrm{sgn}_{\mathcal{C}}(t_1 - t_3) \int_{t_3}^{t_1} dt \, f(t) \, . \end{aligned}$$

Note that the upper relations are true irrespective of whether the times t_1 and t_3 belong to the chronological or the antichronological part of the closed real-time path. Therefore, the upper compact notation is unambiguous.

Danksagung

An dieser Stelle möchte ich mich bei allen bedanken, die zum Gelingen dieser Arbeit beigetragen haben. Insbesondere danke ich

- meinem Betreuer, Herrn Prof. Dr. Manfred Lindner. Er hat mir diese Arbeit an einem sehr interessanten und vielseitigen Thema ermöglicht. Außerdem hat er für exzellente Arbeitsbedingungen gesorgt und hat die Teilnahme an mehreren Sommerschulen und Konferenzen gefördert.
- Florian Bauer, Marc-Thomas Eisele und Markus Michael Müller ("MMM") für die gute Zusammenarbeit.
- Markus Michael Müller für die Erstellung von numerischen Lösungen der Kadanoff-Baym Gleichungen und das Probelesen der Arbeit.
- allen Mitgliedern des ehemaligen Lehrstuhls T30d sowie der Abteilung für Teilchen- und Astroteilchenphysik für die anregende Arbeitsatmosphäre und interessante Diskussionen über physikalische und unphysikalische Themen.
- den Sekretärinnen Karin Ramm und Anja Berneiser für die freundliche Unterstützung bei bürokratischen Angelegenheiten.
- den Systemadministratoren sowie Herrn Köck für die Bereitstellung von Rechnerressourcen.
- A. Anisimov, E. Babichev, J. Berges, S. Borsanyi, H. Gies, U. Reinosa, A. Vikman und C. Wetterich für hilfreiche Kommentare und Diskussionen.
- dem Perimeter Institute für die Finanzierung einer Sommerschule.
- meinen Zimmerkollegen Florian Bauer, Michael Schmidt und Viviana Niro für die gute Gemeinschaft und die Auflockerungen zwischendurch.
- der Deutschen Bahn AG dafür, daß ich das Leben zwischen Heidelberg und München in vollen Zügen genießen durfte.
- und dem `birthday-script` für die Versüßung vieler Nachmittage.

Ganz besonders danke ich meiner Lebensgefährtin Sylvia, die mir jederzeit tatkräftig und liebevoll zur Seite gestanden ist, sowie meinen Eltern Cornelia und Michael und meiner Schwester Hella, die mich immerzu verständnisvoll unterstützt haben. Einen großen Dank haben Gisela und Wilfried verdient, insbesondere für die unkomplizierte Hilfe bei praktischen Aspekten der doppelten Haushaltsführung, und Angelika für vielerlei hilfreiche Ratschläge.

Bibliography

[1] G. Aarts and J. Berges, *Classical aspects of quantum fields far from equilibrium*, Phys. Rev. Lett. **88**, 041603 (2002), hep-ph/0107129.

[2] G. Aarts and J. M. Martínez Resco, *Transport coefficients from the 2PI effective action*, Phys. Rev. **D68**, 085009 (2003), hep-ph/0303216.

[3] G. Aarts and A. Tranberg, *Particle creation and warm inflation*, Phys. Lett. **B650**, 65–71 (2007), hep-ph/0701205.

[4] G. Aarts and A. Tranberg, *Thermal effects on inflaton dynamics* (2007), arXiv:0712.1120[hep-ph].

[5] L. F. Abbott, E. Farhi and M. B. Wise, *Particle Production in the New Inflationary Cosmology*, Phys. Lett. **B117**, 29 (1982).

[6] J. Adams et al., *Experimental and theoretical challenges in the search for the quark gluon plasma: The STAR collaboration's critical assessment of the evidence from RHIC collisions*, Nucl. Phys. **A757**, 102–183 (2005), nucl-ex/0501009.

[7] K. Adcox et al., *Formation of dense partonic matter in relativistic nucleus nucleus collisions at RHIC: Experimental evaluation by the PHENIX collaboration*, Nucl. Phys. **A757**, 184–283 (2005), nucl-ex/0410003.

[8] I. Affleck and M. Dine, *A new mechanism for baryogenesis*, Nucl. Phys. **B249**, 361 (1985).

[9] A. Albrecht and C. Skordis, *Phenomenology of a realistic accelerating universe using only Planck-scale physics*, Phys. Rev. Lett. **84**, 2076–2079 (2000), astro-ph/9908085.

[10] L. Amendola, *Coupled quintessence*, Phys. Rev. **D62**, 043511 (2000), astro-ph/9908023.

[11] L. Amendola, M. Baldi and C. Wetterich, *Growing matter* (2007), arXiv:0706.3064.

[12] L. Amendola, R. Gannouji, D. Polarski and S. Tsujikawa, *Conditions for the cosmological viability of f(R) dark energy models*, Phys. Rev. **D75**, 083504 (2007), gr-qc/0612180.

[13] L. Amendola, C. Quercellini, D. Tocchini-Valentini and A. Pasqui, *Constraints on the interaction and self-interaction of dark energy from cosmic microwave background*, Astrophys. J. **583**, L53 (2003), astro-ph/0205097.

[14] L. Amendola and D. Tocchini-Valentini, *Stationary dark energy: the present universe as a global attractor*, Phys. Rev. **D64**, 043509 (2001), astro-ph/0011243.

[15] L. Anchordoqui and H. Goldberg, *Time variation of the fine structure constant driven by quintessence*, Phys. Rev. **D68**, 083513 (2003), hep-ph/0306084.

[16] C. Armendariz-Picon, V. F. Mukhanov and P. J. Steinhardt, *Essentials of k-essence*, Phys. Rev. **D63**, 103510 (2001), astro-ph/0006373.

[17] A. Arrizabalaga, J. Smit and A. Tranberg, *Equilibration in φ^4 theory in 3+1 dimensions*, Phys. Rev. **D72**, 025014 (2005), hep-ph/0503287.

[18] J. Baacke, K. Heitmann and C. Patzold, *Nonequilibrium dynamics of fermions in a spatially homogeneous scalar background field*, Phys. Rev. **D58**, 125013 (1998), hep-ph/9806205.

[19] K. R. S. Balaji, T. Biswas, R. H. Brandenberger and D. London, *Dynamical CP violation in the early universe*, Phys. Lett. **B595**, 22–27 (2004), hep-ph/0403014.

[20] T. Banks, M. Dine and M. R. Douglas, *Time-varying alpha and particle physics*, Phys. Rev. Lett. **88**, 131301 (2002), hep-ph/0112059.

[21] T. Barreiro, E. J. Copeland and N. J. Nunes, *Quintessence arising from exponential potentials*, Phys. Rev. **D61**, 127301 (2000), astro-ph/9910214.

[22] N. Bartolo and M. Pietroni, *Scalar tensor gravity and quintessence*, Phys. Rev. **D61**, 023518 (2000), hep-ph/9908521.

[23] F. Bauer, M.-T. Eisele and M. Garny, *Leptonic dark energy and baryogenesis*, Phys. Rev. **D74**, 023509 (2006), hep-ph/0510340.

[24] G. Baym, *Selfconsistent approximation in many body systems*, Phys. Rev. **127**, 1391–1401 (1962).

[25] J. Berges, *Controlled nonperturbative dynamics of quantum fields out of equilibrium*, Nucl. Phys. **A699**, 847–886 (2002), hep-ph/0105311.

[26] J. Berges, *n-PI effective action techniques for gauge theories*, Phys. Rev. **D70**, 105010 (2004), hep-ph/0401172.

[27] J. Berges, *Introduction to nonequilibrium quantum field theory*, AIP Conf. Proc. **739**, 3–62 (2005), hep-ph/0409233.

[28] J. Berges, S. Borsanyi, U. Reinosa and J. Serreau, *Nonperturbative renormalization for 2PI effective action techniques*, Annals Phys. **320**, 344–398 (2005), hep-ph/0503240.

[29] J. Berges, S. Borsanyi, U. Reinosa and J. Serreau, *Renormalized thermodynamics from the 2PI effective action*, Phys. Rev. **D71**, 105004 (2005), hep-ph/0409123.

[30] J. Berges, S. Borsanyi and J. Serreau, *Thermalization of fermionic quantum fields*, Nucl. Phys. **B660**, 51–80 (2003), hep-ph/0212404.

[31] J. Berges, S. Borsanyi and C. Wetterich, *Prethermalization*, Phys. Rev. Lett. **93**, 142002 (2004), hep-ph/0403234.

[32] J. Berges and J. Cox, *Thermalization of quantum fields from time-reversal invariant evolution equations*, Phys. Lett. **B517**, 369–374 (2001), hep-ph/0006160.

[33] J. Berges and J. Serreau, *Parametric resonance in quantum field theory*, Phys. Rev. Lett. **91**, 111601 (2003), hep-ph/0208070.

[34] P. Binetruy, *Models of dynamical supersymmetry breaking and quintessence*, Phys. Rev. **D60**, 063502 (1999), hep-ph/9810553.

[35] N. D. Birrell and P. C. W. Davies, *Quantum fields in curved space* (Cambridge University Press, Cambridge, UK, 1982).

[36] O. E. Bjaelde et al., *Neutrino Dark Energy – Revisiting the Stability Issue* (2007), arXiv:0705.2018.

[37] J.-P. Blaizot, E. Iancu and U. Reinosa, *Renormalization of phi-derivable approximations in scalar field theories*, Nucl. Phys. **A736**, 149–200 (2004), hep-ph/0312085.

[38] N. N. Bogoliubov and O. S. Parasiuk, *On the Multiplication of the causal function in the quantum theory of fields*, Acta Math. **97**, 227–266 (1957).

[39] B. Boisseau, G. Esposito-Farese, D. Polarski and A. A. Starobinsky, *Reconstruction of a scalar-tensor theory of gravity in an accelerating universe*, Phys. Rev. Lett. **85**, 2236 (2000), gr-qc/0001066.

[40] L. A. Boyle, R. R. Caldwell and M. Kamionkowski, *Spintessence! New models for dark matter and dark energy*, Phys. Lett. **B545**, 17–22 (2002), astro-ph/0105318.

[41] C. Brans and R. H. Dicke, *Mach's principle and a relativistic theory of gravitation*, Phys. Rev. **124**, 925–935 (1961).

[42] P. Brax and J. Martin, *Quintessence and supergravity*, Phys. Lett. **B468**, 40–45 (1999), astro-ph/9905040.

[43] P. Brax and J. Martin, *The robustness of quintessence*, Phys. Rev. **D61**, 103502 (2000), astro-ph/9912046.

[44] P. Brax and J. Martin, *Dark energy and the MSSM*, Phys. Rev. **D75**, 083507 (2007), hep-th/0605228.

[45] A. W. Brookfield, C. van de Bruck, D. F. Mota and D. Tocchini-Valentini, *Cosmology with massive neutrinos coupled to dark energy*, Phys. Rev. Lett. **96**, 061301 (2006), astro-ph/0503349.

[46] N. Brouzakis, N. Tetradis and C. Wetterich, *Neutrino Lumps in Quintessence Cosmology* (2007), arXiv:0711.2226.

[47] I. L. Buchbinder, S. D. Odintsov and I. L. Shapiro, *Effective action in quantum gravity* (IOP Publishing, Bristol, UK, 1992).

[48] W. Buchmüller, P. Di Bari and M. Plümacher, *Leptogenesis for pedestrians*, Ann. Phys. **315**, 305–351 (2005), hep-ph/0401240.

[49] E. Calzetta and B. L. Hu, *Nonequilibrium quantum fields: closed time path effective action, Wigner function and Boltzmann equation*, Phys. Rev. **D37**, 2878 (1988).

[50] B. A. Campbell and K. A. Olive, *Nucleosynthesis and the time dependence of fundamental couplings*, Phys. Lett. **B345**, 429–434 (1995), hep-ph/9411272.

[51] S. M. Carroll, *Quintessence and the rest of the world*, Phys. Rev. Lett. **81**, 3067–3070 (1998), astro-ph/9806099.

[52] F. C. Carvalho and A. Saa, *Non-minimal coupling, exponential potentials and the w < -1 regime of dark energy*, Phys. Rev. **D70**, 087302 (2004), astro-ph/0408013.

[53] R. Catena, N. Fornengo, A. Masiero, M. Pietroni et al., *Dark matter relic abundance and scalar-tensor dark energy*, Phys. Rev. **D70**, 063519 (2004), astro-ph/0403614.

[54] H. Chand, R. Srianand, P. Petitjean and B. Aracil, *Probing the cosmological variation of the fine-structure constant: Results based on VLT-UVES sample*, Astron. Astrophys. **417**, 853 (2004), astro-ph/0401094.

[55] T. Chiba, *Quintessence, the gravitational constant, and gravity*, Phys. Rev. **D60**, 083508 (1999), gr-qc/9903094.

[56] T. Chiba and K. Kohri, *Quintessence cosmology and varying alpha*, Prog. Theor. Phys. **107**, 631–636 (2002), hep-ph/0111086.

[57] K. Chou, Z. Su, B. Hao and L. Yu, *Equilibrium and Nonequilibrium Formalisms Made Unified*, Phys. Rept. **118**, 1 (1985).

[58] D. J. H. Chung, L. L. Everett and A. Riotto, *Quintessence and the underlying particle physics theory*, Phys. Lett. **B556**, 61–70 (2003), hep-ph/0210427.

[59] S. R. Coleman, *Q balls*, Nucl. Phys. **B262**, 263 (1985).

[60] S. R. Coleman and E. Weinberg, *Radiative Corrections as the Origin of Spontaneous Symmetry Breaking*, Phys. Rev. **D7**, 1888–1910 (1973).

[61] J. C. Collins, *Renormalization* (Cambridge University Press, Cambridge, UK, 1984).

[62] D. Comelli, M. Pietroni and A. Riotto, *Dark energy and dark matter*, Phys. Lett. **B571**, 115–120 (2003), hep-ph/0302080.

[63] F. Cooper et al., *Nonequilibrium quantum fields in the large N expansion*, Phys. Rev. **D50**, 2848–2869 (1994), hep-ph/9405352.

[64] E. J. Copeland, N. J. Nunes and M. Pospelov, *Models of quintessence coupled to the electromagnetic field and the cosmological evolution of alpha*, Phys. Rev. **D69**, 023501 (2004), hep-ph/0307299.

[65] E. J. Copeland, M. Sami and S. Tsujikawa, *Dynamics of dark energy*, Int. J. Mod. Phys. **D15**, 1753–1936 (2006), hep-th/0603057.

[66] J. M. Cornwall, R. Jackiw and E. Tomboulis, *Effective Action for Composite Operators*, Phys. Rev. **D10**, 2428–2445 (1974).

[67] T. L. Curtright and C. B. Thorn, *Conformally Invariant Quantization of the Liouville Theory*, Phys. Rev. Lett. **48**, 1309 (1982).

[68] P. Danielewicz, *Quantum Theory of Nonequilibrium Processes I*, Annals Phys. **152**, 239–304 (1984).

[69] P. Danielewicz, *Quantum theory of nonequilibrium processes. II. Application to nuclear collisions*, Annals Phys. **152**, 305–326 (1984).

[70] S. Davidson and A. Ibarra, *A lower bound on the right-handed neutrino mass from leptogenesis*, Phys. Lett. **B535**, 25–32 (2002), hep-ph/0202239.

[71] S. Davidson, E. Nardi and Y. Nir, *Leptogenesis* (2008), 0802.2962.

[72] A. De Felice, S. Nasri and M. Trodden, *Quintessential baryogenesis*, Phys. Rev. **D67**, 043509 (2003), hep-ph/0207211.

[73] R. de Ritis, A. A. Marino, C. Rubano and P. Scudellaro, *Tracker fields from nonminimally coupled theory*, Phys. Rev. **D62**, 043506 (2000), hep-th/9907198.

[74] C. Deffayet, G. R. Dvali and G. Gabadadze, *Accelerated universe from gravity leaking to extra dimensions*, Phys. Rev. **D65**, 044023 (2002), astro-ph/0105068.

[75] T. Dent, S. Stern and C. Wetterich, *Primordial nucleosynthesis as a probe of fundamental physics parameters*, Phys. Rev. **D76**, 063513 (2007), arXiv:0705.0696.

[76] E. D'Hoker and R. Jackiw, *Liouville field theory*, Phys. Rev. **D26**, 3517 (1982).

[77] K. Dick, M. Lindner, M. Ratz and D. Wright, *Leptogenesis with Dirac neutrinos*, Phys. Rev. Lett. **84**, 4039–4042 (2000), hep-ph/9907562.

[78] M. Dine and A. Kusenko, *The origin of the matter-antimatter asymmetry*, Rev. Mod. Phys. **76**, 1 (2004), hep-ph/0303065.

[79] S. Dodelson and L. M. Widrow, *Baryon symmetric baryogenesis*, Phys. Rev. Lett. **64**, 340–343 (1990).

[80] A. D. Dolgov, *Non GUT baryogenesis*, Phys. Rept. **222**, 309–386 (1992).

[81] J. F. Donoghue, *Spatial gradients in the cosmological constant*, JHEP **03**, 052 (2003), hep-ph/0101130.

[82] M. Doran, *Can we test dark energy with running fundamental constants?*, JCAP **0504**, 016 (2005), astro-ph/0411606.

[83] M. Doran and J. Jaeckel, *Loop corrections to scalar quintessence potentials*, Phys. Rev. **D66**, 043519 (2002), astro-ph/0203018.

[84] M. Doran, M. Lilley and C. Wetterich, *Constraining quintessence with the new CMB data*, Phys. Lett. **B528**, 175–180 (2002), astro-ph/0105457.

[85] M. Doran and G. Robbers, *Early dark energy cosmologies*, JCAP **0606**, 026 (2006), astro-ph/0601544.

[86] M. Doran, G. Robbers and C. Wetterich, *Impact of three years of data from the Wilkinson Microwave Anisotropy Probe on cosmological models with dynamical dark energy*, Phys. Rev. **D75**, 023003 (2007), astro-ph/0609814.

[87] M. Doran and C. Wetterich, *Quintessence and the cosmological constant*, Nucl. Phys. Proc. Suppl. **124**, 57–62 (2003), astro-ph/0205267.

[88] J. F. Dufaux, A. Bergman, G. N. Felder, L. Kofman et al., *Theory and Numerics of Gravitational Waves from Preheating after Inflation*, Phys. Rev. **D76**, 123517 (2007), arXiv:0707.0875.

[89] J. Dunkley et al., *Five-Year Wilkinson Microwave Anisotropy Probe (WMAP) Observations: Likelihoods and Parameters from the WMAP data* (2008), arXiv:0803.0586.

[90] G. V. Dunne, *Heisenberg-Euler effective Lagrangians: Basics and extensions* (2004), hep-th/0406216.

[91] E. Elizalde, *Ten physical applications of spectral zeta functions*, Lect. Notes Phys. **M35**, 1–224 (1995).

[92] E. Elizalde, K. Kirsten and S. D. Odintsov, *Effective Lagrangian and the back reaction problem in a selfinteracting O(N) scalar theory in curved space-time*, Phys. Rev. **D50**, 5137–5147 (1994), hep-th/9404084.

[93] J. R. Ellis, J. E. Kim and D. V. Nanopoulos, *Cosmological Gravitino Regeneration and Decay*, Phys. Lett. **B145**, 181 (1984).

[94] V. Faraoni, *Inflation and quintessence with nonminimal coupling*, Phys. Rev. **D62**, 023504 (2000), gr-qc/0002091.

[95] R. Fardon, A. E. Nelson and N. Weiner, *Dark energy from mass varying neutrinos*, JCAP **0410**, 005 (2004), astro-ph/0309800.

[96] G. R. Farrar and P. J. E. Peebles, *Interacting dark matter and dark energy*, Astrophys. J. **604**, 1–11 (2004), astro-ph/0307316.

[97] E. Fermi, *An attempt of a theory of beta radiation. 1*, Z. Phys. **88**, 161–177 (1934).

[98] P. G. Ferreira and M. Joyce, *Structure formation with a self-tuning scalar field*, Phys. Rev. Lett. **79**, 4740–4743 (1997), astro-ph/9707286.

[99] U. Franca and R. Rosenfeld, *Age constraints and fine tuning in variable-mass particle models*, Phys. Rev. **D69**, 063517 (2004), astro-ph/0308149.

[100] J. Frieman, M. Turner and D. Huterer, *Dark Energy and the Accelerating Universe* (2008), arXiv:0803.0982.

[101] R. Gannouji, D. Polarski, A. Ranquet and A. A. Starobinsky, *Scalar-tensor models of normal and phantom dark energy*, JCAP **0609**, 016 (2006), astro-ph/0606287.

[102] M. Garny, *Quantum corrections in quintessence models*, Phys. Rev. **D74**, 043009 (2006), hep-ph/0606120.

[103] M. Garny, *B-L-symmetric baryogenesis with leptonic quintessence*, J. Phys. **A40**, 7005–7010 (2007), hep-ph/0612145.

[104] F. Gelis, *The Effect of the vertical part of the path on the real time Feynman rules in finite temperature field theory*, Z. Phys. **C70**, 321–331 (1996), hep-ph/9412347.

[105] E. Gildener and S. Weinberg, *Symmetry Breaking and Scalar Bosons*, Phys. Rev. **D13**, 3333 (1976).

[106] J.-A. Gu and W.-Y. P. Hwang, *Can the quintessence be a complex scalar field?*, Phys. Lett. **B517**, 1–6 (2001), astro-ph/0105099.

[107] P. Gu, X. Wang and X. Zhang, *Dark energy and neutrino mass limits from baryogenesis*, Phys. Rev. **D68**, 087301 (2003), hep-ph/0307148.

[108] A. H. Guth, *The inflationary universe: a possible solution to the horizon and flatness problems*, Phys. Rev. **D23**, 347–356 (1981).

[109] J. A. Harvey and M. S. Turner, *Cosmological baryon and lepton number in the presence of electroweak fermion number violation*, Phys. Rev. **D42**, 3344–3349 (1990).

[110] S. W. Hawking, *Zeta function regularization of path intergrals in curved space*, Commun. Math. Phys. **55**, 133 (1977).

[111] A. Hebecker and C. Wetterich, *Natural quintessence?*, Phys. Lett. **B497**, 281–288 (2001), hep-ph/0008205.

[112] U. W. Heinz and P. F. Kolb, *Early thermalization at RHIC*, Nucl. Phys. **A702**, 269–280 (2002), hep-ph/0111075.

[113] K. Hepp, *Proof of the Bogolyubov-Parasiuk theorem on renormalization*, Commun. Math. Phys. **2**, 301–326 (1966).

[114] M. B. Hoffman, *Cosmological constraints on a dark matter: Dark energy interaction* (2003), astro-ph/0307350.

[115] A. Hohenegger, A. Kartavtsev and M. Lindner, *Deriving Boltzmann Equations from Kadanoff-Baym Equations in Curved Space-Time* (2008), arXiv:0807.4551.

[116] B. L. Hu and D. J. O'Connor, *Effective lagrangian for lambda phi**4 theory in curved space-time with varying background fields: quasilocal approximation*, Phys. Rev. **D30**, 743 (1984).

[117] G. Huey and B. D. Wandelt, *Interacting quintessence, the coincidence problem and cosmic acceleration*, Phys. Rev. **D74**, 023519 (2006), astro-ph/0407196.

[118] K. Ichikawa and M. Kawasaki, *Constraining the variation of the coupling constants with big bang nucleosynthesis*, Phys. Rev. **D65**, 123511 (2002), hep-ph/0203006.

[119] A. Ivanchik et al., *A new constraint on the time dependence of the proton-to- electron mass ratio. Analysis of the Q 0347-383 and Q 0405- 443 spectra*, Astron. Astrophys. **440**, 45–52 (2005), astro-ph/0507174.

[120] Y. B. Ivanov, J. Knoll and D. N. Voskresensky, *Self-consistent approximations to non-equilibrium many- body theory*, Nucl. Phys. **A657**, 413–445 (1999), hep-ph/9807351.

[121] I. Jack and L. Parker, *Proof of summed form of proper time expansion for propagator in curved space-time*, Phys. Rev. **D31**, 2439 (1985).

[122] R. Jackiw, *Functional evaluation of the effective potential*, Phys. Rev. **D9**, 1686 (1974).

[123] S. Juchem, W. Cassing and C. Greiner, *Quantum dynamics and thermalization for out-of-equilibrium phi**4-theory*, Phys. Rev. **D69**, 025006 (2004), hep-ph/0307353.

[124] J. I. Kapusta and C. Gale, *Finite-temperature field theory: Principles and applications* (Cambridge University Press, Cambridge, UK, 2006).

[125] B. G. Keating, A. G. Polnarev, N. J. Miller and D. Baskaran, *The Polarization of the Cosmic Microwave Background Due to Primordial Gravitational Waves*, Int. J. Mod. Phys. **A21**, 2459–2479 (2006), astro-ph/0607208.

[126] L. V. Keldysh, *Diagram technique for nonequilibrium processes*, Sov. Phys. JETP **20**, 1018 (1965).

[127] S. Y. Khlebnikov and I. I. Tkachev, *Classical decay of inflaton*, Phys. Rev. Lett. **77**, 219–222 (1996), hep-ph/9603378.

[128] L. Kofman, A. D. Linde and A. A. Starobinsky, *Reheating after inflation*, Phys. Rev. Lett. **73**, 3195–3198 (1994), hep-th/9405187.

[129] L. Kofman, A. D. Linde and A. A. Starobinsky, *Non-Thermal Phase Transitions After Inflation*, Phys. Rev. Lett. **76**, 1011–1014 (1996), hep-th/9510119.

[130] L. Kofman, A. D. Linde and A. A. Starobinsky, *Towards the theory of reheating after inflation*, Phys. Rev. **D56**, 3258–3295 (1997), hep-ph/9704452.

[131] P. F. Kolb and U. W. Heinz, *Hydrodynamic description of ultrarelativistic heavy-ion collisions* (2003), nucl-th/0305084, nucl-th/0305084.

[132] C. F. Kolda and D. H. Lyth, *Quintessential difficulties*, Phys. Lett. **B458**, 197–201 (1999), hep-ph/9811375.

[133] M. Kowalski et al., *Improved Cosmological Constraints from New, Old and Combined Supernova Datasets* (2008), arXiv:0804.4142.

[134] A. Kusenko and M. E. Shaposhnikov, *Supersymmetric Q-balls as dark matter*, Phys. Lett. **B418**, 46–54 (1998), hep-ph/9709492.

[135] N. P. Landsman and C. G. van Weert, *Real and Imaginary Time Field Theory at Finite Temperature and Density*, Phys. Rept. **145**, 141 (1987).

[136] M. Le Bellac, *Thermal Field Theory* (Cambridge University Press, Cambridge, UK, 1996).

[137] S. Lee, K. A. Olive and M. Pospelov, *Quintessence models and the cosmological evolution of alpha*, Phys. Rev. **D70**, 083503 (2004), astro-ph/0406039.

[138] M.-z. Li, X.-l. Wang, B. Feng and X.-m. Zhang, *Quintessence and spontaneous leptogenesis*, Phys. Rev. **D65**, 103511 (2002), hep-ph/0112069.

[139] A. D. Linde, *A New Inflationary Universe Scenario: A Possible Solution of the Horizon, Flatness, Homogeneity, Isotropy and Primordial Monopole Problems*, Phys. Lett. **B108**, 389–393 (1982).

[140] A. D. Linde, *Chaotic Inflation*, Phys. Lett. **B129**, 177–181 (1983).

[141] A. D. Linde, *Particle Physics and Inflationary Cosmology* (Harwood, Chur, Switzerland, 1990), hep-th/0503203.

[142] M. Lindner and M. M. Müller, *Comparison of Boltzmann equations with quantum dynamics for scalar fields*, Phys. Rev. **D73**, 125002 (2006), hep-ph/0512147.

[143] M. Lindner and M. M. Müller, *Comparison of Boltzmann Kinetics with Quantum Dynamics for a Chiral Yukawa Model Far From Equilibrium*, Phys. Rev. **D77**, 025027 (2008), arXiv:0710.2917.

[144] C. Misner, K. Thorne and J. Wheeler, *Gravitation* (Freeman, New York, 1973).

[145] D. F. Mota, V. Pettorino, G. Robbers and C. Wetterich, *Neutrino clustering in growing neutrino quintessence*, Phys. Lett. **B663**, 160–164 (2008), arXiv:0802.1515.

[146] M. M. Müller, *private communications*.

[147] M. M. Müller, *Comparison of Boltzmann Kinetics with Quantum Dynamics for Relativistic Quantum fields*, Ph.D. thesis, Munich, Tech. U. (2006).

[148] Y. Nakayama, *Liouville field theory: A decade after the revolution*, Int. J. Mod. Phys. **A19**, 2771–2930 (2004), hep-th/0402009.

[149] Y. Nambu and G. Jona-Lasinio, *Dynamical model of elementary particles based on an analogy with superconductivity. I*, Phys. Rev. **122**, 345–358 (1961).

[150] I. P. Neupane, *Accelerating cosmologies from exponential potentials*, Class. Quant. Grav. **21**, 4383–4397 (2004), hep-th/0311071.

[151] S. Nojiri and S. D. Odintsov, *Introduction to modified gravity and gravitational alternative for dark energy*, ECONF **C0602061**, 06 (2006), hep-th/0601213.

[152] V. K. Onemli and R. P. Woodard, *Super-acceleration from massless, minimally coupled phi**4*, Class. Quant. Grav. **19**, 4607 (2002), gr-qc/0204065.

[153] L. Parker and D. J. Toms, *New form for the coincidence limit of the feynman propagator, or heat kernel, in curved space-time*, Phys. Rev. **D31**, 953 (1985).

[154] P. J. E. Peebles and A. Vilenkin, *Quintessential inflation*, Phys. Rev. **D59**, 063505 (1999), astro-ph/9810509.

[155] F. Perrotta, C. Baccigalupi and S. Matarrese, *Extended quintessence*, Phys. Rev. **D61**, 023507 (2000), astro-ph/9906066.

[156] A. M. Polyakov, *Quantum geometry of bosonic strings*, Phys. Lett. **B103**, 207–210 (1981).

[157] B. Ratra and P. J. E. Peebles, *Cosmological consequences of a rolling homogeneous scalar field*, Phys. Rev. **D37**, 3406 (1988).

[158] E. Reinhold et al., *Indication of a Cosmological Variation of the Proton - Electron Mass Ratio Based on Laboratory Measurement and Reanalysis of H(2) Spectra*, Phys. Rev. Lett. **96**, 151101 (2006).

[159] A. Riazuelo and J.-P. Uzan, *Cosmological observations in scalar-tensor quintessence*, Phys. Rev. **D66**, 023525 (2002), astro-ph/0107386.

[160] A. G. Riess et al., *Type Ia Supernova Discoveries at z>1 From the Hubble Space Telescope: Evidence for Past Deceleration and Constraints on Dark Energy Evolution*, Astrophys. J. **607**, 665–687 (2004), astro-ph/0402512.

[161] R. Rosenfeld, *Relic abundance of mass-varying cold dark matter particles*, Phys. Lett. **B624**, 158–161 (2005), astro-ph/0504121.

[162] V. Sahni, *Dark matter and dark energy*, Lect. Notes Phys. **653**, 141–180 (2004), astro-ph/0403324.

[163] A. D. Sakharov, *Violation of CP invariance, C asymetry, and baryon asymetry of the universe*, Pisma Zh. Eksp. Teor. Fiz. **5**, 32–35 (1967).

[164] F. Schwabl, *Statistische Mechanik* (Springer, Berlin, Germany, 2000).

[165] J.-M. Schwindt and C. Wetterich, *Dark energy cosmologies for codimension-two branes*, Nucl. Phys. **B726**, 75–92 (2005), hep-th/0501049.

[166] J. S. Schwinger, *Brownian motion of a quantum oscillator*, J. Math. Phys. **2**, 407–432 (1961).

[167] Y. Shtanov, J. H. Traschen and R. H. Brandenberger, *Universe reheating after inflation*, Phys. Rev. **D51**, 5438–5455 (1995), hep-ph/9407247.

[168] R. Srianand, H. Chand, P. Petitjean and B. Aracil, *Limits on the time variation of the electromagnetic fine- structure constant in the low energy limit from absorption lines in the spectra of distant quasars*, Phys. Rev. Lett. **92**, 121302 (2004), astro-ph/0402177.

[169] P. J. Steinhardt, L.-M. Wang and I. Zlatev, *Cosmological tracking solutions*, Phys. Rev. **D59**, 123504 (1999), astro-ph/9812313.

[170] A. Tranberg, *Quantum field thermalization in expanding backgrounds* (2008), arXiv:0806.3158.

[171] J.-P. Uzan, *Cosmological scaling solutions of non-minimally coupled scalar fields*, Phys. Rev. **D59**, 123510 (1999), gr-qc/9903004.

[172] J.-P. Uzan, *The fundamental constants and their variation: Observational status and theoretical motivations*, Rev. Mod. Phys. **75**, 403 (2003), hep-ph/0205340.

[173] H. van Hees and J. Knoll, *Renormalization in self-consistent approximation schemes at finite temperature. III: Global symmetries*, Phys. Rev. **D66**, 025028 (2002), hep-ph/0203008.

[174] H. van Hees and J. Knoll, *Renormalization in self-consistent approximations schemes at finite temperature. I: Theory*, Phys. Rev. **D65**, 025010 (2002), hep-ph/0107200.

[175] H. van Hees and J. Knoll, *Renormalization of self-consistent approximation schemes. II: Applications to the sunset diagram*, Phys. Rev. **D65**, 105005 (2002), hep-ph/0111193.

[176] J. K. Webb et al., *Further Evidence for Cosmological Evolution of the Fine Structure Constant*, Phys. Rev. Lett. **87**, 091301 (2001), astro-ph/0012539.

[177] S. Weinberg, *High-energy behavior in quantum field theory*, Phys. Rev. **118**, 838–849 (1960).

[178] S. Weinberg, *Anthropic Bound on the Cosmological Constant*, Phys. Rev. Lett. **59**, 2607 (1987).

[179] S. Weinberg, *The Quantum theory of fields. Vol. 1: Foundations* (Cambridge University Press, Cambridge, UK, 1995).

[180] S. Weinberg, *The quantum theory of fields. Vol. 2: Modern applications* (Cambridge University Press, Cambridge, UK, 1996).

[181] C. Wetterich, *Cosmologies with variable Newton's "constant"*, Nucl. Phys. **B302**, 645 (1988).

[182] C. Wetterich, *Cosmology and the fate of dilatation symmetry*, Nucl. Phys. **B302**, 668 (1988).

[183] C. Wetterich, *Conformal fixed point, cosmological constant and quintessence*, Phys. Rev. Lett. **90**, 231302 (2003), hep-th/0210156.

[184] C. Wetterich, *Crossover quintessence and cosmological history of fundamental 'constants'*, Phys. Lett. **B561**, 10–16 (2003), hep-ph/0301261.

[185] C. Wetterich, *Probing quintessence with time variation of couplings*, JCAP **0310**, 002 (2003), hep-ph/0203266.

[186] C. Wetterich, *Growing neutrinos and cosmological selection*, Phys. Lett. **B655**, 201–208 (2007), 0706.4427.

[187] M. Yamaguchi, *Generation of cosmological large lepton asymmetry from a rolling scalar field*, Phys. Rev. **D68**, 063507 (2003), hep-ph/0211163.

[188] Y. B. Zel'dovich, *The Cosmological constant and the theory of elementary particles*, Sov. Phys. Usp. **11**, 381–393 (1968).

[189] X. Zhang, *Coupled quintessence in a power-law case and the cosmic coincidence problem*, Mod. Phys. Lett. **A20**, 2575 (2005), astro-ph/0503072.

[190] W. Zimdahl and D. Pavon, *Interacting quintessence*, Phys. Lett. **B521**, 133–138 (2001), astro-ph/0105479.

[191] W. Zimmermann, *Convergence of Bogolyubov's method of renormalization in momentum space*, Commun. Math. Phys. **15**, 208–234 (1969).